RESEARCH MEMORANDUM

SOME STUDIES OF AXISYMMETRIC FREE JETS EXHAUSTING FROM SONIC AND SUPERSONIC NOZZLES INTO STILL AIR AND INTO SUPERSONIC STREAMS

By Eugene S. Love and Carl E. Grigsby

Langley Aeronautical Laboratory
Langley Field, Va.

NATIONAL ADVISORY COMMITTEE
FOR AERONAUTICS

WASHINGTON

May 10, 1955

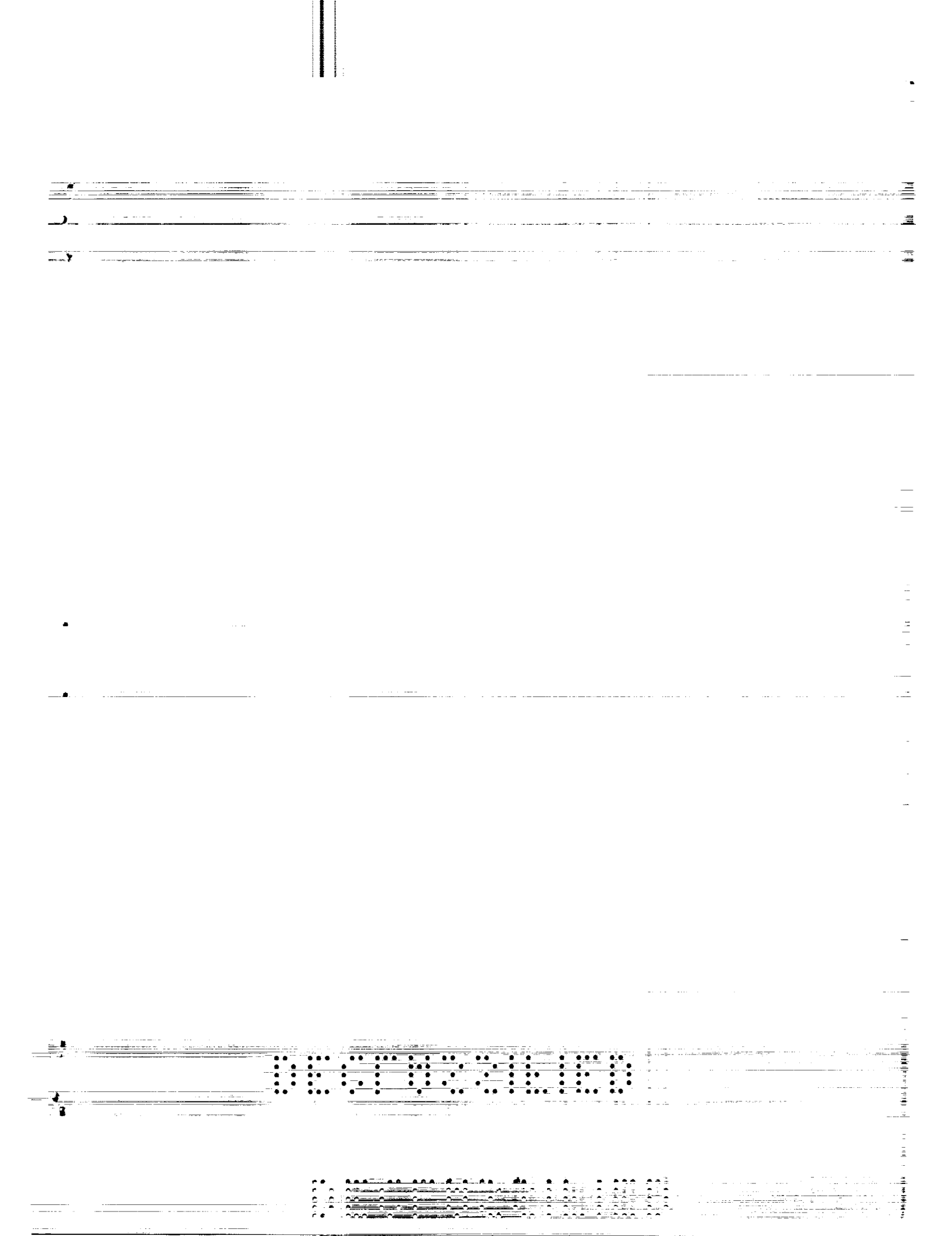

ERRATA

NACA RM L54L31

SOME STUDIES OF AXISYMMETRIC FREE JETS EXHAUSTING FROM SONIC AND SUPERSONIC NOZZLES INTO STILL AIR AND INTO SUPERSONIC STREAMS

By Eugene S. Love and Carl E. Grigsby

May 10, 1955

The statement on page 9 of this paper that Pack's method is semiempirical is incorrect. Consequently, the paragraph on page 9, lines 15 to 32 should be replaced by the following:

> Two of the methods which have had some success in predicting the wavelength were used to calculate the upper and lower curves shown in figure 7(a) for $M_j = 1.00$. The method of Pack (ref. 13) has been advanced as being applicable to all Mach numbers. It is based upon linear theory (and therefore subject to the restrictions of linear theory) and is a correction of Prandtl's formula which is known to be in error. (See refs. 6 and 13, for example.) The older method of Hartmann and Lazarus (ref. 14) is proposed for sonic jets only. This latter method is semiempirical, as are most of the others except those of Prandtl and Pack mentioned above, and it involves constants determined from experimental results for low values of p_j/p_∞. It is not surprising, therefore, to find that both methods are not satisfactory except at very low jet pressure ratios as indicated in figure 7(a). Because of the inadequacy at $M_j = 1$, no comparison has been made between the method of Pack and the present results for higher Mach numbers; further, the assumption of the method that w/d_j is independent of M_j and a function only of the ratio of jet stagnation pressure to the ambient pressure can be shown from these results to be insufficient.

NACA - Langley Field, Va.

[redacted]

CONTENTS

Page

NACA RM L54L31

NATIONAL ADVISORY COMMITTEE FOR AERONAUTICS

RESEARCH MEMORANDUM

SOME STUDIES OF AXISYMMETRIC FREE JETS EXHAUSTING FROM SONIC AND SUPERSONIC NOZZLES INTO STILL AIR AND INTO SUPERSONIC STREAMS

By Eugene S. Love and Carl E. Grigsby

SUMMARY

Some experimental and theoretical studies have been made of axisymmetric free jets exhausting from sonic and supersonic nozzles into still air and into supersonic streams with a view toward current problems associated with propulsive jets and the investigation of these problems.

For jets exhausting into still air, consideration is given to the effects of jet Mach number, nozzle divergence angle, and jet static-pressure ratio upon jet structure, jet wavelength, and the shape and curvature of the jet boundary. Limited studies of the effects of the ratio of specific heats of the jet are included as are observations pertaining to jet noise.

For jets exhausting into supersonic streams, an attempt has been made to present primarily theoretical curves of the type that may be useful in evaluating certain jet interference effects and in formulating experimental studies. The primary variables considered are jet Mach number, free-stream Mach number, jet static-pressure ratio, and the ratio of specific heats of the jet. A few experimental observations are included.

INTRODUCTION

The increasing interest in the problems associated with the use of propulsive jets has in recent years brought about the compilation of several summaries and bibliographies on jets and related subjects - for example, references 1 to 4, chapter IX of reference 5, and the summary studies of reference 6. From these compilations and from numerous investigations of more recent origin the need for further study of free jets is evident.

This report presents results of some experimental and theoretical studies of axisymmetric free jets exhausting from sonic and supersonic nozzles into still air and into supersonic streams with a view toward current problems associated with propulsive jets and the investigation of these problems. The first part of this report deals with jets exhausting into still air; the second part deals with jets exhausting into supersonic streams.

SYMBOLS

A	exit area of nozzle
A_t	throat area of nozzle
$\frac{A_t}{A}$	nozzle area ratio, $M\left(\frac{\frac{\gamma+1}{2}}{1+\frac{\gamma-1}{2}M^2}\right)^{\frac{\gamma+1}{2(\gamma-1)}}$
$\beta_j = \sqrt{M_j^2 - 1}$	
d_j	diameter of jet exit
d_B	diameter of base
δ	two-dimensional turning angle through an oblique shock
δ_j	angle between jet axis and tangent to free jet boundary at nozzle lip
ϵ	shock inclination
γ	ratio of specific heats
l	distance along jet axis from jet exit to shock intersection or to Riemann wave
λ	Kawamura parameter, $\frac{1}{\gamma}(\sin\mu\cos\mu)$
M	Mach number
M_j	jet Mach number at nozzle exit; for a divergent nozzle, value at nozzle lip

μ Mach angle

P Busemann's pressure number

p static pressure

p_o stagnation pressure

$$\frac{p}{p_o} = \left(1 + \frac{\gamma - 1}{2} M^2\right)^{-\frac{\gamma}{\gamma-1}}$$

p_B base pressure

P_B base pressure coefficient, $\frac{p_B - p_\infty}{q_\infty}$

p_j jet static pressure at nozzle exit; for a divergent nozzle, value at nozzle lip

q dynamic pressure

R distance from source

r_j radius of jet exit

ρ average radius of curvature of jet boundary

ρ_o initial radius of curvature of jet boundary (at $x = 0$)

S diameter of Riemann wave

θ direction of velocity with respect to jet axis

θ_N exit angle of nozzle with respect to jet axis

ν Prandtl-Meyer turning angle from sonic velocity

V local velocity

V_l limiting velocity

$\frac{V}{V_l}$ limiting velocity ratio, $\sqrt{1 - \left(\frac{p}{p_o}\right)^{\frac{\gamma-1}{\gamma}}}$

[redacted]

w primary wavelength of jet

x distance from plane of nozzle exit measured parallel to jet axis

y perpendicular distance from jet axis

Subscripts:

j jet, unless more explicitly defined (j', local value in free jet at jet boundary)

∞ free stream (∞', local value at jet boundary)

N nozzle

max maximum value

I. JETS EXHAUSTING INTO STILL AIR

Introduction

Although considerable effort has been devoted to the study of free jets exhausting from sonic and supersonic nozzles into still air, there is still much room for additional study of the effects of the variables involved. Consider the general sketch in figure 1(a) of the first portion of the nonviscous boundary of a jet exhausting supersonically into still air. The well-known characteristic curvature of the boundary is obviously brought about by the requirement that the pressure along the boundary must be constant. The shape and curvature of the inviscid boundary is dependent upon a number of variables; these include the ratio of specific heats of the jet, Mach number of the jet, divergence angle of the nozzle or nozzle geometry in general, and the jet pressure ratio.[1] However, the variation in shape and curvature of the boundary with most of these variables has not been studied except for a few specific and unrelated cases. It might be stated that figure 1(a) is an illustrative sketch of a sonic jet operating at some jet pressure ratio greater than one as shown in figure 1(b), a conically divergent nozzle operating at a jet pressure ratio less than one as shown in figure 1(c), or a number of combinations of

[1]Throughout this paper the term "jet pressure ratio" refers to the ratio of jet static pressure at exit to the ambient or free-stream static pressure. Static-pressure ratio has been used in preference to total-pressure ratio since the latter rarely permits presentation of data in a form that facilitates comparison, does not lend to the elimination of variables, and thereby often obscures conclusions.

variables involved. The jet structure, that is, type of shock or expansion pattern within the jet, would of course be dependent upon these combinations. The exact structure and boundary shape would be unique for a particular combination, but without further study of the effects of the variables involved, the implication of the uniqueness in terms of large or small differences in structure and boundary shape is not clear.

The broadening in recent years of the probable fields of application of free jet characteristics has pointed up, in particular, the need for additional knowledge of boundary shape and curvature. In all such applications the condition of constant pressure along the jet boundary must be a permissible assumption in order to use the characteristics of the jet exhausting into still air. Perhaps the most direct application is in assessing the deflections of the external stream caused by a propulsive jet exhausting from an aircraft flying at low or moderate subsonic speeds as illustrated in figure 2(a). Another application is in the performance of ejectors when the interaction between the primary jet and the subsonic secondary air flow may be assumed to take place at or near constant pressure (fig. 2(b)). A third probable application is in the prediction of the pressure on the base annulus separating an exhausting jet from an external supersonic stream when the ratio of jet exit diameter to base diameter is not very near one (fig. 2(c)). In reference 7 a method based upon the peak-pressure-rise coefficient associated with the separation of a turbulent boundary layer was proposed for predicting the pressure on a two-dimensional base separating supersonic streams having different Mach numbers and pressures. Reference 8, which includes a detailed description of this method, presents results for a two-dimensional base that show this prediction to be satisfactory. For the base annulus, the two-dimensional approach would be expected to be satisfactory when the ratio of the jet exit diameter to the base diameter approaches one since the curvatures of the free boundaries involved are essentially eliminated. This is illustrated in figure 3 which presents the two-dimensional prediction and three of the experimental curves from reference 9. The two-dimensional approach can obviously not be applied to thick base annuli such as illustrated in figure 2(c) without a knowledge of the curvature of the boundaries, the most important of which is the curvature of the jet boundary. These aspects of boundary curvature have been covered in more detail in reference 9.

Besides the interest in boundary curvature, there is also interest in the effects of various parameters upon jet structure. Both combustion problems and problems dealing with jet noise and screech have been shown to be associated with jet structure, in particular with the existence and location of shocks within the free jet. A recent conference on jet noise (ref. 10) led to the conclusion that theories of jet noise cannot make much further headway without a better knowledge of jet structure.

[redacted]

This part of the paper will present the results of theoretical and experimental studies of jets exhausting into still air and will cover the effects of jet Mach number, nozzle divergence angle, and jet pressure ratio upon such characteristics as jet structure, wavelength, and shape and curvature of the jet boundary. Some studies of the effects of the ratio of specific heats of the jet will be included as will be observations pertaining to noise.

APPARATUS AND TESTS

Models.- Twenty-one steel nozzles of identical external geometry were constructed for these tests. A sketch of a typical divergent nozzle installed in the air supply conduit is shown in figure 4. The throat of each nozzle was rounded and smoothly faired, and the interior surface was polished from the start of the convergence to the exit. Sixteen nozzles of the conically divergent type were designed with exit (i.e., divergence) angles θ_N of 5°, 10°, 15°, and 20° for each of four exit Mach numbers M_j of 1.50, 2.00, 2.50, and 3.00. Four nozzles were designed for these same Mach numbers to give $\theta_N = 0^\circ$ at the exit. These four nozzles had contoured profiles that gave essentially isentropic flow throughout and parallel flow at the jet exit. One convergent nozzle was designed for an exit Mach number of 1 ($\theta_N = 0^\circ$). All nozzles were designed with $\gamma_j = 1.400$.

Tests.- The experimental study was confined to schlieren observations. Insofar as possible the tests were conducted with the mixing-zone apparatus (see ref. 8) of the Langley 9-Inch Supersonic Tunnel Section in order to take advantage of its double-image schlieren apparatus which permits both vertical and horizontal density gradients to be recorded separately on a single negative for one spark of the source light. In these tests the nozzles exhausted to atmospheric pressure. Because the tests employed the dry air supply system of the Langley 9-inch supersonic tunnel which is limited to a maximum storage pressure of 500 lb/sq in., supplementary tests for the higher jet Mach numbers and jet pressure ratios were made in the Langley 9-inch supersonic tunnel in which the tunnel was employed as a vacuum box. The schlieren system of the tunnel was used in these tests; consequently, the observations were confined to vertical density gradients. For the sonic nozzle only, tests were also made with the tunnel schlieren system but with the nozzle exhausting to atmospheric pressure.

For each nozzle several runs were made during which the behavior of the jet with varying pressure was observed but not photographed. Based on these runs the intervals were selected for schlieren photography. The stagnation pressure of the jet was measured by means of a mercury manometer

or precision high pressure gages. Calibration tests with the sonic nozzle indicated that the pressure tap shown in figure 4 gave an accurate measurement of stagnation pressure.

Since numerous tests have shown that the pressures in conically divergent nozzles of the type employed in these tests follow closely the theoretical expansion (see ref. 11, for example) and because the nozzles were machined within 0.001 inch of the specified dimensions, no Mach number calibration was made of the conically divergent nozzles. Calibrations were made, however, of the four supersonic nozzles having $\theta_N = 0^\circ$. With the exception of the $M_j = 2.50$ nozzle which was within ± 0.01 of its design value, these nozzles had a maximum Mach number deviation of about -0.04 from their design value. This deviation was felt to be minor for the purpose of these tests, and the static pressure on the nozzle wall just prior to exit p_j was calculated for all nozzles from the measured total pressure and the design Mach number.

Results and Discussion

Schlieren photographs.- Since it was impractical to include all photographs taken in this investigation, only a few representative ones are presented. Figure 5 presents an illustrative sequence of double-image schlieren photographs wherein for a given value of $\frac{p_j}{p_\infty}$ the upper left-hand image accentuates the vertical gradients (horizontal knife edge) and the other image accentuates the horizontal gradients (vertical knife edge).

Jet structure.- The gaseous jet exhausting supersonically into still air has been known to exhibit a periodic or chain-like structure at least as early as the observations of Rayleigh in 1879 (see ref. 6). Rayleigh and many others (see part VI, ref. 1, for example) have offered explanations for and elaborated upon the manner in which the expansion and compression waves within a free jet form the periodic patterns at low jet pressure ratios and the not so periodic patterns at high jet pressure ratios. References 12 to 19 include both theoretical and experimentally deduced explanations for the occurrence of shock waves in jets and their change and growth with varying jet pressure ratio. Reference 15 includes excellent photographs by the Riemann mirror method of the variation in the structure and shock pattern with jet pressure ratio for an axisymmetric jet exhausting sonically. Reference 16 includes characteristics calculations for a two-dimensional jet $\left(M_j = 1.50,\ \theta_N = 0^\circ\right)$ that show clearly how the coalescence of the characteristic lines creates shock waves within the jet; with increasing jet pressure ratio, these shocks are shown to grow in strength and extent from a faintly discernible

compression, to intersecting shocks, to strong shocks of large curvature requiring a Mach reflection. Other calculations of the shock formation that deal in particular with point of origin, factors favoring shock formation, and focusing effects for two-dimensional and axisymmetric jets are given in references 17 to 19. For axisymmetric jets the same general phenomena occur as in two-dimensional jets but at lower jet pressure ratios. In order to distinguish the circular, dish-shaped, normal shocks that occur in axisymmetric jets from the analogous normal shocks associated with the Mach reflection in two-dimensional jets, the former are, in jet studies, often referred to as Riemann waves (rigorously, the term is applicable to all normal shocks). This term will be adopted herein.

Qualitatively, the present studies showed no significant deviations in jet structure or shock patterns that would not be expected ($\theta_N = 0^\circ$). Although a few previous studies include photographs which show that the shock phenomenon begins with a Riemann wave pattern, decays to an intersecting shock pattern, thence to no shocks, and then begins the well-known reverse variation, one is likely to gain the incorrect impression from most past studies that the initial variation begins with the shock-free condition. The decay in shock strength is confined to a narrow range of jet pressure ratios immediately after starting and was observed to take place at all Mach numbers of these tests. Once the Riemann wave reappears the general shock pattern does not change with increasing jet pressure ratio. These variations will become more apparent in the quantitative results to be presented in the sections that follow.

Primary wavelength.- Since the observations of Rayleigh mentioned in the previous section, several theories have been advanced for the prediction of the primary wavelength or the length of the first periodic segment of the free jet and the secondary wavelength or the length of succeeding periodic segments, which are known to differ from the primary, particularly at the higher jet pressure ratios. The predominant interest has been centered upon primary wavelength. An excellent summary of jet wavelength theories in existence prior to 1949 is given in reference 6. Since that time Wada (ref. 12), Pack (ref. 13), and others have added to earlier contributions or advanced new theories. Little has been added to the old and very limited experimental information, most of which is confined to sonic exits and jet pressure ratios of the order of 3 or less.

Figure 6 presents a double-image schlieren photograph in which the primary wavelength w is designated. Figure 7 presents the nondimensional primary wavelength $\frac{w}{d_j}$ as a function of jet pressure ratio $\frac{p_j}{p_\infty}$ for all values of M_j and θ_N of these tests. It will be noted that there are more experimental data for $M_j = 1$ than for the other Mach numbers at a given value of θ_N. The data for $M_j = 1$ represent values measured

from shadowgraphs, schlierens, repeat runs, and photographic enlargements of different sizes. Within the accuracy of the measurements there was no apparent difference in the data from these sources. In general, however, the accuracy of all measurements from any source tended to decrease slightly as $\frac{p_j}{p_\infty}$ increased as a result of the decrease in definition caused by the increased turbulence surrounding the jet.

The experimental results show the increasing wavelength with increasing Mach number that is to be expected $\left(\frac{p_j}{p_\infty}$ and θ_N constant$\right)$. In addition, divergence angle θ_N is indicated to be of secondary importance within the range of 0° to 20°. There tends to be a decrease in wavelength with increasing θ_N; the exceptions to this might be attributable to experimental accuracy. From a consideration of the increasing shock losses within the jet (increasing entropy) that occur with increasing θ_N, one might expect increasing θ_N to cause the wavelength to decrease.

Two of the methods which have had some success in predicting the wavelength were used to calculate the upper and lower curves shown in figure 7(a) for $M_j = 1.00$. The method of Pack (ref. 13) has been advanced as being applicable to all Mach numbers. The older method of Hartmann and Lazarus (ref. 14) is proposed for sonic jets only. These methods, as well as all other methods with the possible exception of the original proposal of Prandtl which is known to be in error (see ref. 6, for example), are semiempirical and involve constants determined from experimental results for $\frac{p_j}{p_\infty} < 3$. It is not surprising, therefore, to find that the methods are not satisfactory except at very low jet pressure ratios as indicated in figure 7(a). In fact, the older prediction of Hartmann and Lazarus is rather remarkable in view of the meager experimental data available at that time. Because of the inadequacy at $M_j = 1$, no comparison has been made between the method of Pack and the present results for higher Mach numbers; further, the assumption of the method that $\frac{w}{d_j}$ is independent of M_j and a function only of the ratio of jet stagnation pressure to the ambient pressure can be shown from these results to be insufficient.

On the basis of these experimental data an attempt was made to derive an empirical relation for the variation of $\frac{w}{d_j}$ with $\frac{p_j}{p_\infty}$ that would apply to $\theta_N = 0^\circ$ and varying M_j. For axisymmetric jets the only

[redacted]

inviscid solution to $\frac{w}{d_j}$ not requiring the combined treatment of a characteristics net and the shock equations is for $\theta_N = 0^\circ$ and $\frac{p_j}{p_\infty} = 1$. For this condition only, the solution is the same for two-dimensional and axisymmetric jets and is $\frac{w}{d_j} = \beta_j$, where $\beta_j = \sqrt{M_j^2 - 1}$. Outside of satisfying this condition and the equally simple requirement that the value of $\frac{p_j}{p_\infty}$ for $\frac{w}{d_j} = 0$ must lie to the right of the theoretical value of $\frac{p_j}{p_\infty}$ for starting (denoted by arrows in the figures and is equal to one at $M_j = 1$), the empirical solutions were derived so as to fit best the results for $M_j = 1$ in preference to the other Mach numbers. Consequently, the abrupt change in the variation of $\frac{w}{d_j}$ with $\frac{p_j}{p_\infty}$ that accompanies the reappearance of the Riemann wave within the jet occurs at about $\frac{p_j}{p_\infty} = 2$. This well-known feature has been treated for sonic jets by many authors (refs. 12 to 16, for example).

The two empirical relations thus derived are:

for $\frac{p_j}{p_\infty} \lessapprox 2$

$$\frac{w}{d_j} = 1.55\sqrt{M_j^2\left(\frac{p_j}{p_\infty}\right) - 1} - 0.55\beta_j \tag{1}$$

and for $\frac{p_j}{p_\infty} \gtrapprox 2$

$$\frac{w}{d_j} = 1.52\left(\frac{p_j}{p_\infty}\right)^{.437} + 1.55\left(\sqrt{2M_j^2 - 1} - 1\right) - 0.55\beta_j + .5\left[\frac{1}{1.55}\sqrt{\left(\frac{p_j}{p_\infty} - 2\right)\beta_j} - 1\right] \tag{2}$$

The curves given by these equations are shown by the solid lines in figures 7(a) to 7(e). It is interesting to note that the theoretical inviscid value of β_j for $\frac{p_j}{p_\infty} = 1$ is in close agreement with the

[redacted]

experimental results for all values of M_j. While equations (1) and (2) generally give a fair prediction of the experimental results, there is a noticeable tendency at the higher jet pressure ratios to overpredict the wavelength at low Mach numbers and to underpredict at the higher Mach numbers. An inherent shortcoming of these equations lies in the assumption that the abrupt change in the variation of wavelength with jet pressure ratio occurs at $\frac{p_j}{p_\infty} = 2$, regardless of the value of M_j. In the following section this region of abrupt change will be shown to vary with M_j.

Existence, location, and diameter of Riemann wave.- Figure 8 presents the nondimensional distance from the plane of the jet exit, measured along the jet axis, to the focal point of the intersecting shock pattern or to the Riemann wave, as the case may be. This distance $\frac{l}{d_j}$ increases with increasing $\frac{p_j}{p_\infty}$ and M_j as would be expected. There is a tendency for increasing θ_N to decrease $\frac{l}{d_j}$.

Figure 9 presents the nondimensional diameter of the Riemann wave $\frac{S}{d_j}$. As $\frac{p_j}{p_\infty}$ increases from the condition of a Riemann wave at the jet exit $\left(\text{starting value of } \frac{p_j}{p_\infty} \text{ is indicated in the figures}\right)$, the Riemann wave first decreases in diameter and for the lower values of θ_N gives way to an intersecting shock pattern $\left(\frac{S}{d_j} = 0\right)$. With further increases in $\frac{p_j}{p_\infty}$ the Riemann wave increases in diameter, or reappears if a condition of $\frac{S}{d_j} = 0$ had been reached, and continues to increase.

From the curves of figure 9, the range of M_j and $\frac{p_j}{p_\infty}$ for which no Riemann wave occurs can be found for a given value of θ_N. The results are shown in figure 10 for $\theta_N = 0^\circ$, 5°, and 10°; there were insufficient data to determine the boundaries of the regions for $\theta_N = 15^\circ$ and 20° but it is evident from figure 9 that for these values of θ_N the Riemann wave is always present for $M_j = 2$ to 3. From figure 10, the effect of increasing θ_N is to reduce significantly the range in which no Riemann wave occurs. The true effect of M_j is not clear in the lower range of M_j; but, for the higher range of M_j, increasing M_j increases the range of $\frac{p_j}{p_\infty}$ in which no Riemann wave occurs. There is little doubt

that an intersecting shock pattern is restricted to low jet pressure ratios. The dashed line to the left of the left-hand boundary for $\theta_N = 0^\circ$ represents the theoretical starting condition (the Riemann wave at the jet exit) and is in fair agreement with the trend of the experimentally determined boundary.

The abrupt change in the variation of wavelength with jet pressure ratio that is associated with the reappearance of the Riemann wave mentioned in the previous section was assumed to take place at $\frac{p_j}{p_\infty} \approx 2$ for $M_j = 1 \left(\theta_N = 0^\circ\right)$ in developing equations (1) and (2). Although figure 10 shows this to be a fair assumption for $M_j = 1$, it also indicates indirectly that the region of abrupt change varies with M_j.

Initial inclination of jet boundary.- When a jet exhausts from a nozzle into still air, it will undergo a two-dimensional expansion or compression exactly at the nozzle lip dependent only upon whether or not the jet pressure ratio $\frac{p_j}{p_\infty}$ is greater or less than one, respectively. The degree of the expansion (or compression) is a function of $\frac{p_j}{p_\infty}$, M_j, and γ_j. For the case of predominant interest, $\frac{p_j}{p_\infty} > 1$, it is instructive to consider the magnitude of the expansion or the initial inclination of the jet boundary that may occur. The calculated initial inclinations for $\theta_N = 0^\circ$ and $\gamma_j = 1.4$ are presented in figure 11. For $\theta_N \neq 0^\circ$, the value of θ_N is added to the value given by the curves. In spite of the large power sources now available and of such rocket-powered units as are now under development $\left(1 \times 10^6 \text{ pounds of thrust}\right)$, the curves of figure 11 indicate that the likelihood of encountering initial inclinations of 90° are remote, even for $M_j = 1$. However, if extreme pressure ratios should be encountered, large initial inclinations would be realized as is indicated by the schlieren photograph in figure 12.

In view of the number of current applications of sonic exits, the variation of δ_j with $\frac{p_j}{p_\infty}$ for $M_j = 1.00$ is presented to enlarged scale in figure 13 for $\gamma_j = 1.115$, 1.400, and 1.667. The upper and lower values of γ_j represent the probable limits encountered in both practical and experimental applications. The effect of decreasing γ_j is to increase δ_j, and this effect increases with $\frac{p_j}{p_\infty}$.

Calculations by method of characteristics.- Several calculations were made by the method of characteristics to obtain the shape of the jet boundary and to observe the formation of the jet structure. The salient features of these calculations are given in appendix A. The characteristic nets are shown in figure 14. Points on the boundary in the region of "foldback" have been circled for clarity.

Figure 14(a) presents the nets for $\frac{p_j}{p_\infty} = 2$, 10, and 20 for $M_j = 1.01$ $\left(\theta_N = 0^\circ, \gamma_j = 1.400\right)$ or essentially a sonic jet. The errors in the nets for $M_j = 1.01$ are discussed in appendix A and, by mere observation, are obviously not negligible in the vicinity of the jet axis. The boundary shape and the general coalescence of the characteristics, also discussed in appendix A, are nevertheless sufficiently accurate to be of value. At $\frac{p_j}{p_\infty} = 2$, there is no indicated presence of a shock within the jet, but if the calculations were carried further, an intersection of like characteristics would probably be realized before the axis is crossed. At $\frac{p_j}{p_\infty} = 10$ and 20, the manner in which the intersection of like characteristics defines the presence of a shock within the jet is clearly illustrated.

Figure 14(b) presents the nets for $M_j = 1.50$ to 3.00 $\left(\theta_N = 0^\circ, \gamma_j = 1.400\right)$ at $\frac{p_j}{p_\infty} = 2$. No shocks are indicated to be present within the jets, but again, the tendency toward intersection of like characteristics would suggest that shocks might appear for all values of M_j before the axis is reached if the calculations were continued.

Figures 14(c) to 14(f) present the nets for $M_j = 1.50$ to 3.00 $\left(\theta_N = 0^\circ, \gamma_j = 1.400\right)$ at $\frac{p_j}{p_\infty} = 10$ and 20. All nets indicate that shocks have formed within the jets.

Figure 14(g) presents nets for $M_j = 2.00$ and $\frac{p_j}{p_\infty} = 1$ to show the effects of nozzle divergence angle θ_N for $\gamma_j = 1.400$, and to show the effects of γ_j for $\theta_N = 10^\circ$. The indicated effect of increasing θ_N is to promote the formation of shocks within the jet. The effect of increasing γ_j from 1.200 to 1.400 to 1.667 is also to favor the formation of shocks within the jet. This effect of γ_j is somewhat understandable from consideration of the effect that γ has in simple two-dimensional

flow upon the maximum turning of the flow δ_{max} for an attached shock. This effect, as well as the effect upon the inclination ϵ_{max} of the associated shock is shown in figure 15. Since at Mach numbers other than one the value of δ_{max} decreases noticeably with increasing γ, it is logical to expect that at high γ compressions of the same family introduced in a flow will, for a given amount of turning, result in an earlier appearance of a shock brought about by the coalescence of these compressions than might occur at lower values of γ.

Although the effect of M_j and $\frac{p_j}{p_\infty}$ $\left(\theta_N = 0^\circ, \quad \gamma_j = 1.400\right)$ upon the shape of the boundary may be observed directly from the nets, this effect is perhaps better illustrated in figure 16 which reproduces these boundaries and compares them directly. Figure 17 shows the effect of M_j and $\frac{p_j}{p_\infty}$ upon the maximum height $\left(\frac{y}{r_j}\right)_{max}$ reached by the boundary and upon its location as estimated by replacing the straight line segments with a smoothly faired curve through the calculated boundary points in the vicinity of $\left(\frac{y}{r_j}\right)_{max}$, at the same time being guided by the sign and value of θ for the last two points on the boundary. The values for $M_j = 2.50$ and $\frac{p_j}{p_\infty} = 20$ do not agree closely with the trend established by the other boundaries; since there is apparently some error in the calculations of this net, the data for this condition were not used in preparing figure 17. The curves of figure 17(a) appear to indicate that beyond $M_j \approx 3$ the increase of $\left(\frac{y}{r_j}\right)_{max}$ with M_j will be small at all values of $\frac{p_j}{p_\infty}$. The theoretical curve for $\frac{p_j}{p_\infty} = 1$ is obviously a straight line for which $\left(\frac{y}{r_j}\right)_{max}$ is always 1. The curves of figure 17(b) indicate that with increasing M_j the location of $\left(\frac{y}{r_j}\right)_{max}$ continues to increase at all values of $\frac{p_j}{p_\infty}$. The theoretical curve for $\frac{p_j}{p_\infty} \to 1$ is half the wavelength and, therefore, equal to $\frac{\beta_j}{2}$.

Figure 18 affords a direct comparison of the boundary shapes for varying θ_N. The increase in $\left(\frac{y}{r_j}\right)_{max}$ with θ_N is observed to be almost linear within this range of θ_N (0° to 20°). Figure 19 presents a comparison of the boundaries for a particular condition of varying γ_j. The

ordinate scale has been enlarged in this figure for clarity, consequently the local slopes of the boundaries are considerably exaggerated as can be seen by referring to figure 18 $\left(\theta_N = 10^\circ\right)$. From figure 19, the effect of increasing γ_j is very small and amounts essentially to a slight increase in $\frac{y}{r_j}$ as $\frac{x}{r_j}$ increases. As $\frac{x}{r_j} \rightarrow 0$, it is obvious that the effect of γ_j will vanish. Emphasis should be placed on the fact that the particular set of initial conditions used in this study of the effects of γ_j were selected to explore what might be considered a sort of "minimum effect" of γ_j on the boundary: namely, $\frac{p_j}{p_\infty} = 1$ and $M_j = 2$. (In the vicinity of $M = 2$, the ratio of static to stagnation pressure $\frac{p}{p_o}$ is relatively insensitive to γ.) Consequently, the effects of γ_j on the boundary for other initial conditions, particularly for $\frac{p_j}{p_\infty} > 1$, may be considerably different from those shown here. Other examples of calculated jet boundaries involving varying γ_j may be seen in figure 20 which reproduce calculations by Johannesen (ref. 5) for a conically divergent nozzle $\left(\theta_N = 4^\circ\right)$. The effect of γ_j is not shown directly because of the varying M_j; but from consideration of the effects of M_j on jet size and the effects of γ_j upon δ_j which have been shown previously, these boundaries show that for $\frac{p_j}{p_\infty} > 1$ the effect of decreasing γ_j is to increase jet size.

The following section on boundary curvature will show indirectly that the theoretical nonviscous boundaries calculated by the method of characteristics agree satisfactorily with the observed experimental boundaries in the schlieren photographs. This favorable agreement has been noted previously at low jet pressure ratios (3 or less), for example, in reference 20. The fact that this agreement extends to high jet pressure ratios is particularly encouraging from the viewpoint of continuous calculation by machine in that the use of foldback as employed herein permits continuous calculation off the axis. No schlieren photograph was available for $\frac{p_j}{p_\infty} = 20$, the highest jet pressure ratio of these calculations, however a comparison between the calculated results at $\frac{p_j}{p_\infty} = 20$ and the experimental results at $\frac{p_j}{p_\infty} = 21.9$ $\left(M_j = 1.5,\ \theta_N = 0^\circ,\ \gamma_j = 1.400\right)$ presented in figure 21 shows sufficient agreement to indicate that the procedure is satisfactory for predicting both boundary and shock. The difference between the experimental and predicted shock and boundary is in the direction to be accounted for by the difference between the

[redacted]

theoretical and experimental values of $\frac{p_j}{p_\infty}$. In addition, mixing tends to diffuse the experimental boundary prior to reaching the theoretically predicted maximum diameter of the jet.

Average and initial curvature of jet boundary.- An examination of the schlieren photographs of these tests indicated that the shape of the portion of the jet boundary from its start to the vicinity of the maximum diameter of the jet (within the primary wavelength) could be fairly well approximated by a circular arc. The radius of this circular arc will, for convenience, be called the average radius of curvature ρ of the jet boundary and, as shown in the sketch in figure 22(a), is laid off along the normal to the free jet boundary at the exit. Figures 22 and 23 present the results of the experimental measurements in nondimensional form $\frac{\rho}{d_j}$ as a function of $\frac{p_j}{p_\infty}$ to show the effects of M_j and θ_N, respectively. Random examples of the applicability of these experimental curves are given in figure 24 which presents the circular-arc boundary and the normal to the free boundary at exit superposed on schlieren photographs.

An assessment was also made of the similarity of the boundaries given by the characteristics calculations to a circular-arc boundary passing through $\left(\frac{y}{r_j}\right)_{max}$ given by the characteristic solution and having its radius laid off along the normal to the free jet boundary at exit. The circular-arc boundary thus defined was in all cases found to be a good approximation of the characteristic boundary; a typical example of this may be seen in figure 25. The values of $\frac{\rho}{d_j}$ obtained from the characteristic solutions in this manner are designated by the symbols in figures 22(a) and 23(b). These values show surprisingly close agreement with the experimental curves even at low jet pressure ratios where the experimental results would be expected to be less accurate. For $M_j = 2.50$ and $\frac{p_j}{p_\infty} = 20$ (fig. 22(a)) a corrected and an uncorrected value are shown; the suspected error in the characteristic solution for these conditions was mentioned earlier. The corrected value for $\left(\frac{y}{r_j}\right)_{max}$ was determined from the faired curve of figure 17(a).

In reference 19, Johannesen and Meyer have obtained a solution for the initial curvature of the axially symmetric free jet boundary (i.e., the curvature at $x = 0$). This solution and its method of application are summarized in appendix B. The nondimensional initial radius of curvature $\frac{\rho_o}{d_j}$ given by the Johannesen-Meyer solution has been calculated for the same jet conditions for which characteristic nets were calculated ($\gamma_j = 1.400$ only). The results are shown in figure 26. In reference 5,

[redacted]

the value of $\frac{\rho_o}{d_j}$ obtained from the Johannesen-Meyer solution was shown to be in close agreement with the value of $\frac{\rho_o}{d_j}$ obtained from the polynomial satisfying the first few points on a boundary calculated by the method of characteristics. It is of interest for practical application, however, to obtain an idea of how far along the characteristic boundary the circular-arc boundary given by $\frac{\rho_o}{d_j}$ will continue to hold good. Comparisons showed that, except at values of $\frac{p_j}{p_\infty} < 2$, the boundary given by $\frac{\rho_o}{d_j}$ is applicable only to regions in close proximity to the exit as illustrated in figure 25. The effects of M_j, $\frac{p_j}{p_\infty}$, and θ_N upon the extent of applicability of $\frac{\rho_o}{d_j}$ are indicated indirectly in figure 27 where the ratio $\frac{\rho}{\rho_o}$ is presented. The values of ρ in this ratio are those corresponding to the circular-arc boundary through $\left(\frac{y}{r_j}\right)_{max}$. For $\theta_N > 0^o$ the extent of applicability is severely restricted even at $\frac{p_j}{p_\infty} = 1$.

From the above results and the fitting of polynomials to the characteristic points on the boundary as in reference 5, the exact boundary is seen to decrease in curvature in proceeding outward along the boundary from the exit toward the maximum diameter of the jet.

Observations on jet breakdown and jet noise.- Within the range of observation of the schlieren photographs, the jet structure for all Mach numbers and divergence angles of these tests deflected from the axis of the jet in an alternate fashion as the jet flow proceeded downstream. Example of this phenomenon for $M_j = 1.00$ may be seen in figure 28. Examination of the present results indicates that the jet breaks down into a vortex pattern closely resembling a vortex street and thereafter into a region of wide turbulent diffusion. This alternate deflection of the jet structure has been noted by Powell in reference 21 in which the relation between the degeneration of the jet, jet structure, and sound generation are discussed.

The type of sound wave that may be observed to be generated by the jet was found to be dependent to some degree on the sensitivity setting of the optical system. For example, the strong, lower frequency sound waves which Powell has described as having their effective source in the region of disintegration of the jet structure, and which are emitted in the upstream direction in an alternate manner according to the degeneration of jet structure, may be seen in the photographs in figure 29 but not in

[redacted]

the photographs in figure 28 for which the schlieren system had a less sensitive setting. Examination of photographs taken at higher sensitivity setting showed that both the structure of the jet and the sound waves moving upstream tend to become masked by turbulence surrounding the jet and, to some extent, by sound waves having their apparent source in the vicinity of the jet exit and at the initial appearance of turbulence on the free jet boundary not far from the exit. These observations seem to indicate that the apparent discrepancies that exist in some previous studies of sound waves associated with jets may be due in part to the different sensitivities of the optical systems employed. The degeneration of the jet is, of course, a highly unstable phenomenon and the apparent source of the sound waves associated with degeneration of jet structure varies accordingly.

At jet pressure ratios slightly greater than that for the reappearance of the Riemann wave, the sound waves associated with the degeneration of jet structure become less prominent, and the sound waves associated with smaller scale turbulence and the initial appearance of turbulence on the jet boundary are observed to predominate. Examples of this are given in figure 30. The photographs of figure 30 also show that as $\frac{p_j}{p_\infty}$ increases, the more intense sound waves coming from the vicinity of the jet exit tend to be more directional and to lie roughly in a band inclined some 30° to 45° with respect to the jet axis in the downstream direction. This directional trend is in agreement with sound measurements from several investigations. (See refs. 10 and 22, for example.)

From the concept of eddy convection velocity as advanced by Lighthill (ref. 23), one would expect the sound waves in the ambient air to change in shape as M_j increases. This concept has its basis in the idea that small vortices or eddies at the jet boundary are convected downstream at some velocity and, as Lighthill states, "not in the sense that eddies are convected downstream with this velocity unchanged, but that they alter slowest when viewed by an observer moving with this velocity." If this convection velocity is supersonic with respect to the ambient air, oblique compression waves must be expected to arise from the jet boundary and to be inclined in the manner of a nose shock or bow wave common to an object in supersonic flight. Consequently, the shape of the sound (or compression) waves emitted in a downstream direction may be expected to change from spherical (subsonic eddy convection velocity) to conical (supersonic eddy convection velocity), or as observed in the schlieren photographs, from circular to straight oblique, as the jet velocity at the jet boundary increases. The present tests indicated that the shape of the sound waves was a function of all the variables: M_j, $\frac{p_j}{p_\infty}$, and θ_N. In general, however, with increasing jet velocity at the boundary the circular sound waves did tend to give

way to oblique compression waves. An example of the latter may be seen in figure 31. In figure 21(a) of reference 8, similar waves may be observed for a two-dimensional jet $\left(M_j = 3.36\right)$.

From the work of Powell, Lighthill, and others the sound intensity and source of generation, and in fact nearly all sound phenomena associated with jets, are known to be primarily dependent upon jet structure. The significant effects that M_j, $\frac{p_j}{p_\infty}$, and θ_N may have upon the structure have been shown in the previous sections for a particular value of γ_j. The effects of γ_j were touched upon briefly. In the generation of jet noise, the effects of γ_j would appear to be of major importance. For example, light gases such as helium are sometimes employed in jet studies to obtain high sonic velocities comparable to those of a hot jet. In so doing, the proper order of magnitude of the eddy convection velocity may be duplicated and this source of sound and compression wave generation is essentially reproduced. However, the shock structure within the jet will be considerably different because of the large differences in γ_j; consequently, one of the predominant sources of sound - that of passage of turbulence through shock patterns - will not be properly duplicated. Conversely, duplication of γ_j satisfies the shock structure within the jet, but eddy convection (and turbulence) at the boundary may or may not be duplicated, although this is felt to be less important. Another factor to consider is that a jet having a high sonic velocity may exhaust through a convergent nozzle at $\frac{p_j}{p_\infty} < 1$ and create supersonic eddy convection velocities (with respect to the ambient air), whereas the jet itself is obviously subsonic with respect to itself and therefore free of shocks.

From the previous discussion the importance of considering separately the effects of γ_j, temperature of the jet, and sonic velocity of the jet in the problem of jet noise becomes obvious. It follows that the general observations made from the present tests will have limited applicability. While investigations of jet noise with small models are known to be subject to scale effects, these effects are essentially concerned with turbulence and have no significant effect upon jet structure.

II. JETS EXHAUSTING INTO SUPERSONIC STREAMS

Introduction

Probably the predominant interest in jets exhausting into supersonic streams is in the aerodynamic interference they may create. Numerous investigations have been made and much effort is presently being devoted to the study of jet interference upon surfaces in close proximity of the jet exit, such as the base annulus, boattail surface, tail surfaces, and the like. Relatively little has been done to explore the jet interference on surfaces considerably downstream of the exit or far removed from the jet axis. A recent experimental study in this direction is given in reference 24.

Consider an aircraft of the type illustrated in figure 32 in which only that portion of the flow field created by jet operation has been included. Here many variables complicate the problem, but there is no doubt that the rear of the fuselage as well as the tail surfaces may be subjected to significant interference pressure fields. These interference fields would begin approximately at the intersection of the exit shock and fuselage and extend rearward. For a given aircraft configuration the inclination of this exit shock would, excluding viscous effects which are usually minor in this regard, be determined by the combined action of the free-stream variables and of all the influencing variables common to a jet exhausting into still air. For the general configuration, the importance of geometry and the relation of the aircraft components to the interference problem is readily apparent. The interference pressure fields downstream of the exit shock are determined by boundary curvature, jet structure and the rate of decay of jet structure, the type of mixing zone (subsonic or supersonic), and viscous mixing at the jet boundary. At the present time there is a noticeable lack of information applicable to interference problems of this type.

This part of the paper will present primarily theoretical curves of the type that may be useful in evaluating jet interference effects for varying jet Mach number, free-stream Mach number, ratio of specific heats of the jet, and jet pressure ratio. These calculations will touch upon one phase of the base pressure problem (effects of γ_j), the initial slope of the jet boundary, the inclination of the exit shock, the jet structure and associated pressure fields, and some results of experimental observations.

Tests

In the course of this portion of the study a minor experimental investigation was conducted in the Langley 9-inch supersonic tunnel to

[redacted]

obtain schlieren photographs of the behavior of the jets exhausting into supersonic streams over a wide field of observation as compared to the base diameter. A description of the Langley 9-inch supersonic tunnel is given in reference 25. The model construction, jet operation, and pressure measuring equipment were essentially the same as employed in the investigation of reference 25. A sketch of the model is shown in figure 33. Tests were conducted at free-stream Mach numbers of 1.62, 1.94, and 2.41 and over a wide range of jet pressure ratios. Two jet nozzles were employed, one having a sonic exit $(\theta_N = 0^\circ)$ and the other having a design area ratio for a Mach number of 2.50 with $\theta_N = 10^\circ$. The ratio of jet to base diameter was 0.75 for both nozzles.

Results and Discussion

The theoretical calculations included in the sections to follow do not form a complete coverage of what might be considered the current range of interest. The number of parameters involved and their possible combinations preclude such consideration herein. The calculations are intended to be illustrative examples, and the conclusions drawn from them are subject to these limitations.

Variation in basic flow parameters with γ.- Inasmuch as the ratio of specific heats γ will be one of the prime variables considered, a review of the not too well-known effects of γ upon the ratio of static to stagnation pressure $\frac{p}{p_o}$ and upon the Prandtl-Meyer turning angle from sonic velocity ν appears worthwhile. Figure 34 presents the variation of ν with M for several values of γ and shows the decrease in ν that accompanies an increase in γ at constant M. Figure 35 presents the variation of $\frac{p}{p_o}$ with M for the same values of γ and shows that at $M \approx 2.25$, γ has a negligible effect on $\frac{p}{p_o}$. Below $M \approx 2.25$ an increase in γ decreases $\frac{p}{p_o}$, whereas the reverse is true above $M \approx 2.25$.

Effects of γ_j upon jet interference on base pressure.- There is a particular interest at present in determining to what extent cold air jets, or unheated gas jets having a value of γ_j simulating hot jets, may be used in experimental studies. In reference 9, the effects of many of the influencing variables associated with jet interference on boattail and base pressures are summarized, and a procedure is presented for correcting the base-pressure data for one value of γ_j to other

[redacted]

values of γ_j. This procedure assumes that jet total pressures that produce the same base pressure for various values of γ_j and any given nozzle-afterbody combination are those which yield the same value of δ_j. Alternatively stated, the procedure is one for correcting the jet pressure ratio for fixed known values of $\frac{p_B}{p_\infty}$ and δ_j. From the comparisons given in reference 9 for $M_j = 1$ (18- by 18-inch tunnel data) and for $M_j = 2.09$ (8- by 6-foot tunnel data) and from applications to other data for $M_j = 1$, this procedure appears suitable for obtaining, at least, a first-order approximation of the effects of γ_j upon the base pressure and boattail pressures.

Figure 36 presents curves obtained directly from the calculations of figures 34 and 35 that may be used in applying the above procedure. In figure 36, the values of $\frac{p}{p_o}$ from figure 35 are designated as $\frac{p_j}{p_{o_j}}$ or $\frac{p_B}{p_{o_j}}$ and the values of ν from figure 34 are designated as ν_j or $\left(\nu_j + \delta_j\right)$. With the value of ν_j corresponding to M_j at the desired γ_j determined and the value of δ_j given, the value of $\left(\nu_j + \delta_j\right)$ at the desired γ_j, that is, the amount of expansion necessary to reach $\frac{p_B}{p_{o_j}}$, is known. The value of $\frac{p_B}{p_{o_j}}$ may thus be read from figure 36 for the desired value of γ_j. Division of the known fixed value of $\frac{p_B}{p_\infty}$ by this value of $\frac{p_B}{p_{o_j}}$ gives the corrected jet total-pressure ratio $\frac{p_{o_j}}{p_\infty}$ which when multiplied by $\frac{p_j}{p_{o_j}}$ corresponding to M_j at the desired value of γ_j gives the corrected jet static-pressure ratio $\frac{p_j}{p_\infty}$. For $M_j = 1$ the dashed lines are ignored and the curves are used directly since ν_j becomes zero. For $M_j > 1$ the value of δ_j must be measured from the base line corresponding to the value of M_j considered (for which $\delta_j = 0^\circ$) such as indicated by the dashed lines. A detailed examination of the curves of figure 36 indicated that at a fixed value of $\frac{p_j}{p_\infty}$ (1 or greater) the base pressure will apparently always increase with decreasing γ_j.

[redacted]

(Emphasis is placed on the fact that the above conclusion is in terms of jet static-pressure ratio which is used throughout in this paper. In terms of jet total-pressure ratio, no such conclusion may be drawn since the reversal in the effect of γ upon $\frac{p}{p_o}$ with varying M (fig. 35) that occurs near $M \approx 2.25$ may or may not reverse the effects of γ_j upon base pressure beyond $M_j \approx 2.25$. Below $M_j \approx 2.25$ the effects of γ_j upon base pressure are apparently the same in terms of either total- or static-pressure ratio.)

The possibility of misuse of the curves of figure 36 in experimental studies bears some note. For $M_j = 1$, the curves have a certain uniqueness in that the nozzle area ratio for $M_j = 1$ is independent of γ_j. For $M_j > 1$ the nozzle area ratio is, of course, a function of γ_j as shown in figure 37, and the use of a scale model of a prototype nozzle in experimental studies employing cold air, for example, results in a different value of M_j from that of the prototype. The correction for γ_j would be incorrect if this different value of M_j were employed to obtain the corrected jet pressure ratio. The preceding statement should not be construed as implying that M_j per se has a significant effect on the variation of base pressure with jet static-pressure ratio; results given in reference 9 and in reference 25, in particular, show that M_j has only small effect on this variation. Of course the nozzle of a model could be designed with the experimental value of γ_j to give the same value of M_j (by varying throat area only) as obtained by the prototype with its value of γ_j.

Initial inclination of jet boundary, constant M_j.- Figures 38(a), (b), and (c) present for $\gamma_j = 1.115$, 1.400, and 1.667, respectively, the effects for a sonic exit ($M_j = 1.00$) of increasing jet pressure ratio $\frac{p_j}{p_\infty}$ upon the initial boundary inclination δ_j at several values of free-stream Mach number M_∞. (These calculations, as well as others to follow, correspond to a base annulus thickness of zero, zero boattailing, and are for $\gamma_\infty = 1.400$ unless otherwise specified.) The curves indicate that for a given value of γ_j the variation of δ_j with $\frac{p_j}{p_\infty}$ experiences small effects from varying M_∞. A comparison of figures 38(a),

(b), and (c) for a constant value of M_∞ shows that for a given jet pressure ratio, decreasing γ_j causes an increase in δ_j. Figures 39(a) (b), and (c) are cross plots of the respective parts of figure 38 and show the variation of $\frac{p_j}{p_\infty}$ with M_∞ for several values of δ_j. From both figures 38 and 39 the effect of increasing M_∞ is seen to be negligible for values of $\frac{p_j}{p_\infty}$ of the order of 2 or less.

A comparison of these calculations (figs. 38 and 39) with those for $M_\infty = 0$ (fig. 13) illustrates the large effect that external supersonic flow has in reducing δ_j for a given jet pressure ratio as a result of the presence of the exit shock. As an example, for $\gamma_j = 1.400$ and $\frac{p_j}{p_\infty} \approx 8$ the value of δ_j is approximately 37.3° for $M_\infty = 0$, whereas for $M_\infty = 3$ the value of δ_j is about 17.1°. It becomes obvious from the outset, therefore, that inclinations of the external flow in the vicinity of the jet boundary caused by jet operation will, for a given value of $\frac{p_j}{p_\infty}$ and γ_j, be considerably less for supersonic external flow as compared to subsonic external flow.

Initial inclination of jet boundary, constant M_∞.- Figure 40 presents for $\gamma_j = 1.115$, 1.300, 1.400, and 1.667 some examples of the effects of M_j upon $\frac{p_j}{p_\infty}$ for several values of δ_j. The data of figure 40(a) are for $M_\infty = 1.30$ while those of figure 40(b) are for $M_\infty = 2.00$. All calculations were made with $\theta_N = 0^\circ$. Examination of the curves indicates that for any value of M_j the effect of decreasing γ_j at constant $\frac{p_j}{p_\infty}$ is to cause an increase in δ_j. Further, the minimum in the curves that occurs between $M_j = 1$ and about 1.5 indicates that for a given value of $\frac{p_j}{p_\infty}$ the effect of increasing M_j is to increase δ_j initially and thereafter to decrease δ_j.

Inclination of the exit shock.- The data of figure 40 may be used to calculate the initial inclination of the exit shock of the type illustrated in figure 32. The results are presented in figure 41(a) and (b) for $M_\infty = 1.30$ and 2.00, respectively. The effects of $\frac{p_j}{p_\infty}$ upon ϵ are shown for $\gamma_j = 1.115$, 1.300, 1.400, and 1.667 at each of several values

of M_j from 1.00 to 4.00. These curves indicate the significant effect that γ_j may have upon the approximate upstream limit (i.e., the exit shock) of the interference pressure field created by a jet as a result of the change in shock inclination. The duplication of γ_j in experimental studies of jet interference upon surfaces as shown in figure 32 would, therefore, appear desireable. This is emphasized by the fact that rocket-powered research aircraft are presently engaging in supersonic flights with conditions of $M_j \approx 2.5$, $M_\infty \approx 2$, and $\frac{p_j}{p_\infty} \approx 30$.

In experimental studies of jet interference, the duplication of γ_j is sometimes not practical or possible. In such instances, curves of the type given in figure 41 may be used to convert the values of $\frac{p_j}{p_\infty}$ corresponding to the experimental value of γ_j to values of $\frac{p_j}{p_\infty}$ for simulated γ_j. For example, consider the case of $M_j = 2.00$, $M_\infty = 2.00$, and an experimental value of $\frac{p_j}{p_\infty} = 20$ for an experimental value of $\gamma_j = 1.667$. A simulation for $\gamma_j = 1.300$ is desired. From figure 41(b) the shock inclination ϵ for the experimental conditions is about 59.4°; the experimental conditions represent, therefore, a value of $\frac{p_j}{p_\infty} \approx 12$ for $\gamma_j = 1.300$. Although this procedure may be used in experimental work to give duplication of the exit shock inclination without duplication of γ_j, it is important to note that the jet structure and, consequently, the interference pressure field downstream of the exit shock is not duplicated. Some aspects of this problem will be covered in the following sections.

Basic considerations of jet structure.- The structure of an axisymmetric supersonic jet bounded by a supersonic stream may be calculated for inviscid flow by the method of characteristics (see refs. 26 and 27), but the complexities involved discourage even machine calculations with the procedures presently available. Of the few calculations which have been made, the most complete example appears to be that of Schäfer (ref. 27). The net for this calculation is reproduced in figure 42. From this calculation the indication is obtained that, theoretically, a supersonic outer stream will permit an intersecting shock pattern to exist within the jet at much higher jet pressure ratios before giving way to a Riemann wave than would be the case for a subsonic outer stream. Previous experimental observations such as presented in reference 28, for example, support this indication.

[redacted]

For a supersonic outer stream, wavelength ceases to be a function of jet properties only and is subject to the additional effects of the outer stream variables. When the mixing boundary between the jet and outer stream is subsonic the jet does tend to exhibit periodic structure however, as shown experimentally in reference 29. So long as the mixing boundary remains subsonic, the shocks which occur within the jet must obviously be reflected at the subsonic boundary and cannot penetrate into the outer stream. Nevertheless, the jet structure and the pressure fields in the outer stream are interrelated because of the pressure balance that must take place at the mixing boundary. When the mixing boundary is supersonic throughout, the shocks which occur within the jet are not reflected upon reaching the mixing boundary but continue through the boundary and into the outer stream and are bent or deflected without discontinuity according to the Mach number distribution and direction of flow in the mixing boundary and outer stream. Examples of shocks passing through the boundary may be seen in references 25 and 29 for jets; an excellent photograph of this phenomenon for two-dimensional flow may be seen in figure 36 of reference 30.

The possibility exists for the case of a supersonic mixing boundary that as the shock from within the jet traverses the mixing boundary, the so-called second-family characteristic or Mach lines having their origins along the portion of the shock within the mixing boundary may diverge, creating an expansion, or may form an envelope thereby creating a weak secondary shock within the jet which has the appearance of a reflected shock. The manner in which this occurs is somewhat analagous to the interaction of incident shocks and the supersonic portions of boundary layers described in reference 31. Examples of this reflection phenomenon for a jet may be seen in reference 25. If a secondary shock (or expansion) occurs, the phenomenon may repeat itself when the secondary shock (or expansion) traverses the mixing boundary and will continue in this fashion until the compressions (or expansions) within the jet are eliminated.

If all initial conditions for which a secondary shock occurs are assumed to remain invariant and the supersonic mixing boundary is pictured as being compressed to zero thickness, the shock from within the jet will have a discontinuity in slope at the point where it crosses the boundary and the secondary shock will have its origin at this point. Thus, the conditions become those amenable to inviscid theoretical treatment, namely, supersonic streams separated by a supersonic interface. A recent two-dimensional study by Kawamura (ref. 32) of the supersonic interface and wave patterns in the two-dimensional supersonic compound jet will be considered in the following section.

Kawamura analysis.- The analysis of Kawamura (ref. 32) is applicable to low jet pressure ratios only, but the results are indicative of what might be expected to occur at much higher jet pressure ratios. In this analysis Kawamura develops expressions for the changes in flow direction

and pressure and establishes the type of secondary or so-called reflected wave and the jet structure on the basis of the parameter $\lambda = (\sin \mu \cos \mu) \frac{1}{\gamma}$. It is shown that if at the supersonic interface the difference between local values of λ for the free jet and the outer stream $\lambda_{j'} - \lambda_{\infty'}$ is positive, a compression wave (or expansion wave) passing from the jet through the supersonic interface and into the outer stream will cause a compression wave (or expansion wave) to be reflected into the jet; that is, the reflected wave is of the same type as the wave which passes through the boundary. If $\lambda_{j'} - \lambda_{\infty'}$ is negative the reflected wave is of opposite type. As the jet structure decays in passing downstream, Kawamura shows that the wave pattern composing this structure is of the same type (compressive or expansive) throughout the jet if $\lambda_{j'} - \lambda_{\infty'}$ is positive and of alternating type if $\lambda_{j'} - \lambda_{\infty'}$ is negative.

The values of the basic Kawamura parameter λ have been computed for $M = 1.00$ to 3.00 and $\gamma = 1.100$ to 1.667. The results are given in figure 43. Values of the difference parameter $\lambda_{j'} - \lambda_{\infty'}$ have also been computed and are presented in figure 44 as a function of $M_{j'}$ for varying γ_j and $M_{\infty'}$. The primes again denote local values at the interface. The values of λ and $\lambda_{j'} - \lambda_{\infty'}$ given by these curves may be used to obtain flow direction and pressures by substitution in the expressions given in reference 32. The curves in figure 44 are of particular significance to the problem of jet interference in that they show the importance of simulation of γ_j in experimental studies which are concerned with the changes in the pressure fields of the outer stream that are caused by the jet. One might expect the indication that the greater the difference between the experimental value of γ_j and the value for true simulation, the greater the error in jet structure and in the interference pressure fields created by the jet. Not so obvious, however, is the indication that such differences in γ_j may result in a type of jet structure and ambient pressure field that is opposite from that for true simulation.

In applying the procedures of Kawamura and in studies of shocks within the jet, a knowledge of the effect of γ upon shock inclination ϵ is helpful. Calculations have been made of the variation in ϵ with δ for $M = 1.50$ to 5.00 and $\gamma = 1.115$ to 1.667. Since, excluding $\gamma = 1.400$, this information is not generally available, it is presented in figure 45.

[redacted]

Conditions for no reflection at supersonic interface.- In reference 31, Barry has shown for the case of two supersonic flows separated by a supersonic interface and having identical values of γ that, if the difference between the Mach numbers of the two flows is small, there will be no reflection at the interface from the passage of a shock through the interface when the average Mach number of the two flows equals $\sqrt{2}$. From the work of Kawamura discussed in the previous section, no reflection would be expected from the passage of compression or expansion waves through a supersonic interface when $\lambda_{j'} - \lambda_{\infty'} = 0$. Figure 46 presents the variation of $M_{\infty'}$ with $M_{j'}$ for no reflection at several values of γ_j as determined from the calculations for figure 44. The 45° line for $\gamma_j = 1.400$ is the trivial solution for $\gamma_j = \gamma_\infty$ and $M_{j'} = M_{\infty'}$. A confirmation of Barry's solution becomes readily apparent at the intersection of the curves for $\gamma_j = 1.400$. Perhaps the most important conclusion to be drawn from figure 46 is that the condition of no reflection is one which may occur quite often in practical applications even from a nonviscous consideration. The inclusion of viscous effects, and therefore a mixing boundary of finite thickness, would tend to weaken a reflection since the origin of the reflections is not confined to a point. Accordingly, reflections within jets having supersonic mixing boundaries would be expected to have a much lesser interference effect upon the pressure fields in the outer stream than the waves which give rise to these reflections, and to eliminate themselves rapidly within the course of a few additional reflections.

Experimental observations.- The schlieren observations of references 8 and 33 demonstrate for a two-dimensional jet with a supersonic mixing boundary the weakness of the reflection associated with the passage of a strong shock from within the jet into the outer stream. Also illustrated is the very rapid elimination of reflections (ref. 33, in particular). In no instance could more than two reflections be detected within the jet, and in most instances only one.

For axisymmetric jets, the schlieren observations of references 25, 28, and 29 never show more than three reflections when a strong shock from within the jet passes through a supersonic boundary into the outer stream. In most instances, there is only one visible reflection and and in some instances, no reflections are visible. The pressure measurements of reference 24 also indicate the rapid elimination of and attenuation in strength of such reflections.

In order to observe the reflections, jet structure, and disturbances introduced into the outer stream at distances considerably farther downstream and away from the jet axis than was possible in the investigations mentioned above, the minor investigation described in the section "Tests"

[redacted]

in this part of the paper was undertaken. From figure 33 and the results of reference 28, some interference upon the jet from the side strut is to be expected; however, this interference is not felt to affect seriously the qualitative results of the tests. Some examples of the schlieren photographs obtained in these tests are shown in figures 47, 48, and 49. In none of the photographs could more than one reflection be detected, after which the jet continued downstream with only small spreading. For a given pressure ratio, the jet for $M_j = 2.50$ did not dissipate so readily in moving downstream as did the jet for $M_j = 1.00$. From these tests, indications are that for jets with supersonic mixing boundaries the reflections associated with the passage of the shock from within the jet into the outer stream may be assumed to have negligible interference effects upon the ambient stream. Downstream of the region where the jet shock passes through the mixing boundary, it appears permissible to assume for interference studies that the jet is cylindrical in shape; this is in agreement with the pressure surveys of reference 28. Insofar as axisymmetric jets are concerned, the main disturbances introduced into the outer stream will, for supersonic mixing boundaries, apparently be the exit shock (or expansion) and the shock from within the jet.

From references 25, 28, and 29, the presence or absence of a Riemann wave within a jet bounded by a supersonic stream is indicated to be a function of the base and afterbody geometry as well as the flow variables of the jet and free stream. In general, however, the Riemann wave occurring at low values of $\frac{p_j}{p_\infty}$ gives way to an intersecting shock pattern at higher values of $\frac{p_j}{p_\infty}$ than for the same jet exhausting into still air. Once the intersecting shock pattern occurs within a jet bounded by a supersonic stream, the present results indicate that it will remain to a value of $\frac{p_j}{p_\infty}$ many times that for which the Riemann wave would reappear in the same jet exhausting into still air; after the Riemann wave reappears, its growth with $\frac{p_j}{p_\infty}$ is much less for the jet bounded by a supersonic stream.

CONCLUDING REMARKS

Some experimental and theoretical studies have been made of axisymmetric free jets exhausting from sonic and supersonic nozzles into still air and into supersonic streams with a view toward current problems associated with propulsive jets and the investigation of these problems. The scope and results of these studies are given below.

[redacted]

Jets Exhausting Into Still Air

For jets exhausting into still air, the primary variables considered were jet Mach number, nozzle divergence angle, jet static-pressure ratio, and, to a lesser extent, the ratio of specific heats of the jet. The effects of most of these variables upon jet structure, primary wavelength, and the shape and curvature of the jet boundary were studied. Observations were also made of features pertaining to jet noise. A summary of the results and the more specific conclusions follow:

1. Divergence angle of the nozzle (0° to 20°) has a small effect upon the primary wavelength of the jet. Existing methods for predicting the wavelength of an axisymmetric jet are inadequate above a jet static-pressure ratio of about 2. Empirical relations are presented which give fair predictions of experimental results for jet Mach numbers from 1 to 3.

2. Curves defining the existence as well as the location and diameter of the Riemann wave are presented. Increasing nozzle divergence angle reduces significantly the range of jet static-pressure ratios in which no Riemann wave occurs. The effect of jet Mach number is not clear in the lower range of jet Mach numbers, but for the higher range of jet Mach numbers an increase in jet Mach number increases the range of jet static-pressure ratios in which no Riemann wave occurs. An intersecting shock pattern is clearly restricted to low jet static-pressure ratios.

3. Within the first wavelength of the jet, calculations by the method of characteristics employing the procedure of foldback will adequately predict both jet boundary shape and shock location within the jet for jet static-pressure ratios at least as high as 20. A tabulated solution is presented for the jet with sonic exit.

4. A circular-arc boundary is a satisfactory prediction, both theoretically and experimentally, of the first portion of the jet boundary from the jet exit to the vicinity of the maximum diameter of the jet. The range of applicability of the Johannesen-Meyer solution for the initial curvature of the boundary is, as the solution implies, restricted to regions in very close proximity to the exit. Values of the integrals in the Johannesen method of characteristics are presented for a broad range of application.

5. For jet static-pressure ratios greater than one, both increasing ratio of specific heats of the jet and increasing jet Mach number reduce the initial inclination of the jet at the exit. For a given jet Mach number and jet static-pressure ratio (>1), decreasing the ratio of specific heats of the jet increases the size of the jet; for a jet static pressure of 1, indications are that the effects upon jet size of a change in the ratio of specific heats of the jet would be negligibly small.

[redacted]

6. Beyond a jet Mach number of about 3 the increase in the theoretical maximum diameter of the jet with increasing jet Mach number will apparently be small; however, the distance from the jet exit to the maximum diameter will continue to increase rapidly with increasing jet Mach number.

7. Observations of the sound waves generated by the jet indicated that the type of sound wave that may be observed is dependent upon the sensitivity of the optical system employed; therein may lie the apparent discrepancies between some of the visual studies of sound waves associated with jets. The present observations tended to confirm in general the hypotheses of Powell and Lighthill regarding sound waves associated with degeneration of jet structure and with eddy convection velocity, respectively.

Jets Exhausting Into Supersonic Streams

For jets exhausting into supersonic streams, an attempt was made to present primarily theoretical curves of the type that may be useful in evaluating certain jet interference effects and in formulating experimental studies. The primary variables considered were jet Mach number, free-stream Mach number, jet static-pressure ratio, and the ratio of specific heats of the jet. A few experimental observations were made. A summary of the types of curves which have been presented and some of the indicated conclusions follow:

1. Curves of the type applicable to the method presented in NACA RM E53H25 for correcting base-pressure data for one value of the ratio of specific heats of the jet to other values are given for a broad range of operation. Apparently the base pressure for a given value of jet static-pressure ratio will always increase with decreasing ratio of specific heats of the jet.

2. At constant jet Mach number, the variation of the initial inclination of the jet boundary with jet static-pressure ratio experiences small effects from varying free-stream Mach number; these effects are negligible below a jet static-pressure ratio of the order of 2.

3. At constant free-stream Mach number, increasing jet Mach number at a fixed value of jet static-pressure ratio first increases the initial inclination of the jet boundary (jet Mach number near one) and thereafter decreases the initial inclination (jet Mach numbers of the order of 1.5 and greater).

4. The initial inclination of the jet boundary is always much less for a supersonic than for a subsonic free stream. Decreasing the ratio of specific heats of the jet always increases the initial inclination of the jet boundary.

[redacted]

5. The ratio of specific heats of the jet can have a significant effect upon the inclination of the exit shock in the external stream and, therefore, upon the upstream limit of the interference pressure field created by the jet. The type of curves presented to show this effect may be used to achieve duplication of exit shock inclination (but not jet structure) in experimental studies without duplication of the ratio of specific heats of the jet.

6. Consideration is given to jet structure and the phenomena to be expected in the presence of subsonic and supersonic mixing boundaries. Curves are presented of the basic Kawamura parameter and of the difference parameter, from which the importance of the ratio of specific heats of the jet to the jet structure and ambient pressure field may be gathered. Curves showing the effects of the ratio of specific heats upon shock inclination are included.

7. In practical application, it is quite possible to have a condition of no reflection from the passage of a shock from within the jet through a supersonic mixing boundary and into the outer stream. Experimental observations indicate that when such reflections do occur they are weak and eliminate themselves rapidly. For jet interference studies, it appears permissible to assume that the jet is cylindrical downstream of the region where the shock arising from within the jet passes through the mixing boundary.

Langley Aeronautical Laboratory,
National Advisory Committee for Aeronautics,
Langley Field, Va., December 31, 1954.

[redacted]

APPENDIX A

CALCULATIONS BY METHOD OF CHARACTERISTICS

Basic Considerations

For several years, the Langley Bell Computing Section has had established procedures for characteristic calculations by machine of the lattice-point type which do not require iterations in the point-to-point flow-field calculations. The characteristic nets thus calculated must, therefore, be somewhat more dense than those employing iterative methods for comparable accuracy. (See refs. 26 and 34 for descriptions of lattice-point type of characteristic calculations.) Insofar as possible the present investigation utilized the procedures of the Langley Bell Computing Section. Nevertheless, certain complications arose in the calculations: the first was the solution for points on and near the jet axis which must be confronted regardless of the type of characteristic calculation employed, second was the choice of procedure to follow when intersecting characteristics of the same family indicated the presence of a shock, third was the solution for divergent nozzles which the existing lattice-point procedures could handle only by time-consuming additions to the calculations, and fourth was the solution for the sonic exit. These four subjects will be covered in the sections to follow.

Points on and Near the Axis

The characteristic calculations for a given set of initial conditions were originally proposed to be carried through only until the maximum height of the jet boundary was reached. This limit was selected for two reasons: first, the boundary shape beyond the maximum height usually has little practical value, and second, the number of solutions required on the jet axis would be reduced. While the latter would not be encountered at the higher values of M_j and θ_N (this accounts for the continuance of some of the calculations for $\theta_N \neq 0^\circ$), they would cause considerable delay in the overall program in that they required transcalculation from machine to manual to machine. The frequency with which this transcalculation is required becomes increasingly severe as M_j decreases. Several procedures are available for refining the calculations near the axis, most of which are discussed in reference 26. The method of successive approximations as described in reference 34 was used in the present calculations with at least two approximations being made for the first point on each first-family characteristic leaving the axis. This procedure gave satisfactory results for all nets except those for $M_j = 1.01$

[redacted]

as can be observed in figure 14(a) where the change in slope of the second family characteristics reverses sign in reaching the axis, an obvious indication of appreciable error. Calculations at higher values of M_j have shown that surprisingly large errors in the flow field near the axis can be present without seriously affecting the shape of the portion of the jet boundary considered herein or the coalescence of characteristics (shock growth) near the boundary. An indication of the error on the axis and its effect on boundary shape for the most critical condition ($M_j = 1$) will be covered in the section on the solution for the sonic exit.

Intersection of Like Characteristics and Shock Growth

The occurrence of a shock is first indicated by the intersection of the last expansion characteristic from the lip of the nozzle and the first reflected characteristic from the boundary. Successive intersections of the same type indicate a growth in strength of the shock and define its shape and location. Several procedures are available for handling the occurrence of a shock. The rigorous solution is to combine the shock equations and the characteristic equations. The ensuing computations become so complicated, however, that this approach is rarely used except to demonstrate the procedure. To date, no satisfactory method has been found to incorporate the procedure in machine calculations. Consequently, it was not considered for use. Of the remaining procedures, all require transcalculation except the use of foldback which permits the machine to make continuous calculations from the axis to the boundary. From a cursory examination, none of the remaining procedures appears to give accuracy better than that obtained with foldback, and some are inferior. For the above reasons, the foldback procedure was used in the present calculations as shown by the characteristic nets in figure 14. This procedure takes its name from the manner in which the characteristic net folds back upon itself as the calculations proceed beyond the point for the occurrence of a shock within the jet. In essence the characteristic equations are permitted to handle their own difficulties by ignoring the intersection of characteristics of the same family. The location of the shock is established by the inner envelope of the intersections of like characteristics, clear examples of which may be seen at $\frac{p_j}{p_\infty} = 10$ and 20 in figure 14(a). The jet flow field between the shock and the jet boundary is defined by the net remaining after the foldback portion of the net is deleted. Thus the method of foldback predicts boundary and shock location and actually gives the type of discontinuities in velocity and direction that occur in crossing a shock.

Solution for Divergent Nozzles

As mentioned previously, the lattice-point procedures available for machine computations at the time of these calculations were not amenable to ready solutions for θ_N other than zero. The centered-expansion characteristic method of Johannesen and Meyer (refs. 5 and 19) is readily applicable to any free jet problem $\left(\frac{p_j}{p_\infty} \geq 1\right)$ but this relatively recent procedure was not available for machine computation nor had the integrals (see appendix B) been evaluated at the time of these calculations except for the range of $M_j = 2.73$ to 3.89 $(\gamma_j = 1.400)$ and for the intervals given in references 5 and 19. In order to take advantage of the existing procedure available for machine, the properties of the leading characteristic were calculated by the Johannesen-Meyer method and used as a base from which the calculations were continued in the same manner as employed for $\theta_N = 0^\circ$. A brief description of the calculation of the leading characteristic by this method follows.

Consider a conically divergent nozzle assumed to give pure source flow and the polar and Cartesian coordinates as shown in the sketch.

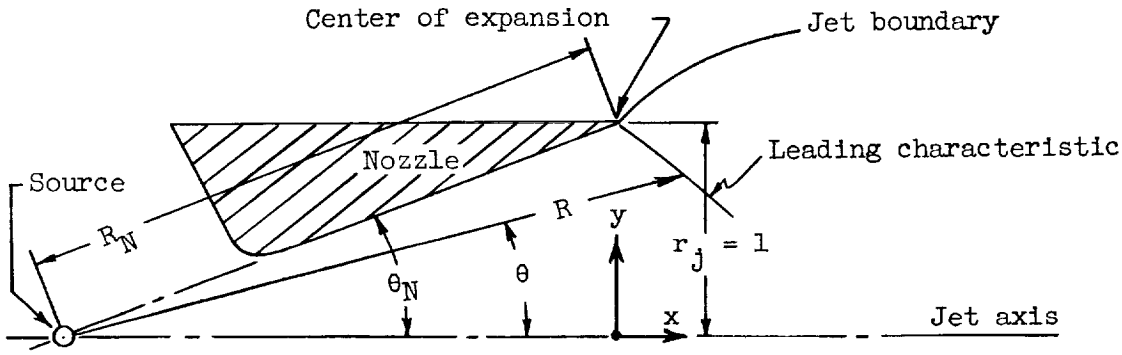

The initial properties of the flow at the nozzle lip just prior to exit are given, namely, M_j, μ_j, γ_j, and θ_N. From the initial conditions and the relation

$$R = C\left(1 + \frac{2}{\gamma-1}\sin^2\mu\right)^{\frac{\gamma_j+1}{4(\gamma_j-1)}}(\sin\mu)^{-\frac{1}{\gamma_j-1}} \tag{A1}$$

the constant C may be determined. With P representing Busemann's pressure number and $t = 1000 - P$, the relation $dt = -2d\theta$ allows the

[redacted]

value of R to be evaluated for any value of $\theta = \theta_N + d\theta$. The flow properties for a given point on the leading characteristic are thus determined and the Cartesian coordinates of the point are

$$\left.\begin{aligned} x &= R\cos\theta - R_N\cos\theta_N \\ y &= R\sin\theta \end{aligned}\right\} \tag{A2}$$

The relation between P and μ was not available for γ_j other than 1.4. Consequently, tables and charts showing this relation for other values of γ_j were prepared for these calculations. Inasmuch as these data are not generally available, they are presented in table I.

An idea of the curvature of the leading characteristic may be gained from reference 5 where an expression for the point of inflexion has been derived in terms of γ_j and the local Mach number on the leading characteristic. This is

$$M = \sqrt{\frac{3}{2 - \gamma_j}} \tag{A3}$$

The curve given by this relation is shown in figure 50. For a constant value of γ_j, the leading characteristic will be concave to the axis for values of M above the curve and convex to the axis for values below.

Solution for the Sonic Exit

A solution to the sonic exit for M_j exactly equal to 1 is difficult since the slope of the leading characteristic is infinite. The usual procedure is to select a value of M_j slightly greater than 1 with the implicit assumption that the difference in this solution from that for M_j exactly equal to 1 is negligible. The first solutions for the sonic exit (fig. 14(a)) were calculated for $M_j = 1.01$ $\left(\mu_j = 81.93^\circ\right)$.

The errors in the calculations near the axis have been discussed and shown to be significant. The advantages of having a so-called universal solution for the expansive flow field leaving a sonic exit for which the errors in the region of the axis are small and for which the properties of the expansive flow field are tabulated have been recognized in the past. Such a solution would not only be valuable to jet studies but to any axisymmetric problem involving flow from a sonic orifice

(for example, in the design of axisymmetric nozzles for supersonic wind tunnels). By using iterative procedures, Owen and Thornhill (ref. 35) have made a characteristic calculation of the flow into a vacumm for $M_j = 1.0038$ $\left(\mu_j = 85^\circ\right)$ with special consideration being given to the flow near the axis of symmetry. The properties of the flow field off the axis are not given; consequently, the additional universal applicability that this solution might otherwise have is lacking. This additional applicability would be somewhat limited, however, since the method employed, while quite accurate, gave large mesh size to the characteristic net. The points defining the flow field are, therefore, few.

In an effort to obtain a solution for the sonic exit that would have the flow field defined in small increments and to assess the effect of errors near the axis upon the jet boundary, the initial conditions of Owen and Thornhill $\left(M_j = 1.0038, \ \mu_j = 85^\circ\right)$ were utilized in a calculation of an exceptionally dense net for $\frac{p_j}{p_\infty} = 2$ with a second approximation being carried out for each axis point by transcalculation.

The results of these calculations are given in table II for the expansion portion of the flow field only. A comparison of the characteristic net at the axis and the boundary shape with the solution for $M_j = 1.01$ (from fig. 14(a)) is shown in figure 51. Figure 52 presents to a sensitive ordinate scale a comparison of the nondimensional velocity distributions along the axis for several conditions. A comparison of the results for $\frac{p_j}{p_\infty} = 2$ in figures 51 and 52 shows that appreciable errors in the characteristic net near the axis and, therefore, in the velocity along the axis, may have negligibly small effects upon the boundary shape through $\left(\frac{y}{r_j}\right)_{max}$ even for the critical condition of $M_j \approx 1$. The initial portions of the velocity distributions for $\frac{p_j}{p_\infty} = 10$ and 20 and $M_j = 1.01$ are included in figure 52 to illustrate the effects of further increasing the mesh size (see fig. 14(a)). From the comparisons of the calculations for $\frac{p_j}{p_\infty} = 2$, the errors in the boundaries for $\frac{p_j}{p_\infty} = 10$ and 20 may be expected to be small.

The calculation of Owen and Thornhill and the present calculation $\left(M_j = 1.0038\right)$ of the velocity along the axis are in good agreement (fig. 52). This agreement would appear to indicate that even near $M = 1$ the simpler noniterative procedure of the present calculation

[redacted]

may be expected to give results equally as satisfactory as those of the more tedious iterative procedures if the net is dense. Experimental measurements of the velocity along the axis have been made by a number of methods (see refs. 14, 15, and 36). The probe results of reference 15 and the interferometric studies of reference 36 appear to contain least error and it is from a comparison with these results that Owen and Thornhill concluded that the agreement between experiment and their calculation was good. For a given accuracy in measuring pressure, the use of total-pressure probes to determine Mach number and velocity introduces large errors as the Mach number decreases from about 1.2 to 1; consequently for values of $\frac{x}{r_j}$ less than about 0.45, the probe results are subject to question. The interferometric measurements (ref. 36) are subject only to the accumulative errors in reducing the data; these results are shown by the cross-hatched band in figure 52 where the width of the band denotes the scatter and probable error. Recently, measurements have been made by Mr. R. M. O'Donnell of the Langley Aeronautical Laboratory utilizing the mixing zone apparatus of the Langley 9-inch supersonic tunnel section. In order to avoid probe interference and the inaccuracies near $M = 1$, a splitter plate technique was used with orifices installed on the plate surface along the jet axis. The results of these measurements are also indicated in figure 52. A comparison of the experimental results with the theoretical calculations would appear to indicate that the expansive flow field properties included in table II are sufficiently accurate to expect good results in application to other problems.

APPENDIX B

CALCULATION OF INITIAL CURVATURE OF A JET BOUNDARY USING THE METHOD OF JOHANNESEN AND MEYER

Johannesen and Meyer (ref. 19) have obtained an approximate solution for the axially symmetrical flow of a perfect gas in the region of an expansion around a corner. This solution which is in the form of an expansion in powers of the distance from the corner replaces the conventional method of characteristics in such a region. An application is made to a jet discharging into still air where the static pressure in the jet nozzle is higher than ambient pressure. A formula is presented for the initial curvature, at the lip of the nozzle, of a jet boundary.

Using the notation of reference 19 (given at the conclusion of this appendix), the initial curvature is given by

$$\left(\frac{d\theta}{dR}\right)_{R=0} - \left(\frac{1}{q_F}\right) \cot \mu_F \left(\frac{dq}{dR}\right)_{R=0} = \frac{-\left[q_F \sin \theta_j \sin^2\mu_F + u_1\left(\phi_F\right)\right]}{q_F \sin^2\mu_F} \tag{B1}$$

Now on the jet boundary, $\frac{dq}{dR} = 0$ and

$$\left(\frac{d\theta}{dR}\right)_{R=0} = \frac{-\left[q_F \sin \theta_j \sin^2\mu_F + u_1\left(\phi_F\right)\right]}{q_F \sin^2\mu_F} \tag{B2}$$

(The initial radius of curvature in the symbology of the text is $\frac{\rho_o}{d_j}$ and is equal to $\frac{1}{2}\left(\frac{dR}{d\theta}\right)_{R=0}$.)

Each of the quantities of equation (B2) except $u_1\left(\phi_F\right)$ may be easily determined once the initial characteristics of the jet flow are given. The velocity component $u_1\left(\phi_F\right)$ is given by

$$u_1(\phi) = K(\phi)\left[I_1(\phi) \cos \beta_o + I_2(\phi) \sin \beta_o - \lambda I_3(\phi) \cos \beta_o + \lambda I_4(\phi) \sin \beta_o + C_2\right] \tag{B3}$$

where $K(\phi) = -\frac{a_s}{2\lambda}\left(1 - z^2\right)^2 \sqrt{z}$

and the integrals $I_1(\phi) \ldots I_4(\phi)$ can be written as

$$\left.\begin{aligned} I_1(\phi) &= \int \frac{\cos\left(\lambda^{-1} \sin^{-1} z\right)}{\left(1 - z^2\right)^2 \sqrt{z}}\, dz \\ I_2(\phi) &= \int \frac{\sin\left(\lambda^{-1} \sin^{-1} z\right)}{\left(1 - z^2\right)^2 \sqrt{z}}\, dz \\ I_3(\phi) &= \int \frac{\sin\left(\lambda^{-1} \sin^{-1} z\right)}{\left(1 - z^2\right)^{3/2} z^{3/2}}\, dz \\ I_4(\phi) &= \int \frac{\cos\left(\lambda^{-1} \sin^{-1} z\right)}{\left(1 - z^2\right)^{3/2} z^{3/2}}\, dz \end{aligned}\right\} \qquad (B4)$$

The limits of integration are determined from the values of z corresponding to ϕ_L and ϕ_F (the values which ϕ takes on the leading and final Mach lines, respectively, at the lip). The relation between z and ϕ is given as

$$z = \sin \lambda\left(\phi + \beta_o\right) \qquad (B5)$$

where

$$\beta_o = \mu_L - \pi - \phi_c + \frac{1}{\lambda} \cot^{-1}\left(\frac{1}{\lambda} \tan \mu_L\right) \qquad (B6)$$

It will be noted that β_o is also given by the Busemann pressure number minus 1,000.

The integrals of equation (B4) have been computed for $\gamma = 1.400$ over a large range of values of z $\left(1.0 \lessapprox M_F \approx 5.2\right)$ and are tabulated in table III. The value of each integral given in table III represents the integral between the limits $z = 0.03$ and the value of z listed in the table. Thus in applying these results to the calculation of the initial curvature of a jet boundary, it is necessary only to obtain z_L and z_F corresponding to the given jet flow boundaries; obtain the corresponding values of $I_1(\phi) \ldots I_4(\phi)$ in table III and the difference between the integrals for z_F and z_L represents the desired solution to equation (B4).

[redacted]

In equation (B3), C_2 is an arbitrary constant and, since the integrals of equation (B4) are zero for $z = z_L$, it is given by

$$C_2 = \frac{u_1(\phi_L)}{K(\phi_L)} \tag{B7}$$

It will be noted that the solutions to equation (B4) given in table III are useful not only in the previously discussed application, but also in the much broader application of the characteristic calculation of the jet flow field as discussed in reference 5.

Notation From Reference 19

(All distances made nondimensional with respect to radius of jet at exit)

R, ϕ	polar coordinates in meridian plane with origin at center of expansion
u, v	velocity components in direction of R and ϕ increasing
q	velocity magnitude
θ	angle between downstream direction on axis and local stream direction
a_s	critical speed of sound
μ	local Mach angle
$I_1(\phi)$ . . . $I_{\ }(\phi)$	integrals occurring in equation (B4)
λ	$\sqrt{\frac{\gamma - 1}{\gamma + 1}}$
M	Mach number

Subscripts:

J	limiting value as center is approached along boundary streamline from downstream
L	limiting value as center is approached along leading Mach line in region of centered expansion

[redacted]

F limiting value as center is approached along final Mach line in region of centered expansion

c limiting value as center is approached along boundary streamline from upstream

REFERENCES

1. Krzywoblocki, M. Z.: Jets. NOTS TM No. 1576, U. S. Naval Ord. Test Station (Inyokern, Calif.), Sept. 1953.

2. Anon: Jets - Flow [Bibliography]. BTI-6070, Armed Services Tech. Information Agency, Document Service Center (Dayton, Ohio), 1954.

3. Anon: Nozzles - Flow [Bibliography]. BTI-6762, Armed Services Tech. Information Agency, Document Service Center (Dayton, Ohio), 1954.

4. Anon: Nozzles, Exhaust [Bibliography]. BTI-6761, Armed Services Tech. Information Agency, Document Service Center (Dayton, Ohio), 1954.

5. Johannesen, N. H.: Ejector Theory and Experiments. A.T.S. No. 1, Trans. Danish Acad. of Tech. Sci., (Copenhagen), 1951.

6. Oudart, Adalbert: L'Étude des jets et la mécanique théorique des fluides. Ministère de l'air. Publications Scientifiques et Techniques No. 234, 1949.

7. Love, Eugene S.: The Base Pressure at Supersonic Speeds on Two-Dimensional Airfoils and Bodies of Revolution (With and Without Fins) Having Turbulent Boundary Layers. NACA RM L53C02, 1953.

8. Coletti, Donald E.: Measurements and Predictions of Flow Conditions on a Two-Dimensional Base Separating a Mach Number 3.36 Jet and a Mach Number 1.55 Outer Stream. NACA RM L54C08, 1954.

9. Cortright, Edgar M., Jr., and Kochendorfer, Fred D.: Jet Effects on Flow Over Afterbodies in Supersonic Stream. NACA RM E53H25, 1953.

10. Powell, Alan: Report on the U.K.-U.S.A. Conference on Jet Noise, Southampton University, 29-30th June 1953. Rep. No. F.M. 1935 (Rep. No. 16,068, British A.R.C.), July 1953.

11. Foster, Charles R., and Cowles, Frederick B.: Experimental Study of Gas-Flow Separation in Overexpanded Exhaust Nozzles for Rocket Motors. Progress Rep. No. 4-103, Jet Propulsion Lab., C.I.T., May 9, 1949.

12. Wada, Yoshimasa: On the Recurrent Figure of a Jet. Jour. Phys. Soc. of Japan, vol. 7, no. 2, Mar.-Apr. 1952, pp. 211-214.

[redacted]

13. Pack, D. C.: A Note on Prandtl's Formula for the Wave-Length of a Supersonic Gas Jet. Quarterly Jour. Mech. and Appl. Math., vol. III, pt. 2, June 1950, pp. 173-181.

14. Hartmann, Jul., and Lazarus, Freimut: The Air-Jet With a Velocity Exceeding That of Sound. Phil. Mag. and Jour. Sci., sec. 7, vol. 31, no. 204, Jan. 1941, pp. 35-50.

15. Hartmann, Jul.: The Acoustic Air-Jet Generator. Ingenirvidenskabelige Skrifter nr. 4, Akademiet for de Tekniske Videnskaber og Dansk Ingenirforening (Copenhagen), 1939.

16. Pack, D. C.: On the Formation of Shock-Waves in Supersonic Gas Jets (Two-Dimensional Flow). Quarterly Jour. of Mech. and Appl. Math., vol. I, pt. 1, Mar. 1948, pp. 1-17.

17. Meyer, R. E.: The Method of Characteristics for Problems of Flow Involving Two Independent Variables.
Part I. The General Theory (With a Note on the Calculation of Axially-Symmetrical Supersonic Flows by S. Goldstein). Jour. Mech. and Appl. Math., vol. I, pt. 2, June 1948, pp. 196-219.
Part II. Integration Along a Mach Line. The Radial Focusing Effect in Axially Symmetrical Flow. Jour. Mech. and Appl. Math., vol. I, pt. 4, Dec. 1948, pp. 451-469.

18. Meyer, R. E.: Focusing Effects in Two-Dimensional Supersonic Flow. Phil. Trans. Roy. Soc. (London), ser. A, vol. 242, Dec. 21, 1949, pp. 153-171.

19. Johannesen, N. H., and Meyer, R. E.: Axially-Symmetrical Supersonic Flow Near the Centre of an Expansion. Aero. Quarterly, vol. II, pt. II, Aug. 1950, pp. 127-142.

20. Rousso, Morris D., and Kochendorfer, Fred D.: Velocity and Temperature Fields in Circular Jet Expanding From Choked Nozzle Into Quiescent Air. NACA RM E51F18, 1951.

21. Powell, Alan: On the Mechanism and Reduction of Choked Jet Noise (Part One). Rep. No. F.M. 1858, Univ. of Southampton (Rep. No. 15,623, British A.R.C.), Dec. 1952.

22. Hubbard, Harvey H.: A Survey of the Aircraft-Noise Problem With Special Reference to Its Physical Aspects. NACA TN 2701, 1952.

23. Lighthill, M. J.: On Sound Generated Aerodynamically. II. Turbulence as a Source of Sound. Rep. No. F.M. 1936, Univ. of Manchester (Rep. No. 16,071, British A.R.C.), July 1953.

[redacted]

24. Bressette, Walter E.: Investigation of the Jet Effects on a Flat Surface Downstream of the Exit of a Simulated Turbojet Nacelle at a Free-Stream Mach Number of 2.02. NACA RM L54E05a, 1954.

25. Bromm, August F., Jr., and O'Donnell, Robert M.: Investigation at Supersonic Speeds of the Effect of Jet Mach Number and Divergence Angle of the Nozzle Upon the Pressure on the Base Annulus of a Body of Revolution. NACA RM L54I16, 1954.

26. Isenberg, J. S.: The Method of Characteristics in Compressible Flow. Part I (Steady Supersonic Flow). Tech. Rep. No. F-TR-1173A-ND, ATI No. 26341, Air Materiel Command, U. S. Air Force, Dec. 1947.

27. Schäfer, M.: Steady Supersonic Flows. British M.A.P. Völkenrode. Reps. and Translations No. 995, Apr. 15, 1948. Reps. and Translations No. 996, May 1, 1948.

28. Rousso, Morris D., and Baughman, L. Eugene: Investigation at Mach Number 1.91 of Spreading Characteristics of Jet Expanding From Choked Nozzles. NACA RM E51L19, 1952.

29. O'Donnell, Robert M., and McDearmon, Russell W.: Experimental Investigation of Effects of Primary Jet Flow and Secondary Flow Through a Zero-Length Ejector on the Base and Boattail Pressures of a Body of Revolution at Free-Stream Mach Numbers of 1.62, 1.93, and 2.41. NACA RM L54I22, 1954.

30. Liepmann, H. W., Roshko, A., and Dhawan S.: On Reflection of Shock Waves From Boundary Layers. NACA Rep. 1100, 1952. (Supersedes NACA TN 2334.)

31. Barry, Frank W.: Interaction of an Oblique Shock Wave With a Boundary Layer on a Flat Plate. S. D. Thesis, M.I.T., 1950.

32. Kawamura, Ryuma: Reflection of a Wave at an Interface of Supersonic Flows and Wave Patterns in a Supersonic Compound Jet. Jour. Phys. Soc. of Japan, vol. 7, no. 5, Sept.-Oct. 1952, pp. 482-485.

33. Wilder, John G., Jr.: Part I of Final Report on Phase I of the Study of Air Exchange Problems in Supersonic Tunnels. Rep. No. AD-570-A-5 (Contract No. W33-038 ac-21809), Cornell Aero. Lab., Inc., Jan. 1949.

34. Ferri, Antonio: Elements of Aerodynamics of Supersonic Flows. The Macmillan Co., 1949.

[redacted]

35. Owen, P. L., and Thornhill, C. K.: The Flow in an Axially Symmetric Supersonic Jet From a Nearly Sonic Orifice Into a Vacuum. Rep. No. 30/48 (Theo. Res. Rep. No. 5/48), Ministry of Supply, Armament Res. Establishment (British), Sept. 1948.

36. Ladenburg, R., Van Voorhis, C. C., and Winckler, J.: Interferometric Study of Supersonic Phenomena: Part I. A Supersonic Air Jet at 60 lb/in^2 Tank Pressure. NAVORD Rep. 69-46, Bur. Ordnance, Navy Dept., Apr. 17, 1946.

[redacted]

TABLE I.- RELATION BETWEEN BUSEMANN'S PRESSURE NUMBER, MACH ANGLE, AND MACH NUMBER FOR SEVERAL VALUES OF THE RATIO OF SPECIFIC HEATS

$$\left[P = 1090^\circ - \mu - \left(\frac{\gamma+1}{\gamma-1}\right)^{\frac{1}{2}} \cot^{-1}\left[\left(\frac{\gamma+1}{\gamma-1}\right)^{\frac{1}{2}} \tan\mu\right]\right]$$

M	μ	P for -				
		$\gamma = 1.200$	$\gamma = 1.300$	$\gamma = 1.400$	$\gamma = 1.500$	$\gamma = 1.667$
1.00	90.00	1000.00	1000.00	1000.00	1000.00	1000.00
1.05	72.25	999.46	999.48	999.51	999.53	999.56
1.10	65.38	998.53	998.60	998.66	998.72	998.81
1.15	60.41	997.37	997.50	997.62	997.73	997.89
1.20	56.44	996.06	996.27	996.46	996.62	996.87
1.25	53.13	994.60	994.89	995.16	995.40	995.75
1.30	50.28	993.09	993.49	993.84	994.16	994.62
1.35	47.79	991.50	992.01	992.46	992.86	993.44
1.40	45.58	989.85	990.48	991.04	991.53	992.24
1.45	43.60	988.14	988.90	989.57	990.16	991.00
1.50	41.81	986.40	987.31	988.09	988.79	989.78
1.55	40.18	984.65	985.70	986.62	987.42	988.56
1.60	38.68	982.87	984.09	985.14	986.05	987.35
1.65	37.31	981.08	982.47	983.65	984.69	986.14
1.70	36.03	979.30	980.86	982.19	983.35	984.96
1.75	34.85	977.49	979.24	980.72	982.01	983.79
1.80	33.75	975.70	977.64	979.28	980.68	982.64
1.85	32.72	973.90	976.04	977.84	979.38	981.50
1.90	31.76	972.11	974.45	976.41	978.08	980.38
1.95	30.85	970.32	972.87	975.01	976.81	979.28
2.00	30.00	968.55	971.32	973.63	975.57	978.22
2.05	29.20	966.77	969.77	972.25	974.33	977.16
2.10	28.44	965.02	968.24	970.90	973.12	976.12
2.15	27.72	963.28	966.74	969.57	971.93	975.12
2.20	27.04	961.55	965.25	968.26	970.77	974.13
2.25	26.39	959.83	963.78	966.98	969.62	973.16
2.30	25.77	958.15	962.34	965.72	968.51	972.22
2.35	25.18	956.47	960.91	964.47	967.41	971.30
2.40	24.62	954.80	959.50	963.25	966.32	970.40
2.45	24.09	953.16	958.11	962.05	965.27	969.52
2.50	23.58	951.53	956.74	960.87	964.23	968.65
2.55	23.09	949.93	955.40	959.72	963.22	967.81
2.60	22.62	948.36	954.09	958.59	962.23	967.00
2.65	22.17	946.78	952.78	957.47	961.26	966.19
2.70	21.74	945.22	951.49	956.37	960.30	965.40
2.75	21.32	943.71	950.25	955.32	959.38	964.65
2.80	20.92	942.20	949.01	954.27	958.47	963.90
2.85	20.54	940.70	947.78	953.22	957.56	963.16
2.90	20.17	939.24	946.59	952.22	956.69	962.45
2.95	19.81	937.78	945.40	951.22	955.83	961.74

[redacted]

TABLE I.- RELATION BETWEEN BUSEMANN'S PRESSURE NUMBER, MACH ANGLE, AND MACH NUMBER FOR SEVERAL VALUES OF THE RATIO OF SPECIFIC HEATS - Concluded

$$\left[P = 1090^\circ - \mu - \left(\frac{\gamma + 1}{\gamma - 1}\right)^{\frac{1}{2}} \cot^{-1}\left[\left(\frac{\gamma + 1}{\gamma - 1}\right)^{\frac{1}{2}} \tan \mu\right]\right]$$

M	μ	P for -				
		$\gamma = 1.200$	$\gamma = 1.300$	$\gamma = 1.400$	$\gamma = 1.500$	$\gamma = 1.667$
3.00	19.47	936.36	944.25	950.25	955.00	961.07
3.05	19.14	934.95	943.11	949.30	954.17	960.40
3.10	18.82	933.54	941.98	948.35	953.36	959.74
3.15	18.51	932.18	940.88	947.44	952.58	959.10
3.20	18.21	930.82	939.80	946.54	951.80	958.48
3.25	17.92	929.49	938.74	945.65	951.05	957.87
3.30	17.64	928.17	937.69	944.78	950.30	957.27
3.35	17.37	926.87	936.67	943.93	949.58	956.69
3.40	17.10	925.58	935.65	943.09	948.86	956.12
3.45	16.85	924.34	934.67	942.28	948.18	955.56
3.50	16.60	923.07	933.67	941.46	947.48	955.01
3.55	16.36	921.84	932.73	940.69	946.82	954.48
3.60	16.13	920.66	931.79	939.91	946.17	953.96
3.65	15.90	919.47	930.86	939.16	945.52	953.45
3.70	15.68	918.28	929.94	938.40	944.89	952.94
3.75	15.47	917.13	929.05	937.67	944.27	952.45
3.80	15.26	916.00	928.17	936.96	943.67	951.97
3.85	15.05	914.88	927.31	936.26	943.08	951.51
3.90	14.86	913.77	926.45	935.56	942.49	951.04
3.95	14.66	912.68	925.62	934.89	941.93	950.60
4.00	14.48	911.60	924.79	934.21	941.36	950.14
4.05	14.29	910.54	923.98	933.57	940.81	949.72
4.10	14.12	909.49	923.18	932.92	940.27	949.28
4.15	13.94	908.48	922.41	932.29	939.75	948.88
4.20	13.77	907.44	921.62	931.66	939.21	948.46
4.25	13.61	906.46	920.88	931.06	938.71	948.06
4.30	13.45	905.46	920.13	930.45	938.21	947.66
4.35	13.29	904.49	919.40	929.87	937.72	947.28
4.40	13.14	903.54	918.68	929.30	937.24	946.91
4.45	12.99	902.59	917.96	928.72	936.76	946.53
4.50	12.84	901.66	917.27	928.16	936.29	946.17
4.55	12.70	900.75	916.59	927.62	935.84	945.81
4.60	12.56	899.83	915.90	927.07	935.39	945.46
4.65	12.42	898.95	915.24	926.55	934.95	945.12
4.70	12.28	898.10	914.61	926.05	934.54	944.80
4.75	12.15	897.23	913.97	925.53	934.11	944.46
4.80	12.02	896.36	913.32	925.02	933.68	944.13

[redacted]

TABLE II.- EXPANSIVE FLOW FIELD OBTAINED BY CHARACTERISTIC CALCULATIONS FOR JET FLOW FROM NEAR-SONIC EXIT ($M_j = 1.0038$; $\mu_j = 85^\circ$)

x/r_j	y/r_j	θ, radians	μ, radians	V/V_l
0.0000000	1.000000	0.0000000	1.483530	0.4095466
.0000000	1.000000	$.1570796 \times 10^{-3}$	1.466077	.4101196
.0000000	1.000000	$.3665190 \times 10^{-3}$	1.448624	.4107984
.0000000	1.000000	$.6108651 \times 10^{-3}$	1.431171	.4115834
.0000000	1.000000	$.9948375 \times 10^{-3}$	1.413715	.4124758
.0000000	1.000000	$.1361357 \times 10^{-2}$	1.396262	.4134764
.0000000	1.000000	$.1919861 \times 10^{-2}$	1.378809	.4145861
.0000000	1.000000	$.2443460 \times 10^{-2}$	1.361357	.4158062
.0000000	1.000000	$.3141592 \times 10^{-2}$	1.343903	.4171382
.0000000	1.000000	$.4014256 \times 10^{-2}$	1.326450	.4185834
.0000000	1.000000	$.4886921 \times 10^{-2}$	1.308997	.4201434
.0000000	1.000000	$.6108651 \times 10^{-2}$	1.291544	.4218200
.0000000	1.000000	$.7330381 \times 10^{-2}$	1.274091	.4236149
.0000000	1.000000	$.8726645 \times 10^{-2}$	1.256638	.4255301
.0000000	1.000000	$.1029744 \times 10^{-1}$	1.239183	.4275681
.0000000	1.000000	$.1204277 \times 10^{-1}$	1.221729	.4297307
.0000000	1.000000	$.1413716 \times 10^{-1}$	1.204276	.4320205
.0000000	1.000000	$.1623156 \times 10^{-1}$	1.186824	.4344399
.0000000	1.000000	$.1867502 \times 10^{-1}$	1.169370	.4369920
.0000000	1.000000	$.2129301 \times 10^{-1}$	1.151916	.4396794
.0000000	1.000000	$.2426007 \times 10^{-1}$	1.134464	.4425051
.0000000	1.000000	$.2740166 \times 10^{-1}$	1.117010	.4454728
.0000000	1.000000	$.3089232 \times 10^{-1}$	1.099557	.4485856
.0000000	1.000000	$.3473204 \times 10^{-1}$	1.082104	.4518470
.0000000	1.000000	$.3874630 \times 10^{-1}$	1.064650	.4552610
.0000000	1.000000	$.4328415 \times 10^{-1}$	1.047197	.4588314
.0000000	1.000000	$.4799654 \times 10^{-1}$	1.029744	.4625626
.0000000	1.000000	$.5305800 \times 10^{-1}$	1.012291	.4664589
.0000000	1.000000	$.5864305 \times 10^{-1}$	.9948374	.4705248
.0000000	1.000000	$.6457717 \times 10^{-1}$	.9773841	.4747653
.0000000	1.000000	$.7103489 \times 10^{-1}$	.9599308	.4791852
.0000000	1.000000	$.7784167 \times 10^{-1}$	.9424776	.4837899
.0000000	1.000000	$.8517205 \times 10^{-1}$	.9250244	.4885848
.0000000	1.000000	$.9285150 \times 10^{-1}$	.9075712	.4935756
.0000000	1.000000	.1012291	.8901177	.4987684
.0000000	1.000000	.1101303	.8726642	.5041691
.0000000	1.000000	.1195550	.8552110	.5097841
.0000000	1.000000	.1296779	.8377581	.5156200
.0000000	1.000000	.1403245	.8203046	.5216837
.0000000	1.000000	.1516691	.8028511	.5279822
.0000000	1.000000	.1638864	.7853980	.5345225
.0000000	1.000000	.1766272	.7679447	.5413120
.0000000	1.000000	.1902408	.7504914	.5483583
.0000000	1.000000	.2047270	.7330381	.5556689
.0000000	1.000000	.2200859	.7155847	.5632514

TABLE II.- EXPANSIVE FLOW FIELD OBTAINED BY CHARACTERISTIC CALCULATIONS FOR JET FLOW FROM NEAR-SONIC EXIT $\left(M_j = 1.0038;\ \mu_j = 85^\circ\right)$ - Continued

x/r_j	y/r_j	θ, radians	μ, radians	V/V_l
0.8748868×10^{-2}	0.9000000	0.0000000	1.483530	0.4095466
$.9555603 \times 10^{-2}$	.9092211	$.1446463 \times 10^{-3}$	1.463211	.4102238
$.1031396 \times 10^{-1}$	.9162524	$.3427840 \times 10^{-3}$	1.444355	.4109805
$.1102749 \times 10^{-1}$	.9218810	$.5896295 \times 10^{-3}$	1.427030	.4117854
$.1170429 \times 10^{-1}$	.9265757	$.9433881 \times 10^{-3}$	1.407850	.4128000
$.1234886 \times 10^{-1}$	.9305198	$.1328176 \times 10^{-2}$	1.391373	.4137761
$.1296833 \times 10^{-1}$	.9339613	$.1856349 \times 10^{-2}$	1.372823	.4149921
$.1356240 \times 10^{-1}$	.9369516	$.2415849 \times 10^{-2}$	1.356551	.4161617
$.1413793 \times 10^{-1}$	.9396278	$.3119539 \times 10^{-2}$	1.339143	.4175210
$.1469872 \times 10^{-1}$	.9420389	$.3972444 \times 10^{-2}$	1.321153	.4190446
$.1524232 \times 10^{-1}$	.9442070	$.4889666 \times 10^{-2}$	1.304468	.4205672
$.1577920 \times 10^{-1}$	.9462136	$.6056157 \times 10^{-2}$	1.285959	.4223814
$.1630253 \times 10^{-1}$	.9480419	$.7297595 \times 10^{-2}$	1.268739	.4241893
$.1681743 \times 10^{-1}$	.9497379	$.8709333 \times 10^{-2}$	1.251399	.4261289
$.1732503 \times 10^{-1}$	.9513189	$.1029699 \times 10^{-1}$	1.234031	.4281934
$.1782630 \times 10^{-1}$	.9527994	$.1206632 \times 10^{-1}$	1.216703	.4303770
$.1832639 \times 10^{-1}$	.9542041	$.1411304 \times 10^{-1}$	1.198692	.4327803
$.1881765 \times 10^{-1}$	.9555173	$.1626392 \times 10^{-1}$	1.181620	.4351867
$.1930905 \times 10^{-1}$	.9567735	$.1870457 \times 10^{-1}$	1.164032	.4377994
$.1979706 \times 10^{-1}$	.9579674	$.2135203 \times 10^{-1}$	1.146674	.4405136
$.2028628 \times 10^{-1}$	.9591157	$.2430263 \times 10^{-1}$	1.129012	.4434169
$.2077330 \times 10^{-1}$	.9602138	$.2747403 \times 10^{-1}$	1.111633	.4464162
$.2126247 \times 10^{-1}$	.9612757	$.3096321 \times 10^{-1}$	1.094076	.4495936
$.2175437 \times 10^{-1}$	.9623052	$.3477736 \times 10^{-1}$	1.076417	.4529425
$.2224544 \times 10^{-1}$	.9632974	$.3883547 \times 10^{-1}$	1.059087	.4563820
$.2274390 \times 10^{-1}$	.9642718	$.4332415 \times 10^{-1}$	1.041362	.4600609
$.2324242 \times 10^{-1}$	.9652153	$.4807383 \times 10^{-1}$	1.023995	.4638276
$.2374527 \times 10^{-1}$	.9661386	$.5318255 \times 10^{-1}$	1.006649	.4677544
$.2425671 \times 10^{-1}$	.9670509	$.5874897 \times 10^{-1}$	.9890757	.4719052
$.2477335 \times 10^{-1}$	.9679471	$.6469384 \times 10^{-1}$	.9716050	.4762087
$.2529941 \times 10^{-1}$	.9688358	$.7111609 \times 10^{-1}$	.9540084	.4807267
$.2583159 \times 10^{-1}$	.9697124	$.7793801 \times 10^{-1}$	.9365624	.4853933
$.2637412 \times 10^{-1}$	.9705850	$.8525964 \times 10^{-1}$	.9190589	.4902683
$.2692374 \times 10^{-1}$	.9714492	$.9300398 \times 10^{-1}$	.9017302	.4952906
$.2748861 \times 10^{-1}$	.9723189	.1013614	.8842062	.5005740
$.2806548 \times 10^{-1}$	.9731895	.1102556	.8667195	.5060573
$.2865502 \times 10^{-1}$	.9740628	.1197001	.8492890	.5117393
$.2926174 \times 10^{-1}$	.9749463	.1297983	.8317795	.5176710
$.2988259 \times 10^{-1}$	.9758361	.1404767	.8143727	.5237977
$.3052228 \times 10^{-1}$	.9767399	.1518400	.7969420	.5301691
$.3118559 \times 10^{-1}$	.9776651	.1639926	.7793900	.5368312
$.3186586 \times 10^{-1}$	.9786032	.1767755	.7619984	.5436835
$.3257201 \times 10^{-1}$	.9795677	.1903837	.7445404	.5508208
$.3330541 \times 10^{-1}$	.9805613	.2048371	.7270520	.5582385
$.3406764 \times 10^{-1}$	.9815874	.2201551	.7095602	.5659332

TABLE II.- EXPANSIVE FLOW FIELD OBTAINED BY CHARACTERISTIC CALCULATIONS FOR JET FLOW FROM NEAR-SONIC EXIT $(M_j = 1.0038;\ \mu_j = 85^\circ)$ - Continued

x/r_j	y/r_j	θ, radians	μ, radians	V/V_l
0.1749774×10^{-1}	0.8000000	0.0000000	1.483530	0.4095466
$.1922838 \times 10^{-1}$	.8197816	$.1510528 \times 10^{-3}$	1.462410	.4102535
$.2078493 \times 10^{-1}$	.8341065	$.3561345 \times 10^{-3}$	1.443067	.4110367
$.2219101 \times 10^{-1}$	.8450858	$.6104594 \times 10^{-3}$	1.425413	.4118659
$.2359168 \times 10^{-1}$	.8546931	$.9737907 \times 10^{-3}$	1.405951	.4129075
$.2483346 \times 10^{-1}$	.8622030	$.1368151 \times 10^{-2}$	1.389276	.4139074
$.2609680 \times 10^{-1}$	.8691397	$.1908553 \times 10^{-2}$	1.370534	.4151507
$.2723855 \times 10^{-1}$	.8748201	$.2480129 \times 10^{-2}$	1.354114	.4163453
$.2838181 \times 10^{-1}$	.8800755	$.3198335 \times 10^{-2}$	1.336568	.4177317
$.2951298 \times 10^{-1}$	.8848843	$.4067796 \times 10^{-2}$	1.318447	.4192844
$.3057419 \times 10^{-1}$	.8890703	$.5001940 \times 10^{-2}$	1.301650	.4208349
$.3167195 \times 10^{-1}$	.8931291	$.6189036 \times 10^{-2}$	1.283029	.4226807
$.3270836 \times 10^{-1}$	.8967120	$.7451460 \times 10^{-2}$	1.265714	.4245190
$.3373199 \times 10^{-1}$	.9000492	$.8885938 \times 10^{-2}$	1.248283	.4264902
$.3474248 \times 10^{-1}$	.9031649	$.1049835 \times 10^{-1}$	1.230834	.4285869
$.3574002 \times 10^{-1}$	.9060823	$.1229410 \times 10^{-1}$	1.213429	.4308037
$.3675098 \times 10^{-1}$	.9088947	$.1437000 \times 10^{-1}$	1.195342	.4332426
$.3772357 \times 10^{-1}$	.9114702	$.1655031 \times 10^{-1}$	1.178202	.4356838
$.3870814 \times 10^{-1}$	.9139638	$.1902332 \times 10^{-1}$	1.160550	.4383330
$.3968146 \times 10^{-1}$	.9163234	$.2170453 \times 10^{-1}$	1.143132	.4410842
$.4066361 \times 10^{-1}$	.9186084	$.2469127 \times 10^{-1}$	1.125413	.4440262
$.4163592 \times 10^{-1}$	.9207817	$.2790017 \times 10^{-1}$	1.107983	.4470645
$.4261623 \times 10^{-1}$	.9228918	$.3142865 \times 10^{-1}$	1.090375	.4502826
$.4360393 \times 10^{-1}$	.9249417	$.3528425 \times 10^{-1}$	1.072668	.4536734
$.4458426 \times 10^{-1}$	.9269063	$.3938457 \times 10^{-1}$	1.055295	.4571552
$.4558644 \times 10^{-1}$	.9288497	$.4391830 \times 10^{-1}$	1.037528	.4608784
$.4658284 \times 10^{-1}$	.9307207	$.4871368 \times 10^{-1}$	1.020123	.4646897
$.4758792 \times 10^{-1}$	.9325520	$.5386963 \times 10^{-1}$	1.002741	.4686622
$.4861403 \times 10^{-1}$	.9343686	$.5948550 \times 10^{-1}$	.9851338	.4728605
$.4964915 \times 10^{-1}$	.9361508	$.6548096 \times 10^{-1}$	.9676321	.4772124
$.5070513 \times 10^{-1}$	.9379218	$.7195563 \times 10^{-1}$	.9500062	.4817805
$.5177143 \times 10^{-1}$	.9396655	$.7883079 \times 10^{-1}$	.9325335	.4864982
$.5285950 \times 10^{-1}$	.9414032	$.8620683 \times 10^{-1}$	.9150035	.4914261
$.5395981 \times 10^{-1}$	.9431214	$.9400620 \times 10^{-1}$	.8976505	.4965021
$.5509334 \times 10^{-1}$	.9448548	.1024201	.8801025	.5018416
$.5625070 \times 10^{-1}$	.9465899	.1113714	.8625933	.5073825
$.5743312 \times 10^{-1}$	.9483301	.1208740	.8451427	.5131234
$.5865110 \times 10^{-1}$	.9500923	.1310312	.8276143	.5191161
$.5989669 \times 10^{-1}$	.9518664	.1417682	.8101875	.5253057
$.6118066 \times 10^{-1}$	.9536693	.1531901	.7927370	.5317423
$.6251329 \times 10^{-1}$	.9555169	.1654019	.7751659	.5384721
$.6387916 \times 10^{-1}$	.9573893	.1782429	.7577551	.5453941
$.6529787 \times 10^{-1}$	.9593157	.1919091	.7402784	.5526036
$.6677184 \times 10^{-1}$	.9613012	.2064194	.7227692	.5600967
$.6830406 \times 10^{-1}$	.9633523	.2217934	.7052569	.5678695

[redacted]

TABLE II.- EXPANSIVE FLOW FIELD OBTAINED BY CHARACTERISTIC CALCULATIONS FOR JET FLOW FROM NEAR-SONIC EXIT ($M_j = 1.0038$; $\mu_j = 85^\circ$) - Continued

x/r_j	y/r_j	θ, radians	μ, radians	V/V_l
0.2624660×10^{-1}	0.7000000	0.0000000	1.483530	0.4095466
$.2893369 \times 10^{-1}$	.7307138	$.1583478 \times 10^{-3}$	1.461485	.4102879
$.3130918 \times 10^{-1}$	.7523903	$.3710463 \times 10^{-3}$	1.441619	.4111006
$.3342216 \times 10^{-1}$	.7687039	$.6334703 \times 10^{-3}$	1.423617	.4119564
$.3555932 \times 10^{-1}$	.7831830	$.1006987 \times 10^{-2}$	1.403861	.4130274
$.3740747 \times 10^{-1}$	.7942188	$.1411383 \times 10^{-2}$	1.386974	.4140532
$.3932387 \times 10^{-1}$	.8046081	$.1964559 \times 10^{-2}$	1.368036	.4153261
$.4102068 \times 10^{-1}$	.8129446	$.2548770 \times 10^{-2}$	1.351464	.4165474
$.4273893 \times 10^{-1}$	.8207462	$.3281926 \times 10^{-2}$	1.333773	.4179631
$.4444764 \times 10^{-1}$	.8279228	$.4168522 \times 10^{-2}$	1.315520	.4195469
$.4603281 \times 10^{-1}$	.8341023	$.5120240 \times 10^{-2}$	1.298611	.4211269
$.4769823 \times 10^{-1}$	.8401893	$.6328608 \times 10^{-2}$	1.279881	.4230062
$.4925383 \times 10^{-1}$	.8455071	$.7612560 \times 10^{-2}$	1.262469	.4248768
$.5079232 \times 10^{-1}$	.8504680	$.9070455 \times 10^{-2}$	1.244949	.4268813
$.5231164 \times 10^{-1}$	.8551027	$.1070791 \times 10^{-1}$	1.227415	.4290125
$.5381138 \times 10^{-1}$	.8594433	$.1253051 \times 10^{-1}$	1.209931	.4312645
$.5533934 \times 10^{-1}$	.8636510	$.1463636 \times 10^{-1}$	1.191772	.4337406
$.5679911 \times 10^{-1}$	.8674782	$.1684683 \times 10^{-1}$	1.174567	.4362181
$.5828285 \times 10^{-1}$	.8711997	$.1935260 \times 10^{-1}$	1.156850	.4389058
$.5974741 \times 10^{-1}$	.8747166	$.2206788 \times 10^{-1}$	1.139373	.4416960
$.6122868 \times 10^{-1}$	.8781307	$.2509120 \times 10^{-1}$	1.121600	.4446785
$.6269242 \times 10^{-1}$	.8813725	$.2833785 \times 10^{-1}$	1.104119	.4477577
$.6417022 \times 10^{-1}$	.8845252	$.3190624 \times 10^{-1}$	1.086465	.4510180
$.6566015 \times 10^{-1}$	.8875906	$.3580388 \times 10^{-1}$	1.068714	.4544523
$.6713615 \times 10^{-1}$	.8905233	$.3994708 \times 10^{-1}$	1.051300	.4579778
$.6864879 \times 10^{-1}$	.8934321	$.4452600 \times 10^{-1}$	1.033495	.4617471
$.7014983 \times 10^{-1}$	.8962276	$.4936738 \times 10^{-1}$	1.016054	.4656045
$.7166413 \times 10^{-1}$	.8989644	$.5457069 \times 10^{-1}$	.9986399	.4696243
$.7321219 \times 10^{-1}$	.9016833	$.6023588 \times 10^{-1}$	.9810016	.4738718
$.7477322 \times 10^{-1}$	.9043502	$.6628181 \times 10^{-1}$	.9634712	.4782739
$.7636689 \times 10^{-1}$	.9070026	$.7280859 \times 10^{-1}$	.9458196	.4828937
$.7797522 \times 10^{-1}$	.9096132	$.7973626 \times 10^{-1}$	.9283209	.4876643
$.7961709 \times 10^{-1}$	.9122162	$.8716646 \times 10^{-1}$	.9107685	.4926464
$.8127664 \times 10^{-1}$	.9147891	$.9502022 \times 10^{-1}$	.8933950	.4977777
$.8298789 \times 10^{-1}$	.9173874	.1034898	.8758271	.5031747
$.8473521 \times 10^{-1}$	.9199887	.1124976	.8582998	.5087745
$.8652037 \times 10^{-1}$	.9225981	.1220566	.8408310	.5145760
$.8835997 \times 10^{-1}$	.9252419	.1322705	.8232859	.5206315
$.9024122 \times 10^{-1}$	.9279038	.1430644	.8058437	.5268853
$.9218093 \times 10^{-1}$	.9306101	.1545428	.7883776	.5333884
$.9419511 \times 10^{-1}$	.9333850	.1668113	.7707916	.5401872
$.9625939 \times 10^{-1}$	.9361974	.1797078	.7533653	.5471800
$.9840438 \times 10^{-1}$	.9390921	.1934286	.7358731	.5544630
.1006337	.9420770	.2079926	.7183484	.5620323
.1029517	.9451616	.2234182	.7008191	.5698843

TABLE II.- EXPANSIVE FLOW FIELD OBTAINED BY CHARACTERISTIC CALCULATIONS FOR JET FLOW FROM NEAR-SONIC EXIT (M_j = 1.0038; μ_j = 85°) - Continued

x/r_j	y/r_j	θ, radians	μ, radians	V/V_l
0.3499547×10^{-1}	0.6000000	0.0000000	1.483530	0.4095466
$.3867622 \times 10^{-1}$	.6420716	$.1668802 \times 10^{-3}$	1.460426	.4103278
$.4189340 \times 10^{-1}$	.6711468	$.3878676 \times 10^{-3}$	1.439972	.4111742
$.4472931 \times 10^{-1}$	.6927650	$.6587788 \times 10^{-3}$	1.421589	.4120600
$.4761713 \times 10^{-1}$	.7120619	$.1042986 \times 10^{-2}$	1.401523	.4131633
$.5008229 \times 10^{-1}$	.7265769	$.1457836 \times 10^{-2}$	1.384418	.4142175
$.5266212 \times 10^{-1}$	.7403686	$.2024218 \times 10^{-2}$	1.365275	.4155226
$.5492242 \times 10^{-1}$	.7513222	$.2621446 \times 10^{-2}$	1.348547	.4167728
$.5722406 \times 10^{-1}$	.7616329	$.3370106 \times 10^{-2}$	1.330714	.4182198
$.5951836 \times 10^{-1}$	.7711436	$.4274451 \times 10^{-2}$	1.312328	.4198367
$.6163473 \times 10^{-1}$	.7792893	$.5244187 \times 10^{-2}$	1.295309	.4214483
$.6387540 \times 10^{-1}$	.7873778	$.6474402 \times 10^{-2}$	1.276469	.4233633
$.6595720 \times 10^{-1}$	.7944091	$.7780502 \times 10^{-2}$	1.258963	.4252680
$.6801737 \times 10^{-1}$	.8009748	$.9262501 \times 10^{-2}$	1.241356	.4273076
$.7005237 \times 10^{-1}$	.8071119	$.1092587 \times 10^{-1}$	1.223742	.4294749
$.7206108 \times 10^{-1}$	.8128611	$.1277601 \times 10^{-1}$	1.206185	.4317638
$.7411297 \times 10^{-1}$	.8184504	$.1491218 \times 10^{-1}$	1.187952	.4342794
$.7606651 \times 10^{-1}$	.8235182	$.1715325 \times 10^{-1}$	1.170684	.4367952
$.7805628 \times 10^{-1}$	.8284574	$.1969240 \times 10^{-1}$	1.152907	.4395231
$.8001887 \times 10^{-1}$	.8331229	$.2244248 \times 10^{-1}$	1.135377	.4423539
$.8200610 \times 10^{-1}$	.8376582	$.2550274 \times 10^{-1}$	1.117550	.4453789
$.8396814 \times 10^{-1}$	.8419619	$.2878747 \times 10^{-1}$	1.100021	.4485009
$.8595049 \times 10^{-1}$	.8461510	$.3239600 \times 10^{-1}$	1.082322	.4518054
$.8794995 \times 10^{-1}$	.8502267	$.3633555 \times 10^{-1}$	1.064528	.4552854
$.8992890 \times 10^{-1}$	.8541233	$.4052162 \times 10^{-1}$	1.047077	.4588566
$.9195961 \times 10^{-1}$	.8579936	$.4514601 \times 10^{-1}$	1.029236	.4626737
$.9397297 \times 10^{-1}$	.8617107	$.5003307 \times 10^{-1}$	1.011763	.4665793
$.9600427 \times 10^{-1}$	.8653507	$.5528355 \times 10^{-1}$	.9943193	.4706482
$.9808241 \times 10^{-1}$	.8689702	$.6099781 \times 10^{-1}$	.9766532	.4749467
.1001777	.8725207	$.6709356 \times 10^{-1}$	.9590975	.4794009
.1023177	.8760539	$.7367184 \times 10^{-1}$	.9414226	.4840743
.1044770	.8795313	$.8065158 \times 10^{-1}$	.9239040	.4888993
.1066820	.8830001	$.8813468 \times 10^{-1}$	.9063316	.4939376
.1089104	.8864287	$.9604133 \times 10^{-1}$	.8889401	.4991261
.1112094	.8898936	.1045653	.8713565	.5045823
.1135572	.8933633	.1136275	.8538146	.5102429
.1159561	.8968447	.1232410	.8363320	.5161067
.1184289	.9003736	.1335098	.8187742	.5222265
.1209579	.9039273	.1443581	.8013205	.5285461
.1235663	.9075417	.1558909	.7838440	.5351168
.1262757	.9112495	.1682129	.7662470	.5419861
.1290528	.9150082	.1811616	.7488100	.5490510
.1319394	.9188786	.1949334	.7313068	.5564087
.1349405	.9228712	.2095466	.7137706	.5640554
.1380618	.9269987	.2250195	.6962298	.5719874

[redacted]

TABLE II.- EXPANSIVE FLOW FIELD OBTAINED BY CHARACTERISTIC CALCULATIONS FOR JET FLOW FROM NEAR-SONIC EXIT ($M_j = 1.0038$; $\mu_j = 85^\circ$) - Continued

x/r_j	y/r_j	θ, radians	μ, radians	V/V_l
0.4374434×10^{-1}	0.5000000	0.0000000	1.483530	0.4095466
$.4846100 \times 10^{-1}$	.5539121	$.1769778 \times 10^{-3}$	1.459177	.4103753
$.5254666 \times 10^{-1}$	.5904221	$.4070187 \times 10^{-3}$	1.438074	.4112601
$.5612414 \times 10^{-1}$	.6173017	$.6869535 \times 10^{-3}$	1.419284	.4121795
$.5977866 \times 10^{-1}$	.6413480	$.1082254 \times 10^{-2}$	1.398890	.4133188
$.6287288 \times 10^{-1}$	.6592853	$.1507881 \times 10^{-2}$	1.381555	.4144042
$.6612807 \times 10^{-1}$	.6764208	$.2088014 \times 10^{-2}$	1.362207	.4157441
$.6896147 \times 10^{-1}$	.6899463	$.2698652 \times 10^{-2}$	1.345323	.4170256
$.7185592 \times 10^{-1}$	.7027234	$.3463248 \times 10^{-2}$	1.327346	.4185064
$.7474510 \times 10^{-1}$	.7145302	$.4385822 \times 10^{-2}$	1.308833	.4201587
$.7740083 \times 10^{-1}$	.7246116	$.5373993 \times 10^{-2}$	1.291702	.4218042
$.8022549 \times 10^{-1}$	.7346720	$.6626444 \times 10^{-2}$	1.272754	.4237574
$.8284144 \times 10^{-1}$	.7433932	$.7955135 \times 10^{-2}$	1.255155	.4256985
$.8543118 \times 10^{-1}$	.7515427	$.9461532 \times 10^{-2}$	1.237464	.4277756
$.8798959 \times 10^{-1}$	.7591641	$.1115108 \times 10^{-1}$	1.219771	.4299813
$.9051491 \times 10^{-1}$	.7663059	$.1302927 \times 10^{-1}$	1.202143	.4323092
$.9309869 \times 10^{-1}$	.7732625	$.1519639 \times 10^{-1}$	1.183843	.4348662
$.9555355 \times 10^{-1}$	.7795588	$.1746859 \times 10^{-1}$	1.166515	.4374222
$.9805710 \times 10^{-1}$	.7857050	$.2004151 \times 10^{-1}$	1.148683	.4401924
.1005254	.7915096	$.2282650 \times 10^{-1}$	1.131099	.4430661
.1030266	.7971580	$.2592415 \times 10^{-1}$	1.113225	.4461355
.1054948	.8025166	$.2924732 \times 10^{-1}$	1.095652	.4493022
.1079898	.8077361	$.3289624 \times 10^{-1}$	1.077912	.4526529
.1105070	.8128170	$.3687826 \times 10^{-1}$	1.060083	.4561801
.1129972	.8176732	$.4110714 \times 10^{-1}$	1.042597	.4597991
.1155546	.8225015	$.4577706 \times 10^{-1}$	1.024726	.4636658
.1180889	.8271374	$.5071022 \times 10^{-1}$	1.007226	.4676211
.1206461	.8316785	$.5600762 \times 10^{-1}$	.9897562	.4717411
.1232636	.8361971	$.6177063 \times 10^{-1}$	.9720677	.4760924
.1259026	.8406303	$.6791599 \times 10^{-1}$	.9544913	.4806003
.1285988	.8450441	$.7454492 \times 10^{-1}$	.9367972	.4853293
.1313192	.8493886	$.8157598 \times 10^{-1}$	.9192626	.4902105
.1340979	.8537241	$.8911124 \times 10^{-1}$	.9016766	.4953066
.1369059	.8580101	$.9706993 \times 10^{-1}$	.8842714	.5005539
.1398041	.8623437	.1056470	.8666767	.5060709
.1427642	.8666847	.1147623	.8491248	.5117938
.1457892	.8710415	.1244286	.8316339	.5177214
.1489083	.8754596	.1347503	.8140683	.5239070
.1520988	.8799099	.1456506	.7966075	.5302938
.1553901	.8844381	.1572345	.7791243	.5369339
.1588101	.8890853	.1696070	.7615211	.5438751
.1623162	.8937976	.1826045	.7440788	.5510132
.1659616	.8986520	.1964235	.7265701	.5584467
.1697527	.9036618	.2110815	.7090277	.5661719
.1736970	.9088429	.2265971	.6914804	.5741848

TABLE II.- EXPANSIVE FLOW FIELD OBTAINED BY CHARACTERISTIC CALCULATIONS

FOR JET FLOW FROM NEAR-SONIC EXIT ($M_j = 1.0038$; $\mu_j = 85^\circ$) - Continued

x/r_j	y/r_j	θ, radians	μ, radians	V/V_l
0.5249321×10^{-1}	0.4000000	0.0000000	1.483530	0.4095466
$.5829498 \times 10^{-1}$	.4663154	$.1892671 \times 10^{-3}$	1.457683	.4104328
$.6328018 \times 10^{-1}$	.5102741	$.4288965 \times 10^{-3}$	1.435842	.4113629
$.6762103 \times 10^{-1}$	.5423475	$.7180689 \times 10^{-3}$	1.416603	.4123207
$.7206156 \times 10^{-1}$	.5710534	$.1124717 \times 10^{-2}$	1.395870	.4135001
$.7579934 \times 10^{-1}$	.5923424	$.1561331 \times 10^{-2}$	1.378302	.4146199
$.7974398 \times 10^{-1}$	.6127506	$.2155338 \times 10^{-2}$	1.358749	.4159981
$.8316185 \times 10^{-1}$	.6287947	$.2779654 \times 10^{-2}$	1.341710	.4173135
$.8666033 \times 10^{-1}$	.6439889	$.3560444 \times 10^{-2}$	1.323594	.4188308
$.9015518 \times 10^{-1}$	.6580482	$.4501390 \times 10^{-2}$	1.304953	.4205215
$.9336009 \times 10^{-1}$	.6700310	$.5508342 \times 10^{-2}$	1.287719	.4222032
$.9677905 \times 10^{-1}$	.6820305	$.6783516 \times 10^{-2}$	1.268668	.4241970
$.9993860 \times 10^{-1}$	.6924155	$.8135174 \times 10^{-2}$	1.250983	.4261768
.1030671	.7021261	$.9666313 \times 10^{-2}$	1.233212	.4282938
.1061581	.7112121	$.1138255 \times 10^{-1}$	1.215448	.4305400
.1092090	.7197296	$.1328895 \times 10^{-1}$	1.197754	.4329093
.1123340	.7280379	$.1548740 \times 10^{-1}$	1.179393	.4355101
.1152990	.7355502	$.1779083 \times 10^{-1}$	1.162009	.4381087
.1183254	.7428920	$.2039773 \times 10^{-1}$	1.144126	.4409235
.1213085	.7498263	$.2321800 \times 10^{-1}$	1.126497	.4438421
.1243329	.7565793	$.2635318 \times 10^{-1}$	1.108580	.4469581
.1273166	.7629857	$.2971503 \times 10^{-1}$	1.090969	.4501715
.1303336	.7692297	$.3340455 \times 10^{-1}$	1.073195	.4535704
.1333782	.7753107	$.3742883 \times 10^{-1}$	1.055334	.4571472
.1363893	.7811225	$.4170062 \times 10^{-1}$	1.037820	.4608159
.1394834	.7869056	$.4641547 \times 10^{-1}$	1.019923	.4647346
.1425488	.7924577	$.5139394 \times 10^{-1}$	1.002399	.4687420
.1456422	.7978984	$.5673795 \times 10^{-1}$	.9849107	.4729149
.1488097	.8033152	$.6254921 \times 10^{-1}$	.9672045	.4773210
.1520035	.8086308	$.6874335 \times 10^{-1}$	.9496129	.4818847
.1552675	.8139254	$.7542225 \times 10^{-1}$	.9319064	.4866710
.1585608	.8191381	$.8250338 \times 10^{-1}$	.9143605	.4916105
.1619253	.8243421	$.9008921 \times 10^{-1}$	.8967649	.4967665
.1653256	.8294877	$.9809850 \times 10^{-1}$	.8793534	.5020743
.1688362	.8346931	.1067266	.8617523	.5076541
.1724224	.8399091	.1158930	.8441961	.5134411
.1760879	.8451458	.1256096	.8267019	.5194343
.1798684	.8504583	.1359815	.8091342	.5256874
.1837360	.8558114	.1469309	.7916717	.5321431
.1877270	.8612601	.1585628	.7741886	.5388540
.1918753	.8668545	.1709824	.7565855	.5458684
.1961290	.8725292	.1840245	.7391430	.5530812
.2005530	.8783775	.1978861	.7216345	.5605918
.2051553	.8844156	.2125846	.7040924	.5683963
.2099451	.8906628	.2281373	.6865449	.5764911

[redacted]

TABLE II.- EXPANSIVE FLOW FIELD OBTAINED BY CHARACTERISTIC CALCULATIONS FOR JET FLOW FROM NEAR-SONIC EXIT ($M_j = 1.0038$; $\mu_j = 85^\circ$) - Continued

x/r_j	y/r_j	θ, radians	μ, radians	V/V_l
0.6124208×10^{-1}	0.3000000	0.0000000	1.483530	0.4095466
$.6818709 \times 10^{-1}$	.3793820	$.2046700 \times 10^{-3}$	1.455848	.4105046
$.7410973 \times 10^{-1}$	.4307716	$.4539568 \times 10^{-3}$	1.433143	.4114894
$.7924108 \times 10^{-1}$	.4679374	$.7521654 \times 10^{-3}$	1.413425	.4124916
$.8449095 \times 10^{-1}$	.5011833	$.1169917 \times 10^{-2}$	1.392335	.4137164
$.8888973 \times 10^{-1}$	.5257342	$.1617429 \times 10^{-2}$	1.374541	.4148742
$.9354089 \times 10^{-1}$	.5493280	$.2225322 \times 10^{-2}$	1.354791	.4162941
$.9755704 \times 10^{-1}$	.5678273	$.2863299 \times 10^{-2}$	1.337606	.4176465
.1016731	.5853805	$.3660290 \times 10^{-2}$	1.319359	.4192033
.1057869	.6016422	$.4619959 \times 10^{-2}$	1.300604	.4209350
.1095527	.6154870	$.5645864 \times 10^{-2}$	1.283275	.4226555
.1135784	.6293890	$.6943925 \times 10^{-2}$	1.264133	.4246928
.1172928	.6414088	$.8318573 \times 10^{-2}$	1.246370	.4267141
.1209713	.6526554	$.9874819 \times 10^{-2}$	1.228529	.4288733
.1246058	.6631845	$.1161785 \times 10^{-1}$	1.210701	.4311626
.1281933	.6730591	$.1355278 \times 10^{-1}$	1.192950	.4335757
.1318706	.6827029	$.1578292 \times 10^{-1}$	1.174536	.4362226
.1353564	.6914182	$.1811804 \times 10^{-1}$	1.157107	.4388658
.1389166	.6999439	$.2075924 \times 10^{-1}$	1.139181	.4417275
.1424253	.7079981	$.2361493 \times 10^{-1}$	1.121514	.4446933
.1459840	.7158474	$.2678776 \times 10^{-1}$	1.103561	.4478583
.1494941	.7232950	$.3018798 \times 10^{-1}$	1.085920	.4511210
.1530444	.7305578	$.3391800 \times 10^{-1}$	1.068118	.4545704
.1566279	.7376344	$.3798433 \times 10^{-1}$	1.050233	.4581991
.1601714	.7443983	$.4229866 \times 10^{-1}$	1.032698	.4619198
.1638142	.7511336	$.4705846 \times 10^{-1}$	1.014782	.4658925
.1674226	.7576006	$.5208180 \times 10^{-1}$	.9972434	.4699541
.1710646	.7639398	$.5747163 \times 10^{-1}$	.9797411	.4741822
.1747950	.7702547	$.6333010 \times 10^{-1}$	.9620242	.4786455
.1785567	.7764534	$.6957195 \times 10^{-1}$	.9444241	.4832671
.1824019	.7826305	$.7629980 \times 10^{-1}$	.9267116	.4881128
.1862819	.7887137	$.8342972 \times 10^{-1}$	.9091618	.4931126
.1902467	.7947891	$.9106489 \times 10^{-1}$	.8915638	.4983303
.1942540	.8007980	$.9912289 \times 10^{-1}$	.8741514	.5037007
.1983926	.8068797	.1078003	.8565517	.5093451
.2026211	.8129759	.1170153	.8389974	.5151981
.2069439	.8190985	.1267798	.8215065	.5212587
.2114035	.8253123	.1371988	.8039429	.5275812
.2159669	.8315757	.1481939	.7864864	.5341075
.2206771	.8379536	.1598703	.7690086	.5408908
.2255745	.8445050	.1723332	.7514124	.5479799
.2305974	.8511529	.1854155	.7339768	.5552688
.2358232	.8580072	.1993149	.7164755	.5628577
.2412614	.8650870	.2140484	.6989406	.5707428
.2469232	.8724153	.2296329	.6813999	.5789202

TABLE II.- EXPANSIVE FLOW FIELD OBTAINED BY CHARACTERISTIC CALCULATIONS FOR JET FLOW FROM NEAR-SONIC EXIT $(M_j = 1.0038;\ \mu_j = 85^\circ)$ - Continued

x/r_j	y/r_j	θ, radians	μ, radians	V/V_l
0.6999094×10^{-1}	0.2000000	0.0000000	1.483530	0.4095466
$.7814935 \times 10^{-1}$	.2932515	$.2247088 \times 10^{-3}$	1.453487	.4105986
$.8505892 \times 10^{-1}$	.3519959	$.4821653 \times 10^{-3}$	1.429748	.4116522
$.9101575 \times 10^{-1}$	.3940939	$.7881754 \times 10^{-3}$	1.409518	.4127066
$.9710577 \times 10^{-1}$	.4317140	$.1216019 \times 10^{-2}$	1.388083	.4139827
.1021880	.4594072	$.1673625 \times 10^{-2}$	1.370074	.4151829
.1075677	.4860763	$.2294754 \times 10^{-2}$	1.350148	.4166487
.1121998	.5069522	$.2945972 \times 10^{-2}$	1.332837	.4180413
.1169509	.5267952	$.3758884 \times 10^{-2}$	1.314481	.4196408
.1217005	.5452002	$.4736880 \times 10^{-2}$	1.295630	.4214169
.1260422	.5608616	$.5781489 \times 10^{-2}$	1.278224	.4231790
.1306907	.5766236	$.7102420 \times 10^{-2}$	1.259009	.4252627
.1349745	.5902456	$.8500224 \times 10^{-2}$	1.241187	.4273279
.1392172	.6030010	$.1008146 \times 10^{-1}$	1.223291	.4295321
.1434093	.6149500	$.1185140 \times 10^{-1}$	1.205415	.4318671
.1475471	.6261626	$.1381485 \times 10^{-1}$	1.187620	.4343266
.1517909	.6371252	$.1607636 \times 10^{-1}$	1.169165	.4370226
.1558109	.6470301	$.1844303 \times 10^{-1}$	1.151703	.4397131
.1599187	.6567285	$.2111829 \times 10^{-1}$	1.133746	.4426244
.1639668	.6658933	$.2400926 \times 10^{-1}$	1.116052	.4456400
.1680739	.6748313	$.2721963 \times 10^{-1}$	1.098076	.4488565
.1721244	.6833140	$.3065816 \times 10^{-1}$	1.080414	.4521708
.1762224	.6915909	$.3442824 \times 10^{-1}$	1.062595	.4556734
.1803594	.6996596	$.3853618 \times 10^{-1}$	1.044695	.4593565
.1844498	.7073737	$.4289255 \times 10^{-1}$	1.027148	.4631316
.1886564	.7150602	$.4769630 \times 10^{-1}$	1.009223	.4671611
.1928230	.7224419	$.5276399 \times 10^{-1}$	.9916790	.4712791
.1970289	.7296808	$.5819882 \times 10^{-1}$	.9741735	.4755647
.2013382	.7368956	$.6410367 \times 10^{-1}$	.9564550	.4800874
.2056841	.7439802	$.7039212 \times 10^{-1}$	.9388551	.4847692
.2101275	.7510433	$.7716695 \times 10^{-1}$	.9211450	.4896769
.2146117	.7580012	$.8434381 \times 10^{-1}$	.9035992	.4947394
.2191948	.7649533	$.9202616 \times 10^{-1}$	.8860077	.5000212
.2238276	.7718315	.1001310	.8686035	.5054562
.2286136	.7787963	.1088551	.8510128	.5111674
.2335046	.7857805	.1181159	.8334690	.5170887
.2385057	.7927976	.1279254	.8159898	.5232186
.2436665	.7999223	.1383884	.7984393	.5296123
.2489486	.8071068	.1494258	.7809963	.5362110
.2544021	.8144258	.1611428	.7635334	.5430684
.2600741	.8219473	.1736441	.7459518	.5502340
.2658930	.8295828	.1867621	.7285314	.5576004
.2719490	.8374589	.2006942	.7110456	.5652689
.2782534	.8455980	.2154575	.6935263	.5732356
.2848195	.8540266	.2310674	.6760010	.5814967

[redacted]

TABLE II.- EXPANSIVE FLOW FIELD OBTAINED BY CHARACTERISTIC CALCULATIONS FOR JET FLOW FROM NEAR-SONIC EXIT $\left(M_j = 1.0038;\ \mu_j = 85^\circ\right)$ - Continued

x/r_j	y/r_j	θ, radians	μ, radians	V/V_l
0.7436538×10^{-1}	0.1500000	0.0000000	1.483530	0.4095466
$.8317474 \times 10^{-1}$	.2506917	$.2386524 \times 10^{-3}$	1.451882	.4106636
$.9060919 \times 10^{-1}$	.3130420	$.4982903 \times 10^{-3}$	1.427539	.4117602
$.9699916 \times 10^{-1}$	.3574981	$.8071739 \times 10^{-3}$	1.407067	.4128441
.1035258	.3972036	$.1239396 \times 10^{-2}$	1.385492	.4141482
.1089613	.4263999	$.1701726 \times 10^{-2}$	1.367401	.4153710
.1147162	.4545451	$.2329333 \times 10^{-2}$	1.347415	.4168611
.1196649	.4765663	$.2987052 \times 10^{-2}$	1.330061	.4182750
.1247419	.4975168	$.3807868 \times 10^{-2}$	1.311667	.4198972
.1298175	.5169622	$.4795145 \times 10^{-2}$	1.292788	.4216966
.1344541	.5335087	$.5849218 \times 10^{-2}$	1.275356	.4234807
.1394214	.5501795	$.7181786 \times 10^{-2}$	1.256122	.4255887
.1439965	.5645866	$.8591396 \times 10^{-2}$	1.238280	.4276770
.1485279	.5780827	$.1018549 \times 10^{-1}$	1.220369	.4299046
.1530053	.5907303	$.1196911 \times 10^{-1}$	1.202479	.4322636
.1574246	.6026027	$.1394722 \times 10^{-1}$	1.184673	.4347472
.1619583	.6142166	$.1622486 \times 10^{-1}$	1.166208	.4374687
.1662516	.6247101	$.1860736 \times 10^{-1}$	1.148736	.4401841
.1706396	.6349897	$.2130002 \times 10^{-1}$	1.130771	.4431212
.1749637	.6447058	$.2420885 \times 10^{-1}$	1.113070	.4461628
.1793514	.6541850	$.2743800 \times 10^{-1}$	1.095088	.4494063
.1836786	.6631828	$.3089573 \times 10^{-1}$	1.077422	.4527476
.1880569	.6719652	$.3468587 \times 10^{-1}$	1.059600	.4562779
.1924773	.6805290	$.3881461 \times 10^{-1}$	1.041699	.4599893
.1968479	.6887175	$.4319203 \times 10^{-1}$	1.024153	.4637926
.2013435	.6968795	$.4801800 \times 10^{-1}$	1.006230	.4678513
.2057962	.7047190	$.5310770 \times 10^{-1}$	.9886891	.4719985
.2102912	.7124086	$.5856505 \times 10^{-1}$	.9711876	.4763137
.2148974	.7200747	$.6449304 \times 10^{-1}$	.9534734	.4808670
.2195430	.7276040	$.7080453 \times 10^{-1}$	.9358805	.4855797
.2242934	.7351123	$.7760280 \times 10^{-1}$	.9181773	.4905191
.2290877	.7425102	$.8480291 \times 10^{-1}$	.9006386	.4956137
.2339883	.7499036	$.9250828 \times 10^{-1}$	.8830554	.5009283
.2389425	.7572198	.1006356	.8656597	.5063966
.2440612	.7646300	.1093821	.8480784	.5121421
.2492929	.7720624	.1186651	.8305447	.5180980
.2546430	.7795313	.1284958	.8130760	.5242634
.2601646	.7871167	.1389796	.7955368	.5306933
.2658167	.7947674	.1500364	.7781049	.5373289
.2716532	.8025630	.1617719	.7606537	.5442239
.2777245	.8105764	.1742904	.7430838	.5514283
.2839541	.8187130	.1874243	.7256758	.5588338
.2904386	.8271081	.2013705	.7082021	.5665424
.2971902	.8357857	.2161456	.6906951	.5745503
.3042234	.8447744	.2317650	.6731811	.5828536

[redacted]

TABLE II.- EXPANSIVE FLOW FIELD OBTAINED BY CHARACTERISTIC CALCULATIONS FOR JET FLOW FROM NEAR-SONIC EXIT $(M_j = 1.0038;\ \mu_j = 85^\circ)$ - Continued

x/r_j	y/r_j	θ, radians	μ, radians	V/V_l
0.7873981×10^{-1}	0.1000000	0.0000000	1.483530	0.4095466
$.8822959 \times 10^{-1}$	.2084695	$.2556294 \times 10^{-3}$	1.449943	.4107434
$.9621177 \times 10^{-1}$	.2743377	$.5141673 \times 10^{-3}$	1.424918	.4118908
.1030506	.3210518	$.8245088 \times 10^{-3}$	1.404224	.4130064
.1100271	.3627573	$.1260242 \times 10^{-2}$	1.382538	.4143397
.1158255	.3934025	$.1726781 \times 10^{-2}$	1.364394	.4155859
.1219648	.4229777	$.2360357 \times 10^{-2}$	1.344369	.4171012
.1272373	.4461141	$.3024302 \times 10^{-2}$	1.326990	.4185370
.1326474	.4681468	$.3852923 \times 10^{-2}$	1.308578	.4201823
.1380558	.4886121	$.4849346 \times 10^{-2}$	1.289684	.4220056
.1429935	.5060287	$.5912788 \times 10^{-2}$	1.272240	.4238122
.1482860	.5235951	$.7256931 \times 10^{-2}$	1.252995	.4259453
.1531584	.5387772	$.8678228 \times 10^{-2}$	1.235144	.4280573
.1579842	.5530065	$.1028505 \times 10^{-1}$	1.217228	.4303091
.1627525	.5663467	$.1208232 \times 10^{-1}$	1.199330	.4326928
.1674589	.5788740	$.1407484 \times 10^{-1}$	1.181519	.4352014
.1722882	.5911355	$.1636853 \times 10^{-1}$	1.163051	.4379492
.1768602	.6022150	$.1876707 \times 10^{-1}$	1.145575	.4406900
.1815340	.6130738	$.2147700 \times 10^{-1}$	1.127609	.4436536
.1861396	.6233400	$.2440380 \times 10^{-1}$	1.109907	.4467218
.1908136	.6333596	$.2765189 \times 10^{-1}$	1.091928	.4499928
.1954230	.6428724	$.3112905 \times 10^{-1}$	1.074264	.4533615
.2000874	.6521604	$.3493948 \times 10^{-1}$	1.056444	.4569200
.2047971	.6612198	$.3908901 \times 10^{-1}$	1.038547	.4606604
.2094536	.6698838	$.4348733 \times 10^{-1}$	1.021005	.4644927
.2142441	.6785228	$.4833524 \times 10^{-1}$	1.003088	.4685814
.2189888	.6868218	$.5344646 \times 10^{-1}$	.9855518	.4727588
.2237790	.6949641	$.5892553 \times 10^{-1}$	.9680567	.4771047
.2286884	.7030838	$.6487617 \times 10^{-1}$	.9503516	.4816893
.2336401	.7110603	$.7121040 \times 10^{-1}$	.9327677	.4864337
.2387042	.7190166	$.7803149 \times 10^{-1}$	.9150741	.4914057
.2438154	.7268575	$.8525399 \times 10^{-1}$	.8975462	.4965332
.2490406	.7346955	$.9298199 \times 10^{-1}$	.8799746	.5018813
.2543234	.7424532	.1011313	.8625908	.5073834
.2597823	.7503128	.1098997	.8450224	.5131637
.2653624	.7581976	.1192035	.8275017	.5191553
.2710695	.7661229	.1290548	.8100463	.5253567
.2769604	.7741738	.1395581	.7925212	.5318236
.2829914	.7822958	.1506336	.7751036	.5384965
.2892199	.7905738	.1623862	.7576670	.5454298
.2957002	.7990851	.1749211	.7401124	.5526733
.3023504	.8077294	.1880694	.7227197	.5601183
.3092743	.8166504	.2020282	.7052613	.5678675
.3164847	.8258741	.2168137	.6877689	.5759170
.3239973	.8354310	.2324409	.6702701	.5842627

[redacted]

TABLE II.- EXPANSIVE FLOW FIELD OBTAINED BY CHARACTERISTIC CALCULATIONS FOR JET FLOW FROM NEAR-SONIC EXIT ($M_j = 1.0038$; $\mu_j = 85^\circ$) - Continued

x/r_j	y/r_j	θ, radians	μ, radians	V/V_l
0.8223936×10^{-1}	0.6000000×10^{-1}	0.0000000	1.483530	0.4095466
$.9230156 \times 10^{-1}$	.1750118	$.2728449 \times 10^{-3}$	1.448016	.4108239
.1007453	.2435908	$.5254415 \times 10^{-3}$	1.422354	.4120208
.1079591	.2920036	$.8354714 \times 10^{-3}$	1.401534	.4131627
.1153084	.3352248	$.1273159 \times 10^{-2}$	1.379806	.4145197
.1214059	.3669786	$.1742626 \times 10^{-2}$	1.361651	.4157847
.1278613	.3976561	$.2380778 \times 10^{-2}$	1.341628	.4173202
.1333997	.4216570	$.3049612 \times 10^{-2}$	1.324251	.4187736
.1390828	.4445335	$.3884348 \times 10^{-2}$	1.305843	.4204377
.1447637	.4657976	$.4887969 \times 10^{-2}$	1.286954	.4222805
.1499480	.4838975	$.5958929 \times 10^{-2}$	1.269514	.4241054
.1555067	.5021695	$.7312255 \times 10^{-2}$	1.250272	.4262591
.1606222	.5179644	$.8742921 \times 10^{-2}$	1.232426	.4283905
.1656888	.5327743	$.1035993 \times 10^{-1}$	1.214511	.4306622
.1706950	.5466643	$.1216819 \times 10^{-1}$	1.196618	.4330661
.1756362	.5597122	$.1417240 \times 10^{-1}$	1.178809	.4355951
.1807072	.5724894	$.1647885 \times 10^{-1}$	1.160345	.4383646
.1855072	.5840361	$.1889034 \times 10^{-1}$	1.142874	.4411261
.1904147	.5953574	$.2161420 \times 10^{-1}$	1.124912	.4441115
.1952506	.6060633	$.2455538 \times 10^{-1}$	1.107216	.4472015
.2001587	.6165155	$.2781881 \times 10^{-1}$	1.089241	.4504950
.2049990	.6264408	$.3131135 \times 10^{-1}$	1.071583	.4538864
.2098974	.6361344	$.3513791 \times 10^{-1}$	1.053771	.4574681
.2148437	.6455918	$.3930410 \times 10^{-1}$	1.035881	.4612322
.2197341	.6546380	$.4371924 \times 10^{-1}$	1.018347	.4650881
.2247659	.6636605	$.4858451 \times 10^{-1}$	1.000437	.4692015
.2297497	.6723292	$.5371339 \times 10^{-1}$	.9829109	.4734033
.2347817	.6808359	$.5921025 \times 10^{-1}$	.9654258	.4777740
.2399393	.6893212	$.6517869 \times 10^{-1}$	.9477298	.4823844
.2451417	.6976584	$.7153049 \times 10^{-1}$	.9301556	.4871550
.2504627	.7059762	$.7836962 \times 10^{-1}$	.9124741	.4921535
.2558336	.7141748	$.8560992 \times 10^{-1}$	.8949575	.4973079
.2613248	.7223721	$.9335522 \times 10^{-1}$	.8773974	.5026836
.2668769	.7304868	.1015214	.8600251	.5082135
.2726148	.7387098	.1103065	.8424698	.5140224
.2784807	.7469608	.1196270	.8249627	.5200427
.2844805	.7552559	.1294940	.8075212	.5262734
.2906744	.7636841	.1400123	.7900095	.5327704
.2970164	.7721883	.1511018	.7726063	.5394737
.3035670	.7808575	.1628676	.7551846	.5464379
.3103833	.7897730	.1754143	.7376447	.5537133
.3173794	.7988295	.1885726	.7202657	.5611906
.3246643	.8081781	.2025405	.7028223	.5689726
.3322520	.8178459	.2173331	.6853444	.5770556
.3401592	.8278651	.2329653	.6678605	.5854354

[redacted]

TABLE II.- EXPANSIVE FLOW FIELD OBTAINED BY CHARACTERISTIC CALCULATIONS FOR JET FLOW FROM NEAR-SONIC EXIT $(M_j = 1.0038;\ \mu_j = 85^\circ)$ - Continued

x/r_j	y/r_j	θ, radians	μ, radians	V/V_l
0.8398913×10^{-1}	0.4000000×10^{-1}	0.0000000	1.483530	0.4095466
$.9435119 \times 10^{-1}$	.1584395	$.2836015 \times 10^{-3}$	1.446832	.4108741
.1030377	.2283162	$.5300123 \times 10^{-3}$	1.420832	.4120990
.1104461	.2775238	$.8392017 \times 10^{-3}$	1.399983	.4132539
.1179873	.3214634	$.1277553 \times 10^{-2}$	1.378266	.4146224
.1242382	.3537480	$.1748338 \times 10^{-2}$	1.360123	.4158966
.1308553	.3849577	$.2388767 \times 10^{-2}$	1.340118	.4174420
.1365294	.4093794	$.3059989 \times 10^{-2}$	1.322753	.4189042
.1423518	.4326681	$.3897827 \times 10^{-2}$	1.304358	.4205776
.1481717	.4543240	$.4905148 \times 10^{-2}$	1.285478	.4224302
.1534815	.4727609	$.5979965 \times 10^{-2}$	1.268049	.4242642
.1591757	.4913818	$.7338026 \times 10^{-2}$	1.248815	.4264282
.1644150	.5074801	$.8773406 \times 10^{-2}$	1.230975	.4285695
.1696042	.5225782	$.1039552 \times 10^{-1}$	1.213066	.4308513
.1747315	.5367415	$.1220948 \times 10^{-1}$	1.195179	.4332653
.1797922	.5500487	$.1421949 \times 10^{-1}$	1.177375	.4358049
.1849862	.5630832	$.1653241 \times 10^{-1}$	1.158914	.4385854
.1899022	.5748632	$.1895033 \times 10^{-1}$	1.141448	.4413576
.1949287	.5864157	$.2168122 \times 10^{-1}$	1.123491	.4443541
.1998818	.5973416	$.2462951 \times 10^{-1}$	1.105800	.4474553
.2049092	.6080103	$.2790045 \times 10^{-1}$	1.087830	.4507604
.2098670	.6181424	$.3140083 \times 10^{-1}$	1.070177	.4541633
.2148846	.6280394	$.3523550 \times 10^{-1}$	1.052370	.4577568
.2199514	.6376966	$.3941006 \times 10^{-1}$	1.034485	.4615330
.2249610	.6469347	$.4383367 \times 10^{-1}$	1.016957	.4654009
.2301157	.6561501	$.4870760 \times 10^{-1}$	.9990534	.4695269
.2352212	.6650049	$.5384508 \times 10^{-1}$	.9815326	.4737413
.2403763	.6736951	$.5935046 \times 10^{-1}$	.9640532	.4781248
.2456604	.6823645	$.6532786 \times 10^{-1}$	.9463645	.4827482
.2509906	.6908834	$.7168892 \times 10^{-1}$	.9287973	.4875318
.2564426	.6993835	$.7853689 \times 10^{-1}$	.9111227	.4925439
.2619459	.7077625	$.8578595 \times 10^{-1}$	.8936131	.4977120
.2675727	.7161411	$.9354010 \times 10^{-1}$	.8760607	.5031015
.2732621	.7244361	.1017149	.8586966	.5086453
.2791424	.7328427	.1105084	.8411490	.5144686
.2851540	.7412788	.1198369	.8236498	.5205035
.2913034	.7497607	.1297116	.8062167	.5267491
.2976521	.7583797	.1402373	.7887130	.5332612
.3041528	.7670773	.1513335	.7713183	.5399799
.3108678	.7759447	.1631054	.7539044	.5469598
.3178556	.7850650	.1756576	.7363728	.5542513
.3250282	.7943305	.1888208	.7190026	.5617448
.3324975	.8038959	.2027927	.7015672	.5695433
.3402780	.8137890	.2175884	.6840981	.5776431
.3483869	.8240429	.2332230	.6666225	.5860399

[redacted]

TABLE II.- EXPANSIVE FLOW FIELD OBTAINED BY CHARACTERISTIC CALCULATIONS FOR JET FLOW FROM NEAR-SONIC EXIT $\left(M_j = 1.0038;\ \mu_j = 85^\circ\right)$ - Continued

x/r_j	y/r_j	θ, radians	μ, radians	V/V_l
0.8573891×10^{-1}	0.2000000×10^{-1}	0.0000000	1.483530	0.4095466
$.9640913 \times 10^{-1}$	.1419617	$.2957617 \times 10^{-3}$	1.445495	.4109313
.1053469	.2130881	$.5327943 \times 10^{-3}$	1.419124	.4121878
.1129557	.2630474	$.8407074 \times 10^{-3}$	1.398279	.4133552
.1206934	.3076758	$.1279626 \times 10^{-2}$	1.376596	.4147346
.1271007	.3404757	$.1751733 \times 10^{-2}$	1.358486	.4160176
.1338823	.3722060	$.2394370 \times 10^{-2}$	1.338508	.4175728
.1396945	.3970407	$.3067911 \times 10^{-2}$	1.321163	.4190438
.1456583	.4207365	$.3908738 \times 10^{-2}$	1.302786	.4207266
.1516193	.4427803	$.4919721 \times 10^{-2}$	1.283923	.4225890
.1570566	.4615510	$.5998251 \times 10^{-2}$	1.266506	.4244323
.1628884	.4805185	$.7361128 \times 10^{-2}$	1.247287	.4266066
.1682533	.4969190	$.8801193 \times 10^{-2}$	1.229456	.4287578
.1735669	.5123044	$.1042857 \times 10^{-1}$	1.211557	.4310497
.1788170	.5267407	$.1224802 \times 10^{-1}$	1.193678	.4334741
.1839989	.5403071	$.1426407 \times 10^{-1}$	1.175882	.4360241
.1893178	.5535987	$.1658363 \times 10^{-1}$	1.157431	.4388156
.1943515	.5656123	$.1900813 \times 10^{-1}$	1.139970	.4415985
.1994987	.5773964	$.2174599 \times 10^{-1}$	1.122020	.4446063
.2045707	.5885429	$.2470155 \times 10^{-1}$	1.104336	.4477187
.2097190	.5994290	$.2798032 \times 10^{-1}$	1.086373	.4510354
.2147960	.6097688	$.3148850 \times 10^{-1}$	1.068726	.4544499
.2199345	.6198701	$.3533131 \times 10^{-1}$	1.050926	.4580554
.2251236	.6297280	$.3951431 \times 10^{-1}$	1.033048	.4618438
.2302541	.6391590	$.4394629 \times 10^{-1}$	1.015526	.4657240
.2355336	.6485683	$.4882919 \times 10^{-1}$	.9976309	.4698625
.2407628	.6576101	$.5397533 \times 10^{-1}$	.9801170	.4740896
.2460429	.6664849	$.5948947 \times 10^{-1}$	.9626444	.4784860
.2514554	.6753397	$.6547586 \times 10^{-1}$	.9449635	.4831226
.2569153	.6840416	$.7184545 \times 10^{-1}$	.9274036	.4879198
.2625002	.6927254	$.7870217 \times 10^{-1}$	.9097362	.4929457
.2681379	.7012863	$.8596008 \times 10^{-1}$	.8922349	.4981275
.2739025	.7098476	$.9372271 \times 10^{-1}$	.8746905	.5035312
.2797314	.7183244	.1019057	.8573346	.5090893
.2857563	.7269162	.1107078	.8397960	.5149270
.2919160	.7355390	.1200442	.8223060	.5209767
.2982172	.7442096	.1299266	.8048812	.5272372
.3047231	.7530213	.1404597	.7873875	.5337646
.3113852	.7619142	.1515623	.7700009	.5404989
.3182673	.7709818	.1633403	.7525964	.5474946
.3254297	.7803089	.1758979	.7350737	.5548023
.3327820	.7897855	.1890656	.7177124	.5623122
.3404391	.7995700	.2030413	.7002863	.5701274
.3484158	.8096910	.2178394	.6828258	.5782444
.3567298	.8201823	.2334753	.6653590	.5866587

[redacted]

[redacted]

TABLE II.- EXPANSIVE FLOW FIELD OBTAINED BY CHARACTERISTIC CALCULATIONS

FOR JET FLOW FROM NEAR-SONIC EXIT $\left(M_j = 1.0038;\ \mu_j = 85^\circ\right)$ - Continued

x/r_j	y/r_j	θ, radians	μ, radians	V/V_l
0.8748868×10^{-1}	0.0000000	0.0000000	1.483530	0.4095466
$.9847630 \times 10^{-1}$	.1255896	$.5022097 \times 10^{-4}$	1.468986	.4100168
.1065861	.2050094	$.5568377 \times 10^{-3}$	1.419323	.4121774
.1142703	.2555404	$.8599938 \times 10^{-3}$	1.398091	.4133664
.1220925	.3006100	$.1296705 \times 10^{-2}$	1.376211	.4147606
.1285713	.3337110	$.1768165 \times 10^{-2}$	1.358007	.4160531
.1354303	.3657314	$.2410894 \times 10^{-2}$	1.337964	.4176172
.1413086	.3907899	$.3085008 \times 10^{-2}$	1.320581	.4190951
.1473411	.4147012	$.3926850 \times 10^{-2}$	1.302175	.4207848
.1533711	.4369481	$.4939281 \times 10^{-2}$	1.283291	.4226539
.1588711	.4558921	$.6019411 \times 10^{-2}$	1.265857	.4245033
.1647709	.4750381	$.7384276 \times 10^{-2}$	1.246624	.4266842
.1701982	.4915933	$.8826518 \times 10^{-2}$	1.228785	.4288414
.1755736	.5071256	$.1045614 \times 10^{-1}$	1.210876	.4311395
.1808850	.5217007	$.1227820 \times 10^{-1}$	1.192991	.4335700
.1861275	.5353986	$.1429698 \times 10^{-1}$	1.175190	.4361261
.1915088	.5488207	$.1661972 \times 10^{-1}$	1.156736	.4389237
.1966015	.5609525	$.1904735 \times 10^{-1}$	1.139273	.4417126
.2018092	.5728538	$.2178862 \times 10^{-1}$	1.121321	.4447266
.2069408	.5841118	$.2474766 \times 10^{-1}$	1.103634	.4478452
.2121498	.5951077	$.2803001 \times 10^{-1}$	1.085670	.4511683
.2172868	.6055522	$.3154209 \times 10^{-1}$	1.068024	.4545890
.2224860	.6157567	$.3538870 \times 10^{-1}$	1.050223	.4582011
.2277366	.6257158	$.3957580 \times 10^{-1}$	1.032346	.4619960
.2329280	.6352440	$.4401178 \times 10^{-1}$	1.014825	.4658827
.2382703	.6447510	$.4889869 \times 10^{-1}$	.9969308	.4700281
.2435617	.6538872	$.5404916 \times 10^{-1}$	.9794186	.4742618
.2489047	.6628551	$.5956781 \times 10^{-1}$	.9619493	.4786647
.2543819	.6718033	$.6555845 \times 10^{-1}$	.9442705	.4833083
.2599072	.6805974	$.7193277 \times 10^{-1}$	.9267138	.4881122
.2655591	.6893738	$.7879381 \times 10^{-1}$	.9090488	.4931453
.2712645	.6980264	$.8605600 \times 10^{-1}$	.8915508	.4983342
.2770985	.7066798	$.9382311 \times 10^{-1}$	.8740106	.5037450
.2829977	.7152482	.1020103	.8566582	.5093103
.2890955	.7239334	.1108162	.8391225	.5151557
.2953298	.7326504	.1201561	.8216353	.5212132
.3017075	.7414161	.1300423	.8042153	.5274813
.3082927	.7503249	.1405787	.7867253	.5340166
.3150361	.7593164	.1516847	.7693430	.5407587
.3220026	.7684848	.1634651	.7519420	.5477627
.3292530	.7779163	.1760256	.7344240	.5550785
.3366958	.7874995	.1891957	.7170672	.5625966
.3444474	.7973946	.2031729	.6996454	.5704203
.3525230	.8076305	.2179723	.6821891	.5785459
.3609406	.8182415	.2336091	.6647269	.5869688

[redacted]

TABLE II.- EXPANSIVE FLOW FIELD OBTAINED BY CHARACTERISTIC CALCULATIONS FOR JET FLOW FROM NEAR-SONIC EXIT (M_j = 1.0038; μ_j = 85°) - Continued

x/r_j	y/r_j	θ, radians	μ, radians	V/V_l
0.1113133	0.0000000	0.0000000	1.458017	0.4104199
.1226543	.1001341	$.1093971 \times 10^{-3}$	1.439118	.4112127
.1307679	.1614455	$.9267815 \times 10^{-3}$	1.388465	.4139586
.1398650	.2110428	$.1330155 \times 10^{-2}$	1.365541	.4155035
.1473816	.2473901	$.1793538 \times 10^{-2}$	1.347105	.4168853
.1553399	.2826643	$.2437950 \times 10^{-2}$	1.327019	.4185345
.1621432	.3103040	$.3119146 \times 10^{-2}$	1.309662	.4200819
.1691254	.3367619	$.3973541 \times 10^{-2}$	1.291315	.4218428
.1761033	.3614450	$.5003369 \times 10^{-2}$	1.272504	.4237840
.1824600	.3824943	$.6102750 \times 10^{-2}$	1.255139	.4257004
.1892846	.4038321	$.7492855 \times 10^{-2}$	1.235983	.4279553
.1955566	.4223038	$.8961520 \times 10^{-2}$	1.218210	.4301822
.2017686	.4396642	$.1062050 \times 10^{-1}$	1.200366	.4325511
.2079063	.4559798	$.1247478 \times 10^{-1}$	1.182543	.4350534
.2139641	.4713352	$.1452821 \times 10^{-1}$	1.164803	.4376820
.2201850	.4864058	$.1688941 \times 10^{-1}$	1.146408	.4405562
.2260694	.5000380	$.1935564 \times 10^{-1}$	1.129000	.4434188
.2320891	.5134299	$.2213884 \times 10^{-1}$	1.111103	.4465099
.2380207	.5261101	$.2514135 \times 10^{-1}$	1.093472	.4497056
.2440436	.5385092	$.2846995 \times 10^{-1}$	1.075564	.4531082
.2499831	.5502965	$.3202882 \times 10^{-1}$	1.057971	.4566087
.2559963	.5618243	$.3592440 \times 10^{-1}$	1.040224	.4603026
.2620702	.5730853	$.4016213 \times 10^{-1}$	1.022404	.4641809
.2680758	.5838667	$.4464885 \times 10^{-1}$	1.004938	.4681508
.2742584	.5946346	$.4958879 \times 10^{-1}$	.9871017	.4723825
.2803825	.6049893	$.5479161 \times 10^{-1}$	.9696460	.4767024
.2865678	.6151608	$.6036287 \times 10^{-1}$	.9522338	.4811928
.2929106	.6253185	$.6640718 \times 10^{-1}$	.9346141	.4859263
.2993106	.6353084	$.7283452 \times 10^{-1}$	.9171172	.4908212
.3058593	.6452857	$.7974912 \times 10^{-1}$	.8995153	.4959470
.3124716	.6551289	$.8706345 \times 10^{-1}$	.8820792	.5012296
.3192350	.6649802	$.9488181 \times 10^{-1}$	.8646014	.5067360
.3260760	.6747410	.1031187	.8473129	.5123973
.3331501	.6846423	.1119731	.8298427	.5183413
.3403852	.6945867	.1213599	.8124229	.5244986
.3477893	.7045936	.1312899	.7950687	.5308682
.3554373	.7147712	.1418674	.7776459	.5375069
.3632723	.7250504	.1530108	.7603317	.5443536
.3713701	.7355393	.1648252	.7429987	.5514639
.3798019	.7463374	.1774150	.7255489	.5588887
.3884616	.7573169	.1906087	.7082596	.5665166
.3974856	.7686622	.2046043	.6909056	.5744522
.4068921	.7804073	.2194157	.6735169	.5826916
.4167025	.7925924	.2350568	.6561219	.5912301

[redacted]

TABLE II.- EXPANSIVE FLOW FIELD OBTAINED BY CHARACTERISTIC CALCULATIONS FOR JET FLOW FROM NEAR-SONIC EXIT (M_j = 1.0038; μ_j = 85°) - Continued

x/r_j	y/r_j	θ, radians	μ, radians	V/V_l
0.1359276	0.0000000	0.0000000	1.424893	0.4118920
.1468782	$.7452140 \times 10^{-1}$	$.1906271 \times 10^{-3}$	1.405021	.4129607
.1564600	.1318588	$.1411773 \times 10^{-2}$	1.354225	.4163369
.1649605	.1707552	$.1808748 \times 10^{-2}$	1.334821	.4178760
.1739711	.2085292	$.2422358 \times 10^{-2}$	1.314519	.4196373
.1816614	.2381696	$.3093383 \times 10^{-2}$	1.297206	.4212632
.1895540	.2666323	$.3947162 \times 10^{-2}$	1.278987	.4230993
.1974399	.2932662	$.4983637 \times 10^{-2}$	1.260338	.4251140
.2046169	.3160257	$.6093961 \times 10^{-2}$	1.243126	.4270970
.2123265	.3391683	$.7501300 \times 10^{-2}$	1.224139	.4294246
.2194065	.3592373	$.8989216 \times 10^{-2}$	1.206515	.4317196
.2264186	.3781363	$.1067089 \times 10^{-1}$	1.188814	.4341573
.2333468	.3959293	$.1255063 \times 10^{-1}$	1.171125	.4367292
.2401848	.4127019	$.1463214 \times 10^{-1}$	1.153512	.4394280
.2472088	.4291934	$.1702506 \times 10^{-1}$	1.135243	.4423760
.2538511	.4441262	$.1952326 \times 10^{-1}$	1.117949	.4453097
.2606482	.4588175	$.2234166 \times 10^{-1}$	1.100165	.4484748
.2673459	.4727438	$.2538041 \times 10^{-1}$	1.082639	.4517448
.2741485	.4863785	$.2874769 \times 10^{-1}$	1.064836	.4552240
.2808573	.4993530	$.3234617 \times 10^{-1}$	1.047344	.4588008
.2876509	.5120558	$.3628307 \times 10^{-1}$	1.029697	.4625729
.2945145	.5244770	$.4056324 \times 10^{-1}$	1.011974	.4665311
.3013016	.5363792	$.4509258 \times 10^{-1}$	.9946041	.4705804
.3082911	.5482784	$.5007684 \times 10^{-1}$	.9768637	.4748944
.3152154	.5597296	$.5532335 \times 10^{-1}$	.9595018	.4792962
.3222105	.5709876	$.6093845 \times 10^{-1}$	.9421818	.4838696
.3293861	.5822401	$.6702722 \times 10^{-1}$	.9246555	.4886882
.3366282	.5933152	$.7349830 \times 10^{-1}$	.9072512	.4936690
.3440409	.6043851	$.8045583 \times 10^{-1}$	.8897409	.4988828
.3515276	.6153143	$.8781199 \times 10^{-1}$	.8723959	.5042538
.3591879	.6262609	$.9567126 \times 10^{-1}$	.8550108	.5098499
.3669383	.6371146	.1039465	.8378118	.5156017
.3749557	.6481332	.1128377	.8204325	.5216384
.3831586	.6592078	.1222585	.8031029	.5278896
.3915563	.6703600	.1322196	.7858393	.5343541
.4002343	.6817109	.1428252	.7685067	.5410895
.4091281	.6931834	.1539926	.7512817	.5480336
.4183245	.7048987	.1658269	.7340381	.5552427
.4279050	.7169685	.1784318	.7166780	.5627683
.4377493	.7292502	.1916356	.6994775	.5704971
.4480131	.7419510	.2056355	.6822119	.5785351
.4587184	.7551097	.2204450	.6649119	.5868780
.4698901	.7687723	.2360769	.6476040	.5955211

[redacted]

TABLE II.- EXPANSIVE FLOW FIELD OBTAINED BY CHARACTERISTIC CALCULATIONS FOR JET FLOW FROM NEAR-SONIC EXIT ($M_j = 1.0038$; $\mu_j = 85^\circ$) - Continued

x/r_j	y/r_j	θ, radians	μ, radians	V/V_l
0.1593610	0.0000000	0.0000000	1.389366	0.4139017
.1712780	.6496121 × 10-1	.2958171 × 10-3	1.369307	.4152366
.1801082	.1082568	.1891990 × 10-2	1.323004	.4188823
.1900372	.1478175	.2380173 × 10-2	1.301648	.4208350
.1985121	.1788292	.3006475 × 10-2	1.284288	.4225516
.2072104	.2086840	.3837739 × 10-2	1.266224	.4244632
.2158995	.2367004	.4865631 × 10-2	1.247804	.4265461
.2238017	.2606960	.5976022 × 10-2	1.230821	.4285885
.2322933	.2851672	.7390206 × 10-2	1.212084	.4309803
.2400871	.3064308	.8888718 × 10-2	1.194679	.4333347
.2478057	.3264966	.1058471 × 10-1	1.177188	.4358322
.2554317	.3454236	.1248187 × 10-1	1.159697	.4384645
.2629584	.3632953	.1458323 × 10-1	1.142268	.4412243
.2706918	.3808982	.1699955 × 10-1	1.124182	.4442361
.2780034	.3968569	.1952182 × 10-1	1.107051	.4472312
.2854871	.4125809	.2236693 × 10-1	1.089426	.4504603
.2928620	.4275034	.2543364 × 10-1	1.072051	.4537944
.3003540	.4421318	.2883053 × 10-1	1.054394	.4573400
.3077432	.4560663	.3245919 × 10-1	1.037040	.4609831
.3152274	.4697238	.3642788 × 10-1	1.019528	.4648229
.3227902	.4830920	.4074068 × 10-1	1.001937	.4688502
.3302695	.4959128	.4530229 × 10-1	.9846905	.4729686
.3379742	.5087428	.5031998 × 10-1	.9670745	.4773541
.3456081	.5210996	.5559921 × 10-1	.9498311	.4818269
.3533218	.5332579	.6124692 × 10-1	.9326279	.4864722
.3612369	.5454206	.6736827 × 10-1	.9152172	.4913647
.3692272	.5574007	.7387141 × 10-1	.8979266	.4964197
.3774081	.5693845	.8086053 × 10-1	.8805296	.5017091
.3856729	.5812246	.8824655 × 10-1	.8632956	.5071561
.3941319	.5930922	.9613430 × 10-1	.8460200	.5128295
.4026928	.6048675	.1044363	.8289288	.5186586
.4115520	.6168304	.1133522	.8116574	.5247745
.4206191	.6288626	.1227952	.7944338	.5311058
.4299050	.6409875	.1327756	.7772752	.5376509
.4395046	.6533373	.1433976	.7600473	.5444681
.4493467	.6658281	.1545779	.7429257	.5514944
.4595279	.6785925	.1664208	.7257847	.5587866
.4701393	.6917526	.1790300	.7085266	.5663967
.4810478	.7051533	.1922325	.6914257	.5742102
.4924271	.7190215	.2062254	.6742593	.5823339
.5043020	.7334006	.2210215	.6570568	.5907634
.5167016	.7483415	.2366330	.6398455	.5994935

[redacted]

TABLE II.- EXPANSIVE FLOW FIELD OBTAINED BY CHARACTERISTIC CALCULATIONS FOR JET FLOW FROM NEAR-SONIC EXIT (M_j = 1.0038; μ_j = 85°) - Continued

x/r_j	y/r_j	θ, radians	μ, radians	V/V_l
0.1845671	0.0000000	0.0000000	1.352877	0.4164393
.1953253	.4858321 × 10^{-1}	.4086221 × 10^{-3}	1.333616	.4179762
.2056973	.9156796 × 10^{-1}	.2443964 × 10^{-2}	1.288541	.4221204
.2149323	.1237064	.2901022 × 10^{-2}	1.270182	.4240332
.2244255	.1546463	.3654033 × 10^{-2}	1.252043	.4260547
.2339109	.1837465	.4643372 × 10^{-2}	1.233824	.4282188
.2425331	.2087289	.5736389 × 10^{-2}	1.217102	.4303254
.2518018	.2342824	.7144294 × 10^{-2}	1.198673	.4327830
.2603054	.2565373	.8644308 × 10^{-2}	1.181552	.4351966
.2687271	.2775857	.1034697 × 10^{-1}	1.164335	.4377532
.2770478	.2974810	.1225510 × 10^{-1}	1.147105	.4404446
.2852605	.3163026	.1437066 × 10^{-1}	1.129921	.4432638
.2937005	.3348769	.1680490 × 10^{-1}	1.112077	.4463378
.3016790	.3517408	.1934601 × 10^{-1}	1.095161	.4493928
.3098475	.3683829	.2221238 × 10^{-1}	1.077748	.4526847
.3178978	.3841982	.2530155 × 10^{-1}	1.060570	.4560816
.3260775	.3997233	.2872307 × 10^{-1}	1.043105	.4596917
.3341461	.4145289	.3237689 × 10^{-1}	1.025932	.4633993
.3423203	.4290574	.3637188 × 10^{-1}	1.008597	.4673052
.3505822	.4432938	.4071180 × 10^{-1}	.9911754	.4713999
.3587541	.4569607	.4530066 × 10^{-1}	.9740920	.4755851
.3671748	.4706519	.5034636 × 10^{-1}	.9566370	.4800399
.3755194	.4838499	.5565310 × 10^{-1}	.9395479	.4845814
.3839534	.4968476	.6132788 × 10^{-1}	.9224937	.4892962
.3926103	.5098618	.6747627 × 10^{-1}	.9052311	.4942600
.4013516	.5226914	.7400515 × 10^{-1}	.8880837	.4993869
.4103042	.5355358	.8101896 × 10^{-1}	.8708282	.5047496
.4193511	.5482364	.8842834 × 10^{-1}	.8537317	.5102700
.4286136	.5609765	.9633752 × 10^{-1}	.8365916	.5160181
.4379906	.5736273	.1046588	.8196320	.5219219
.4476979	.5864897	.1135922	.8024934	.5281138
.4576366	.5994365	.1230496	.7853990	.5345220
.4678190	.6124928	.1330417	.7683685	.5411442
.4783497	.6258014	.1436715	.7512663	.5480399
.4891509	.6392721	.1548557	.7342678	.5551449
.5003292	.6530483	.1666984	.7172493	.5625163
.5119855	.6672625	.1793024	.7001127	.5702067
.5239740	.6817476	.1924953	.6831314	.5780999
.5364865	.6967497	.2064725	.6660830	.5863040
.5495517	.7123167	.2212469	.6489973	.5948142
.5632023	.7285050	.2368299	.6319015	.6036249

[redacted]

TABLE II.- EXPANSIVE FLOW FIELD OBTAINED BY CHARACTERISTIC CALCULATIONS FOR JET FLOW FROM NEAR-SONIC EXIT (M_j = 1.0038; μ_j = 85°) - Continued

x/r_j	y/r_j	θ, radians	μ, radians	V/V_l
0.2070903	0.0000000	0.0000000	1.317271	0.4193894
.2190201	.4604310 × 10^{-1}	.5277630 × 10^{-3}	1.298912	.4210979
.2285396	.8025925 × 10^{-1}	.2954295 × 10^{-2}	1.258188	.4253552
.2386838	.1119649	.3480637 × 10^{-2}	1.239067	.4275822
.2488352	.1417719	.4376756 × 10^{-2}	1.220848	.4298433
.2580621	.1674012	.5427922 × 10^{-2}	1.204343	.4320115
.2679844	.1936801	.6812723 × 10^{-2}	1.186209	.4345274
.2770853	.2166143	.8303044 × 10^{-2}	1.169376	.4369911
.2860990	.2383493	.1000360 × 10^{-1}	1.152442	.4395965
.2950050	.2589328	.1191467 × 10^{-1}	1.135481	.4423366
.3037960	.2784397	.1403705 × 10^{-1}	1.118554	.4452044
.3128321	.2977235	.1648157 × 10^{-1}	1.100963	.4483293
.3213737	.3152559	.1903439 × 10^{-1}	1.084274	.4514333
.3301204	.3325831	.2191512 × 10^{-1}	1.067082	.4547761
.3387416	.3490701	.2501995 × 10^{-1}	1.050114	.4582238
.3475032	.3652749	.2845844 × 10^{-1}	1.032851	.4618866
.3561466	.3807460	.3212999 × 10^{-1}	1.015868	.4656467
.3649049	.3959441	.3614369 × 10^{-1}	.9987163	.4696063
.3737589	.4108521	.4050278 × 10^{-1}	.9814729	.4737559
.3825181	.4251764	.4511056 × 10^{-1}	.9645571	.4779958
.3915460	.4395404	.5017555 × 10^{-1}	.9472682	.4825073
.4004942	.4533980	.5550123 × 10^{-1}	.9303367	.4871049
.4095404	.4670567	.6119462 × 10^{-1}	.9134356	.4918764
.4188278	.4807445	.6736103 × 10^{-1}	.8963240	.4968984
.4282082	.4942484	.7390690 × 10^{-1}	.8793224	.5020839
.4378180	.5077782	.8093681 × 10^{-1}	.8622103	.5075062
.4475313	.5211666	.8836078 × 10^{-1}	.8452536	.5130862
.4574791	.5346063	.9628302 × 10^{-1}	.8282497	.5188947
.4675530	.5479608	.1046156	.8114238	.5248588
.4779847	.5615488	.1135582	.7944167	.5311122
.4886685	.5752355	.1230225	.7774521	.5375821
.4996181	.5890472	.1330183	.7605480	.5442665
.5109463	.6031355	.1436492	.7435710	.5512249
.5225699	.6174051	.1548309	.7266951	.5583926
.5346041	.6320082	.1666674	.7097973	.5658270
.5471583	.6470860	.1792609	.6927807	.5735811
.5600761	.6624617	.1924388	.6759158	.5815376
.5735648	.6783973	.2063959	.6589823	.5898052
.5876564	.6949447	.2211451	.6420108	.5983787
.6023871	.7121651	.2366964	.6250267	.6072526

TABLE II.- EXPANSIVE FLOW FIELD OBTAINED BY CHARACTERISTIC CALCULATIONS FOR JET FLOW FROM NEAR-SONIC EXIT $(M_j = 1.0038;\ \mu_j = 85^\circ)$ - Continued

x/r_j	y/r_j	θ, radians	μ, radians	V/V_l
0.2318825	0.0000000	0.0000000	1.282917	0.4226923
.2427547	.3671761 × 10-1	.6490770 × 10-3	1.265473	.4245454
.2532597	.7012302 × 10-1	.3497615 × 10-2	1.226097	.4291777
.2640742	.1005785	.4082347 × 10-2	1.206734	.4316902
.2739210	.1267404	.5021827 × 10-2	1.190241	.4339558
.2845175	.1536186	.6346171 × 10-2	1.172359	.4365454
.2942365	.1771229	.7807542 × 10-2	1.155828	.4390652
.3038636	.1994461	.9493340 × 10-2	1.139211	.4417227
.3133767	.2206300	.1139874 × 10-1	1.122563	.4445131
.3227681	.2407438	.1352129 × 10-1	1.105937	.4474306
.3324239	.2606644	.1597074 × 10-1	1.088644	.4506072
.3415511	.2788043	.1853093 × 10-1	1.072223	.4537607
.3508999	.2967601	.2142203 × 10-1	1.055296	.4571549
.3601157	.3138695	.2453859 × 10-1	1.038576	.4606542
.3694837	.3307093	.2799074 × 10-1	1.021554	.4643700
.3787267	.3468064	.3167662 × 10-1	1.004799	.4681831
.3880949	.3626384	.3570563 × 10-1	.9878679	.4721969
.3975678	.3781857	.4008097 × 10-1	.9708384	.4764016
.4069407	.3931399	.4470445 × 10-1	.9541242	.4806965
.4166040	.4081512	.4978579 × 10-1	.9370344	.4852647
.4261839	.4226469	.5512686 × 10-1	.9202905	.4899189
.4358710	.4369479	.6083533 × 10-1	.9035724	.4947473
.4458196	.4512922	.6701635 × 10-1	.8866402	.4998276
.4558702	.4654562	.7357571 × 10-1	.8698127	.5050717
.4661697	.4796594	.8061807 × 10-1	.8528715	.5105534
.4765835	.4937252	.8805279 × 10-1	.8360800	.5161930
.4872518	.5078566	.9598421 × 10-1	.8192384	.5220617
.4980588	.5219090	.1043237	.8025693	.5280859
.5092542	.5362179	.1132709	.7857174	.5344006
.5207239	.5506420	.1227371	.7689047	.5409320
.5324832	.5652089	.1327319	.7521488	.5476780
.5446542	.5800786	.1433585	.7353180	.5546986
.5571475	.5951509	.1545324	.7185851	.5619282
.5700880	.6105868	.1663570	.7018275	.5694248
.5835938	.6265368	.1789344	.6849503	.5772413
.5974975	.6428140	.1920918	.6682208	.5852595
.6120234	.6596968	.2060230	.6514216	.5935888
.6272064	.6772417	.2207399	.6345813	.6022240
.6430871	.6955146	.2362534	.6177268	.6111587

[redacted]

TABLE II.- EXPANSIVE FLOW FIELD OBTAINED BY CHARACTERISTIC CALCULATIONS FOR JET FLOW FROM NEAR-SONIC EXIT ($M_j = 1.0038$; $\mu_j = 85°$) - Continued

x/r_j	y/r_j	θ, radians	μ, radians	V/V_l
0.2543535	0.0000000	0.0000000	1.249970	0.4262942
.2659960	$.3503552 \times 10^{-1}$	$.7663570 \times 10^{-3}$	1.233484	.4282604
.2771064	$.6679266 \times 10^{-1}$	$.4120058 \times 10^{-2}$	1.195624	.4332035
.2874561	$.9339402 \times 10^{-1}$	$.4744754 \times 10^{-2}$	1.178142	.4356925
.2986175	.1207087	$.5927367 \times 10^{-2}$	1.160157	.4383934
.3088600	.1446194	$.7324464 \times 10^{-2}$	1.143779	.4409795
.3190091	.1673649	$.8974450 \times 10^{-2}$	1.127386	.4436915
.3290408	.1889848	$.1085975 \times 10^{-1}$	1.110984	.4465310
.3389463	.2095451	$.1297177 \times 10^{-1}$	1.094609	.4494949
.3491333	.2299412	$.1541684 \times 10^{-1}$	1.077572	.4527187
.3587638	.2485388	$.1797689 \times 10^{-1}$	1.061388	.4559163
.3686306	.2669733	$.2087098 \times 10^{-1}$	1.044697	.4593560
.3783587	.2845608	$.2399265 \times 10^{-1}$	1.028201	.4629003
.3882500	.3018922	$.2745190 \times 10^{-1}$	1.011401	.4666621
.3980110	.3184774	$.3114582 \times 10^{-1}$	.9948546	.4705208
.4079063	.3348075	$.3518379 \times 10^{-1}$	.9781269	.4745812
.4179143	.3508605	$.3956881 \times 10^{-1}$	.9612954	.4788331
.4278188	.3663151	$.4420233 \times 10^{-1}$	.9447695	.4831745
.4380328	.3818435	$.4929375 \times 10^{-1}$	.9278657	.4877909
.4481605	.3968517	$.5464469 \times 10^{-1}$	.9112996	.4924926
.4584043	.4116702	$.6036206 \times 10^{-1}$	.8947532	.4973692
.4689275	.4265458	$.6655171 \times 10^{-1}$	.8779906	.5024985
.4795613	.4412459	$.7311894 \times 10^{-1}$	.8613272	.5077916
.4904614	.4559981	$.8016804 \times 10^{-1}$	.8445474	.5133231
.5014857	.4706180	$.8760796 \times 10^{-1}$	.8279114	.5190125
.5127829	.4853167	$.9554294 \times 10^{-1}$	.8112228	.5249314
.5242299	.4999438	.1038840	.7947008	.5310057
.5360921	.5148484	.1128307	.7779957	.5373712
.5482492	.5298831	.1222943	.7613263	.5439534
.5607172	.5450772	.1322839	.7447102	.5507501
.5736265	.5605977	.1429023	.7280179	.5578217
.5868829	.5763400	.1540654	.7114201	.5651018
.6006192	.5924730	.1658753	.6947949	.5726490
.6149614	.6091548	.1784338	.6780483	.5805163
.6297322	.6261906	.1915687	.6614469	.5885844
.6451707	.6438725	.2054724	.6447731	.5969635
.6613161	.6622605	.2201573	.6280563	.6056478
.6782127	.6814249	.2356332	.6113236	.6146311

[redacted]

TABLE II.- EXPANSIVE FLOW FIELD OBTAINED BY CHARACTERISTIC CALCULATIONS FOR JET FLOW FROM NEAR-SONIC EXIT $(M_j = 1.0038;\ \mu_j = 85^\circ)$ - Continued

x/r_j	y/r_j	θ, radians	μ, radians	V/V_l
0.2783136	0.0000000	0.0000000	1.218597	0.4301322
.2905062	$.3317486 \times 10^{-1}$	$.9090577 \times 10^{-3}$	1.202505	.4322601
.3011374	$.6079862 \times 10^{-1}$	$.4760397 \times 10^{-2}$	1.166519	.4374215
.3128506	$.8854062 \times 10^{-1}$	$.5512074 \times 10^{-2}$	1.147344	.4404062
.3236224	.1127961	$.6758233 \times 10^{-2}$	1.130924	.4430955
.3343033	.1358953	$.8331294 \times 10^{-2}$	1.114705	.4458755
.3448648	.1578849	$.1017342 \times 10^{-1}$	1.098547	.4487701
.3552963	.1788299	$.1226032 \times 10^{-1}$	1.082437	.4517833
.3660279	.1996411	$.1469067 \times 10^{-1}$	1.065678	.4550557
.3761744	.2186447	$.1724329 \times 10^{-1}$	1.049756	.4582980
.3865730	.2375085	$.2013483 \times 10^{-1}$	1.033328	.4617831
.3968273	.2555297	$.2325702 \times 10^{-1}$	1.017084	.4653722
.4072564	.2733111	$.2671938 \times 10^{-1}$	1.000531	.4691796
.4175503	.2903468	$.3041801 \times 10^{-1}$	.9842202	.4730833
.4279887	.3071394	$.3446174 \times 10^{-1}$	.9677220	.4771897
.4385486	.3236649	$.3885331 \times 10^{-1}$	.9511130	.4814882
.4490016	.3395903	$.4349335 \times 10^{-1}$	.9347981	.4858759
.4597842	.3556080	$.4859175 \times 10^{-1}$	.9181040	.4905399
.4704782	.3711032	$.5394936 \times 10^{-1}$	.9017369	.4952886
.4812974	.3864164	$.5967315 \times 10^{-1}$	.8853843	.5002123
.4924150	.4018020	$.6586822 \times 10^{-1}$	.8688115	.5053899
.5036528	.4170186	$.7244002 \times 10^{-1}$	.8523319	.5107314
.5151757	.4323015	$.7949240 \times 10^{-1}$	.8357324	.5163119
.5268327	.4474598	$.8693465 \times 10^{-1}$	.8192719	.5220499
.5387822	.4627115	$.9487026 \times 10^{-1}$	.8027546	.5280177
.5508941	.4779002	.1032101	.7863990	.5341406
.5634496	.4933888	.1121533	.7698576	.5405555
.5763219	.5090240	.1216111	.7533485	.5471870
.5895282	.5248364	.1315923	.7368889	.5540328
.6032072	.5410003	.1421993	.7203502	.5611536
.6172593	.5574073	.1533474	.7039021	.5684826
.6318259	.5742337	.1651389	.6874244	.5760785
.6470426	.5916448	.1776747	.6708227	.5839946
.6627209	.6094385	.1907825	.6543617	.5921107
.6791166	.6279204	.2046553	.6378272	.6005370
.6962712	.6471552	.2193036	.6212473	.6092680
.7142343	.6672171	.2347382	.6046487	.6182968

[redacted]

TABLE II.- EXPANSIVE FLOW FIELD OBTAINED BY CHARACTERISTIC CALCULATIONS FOR JET FLOW FROM NEAR-SONIC EXIT $\left(M_j = 1.0038;\ \mu_j = 85^\circ\right)$ - Continued

x/r_j	y/r_j	θ, radians	μ, radians	V/V_l
0.3033430	0.0000000	0.0000000	1.187828	0.4342970
.3149758	$.2887517 \times 10^{-1}$	$.1055983 \times 10^{-2}$	1.172168	.4365738
.3270209	$.5755836 \times 10^{-1}$	$.5519920 \times 10^{-2}$	1.135775	.4422879
.3382915	$.8216565 \times 10^{-1}$	$.6294589 \times 10^{-2}$	1.118202	.4452655
.3494929	.1055748	$.7675911 \times 10^{-2}$	1.101854	.4481675
.3605786	.1278792	$.9420302 \times 10^{-2}$	1.085823	.4511394
.3715333	.1491520	$.1145104 \times 10^{-1}$	1.069925	.4542131
.3828085	.1703202	$.1384641 \times 10^{-1}$	1.053418	.4575407
.3934716	.1896759	$.1637810 \times 10^{-1}$	1.037746	.4608316
.4044034	.2089165	$.1925638 \times 10^{-1}$	1.021577	.4643649
.4151862	.2273219	$.2237090 \times 10^{-1}$	1.005586	.4680004
.4261563	.2455057	$.2582938 \times 10^{-1}$	.9892860	.4718544
.4369869	.2629474	$.2952644 \times 10^{-1}$	.9732174	.4758040
.4479726	.2801604	$.3357069 \times 10^{-1}$	.9569575	.4799565
.4590895	.2971181	$.3796391 \times 10^{-1}$	.9405814	.4843016
.4700963	.3134772	$.4260653 \times 10^{-1}$	.9244891	.4887349
.4814539	.3299478	$.4770778 \times 10^{-1}$	.9080163	.4934458
.4927212	.3458960	$.5306815 \times 10^{-1}$	.8918604	.4982406
.5041235	.3616715	$.5879414 \times 10^{-1}$	.8757118	.5032108
.5158439	.3775362	$.6499103 \times 10^{-1}$	.8593418	.5084355
.5276946	.3932401	$.7156402 \times 10^{-1}$	.8430587	.5138238
.5398497	.4090260	$.7861628 \times 10^{-1}$	.8266519	.5194517
.5521505	.4246957	$.8605688 \times 10^{-1}$	.8103775	.5252370
.5647639	.4404749	$.9398895 \times 10^{-1}$	.7940424	.5312524
.5775532	.4562010	.1023238	.7778643	.5374222
.5908156	.4722504	.1112597	.7614970	.5438847
.6044179	.4884639	.1207079	.7451589	.5505634
.6183785	.5048737	.1306768	.7288663	.5574562
.6328441	.5216614	.1412685	.7124923	.5646239
.6477111	.5387139	.1523978	.6962039	.5719994
.6631290	.5562156	.1641669	.6798826	.5796414
.6792425	.5743393	.1766767	.6634363	.5876032
.6958530	.5928753	.1897545	.6471263	.5957639
.7132321	.6121432	.2035925	.6307400	.6042343
.7314265	.6322112	.2182013	.6143061	.6130083
.7504885	.6531592	.2335903	.5978499	.6220793

[redacted]

TABLE II.- EXPANSIVE FLOW FIELD OBTAINED BY CHARACTERISTIC CALCULATIONS FOR JET FLOW FROM NEAR-SONIC EXIT $\left(M_j = 1.0038;\ \mu_j = 85^\circ\right)$ - Continued

x/r_j	y/r_j	θ, radians	μ, radians	V/V_l
0.3271733	0.0000000	0.0000000	1.157766	0.4387635
.3401724	$.2966202 \times 10^{-1}$	$.1221280 \times 10^{-2}$	1.142362	.4412090
.3517103	$.5500565 \times 10^{-1}$	$.6326061 \times 10^{-2}$	1.107516	.4471478
.3633643	$.7870891 \times 10^{-1}$	$.7177738 \times 10^{-2}$	1.090053	.4503428
.3749241	.1012664	$.8709378 \times 10^{-2}$	1.073888	.4534349
.3863570	.1227946	$.1063132 \times 10^{-1}$	1.058098	.4565829
.3981312	.1442418	$.1296168 \times 10^{-1}$	1.041789	.4599702
.4092697	.1638755	$.1545500 \times 10^{-1}$	1.026339	.4633097
.4206932	.1834167	$.1830773 \times 10^{-1}$	1.010407	.4668895
.4319644	.2021316	$.2140537 \times 10^{-1}$	.9946528	.4705688
.4434349	.2206432	$.2485244 \times 10^{-1}$	.9785914	.4744662
.4547623	.2384191	$.2854244 \times 10^{-1}$	.9627553	.4784575
.4662556	.2559805	$.3258208 \times 10^{-1}$	.9467245	.4826520
.4778891	.2732999	$.3697254 \times 10^{-1}$	.9305745	.4870390
.4894106	.2900236	$.4161316 \times 10^{-1}$	.9146985	.4915135
.5013030	.3068776	$.4671325 \times 10^{-1}$	.8984411	.4962665
.5131039	.3232116	$.5207249 \times 10^{-1}$	.8824901	.5011027
.5250497	.3393827	$.5779756 \times 10^{-1}$	.8665417	.5061141
.5373326	.3556593	$.6399322 \times 10^{-1}$	.8503700	.5113805
.5497555	.3717843	$.7056383 \times 10^{-1}$	.8342778	.5168106
.5625013	.3880068	$.7761273 \times 10^{-1}$	.8180597	.5224805
.5754040	.4041224	$.8504885 \times 10^{-1}$	.8019676	.5283074
.5886389	.4203631	$.9297483 \times 10^{-1}$	.7858119	.5343646
.6020627	.4365612	.1013018	.7698064	.5405757
.6159882	.4531046	.1102281	.7536109	.5470798
.6302755	.4698296	.1196643	.7374400	.5537997
.6449448	.4867692	.1296189	.7213105	.5607334
.6601511	.5041113	.1401931	.7050963	.5679421
.6757852	.5217399	.1513024	.6889644	.5753576
.6920056	.5398458	.1630480	.6727969	.5830392
.7089654	.5586090	.1755309	.6565020	.5910402
.7264565	.5778129	.1885779	.6403390	.5992391
.7447665	.5977896	.2023807	.6240971	.6077469
.7639445	.6186119	.2169496	.6078052	.6165574
.7840482	.6403638	.2322943	.5914887	.6256633

[redacted]

TABLE II.- EXPANSIVE FLOW FIELD OBTAINED BY CHARACTERISTIC CALCULATIONS FOR JET FLOW FROM NEAR-SONIC EXIT $\left(M_j = 1.0038;\ \mu_j = 85^\circ\right)$ - Continued

x/r_j	y/r_j	θ, radians	μ, radians	V/V_l
0.3537636	0.0000000	0.0000000	1.128109	0.4435692
.3662539	$.2634665 \times 10^{-1}$	$.1409306 \times 10^{-2}$	1.112822	.4462065
.3782223	$.5071303 \times 10^{-1}$	$.7148561 \times 10^{-2}$	1.078285	.4525808
.3902680	$.7355075 \times 10^{-1}$	$.8016011 \times 10^{-2}$	1.060889	.4560172
.4022118	$.9531618 \times 10^{-1}$	$.9677773 \times 10^{-2}$	1.044974	.4592977
.4145247	.1170150	$.1187141 \times 10^{-1}$	1.028805	.4627680
.4261786	.1369001	$.1429014 \times 10^{-1}$	1.013576	.4661662
.4381364	.1567169	$.1709468 \times 10^{-1}$	.9979028	.4697983
.4499392	.1757192	$.2016106 \times 10^{-1}$	.9824147	.4735249
.4619551	.1945392	$.2358661 \times 10^{-1}$	.9666256	.4774683
.4738246	.2126330	$.2726169 \times 10^{-1}$	.9510547	.4815036
.4858719	.2305298	$.3129081 \times 10^{-1}$	.9352877	.4857418
.4980702	.2482000	$.3567373 \times 10^{-1}$	.9193967	.4901723
.5101546	.2652807	$.4030849 \times 10^{-1}$	.9037692	.4946894
.5226326	.2825126	$.4540398 \times 10^{-1}$	.8877590	.4994858
.5350180	.2992299	$.5075898 \times 10^{-1}$	.8720453	.5043646
.5475597	.3157963	$.5648007 \times 10^{-1}$	.8563274	.5094184
.5604597	.3324869	$.6267138 \times 10^{-1}$	.8403835	.5147277
.5735112	.3490371	$.6923715 \times 10^{-1}$	.8245131	.5202004
.5869067	.3657025	$.7628019 \times 10^{-1}$	.8085117	.5259132
.6004716	.3822727	$.8370872 \times 10^{-1}$	.7926297	.5317828
.6143911	.3989858	$.9162608 \times 10^{-1}$	.7766796	.5378824
.6285145	.4156690	$.9994236 \times 10^{-1}$	.7608730	.5441356
.6431715	.4327222	.1088561	.7448746	.5506818
.6582153	.4499768	.1182770	.7288956	.5574436
.6736675	.4674673	.1282138	.7129538	.5644185
.6896929	.4853877	.1387675	.6969238	.5716681
.7061764	.5036190	.1498530	.6809710	.5791238
.7232869	.5223586	.1615716	.6649795	.5868449
.7411856	.5417950	.1740232	.6488578	.5948849
.7596555	.5617038	.1870349	.6328625	.6031216
.7790000	.5824313	.2007980	.6167862	.6116661
.7992739	.6040542	.2153227	.6006565	.6205119
.8205395	.6266619	.2306177	.5844988	.6296517

[redacted]

TABLE II.- EXPANSIVE FLOW FIELD OBTAINED BY CHARACTERISTIC CALCULATIONS FOR JET FLOW FROM NEAR-SONIC EXIT ($M_j = 1.0038$; $\mu_j = 85^\circ$) - Continued

x/r_j	y/r_j	θ, radians	μ, radians	V/V_l
0.3792871	0.0000000	0.0000000	1.098609	0.4487588
.3921533	$.2519185 \times 10^{-1}$	$.1587275 \times 10^{-2}$	1.083670	.4515482
.4044956	$.4858162 \times 10^{-1}$	$.7993560 \times 10^{-2}$	1.049918	.4582646
.4168861	$.7058406 \times 10^{-1}$	$.8928142 \times 10^{-2}$	1.032836	.4618897
.4296922	$.9248926 \times 10^{-1}$	$.1082943 \times 10^{-1}$	1.016540	.4654949
.4418241	.1125719	$.1310970 \times 10^{-1}$	1.001440	.4689665
.4542796	.1326060	$.1583111 \times 10^{-1}$	.9859765	.4726556
.4665789	.1518374	$.1884560 \times 10^{-1}$	.9707266	.4764299
.4791055	.1709058	$.2223612 \times 10^{-1}$	.9551895	.4804176
.4914836	.1892587	$.2588704 \times 10^{-1}$	.9398696	.4844942
.5040513	.2074319	$.2989846 \times 10^{-1}$	.9243540	.4887729
.5167810	.2253938	$.3426785 \times 10^{-1}$	.9087111	.4932435
.5293955	.2427743	$.3889214 \times 10^{-1}$	.8933233	.4977993
.5424250	.2603267	$.4397905 \times 10^{-1}$	.8775539	.5026348
.5553622	.2773704	$.4932644 \times 10^{-1}$	.8620688	.5075519
.5684667	.2942762	$.5504018 \times 10^{-1}$	.8465748	.5126438
.5819504	.3113240	$.6122420 \times 10^{-1}$	.8308525	.5179916
.5955968	.3282435	$.6778215 \times 10^{-1}$	.8151964	.5235024
.6096078	.3452955	$.7481684 \times 10^{-1}$	.7994074	.5292533
.6238013	.3622639	$.8223601 \times 10^{-1}$	.7837296	.5351605
.6383707	.3793932	$.9014249 \times 10^{-1}$	.7679810	.5412976
.6531592	.3965054	$.9844665 \times 10^{-1}$	.7523691	.5475876
.6685120	.4140114	.1073462	.7365632	.5541706
.6842770	.4317378	.1167505	.7207719	.5609690
.7004765	.4497207	.1266681	.7050125	.5679800
.7172837	.4681604	.1371999	.6891620	.5752652
.7345796	.4869344	.1482613	.6733846	.5827554
.7525408	.5062474	.1599525	.6575650	.5905102
.7713396	.5262939	.1723725	.6416122	.5985836
.7907472	.5468445	.1853495	.6257814	.6068521
.8110853	.5682570	.1990737	.6098662	.6154273
.8324127	.5906128	.2135549	.5938948	.6243026
.8547964	.6140063	.2288016	.5778919	.6334703

[redacted]

TABLE II.- EXPANSIVE FLOW FIELD OBTAINED BY CHARACTERISTIC CALCULATIONS FOR JET FLOW FROM NEAR-SONIC EXIT $\left(M_j = 1.0038;\ \mu_j = 85^\circ\right)$ - Continued

x/r_j	y/r_j	θ, radians	μ, radians	V/V_l
0.4055487	0.0000000	0.0000000	1.069709	0.4542555
.4187748	$.2414776 \times 10^{-1}$	$.1777096 \times 10^{-2}$	1.055060	.4572032
.4314689	$.4663196 \times 10^{-1}$	$.8892727 \times 10^{-2}$	1.021980	.4642751
.4447341	$.6876598 \times 10^{-1}$	$.9945947 \times 10^{-2}$	1.004457	.4682625
.4573342	$.8902532 \times 10^{-1}$	$.1192228 \times 10^{-1}$	.9892515	.4718628
.4702838	.1092454	$.1448345 \times 10^{-1}$	.9739126	.4756299
.4830787	.1286724	$.1740603 \times 10^{-1}$	.9588666	.4794606
.4961162	.1479555	$.2073683 \times 10^{-1}$	.9435671	.4834969
.5090045	.1665342	$.2434784 \times 10^{-1}$	.9284929	.4876166
.5220954	.1849506	$.2833049 \times 10^{-1}$	.9132271	.4919365
.5353597	.2031724	$.3267846 \times 10^{-1}$	.8978362	.4964467
.5485085	.2208219	$.3728654 \times 10^{-1}$	.8826923	.5010403
.5620950	.2386639	$.4235948 \times 10^{-1}$	.8671671	.5059142
.5755893	.2560057	$.4769533 \times 10^{-1}$	.8519180	.5108682
.5892630	.2732231	$.5339870 \times 10^{-1}$	.8366549	.5159965
.6033375	.2906010	$.5957215 \times 10^{-1}$	.8211598	.5213812
.6175867	.3078637	$.6611954 \times 10^{-1}$	.8057258	.5269284
.6322219	.3252770	$.7314317 \times 10^{-1}$	.7901548	.5327155
.6470532	.3426197	$.8055086 \times 10^{-1}$	.7746897	.5386581
.6622834	.3601413	$.8844424 \times 10^{-1}$	.7591485	.5448307
.6777483	.3776600	$.9673382 \times 10^{-1}$	.7437375	.5511554
.6938107	.3955961	.1056169	.7281305	.5577732
.7103098	.4137737	.1150030	.7125338	.5646054
.7272714	.4322289	.1249000	.6969639	.5716497
.7448773	.4511680	.1354087	.6813000	.5789676
.7630032	.4704662	.1464433	.6657035	.5864899
.7818354	.4903344	.1581049	.6500610	.5942758
.8015557	.5109740	.1704923	.6342834	.6023792
.8219262	.5321496	.1834328	.6186221	.6106766
.8432848	.5542317	.1971160	.6028740	.6192795
.8656956	.5773061	.2115521	.5870658	.6281809
.8892308	.6014723	.2267494	.5712231	.6373729

[redacted]

TABLE II.- EXPANSIVE FLOW FIELD OBTAINED BY CHARACTERISTIC CALCULATIONS FOR JET FLOW FROM NEAR-SONIC EXIT $\left(M_j = 1.0038;\ \mu_j = 85^\circ\right)$ - Concluded

x/r_j	y/r_j	θ, radians	μ, radians	V/V_l
0.4325213	0.0000000	0.0000000	1.041314	0.4600710
.4460920	$.2318861 \times 10^{-1}$	$.1978676 \times 10^{-2}$	1.026918	.4631821
.4596826	$.4576376 \times 10^{-1}$	$.9925832 \times 10^{-2}$	.9939206	.4707432
.4727123	$.6622906 \times 10^{-1}$	$.1101560 \times 10^{-1}$	.9775566	.4747224
.4861397	$.8662500 \times 10^{-1}$	$.1321216 \times 10^{-1}$	.9620467	.4786396
.4994218	.1062261	$.1595126 \times 10^{-1}$	.9470897	.4825548
.5129656	.1256974	$.1917176 \times 10^{-1}$	.9319692	.4866537
.5263613	.1444747	$.2271253 \times 10^{-1}$	.9171075	.4908240
.5399739	.1631067	$.2664631 \times 10^{-1}$	.9020738	.4951892
.5537730	.1815599	$.3095787 \times 10^{-1}$	.8869201	.4997421
.5674568	.1994513	$.3553849 \times 10^{-1}$	.8720113	.5043753
.5816018	.2175557	$.4058909 \times 10^{-1}$	.8567256	.5092882
.5956560	.2351689	$.4590621 \times 10^{-1}$	.8417080	.5142795
.6099024	.2526719	$.5159314 \times 10^{-1}$	.8266734	.5194443
.6245717	.2703547	$.5775143 \times 10^{-1}$	.8114062	.5248650
.6394292	.2879353	$.6428410 \times 10^{-1}$	.7961947	.5304477
.6546950	.3056851	$.7129265 \times 10^{-1}$	.7808433	.5362700
.6701711	.3233783	$.7868470 \times 10^{-1}$	.7655912	.5422471
.6860703	.3412687	$.8656205 \times 10^{-1}$	.7502597	.5484536
.7022206	.3591715	$.9483405 \times 10^{-1}$	.7350522	.5548114
.7190014	.3775165	.1036975	.7196462	.5614622
.7362471	.3961229	.1130621	.7042462	.5683267
.7539839	.4150291	.1229359	.6888688	.5754023
.7724028	.4344472	.1334186	.6733941	.5827509
.7913745	.4542497	.1444250	.6579819	.5903026
.8110956	.4746538	.1560552	.6425209	.5981169
.8317574	.4958677	.1684074	.6269214	.6062479
.8531116	.5176510	.1813101	.6114335	.6145710
.8755148	.5403858	.1949512	.5958553	.6231984
.8990361	.5641626	.2093411	.5802143	.6321226
.9237540	.5890861	.2244879	.5645351	.6413355
.9365753	.6020008	.2073650	.5737721	.6358754

[redacted]

TABLE III.- VALUES OF INTEGRALS IN JOHANNESEN-MEYER METHOD OF CHARACTERISTICS, $\gamma = 1.400$

[See appendix B]

z_n	$I_1(\phi)$		$I_2(\phi)$		$I_3(\phi)$		$I_4(\phi)$	
	$\int_{z_{n-1}}^{z_n}$	$\int_{z=0.03}^{z_n}$	$\int_{z_{n-1}}^{z_n}$	$\int_{z=0.03}^{z_n}$	$\int_{z_{n-1}}^{z_n}$	$\int_{z=0.03}^{z_n}$	$\int_{z_{n-1}}^{z_n}$	$\int_{z=0.03}^{z_n}$
0.04	0.5352399×10^{-1}	0.5352399×10^{-1}	0.4585197×10^{-2}	0.4585197×10^{-2}	0.1313719	0.1313719	1.544196	1.544196
.05	$.4711751 \times 10^{-1}$	$.1006415$	$.5205754 \times 10^{-2}$	$.9790952 \times 10^{-2}$	.1158030	.2471749	1.052538	2.596735
.06	$.4255425 \times 10^{-1}$	$.1431957$	$.5762908 \times 10^{-2}$	$.1555386 \times 10^{-1}$	.1047641	.3519390	.7757746	3.372510
.07	$.3908471 \times 10^{-1}$	$.1822804$	$.6274384 \times 10^{-2}$	$.2182824 \times 10^{-1}$	$.9641819 \times 10^{-1}$	.4483572	.6018302	3.974340
.08	$.3632673 \times 10^{-1}$	$.2186072$	$.6751271 \times 10^{-2}$	$.2857951 \times 10^{-1}$	$.8982827 \times 10^{-1}$	.5381855	.4840817	4.458422
.09	$.3406212 \times 10^{-1}$	$.2526693$	$.7201104 \times 10^{-2}$	$.3578062 \times 10^{-1}$	$.8445935 \times 10^{-1}$	.6226449	.3999835	4.858405
.10	$.3215590 \times 10^{-1}$	$.2848252$	$.7629288 \times 10^{-2}$	$.4340991 \times 10^{-1}$	$.7998045 \times 10^{-1}$	.7026253	.3374288	5.195834
.11	$.3051953 \times 10^{-1}$	$.3153447$	$.8039885 \times 10^{-2}$	$.5144979 \times 10^{-1}$	$.7617435 \times 10^{-1}$	.7787997	.2893914	5.485226
.12	$.2909210 \times 10^{-1}$	$.3444368$	$.8436044 \times 10^{-2}$	$.5988584 \times 10^{-1}$	$.7289173 \times 10^{-1}$	.8516914	.2515410	5.736767
.13	$.2783018 \times 10^{-1}$	$.3722670$	$.8820295 \times 10^{-2}$	$.6870613 \times 10^{-1}$	$.7002619 \times 10^{-1}$	.9217176	.2210781	5.957845
.14	$.2670182 \times 10^{-1}$	$.3989688$	$.9194703 \times 10^{-2}$	$.7790084 \times 10^{-1}$	$.6749949 \times 10^{-1}$	.9892171	.1961205	6.153965
.15	$.2568292 \times 10^{-1}$	$.4246518$	$.9560992 \times 10^{-2}$	$.8746183 \times 10^{-1}$	$.6525263 \times 10^{-1}$	1.054469	.1753608	6.329326
.16	$.2475490 \times 10^{-1}$	$.4494067$	$.9920643 \times 10^{-2}$	$.9738247 \times 10^{-1}$	$.6324029 \times 10^{-1}$	1.117710	.1578654	6.487192
.17	$.2390314 \times 10^{-1}$	$.4733098$	$.1027491 \times 10^{-1}$	.1076573	$.6142684 \times 10^{-1}$	1.179136	.1429516	6.630143
.18	$.2311597 \times 10^{-1}$	$.4964258$	$.1062493 \times 10^{-1}$	.1182823	$.5978392 \times 10^{-1}$	1.238920	.1301098	6.760253
.19	$.2238393 \times 10^{-1}$	$.5188097$	$.1097170 \times 10^{-1}$	.1292540	$.5828868 \times 10^{-1}$	1.297209	.1189527	6.879206
.20	$.2169923 \times 10^{-1}$	$.5405090$	$.1131612 \times 10^{-1}$	.1405701	$.5692242 \times 10^{-1}$	1.354131	.1091811	6.988387
.21	$.2105540 \times 10^{-1}$	$.5615644$	$.1165899 \times 10^{-1}$	.1522291	$.5566962 \times 10^{-1}$	1.409801	.1005609	7.088948
.22	$.2044699 \times 10^{-1}$	$.5820114$	$.1200110 \times 10^{-1}$	.1642302	$.5451743 \times 10^{-1}$	1.464318	$.9290630 \times 10^{-1}$	7.181854
.23	$.1986935 \times 10^{-1}$	$.6018807$	$.1234313 \times 10^{-1}$	.1765734	$.5345499 \times 10^{-1}$	1.517773	$.8606796 \times 10^{-1}$	7.267922
.24	$.1931851 \times 10^{-1}$	$.6211992$	$.1268577 \times 10^{-1}$	.1892591	$.5247307 \times 10^{-1}$	1.570247	$.7992504 \times 10^{-1}$	7.347847
.25	$.1879101 \times 10^{-1}$	$.6399902$	$.1302963 \times 10^{-1}$	.2022888	$.5156380 \times 10^{-1}$	1.621810	$.7437852 \times 10^{-1}$	7.422226
.26	$.1828381 \times 10^{-1}$	$.6582741$	$.1337534 \times 10^{-1}$	.2156641	$.5072044 \times 10^{-1}$	1.672531	$.6934663 \times 10^{-1}$	7.491572
.27	$.1779423 \times 10^{-1}$	$.6760683$	$.1372349 \times 10^{-1}$	.2293876	$.4993715 \times 10^{-1}$	1.722468	$.6476130 \times 10^{-1}$	7.556334
.28	$.1731989 \times 10^{-1}$	$.6933882$	$.1407465 \times 10^{-1}$	.2434623	$.4920884 \times 10^{-1}$	1.771677	$.6056543 \times 10^{-1}$	7.616899
.29	$.1685863 \times 10^{-1}$	$.7102468$	$.1442939 \times 10^{-1}$	.2578917	$.4853107 \times 10^{-1}$	1.820208	$.5671081 \times 10^{-1}$	7.673610
.30	$.1640848 \times 10^{-1}$	$.7266553$	$.1478827 \times 10^{-1}$	.2726799	$.4789999 \times 10^{-1}$	1.868108	$.5315543 \times 10^{-1}$	7.726766
.31	$.1596765 \times 10^{-1}$	$.7426230$	$.1515186 \times 10^{-1}$	.2878318	$.4731217 \times 10^{-1}$	1.915420	$.4986723 \times 10^{-1}$	7.776633
.32	$.1553445 \times 10^{-1}$	$.7581574$	$.1552071 \times 10^{-1}$	.3033525	$.4676459 \times 10^{-1}$	1.962185	$.4681307 \times 10^{-1}$	7.823447

TABLE III.- VALUES OF INTEGRALS IN JOHANNESEN-MEYER METHOD OF CHARACTERISTICS, $\gamma = 1.400$ - Continued

[See appendix B]

z_n	$I_1(\phi)$		$I_2(\phi)$		$I_3(\phi)$		$I_4(\phi)$	
	$\int_{z_{n-1}}^{z_n}$	$\int_{z=0.03}^{z_n}$	$\int_{z_{n-1}}^{z_n}$	$\int_{z=0.03}^{z_n}$	$\int_{z_{n-1}}^{z_n}$	$\int_{z=0.03}^{z_n}$	$\int_{z_{n-1}}^{z_n}$	$\int_{z=0.03}^{z_n}$
0.33	0.1510733×10^{-1}	0.7732648	0.1589541×10^{-1}	0.3192479	0.4625459×10^{-1}	2.008439	0.4396785×10^{-1}	7.867414
.34	$.1468479 \times 10^{-1}$	.7879496	$.1627653 \times 10^{-1}$	.3355245	$.4577979 \times 10^{-1}$	2.054219	$.4130889 \times 10^{-1}$	7.908723
.35	$.1426544 \times 10^{-1}$	.8022150	$.1666465 \times 10^{-1}$	.3521891	$.4533810 \times 10^{-1}$	2.099557	$.3881638 \times 10^{-1}$	7.947540
.36	$.1384789 \times 10^{-1}$	.8160629	$.1706040 \times 10^{-1}$	.3692495	$.4492764 \times 10^{-1}$	2.144485	$.3647290 \times 10^{-1}$	7.984013
.37	$.1343081 \times 10^{-1}$	.8294937	$.1746439 \times 10^{-1}$	.3867139	$.4454674 \times 10^{-1}$	2.189031	$.3426313 \times 10^{-1}$	8.018276
.38	$.1301288 \times 10^{-1}$	.8425066	$.1787726 \times 10^{-1}$	.4045912	$.4419392 \times 10^{-1}$	2.233225	$.3217343 \times 10^{-1}$	8.050449
.39	$.1259280 \times 10^{-1}$	.8550994	$.1829970 \times 10^{-1}$	.4228909	$.4386783 \times 10^{-1}$	2.277093	$.3019169 \times 10^{-1}$	8.080641
.40	$.1216925 \times 10^{-1}$	.8672687	$.1873240 \times 10^{-1}$	.4416233	$.4356731 \times 10^{-1}$	2.320660	$.2830706 \times 10^{-1}$	8.108948
.41	$.1174090 \times 10^{-1}$	.8790096	$.1917609 \times 10^{-1}$	.4607994	$.4329129 \times 10^{-1}$	2.363952	$.2650979 \times 10^{-1}$	8.135458
.42	$.1130639 \times 10^{-1}$	.8903160	$.1963154 \times 10^{-1}$	.4804310	$.4303884 \times 10^{-1}$	2.406991	$.2479110 \times 10^{-1}$	8.160249
.43	$.1086430 \times 10^{-1}$	.9011803	$.2009956 \times 10^{-1}$	.5005305	$.4280913 \times 10^{-1}$	2.449800	$.2314296 \times 10^{-1}$	8.183392
.44	$.1041319 \times 10^{-1}$	.9115935	$.2058100 \times 10^{-1}$	.5211115	$.4260141 \times 10^{-1}$	2.492401	$.2155811 \times 10^{-1}$	8.204950
.45	$.9951523 \times 10^{-2}$	.9215450	$.2107676 \times 10^{-1}$	.5421883	$.4241506 \times 10^{-1}$	2.534816	$.2002984 \times 10^{-1}$	8.224980
.46	$.9477678 \times 10^{-2}$	.9310227	$.2158779 \times 10^{-1}$	.5637761	$.4224951 \times 10^{-1}$	2.577066	$.1855198 \times 10^{-1}$	8.243532
.47	$.8989955 \times 10^{-2}$	.9400126	$.2211511 \times 10^{-1}$	.5858912	$.4210428 \times 10^{-1}$	2.619170	$.1711880 \times 10^{-1}$	8.260651
.48	$.8486536 \times 10^{-2}$	.9484992	$.2265979 \times 10^{-1}$	.6085510	$.4197896 \times 10^{-1}$	2.661149	$.1572496 \times 10^{-1}$	8.276376
.49	$.7965466 \times 10^{-2}$	.9564646	$.2322299 \times 10^{-1}$	.6317740	$.4187320 \times 10^{-1}$	2.703022	$.1436542 \times 10^{-1}$	8.290741
.50	$.7424635 \times 10^{-2}$	.9638893	$.2380593 \times 10^{-1}$	.6555799	$.4178675 \times 10^{-1}$	2.744809	$.1303540 \times 10^{-1}$	8.303776
.51	$.6861774 \times 10^{-2}$	.9707511	$.2440994 \times 10^{-1}$	.6799899	$.4171937 \times 10^{-1}$	2.786528	$.1173038 \times 10^{-1}$	8.315507
.52	$.6274398 \times 10^{-2}$	.9770255	$.2503642 \times 10^{-1}$	.7050263	$.4167092 \times 10^{-1}$	2.828199	$.1044597 \times 10^{-1}$	8.325953
.53	$.5659799 \times 10^{-2}$	.9826853	$.2568690 \times 10^{-1}$	.7307132	$.4164131 \times 10^{-1}$	2.869841	$.9177912 \times 10^{-2}$	8.335131
.54	$.5015011 \times 10^{-2}$	.9877003	$.2636302 \times 10^{-1}$	.7570762	$.4163049 \times 10^{-1}$	2.911471	$.7922054 \times 10^{-2}$	8.343053
.55	$.4336768 \times 10^{-2}$	.9920370	$.2706654 \times 10^{-1}$	.7841428	$.4163848 \times 10^{-1}$	2.953110	$.6674287 \times 10^{-2}$	8.349727
.56	$.3621465 \times 10^{-2}$	.9956585	$.2779937 \times 10^{-1}$	.8119422	$.4166536 \times 10^{-1}$	2.994775	$.5430515 \times 10^{-2}$	8.355158
.57	$.2865101 \times 10^{-2}$	.9985236	$.2856359 \times 10^{-1}$	.8405058	$.4171125 \times 10^{-1}$	3.036486	$.4186601 \times 10^{-2}$	8.359344
.58	$.2063230 \times 10^{-2}$	1.000586	$.2936144 \times 10^{-1}$	.8698672	$.4177635 \times 10^{-1}$	3.078263	$.2938347 \times 10^{-2}$	8.362282
.59	$.1210885 \times 10^{-2}$	1.001797	$.3019535 \times 10^{-1}$	.9000626	$.4186088 \times 10^{-1}$	3.120124	$.1681434 \times 10^{-2}$	8.363964
.60	$.3025175 \times 10^{-3}$	1.002100	$.3106800 \times 10^{-1}$	.9311306	$.4196513 \times 10^{-1}$	3.162089	$.4113994 \times 10^{-3}$	8.364375
.61	$-.6681245 \times 10^{-3}$	1.001432	$.3198228 \times 10^{-1}$	.9631128	$.4208948 \times 10^{-1}$	3.204178	$-.8764540 \times 10^{-3}$	8.363499

TABLE III.- VALUES OF INTEGRALS IN JOHANNESEN-MEYER METHOD OF CHARACTERISTICS, $\gamma = 1.400$ - Concluded

[See appendix B]

z_n	$I_1(\phi)$		$I_2(\phi)$		$I_3(\phi)$		$I_4(\phi)$	
	$\int_{z_{n-1}}^{z_n}$	$\int_{z=0.03}^{z_n}$	$\int_{z_{n-1}}^{z_n}$	$\int_{z=0.03}^{z_n}$	$\int_{z_{n-1}}^{z_n}$	$\int_{z=0.03}^{z_n}$	$\int_{z_{n-1}}^{z_n}$	$\int_{z=0.03}^{z_n}$
0.62	$-0.1708075 \times 10^{-2}$	0.9997241	0.3294136×10^{-1}	0.9960542	0.4223432×10^{-1}	3.246412	$-0.2187067 \times 10^{-2}$	8.361312
.63	$-.2825310 \times 10^{-2}$	.9968987	$.3394871 \times 10^{-1}$	1.030003	$.4240011 \times 10^{-1}$	3.288813	$-.3525729 \times 10^{-2}$	8.357786
.64	$-.4028873 \times 10^{-2}$	.9928699	$.3500815 \times 10^{-1}$	1.065011	$.4258739 \times 10^{-1}$	3.331400	$-.4898113 \times 10^{-2}$	8.352888
.65	$-.5329072 \times 10^{-2}$	.9875408	$.3612387 \times 10^{-1}$	1.101135	$.4279675 \times 10^{-1}$	3.374197	$-.6310369 \times 10^{-2}$	8.346578
.66	$-.6737714 \times 10^{-2}$	.9808031	$.3730048 \times 10^{-1}$	1.138435	$.4302883 \times 10^{-1}$	3.417226	$-.7769236 \times 10^{-2}$	8.338808
.67	$-.8268349 \times 10^{-2}$	.9725347	$.3854308 \times 10^{-1}$	1.176978	$.4328435 \times 10^{-1}$	3.460510	$-.9282118 \times 10^{-2}$	8.329525
.68	$-.9936617 \times 10^{-2}$	.9625981	$.3985732 \times 10^{-1}$	1.216836	$.4356407 \times 10^{-1}$	3.504074	$-.1085724 \times 10^{-1}$	8.318569
.69	$-.1176063 \times 10^{-1}$	.9508375	$.4124943 \times 10^{-1}$	1.258085	$.4386883 \times 10^{-1}$	3.547943	$-.1250380 \times 10^{-1}$	8.306165
.70	$-.1376151 \times 10^{-1}$	.9370760	$.4272634 \times 10^{-1}$	1.300811	$.4419951 \times 10^{-1}$	3.592142	$-.1423214 \times 10^{-1}$	8.291935
.71	$-.1596390 \times 10^{-1}$	.9211121	$.4429578 \times 10^{-1}$	1.345107	$.4455705 \times 10^{-1}$	3.636699	$-.1605397 \times 10^{-1}$	8.275879
.72	$-.1839683 \times 10^{-1}$	.9027152	$.4596633 \times 10^{-1}$	1.391073	$.4494241 \times 10^{-1}$	3.681642	$-.1798267 \times 10^{-1}$	8.257896
.73	$-.2109460 \times 10^{-1}$	.8816206	$.4774760 \times 10^{-1}$	1.438821	$.4535658 \times 10^{-1}$	3.726998	$-.2003360 \times 10^{-1}$	8.237863
.74	$-.2409803 \times 10^{-1}$	.8575226	$.4965030 \times 10^{-1}$	1.488471	$.4580056 \times 10^{-1}$	3.772799	$-.2222450 \times 10^{-1}$	8.215638
.75	$-.2745595 \times 10^{-1}$	.8300667	$.5168645 \times 10^{-1}$	1.540158	$.4627530 \times 10^{-1}$	3.819074	$-.2457605 \times 10^{-1}$	8.191062
.76	$-.3122721 \times 10^{-1}$	.7988394	$.5386948 \times 10^{-1}$	1.594027	$.4678165 \times 10^{-1}$	3.865856	$-.2711252 \times 10^{-1}$	8.163950
.77	$-.3548324 \times 10^{-1}$	.7633562	$.5621443 \times 10^{-1}$	1.650242	$.4732033 \times 10^{-1}$	3.913176	$-.2986256 \times 10^{-1}$	8.134087
.78	$-.4031146 \times 10^{-1}$	.7230447	$.5873818 \times 10^{-1}$	1.708980	$.4789176 \times 10^{-1}$	3.961068	$-.3286031 \times 10^{-1}$	8.101227
.79	$-.4581971 \times 10^{-1}$	.6772250	$.6145953 \times 10^{-1}$	1.770439	$.4849597 \times 10^{-1}$	4.009564	$-.3614678 \times 10^{-1}$	8.065080
.80	$-.5214234 \times 10^{-1}$	.6250827	$.6439940 \times 10^{-1}$	1.834839	$.4913233 \times 10^{-1}$	4.058696	$-.3977166 \times 10^{-1}$	8.025308
.81	$-.5944837 \times 10^{-1}$	.5656343	$.6758087 \times 10^{-1}$	1.902420	$.4979922 \times 10^{-1}$	4.108496	$-.4379578 \times 10^{-1}$	7.981513
.82	$-.6795293 \times 10^{-1}$	.4976814	$.7102914 \times 10^{-1}$	1.973449	$.5049361 \times 10^{-1}$	4.158989	$-.4829433 \times 10^{-1}$	7.933218
.83	$-.7793315 \times 10^{-1}$	.4197482	$.7477106 \times 10^{-1}$	2.048220	$.5121030 \times 10^{-1}$	4.210200	$-.5336135 \times 10^{-1}$	7.879857
.84	$-.8975104 \times 10^{-1}$	.3299972	$.7883422 \times 10^{-1}$	2.127054	$.5194083 \times 10^{-1}$	4.262140	$-.5911600 \times 10^{-1}$	7.820741
.85	-.1038868	.2261104	$.8324503 \times 10^{-1}$	2.210299	$.5267185 \times 10^{-1}$	4.314812	$-.6571129 \times 10^{-1}$	7.755030
.86	-.1209884	.1051220	$.8802483 \times 10^{-1}$	2.298324	$.5338258 \times 10^{-1}$	4.368195	$-.7334691 \times 10^{-1}$	7.681683
.87	-.1419476	$-.3682561 \times 10^{-1}$	$.9318267 \times 10^{-1}$	2.391507	$.5404066 \times 10^{-1}$	4.422236	$-.8228804 \times 10^{-1}$	7.599395
.88	-.1680194	-.2048450	$.9870152 \times 10^{-1}$	2.490208	$.5459551 \times 10^{-1}$	4.476831	$-.9289409 \times 10^{-1}$	7.506501
.89	-.2010158	-.4058609	.1045119	2.594720	$.5496715 \times 10^{-1}$	4.531798	-.1056635	7.400837
.90	-.2436336	-.6494945	.1104406	2.705161	$.5502670 \times 10^{-1}$	4.586825	-.1213067	7.279531

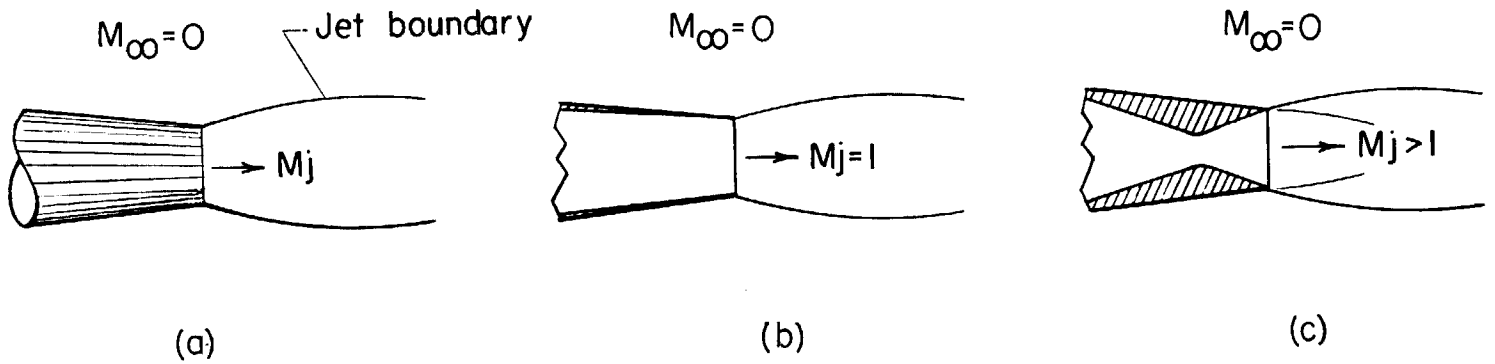

Figure 1.- Sketch of jets exhausting into still air.

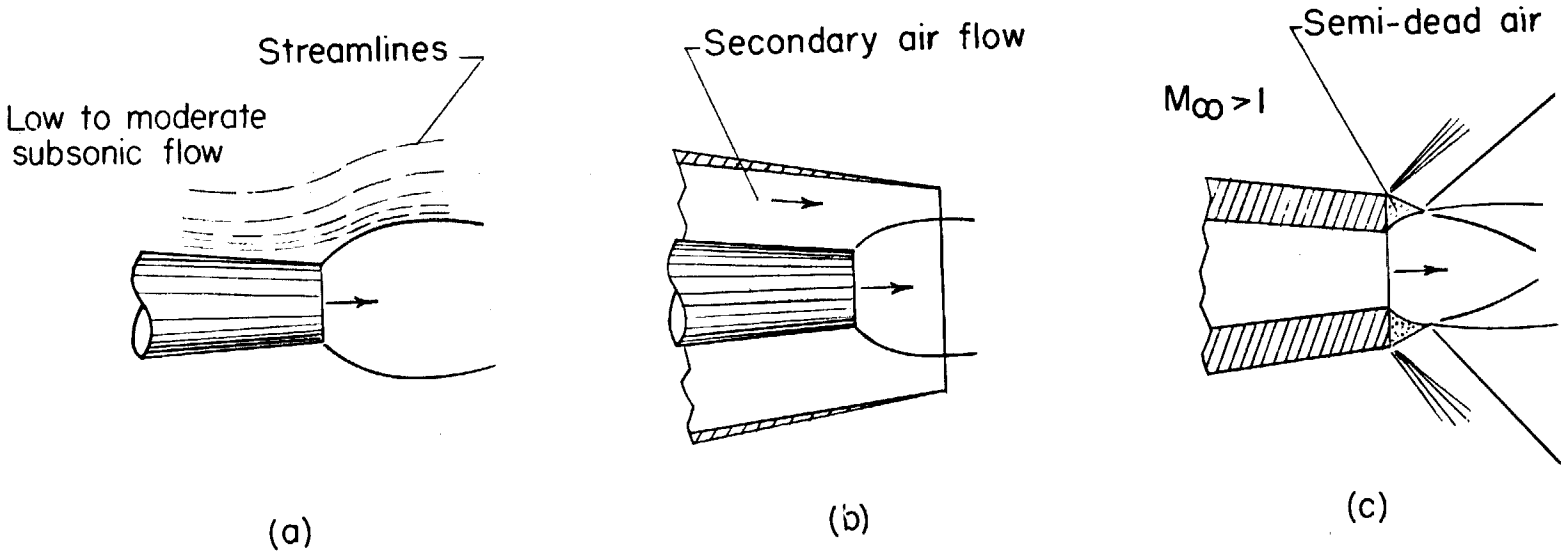

Figure 2.- Sketch of probable fields of application of free jet characteristics.

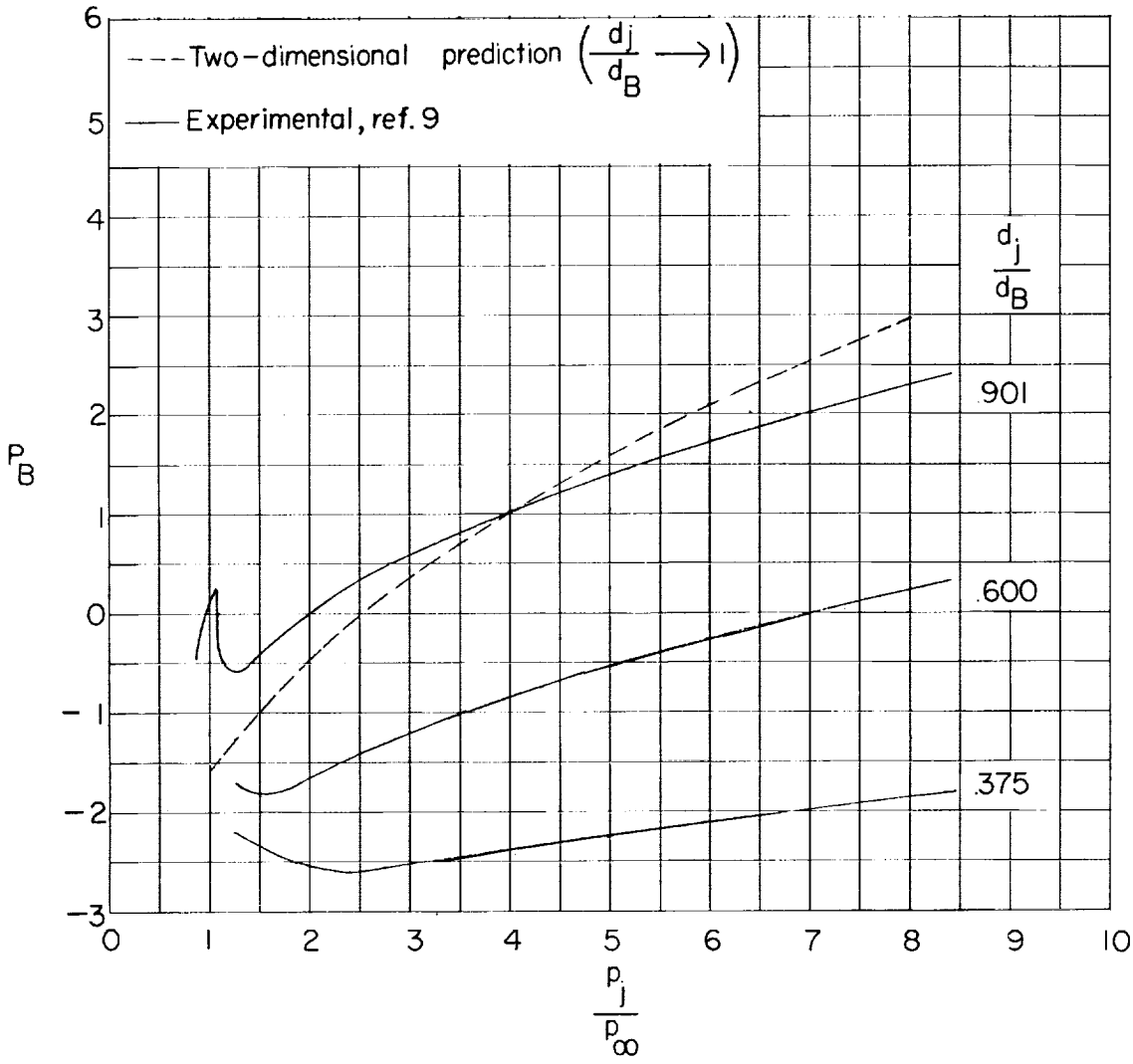

Figure 3.- Example of effects of ratio of jet exit diameter to base diameter upon base pressure. $M_\infty = 1.91$; $M_j = 1.00$; conical boattail angle, 5.6°; ratio of jet exit diameter to maximum body diameter, 0.37.

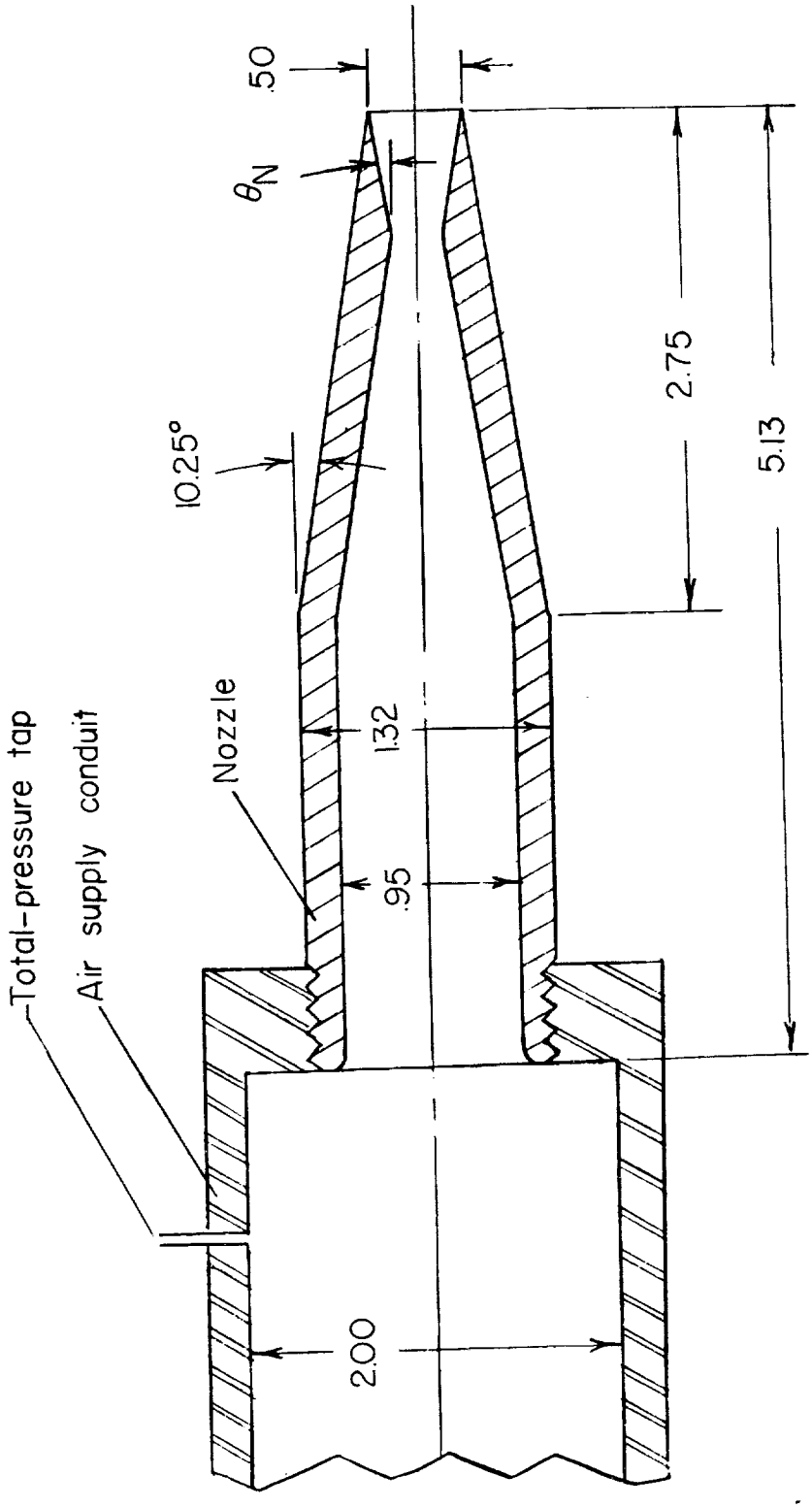

Figure 4.- Sketch of typical divergent nozzle employed in tests. All dimensions are in inches unless otherwise specified.

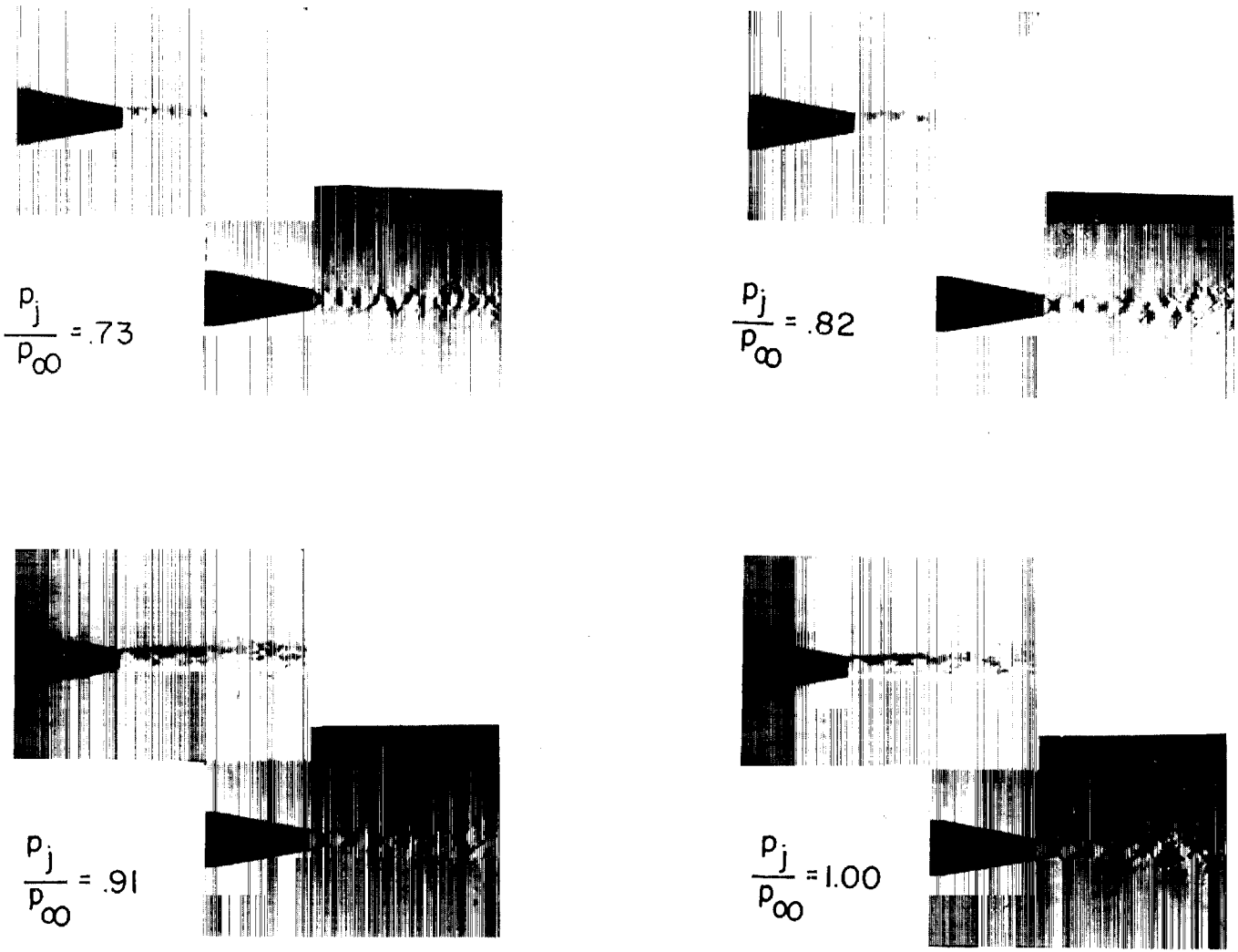

L-86497

Figure 5.- Illustrative sequence of double-image schlieren photographs. $M_j = 1.50$; $\theta_N = 5^\circ$.

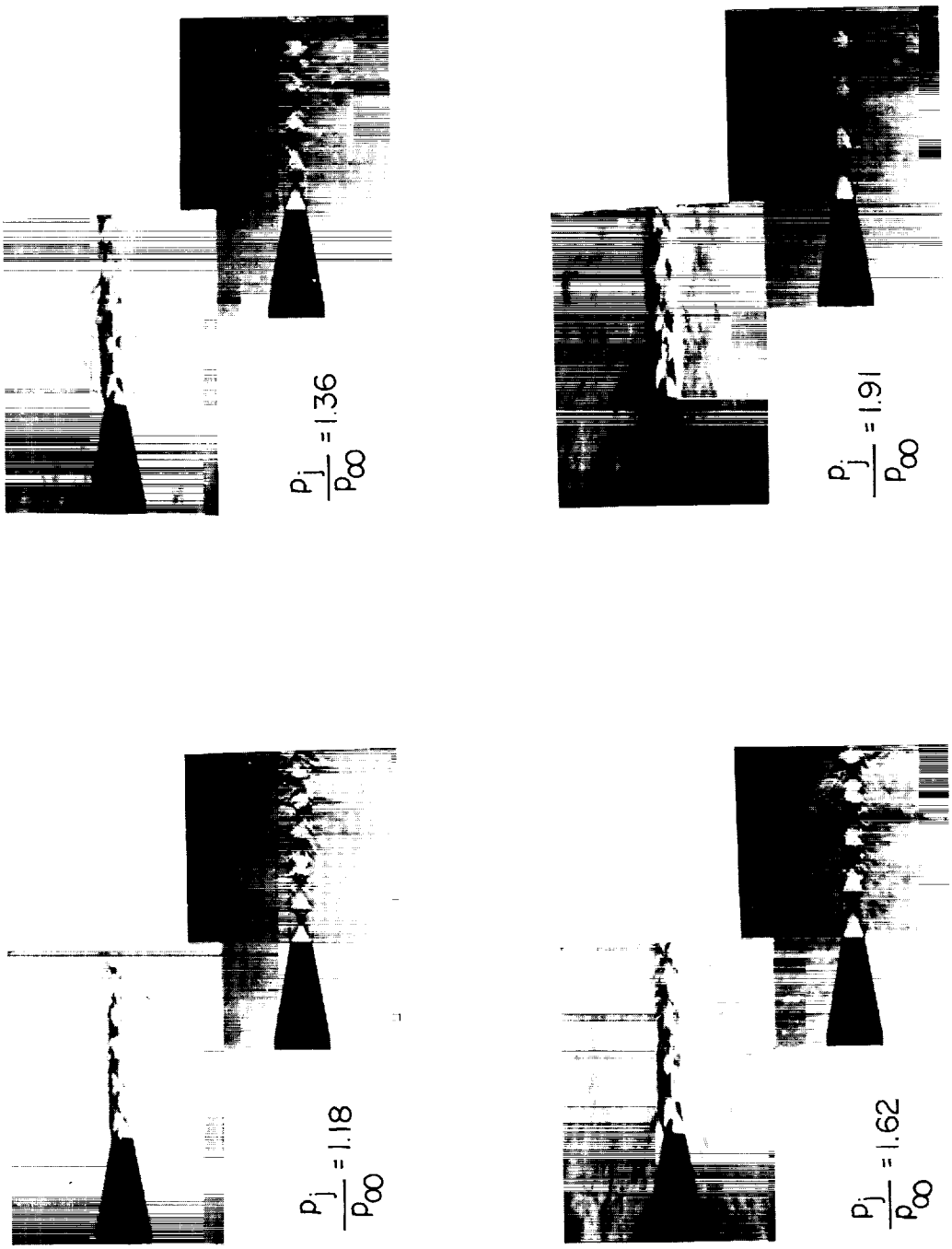

Figure 5.- Continued.

L-86499

Figure 5.- Concluded.

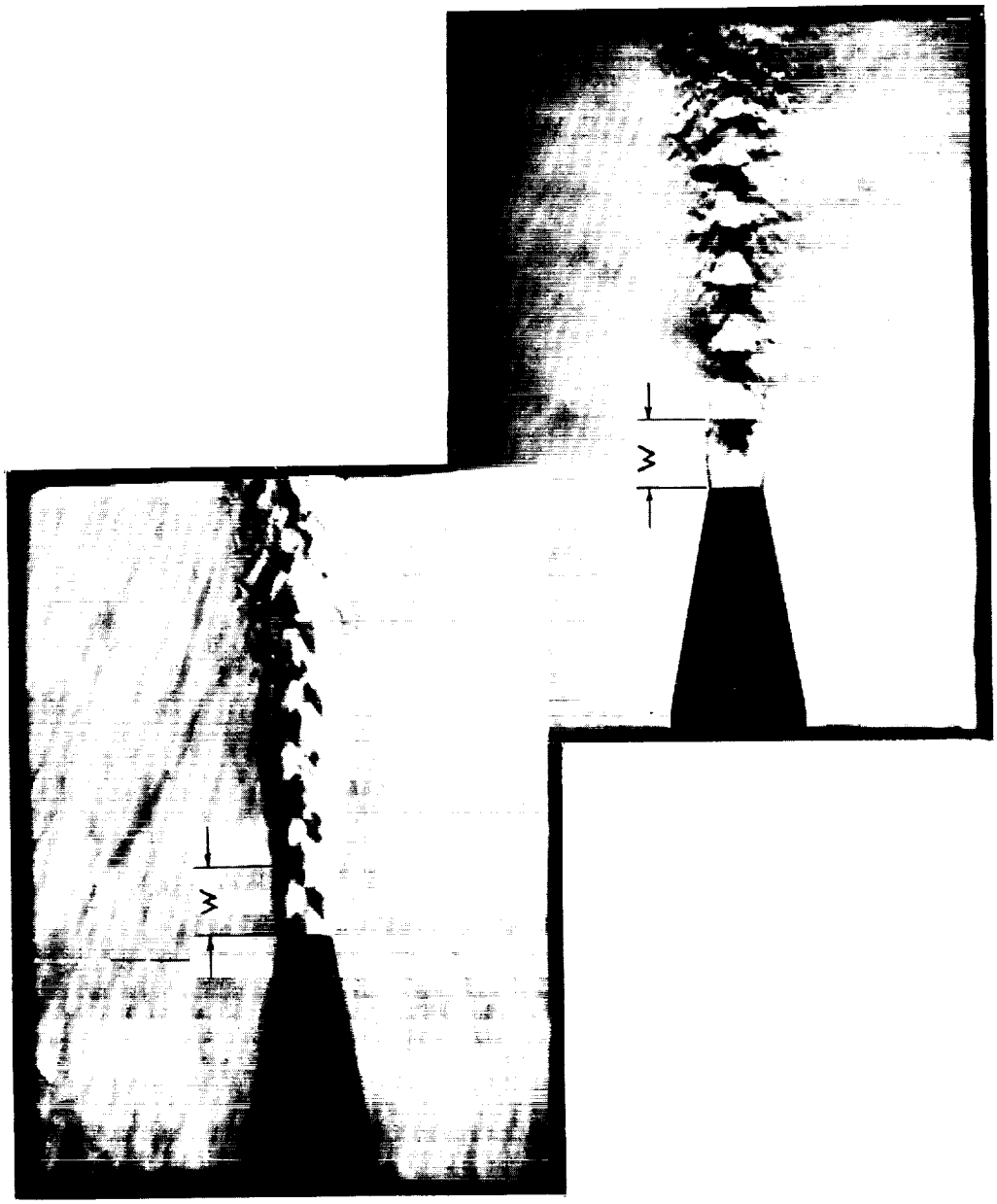

L-86500

Figure 6.- Example of primary wave length. $M_j = 1.00$; $\theta_N = 0°$; $\frac{p_j}{p_\infty} = 1.76$.

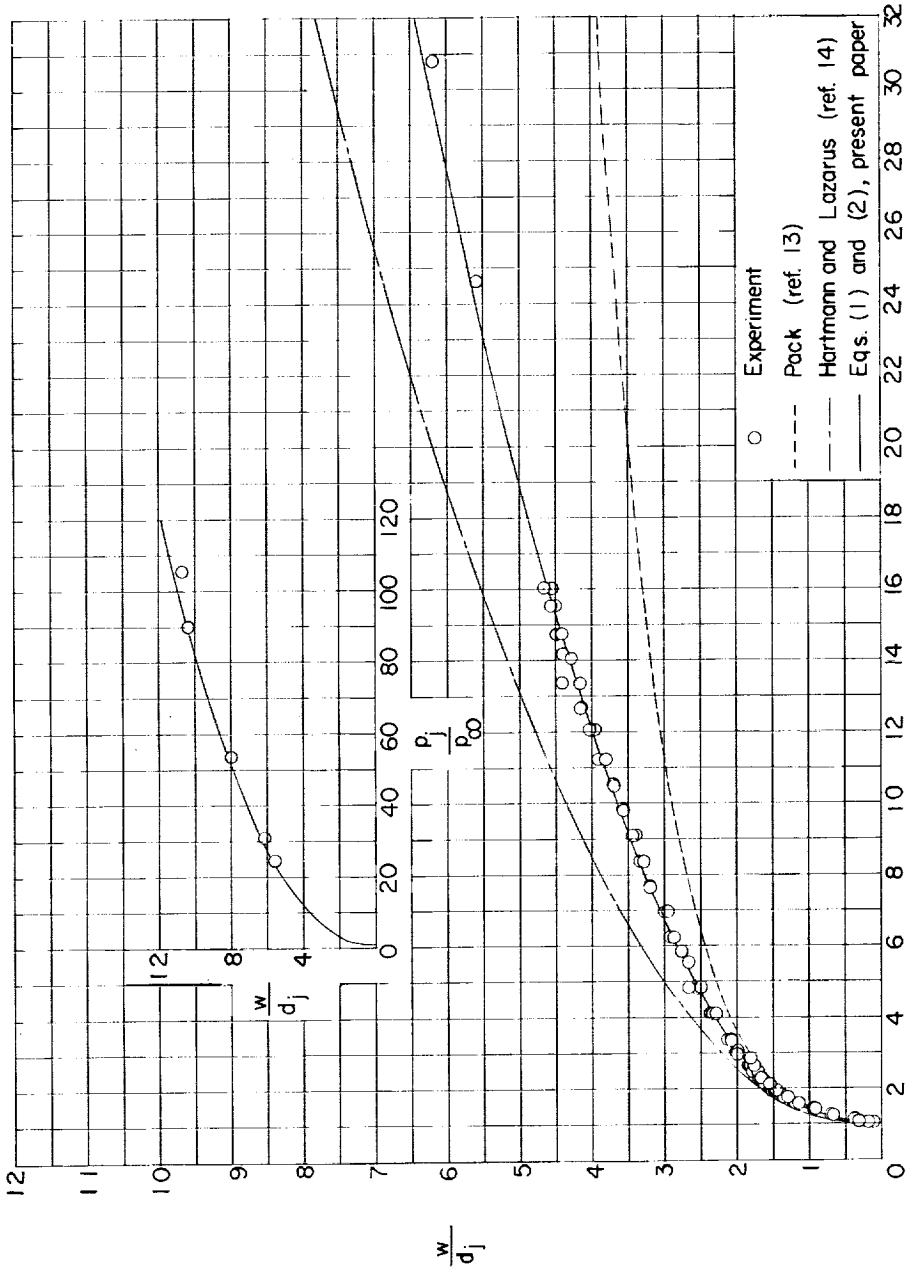

(a) $M_j = 1.00$.

Figure 7.- Effects of jet pressure ratio and nozzle divergence angle upon nondimensional primary wave length.

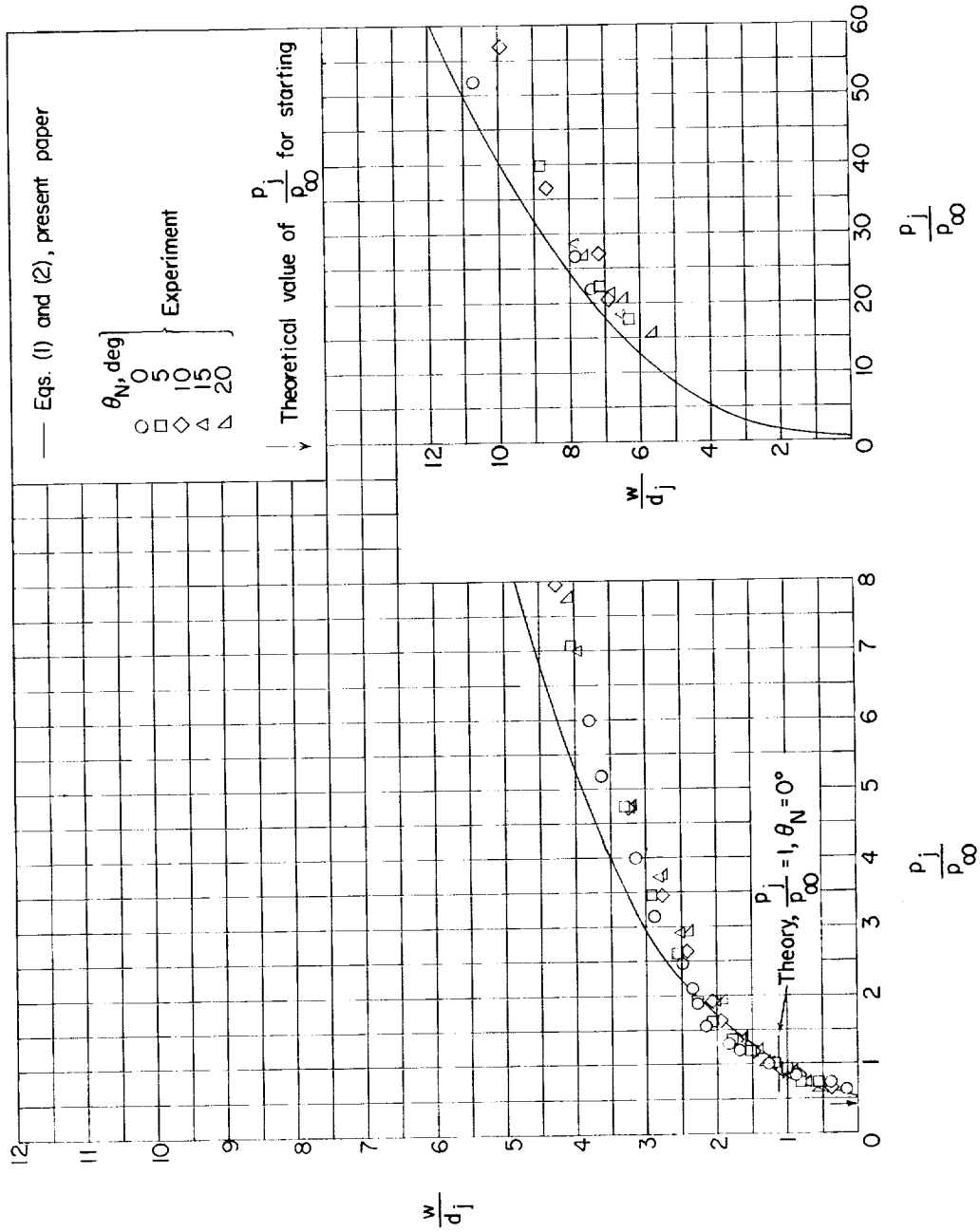

(b) $M_j = 1.50$.

Figure 7.- Continued.

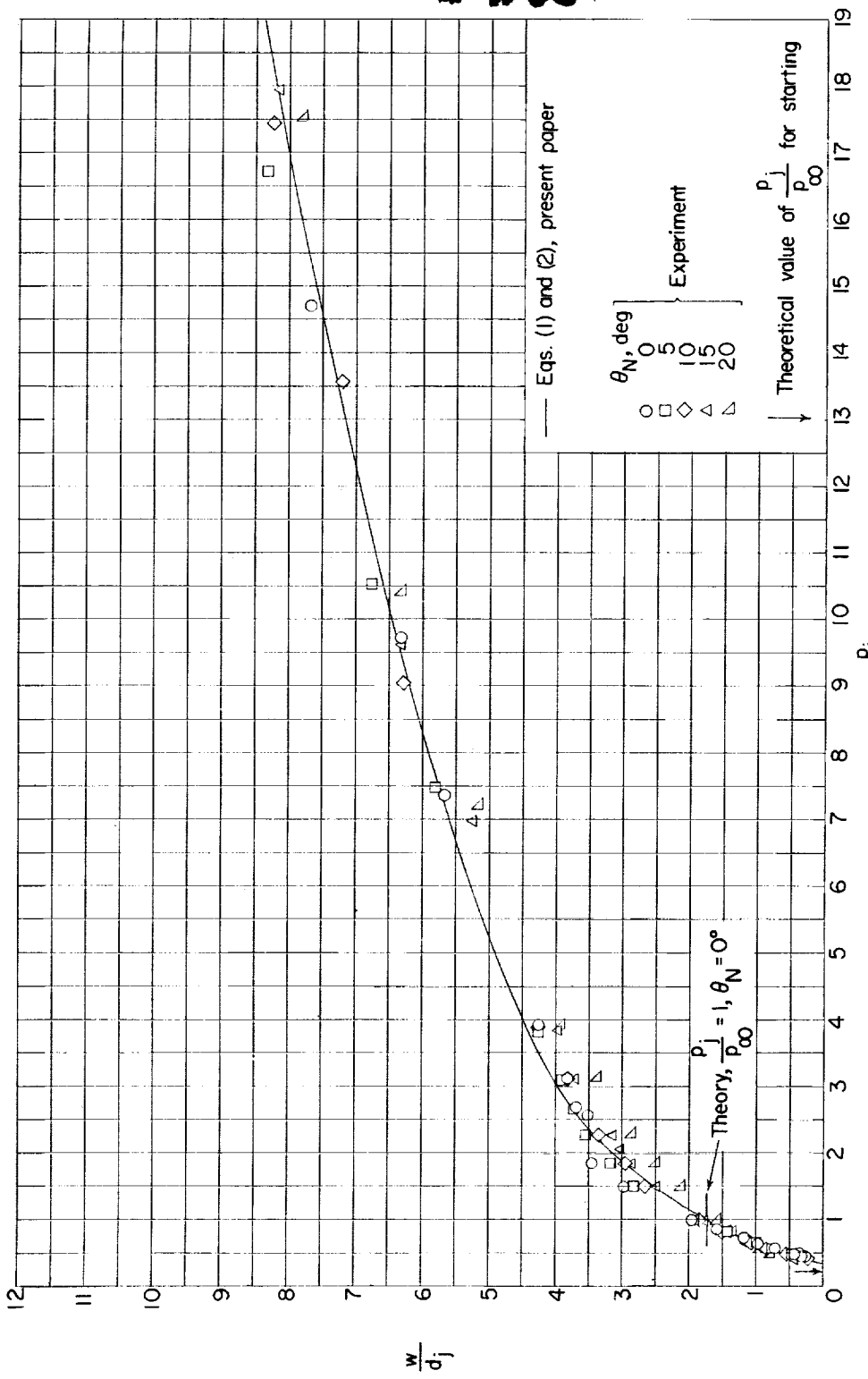

(c) $M_j = 2.00$.

Figure 7.- Continued.

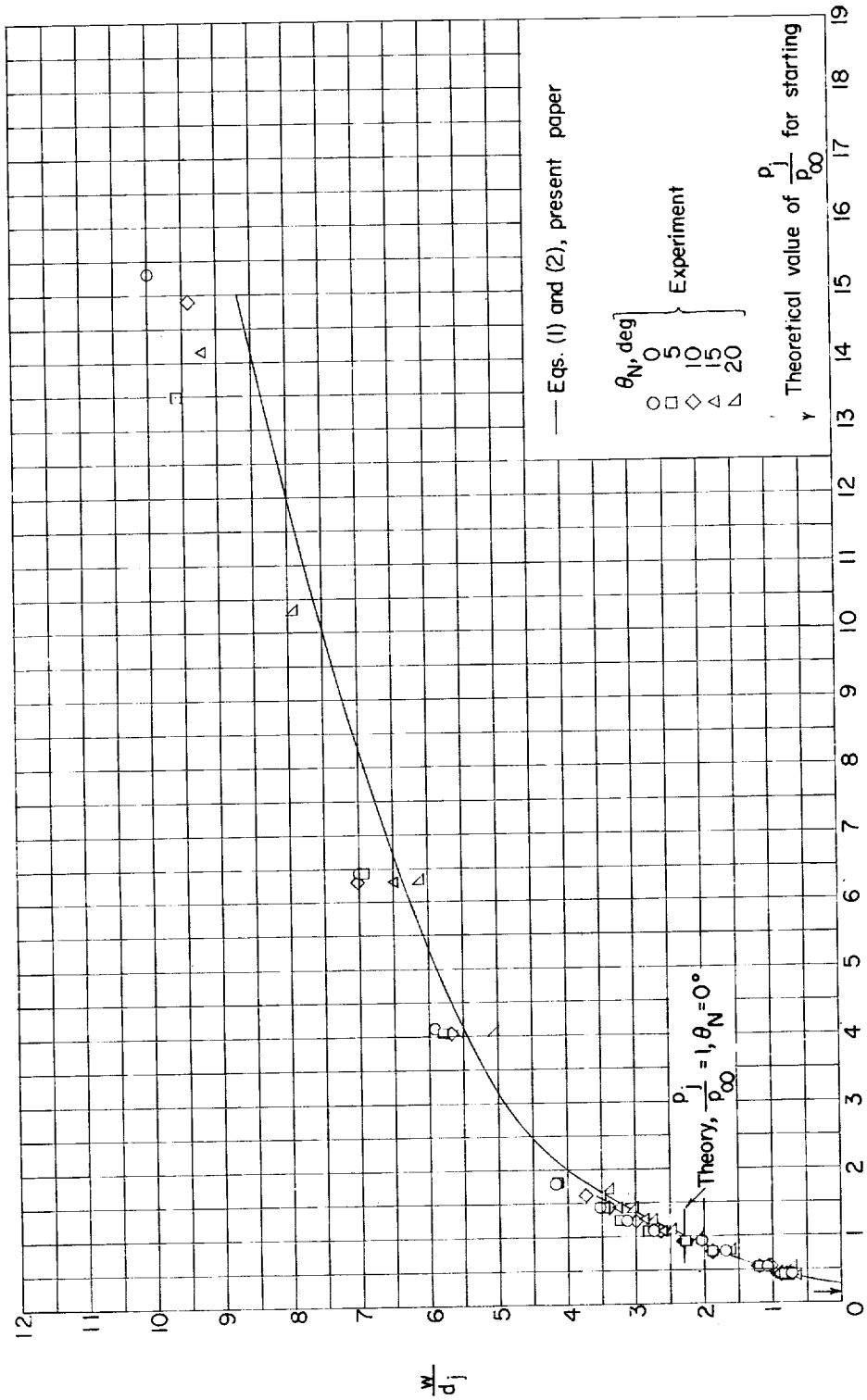

(d) M_j=2.50.

Figure 7.- Continued.

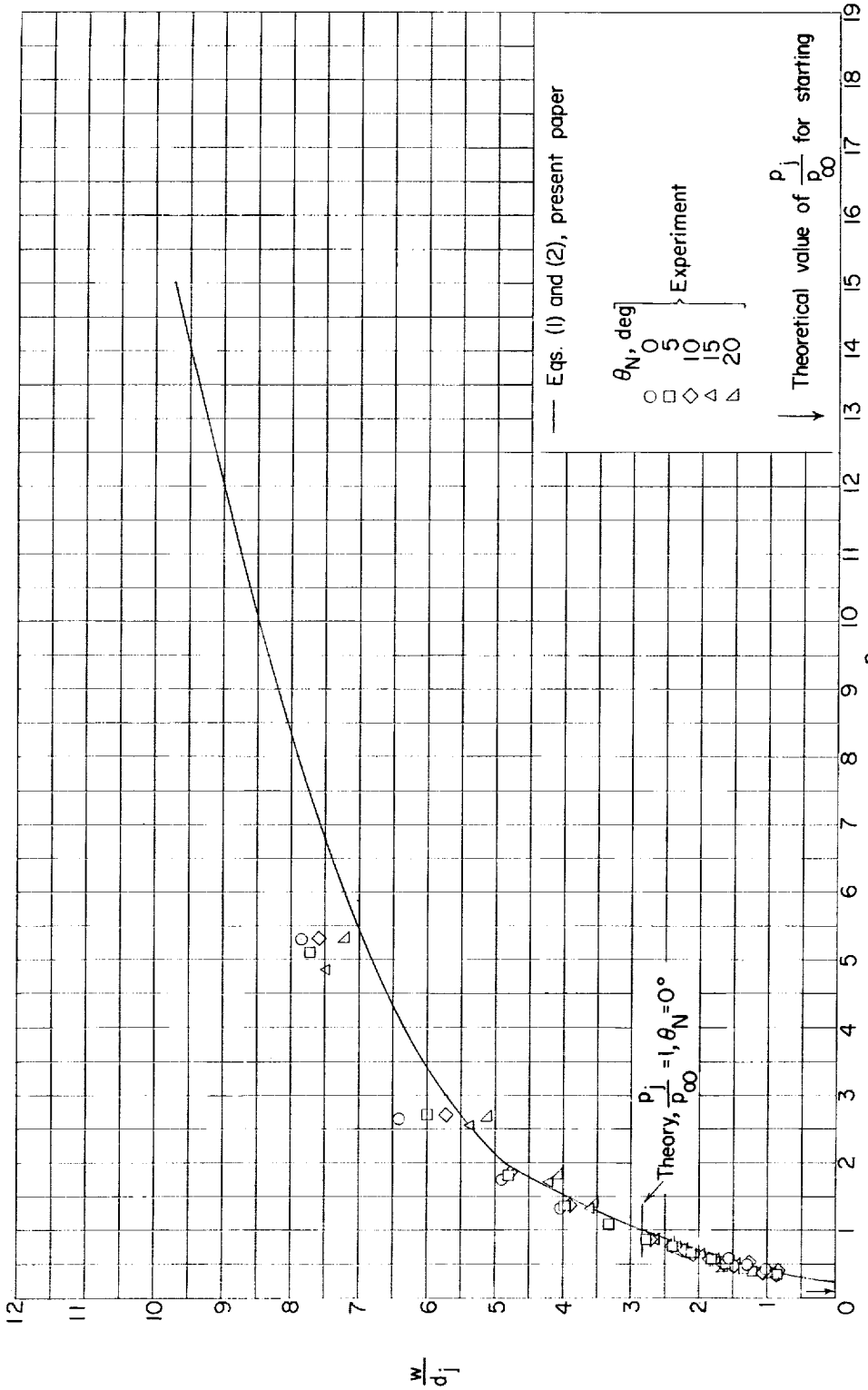

(e) $M_j = 3.00$.

Figure 7.- Concluded.

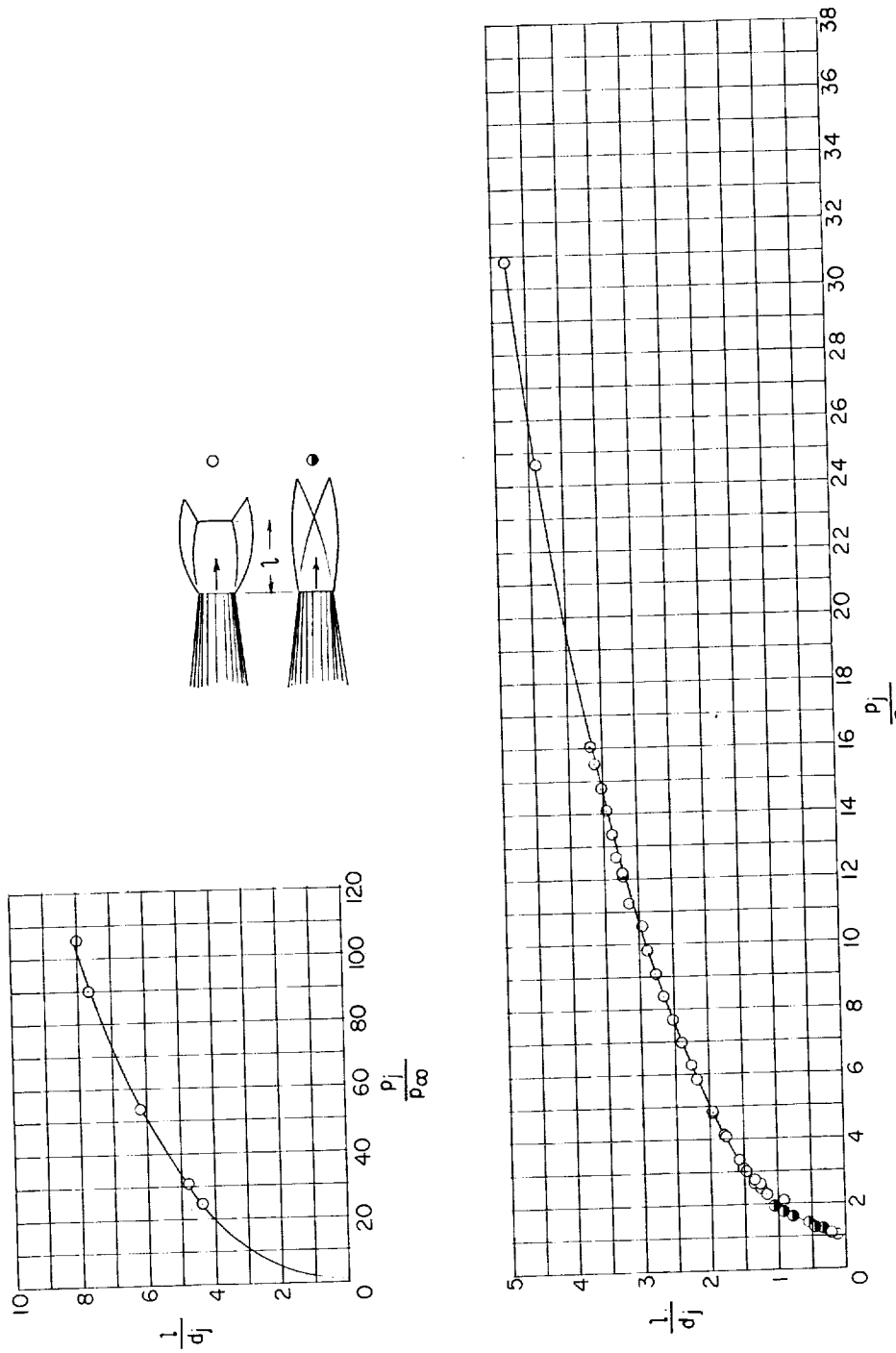

(a) $M_j = 1.00$.

Figure 8.- Effects of jet pressure ratio and nozzle divergence angle upon nondimensional distance along jet axis from plane of jet exit to focal point of intersecting shock pattern or to Riemann wave.

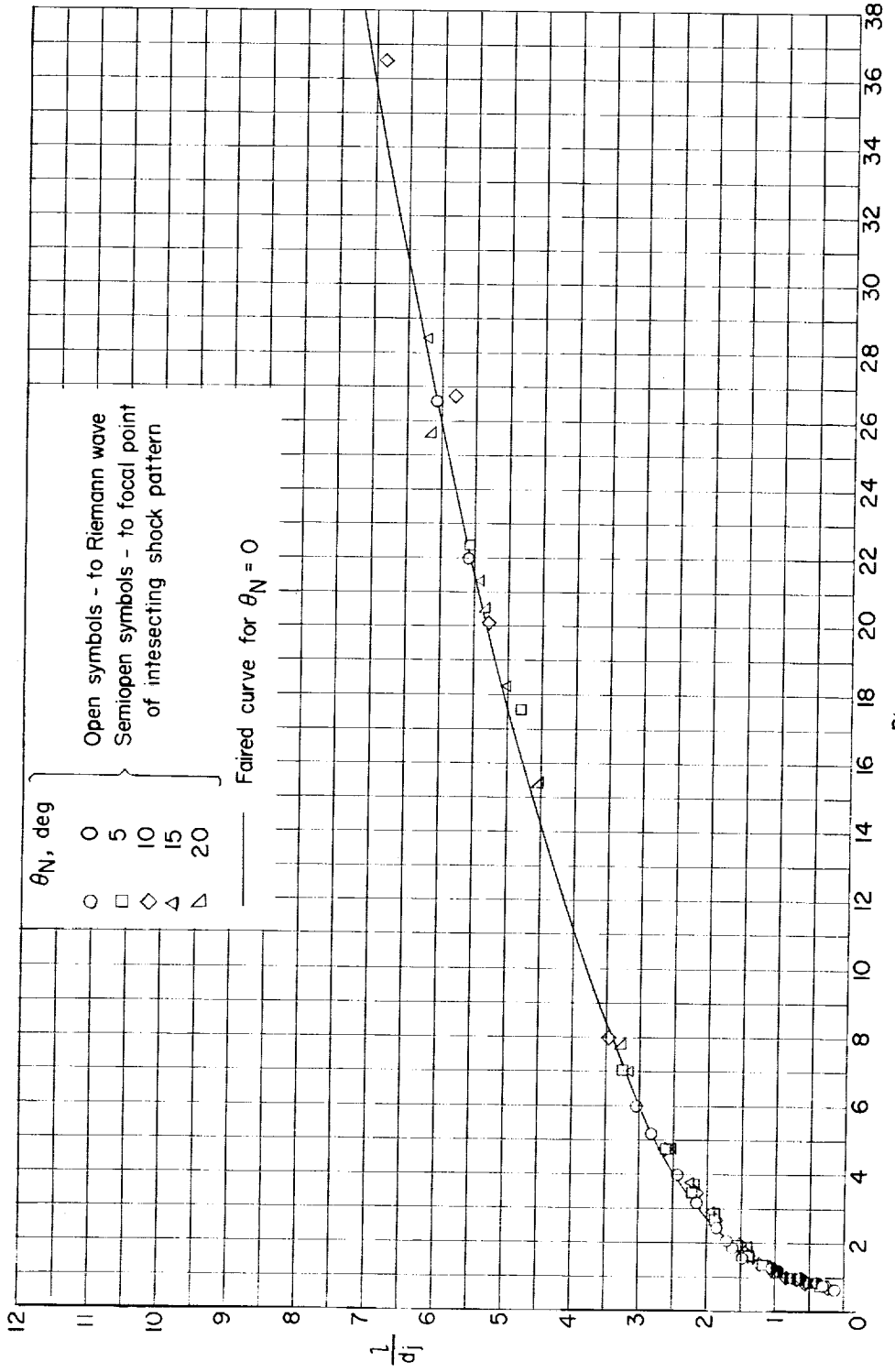

(b) $M_j = 1.50$

Figure 8.- Continued.

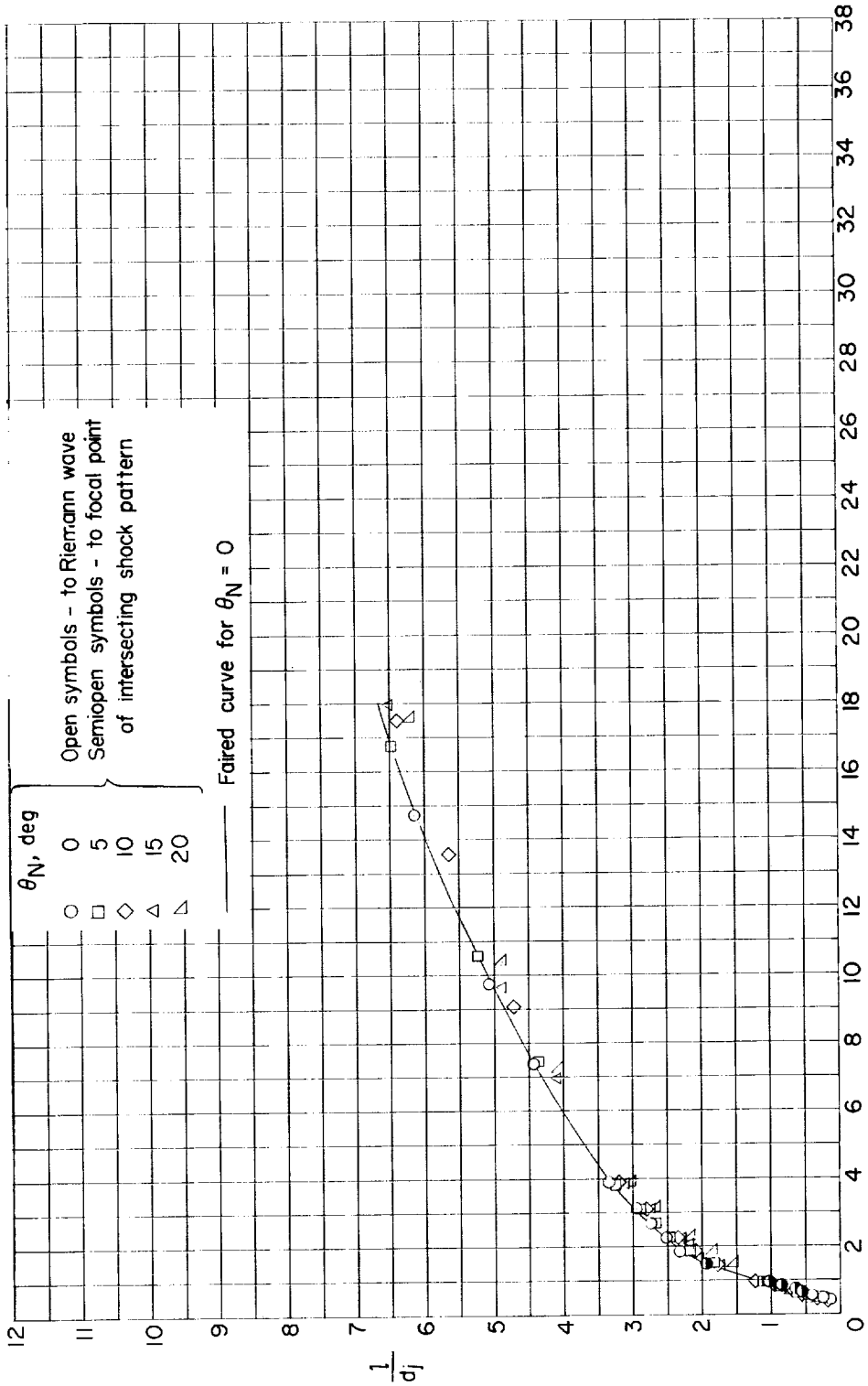

(c) $M_j = 2.00$.

Figure 8.- Continued.

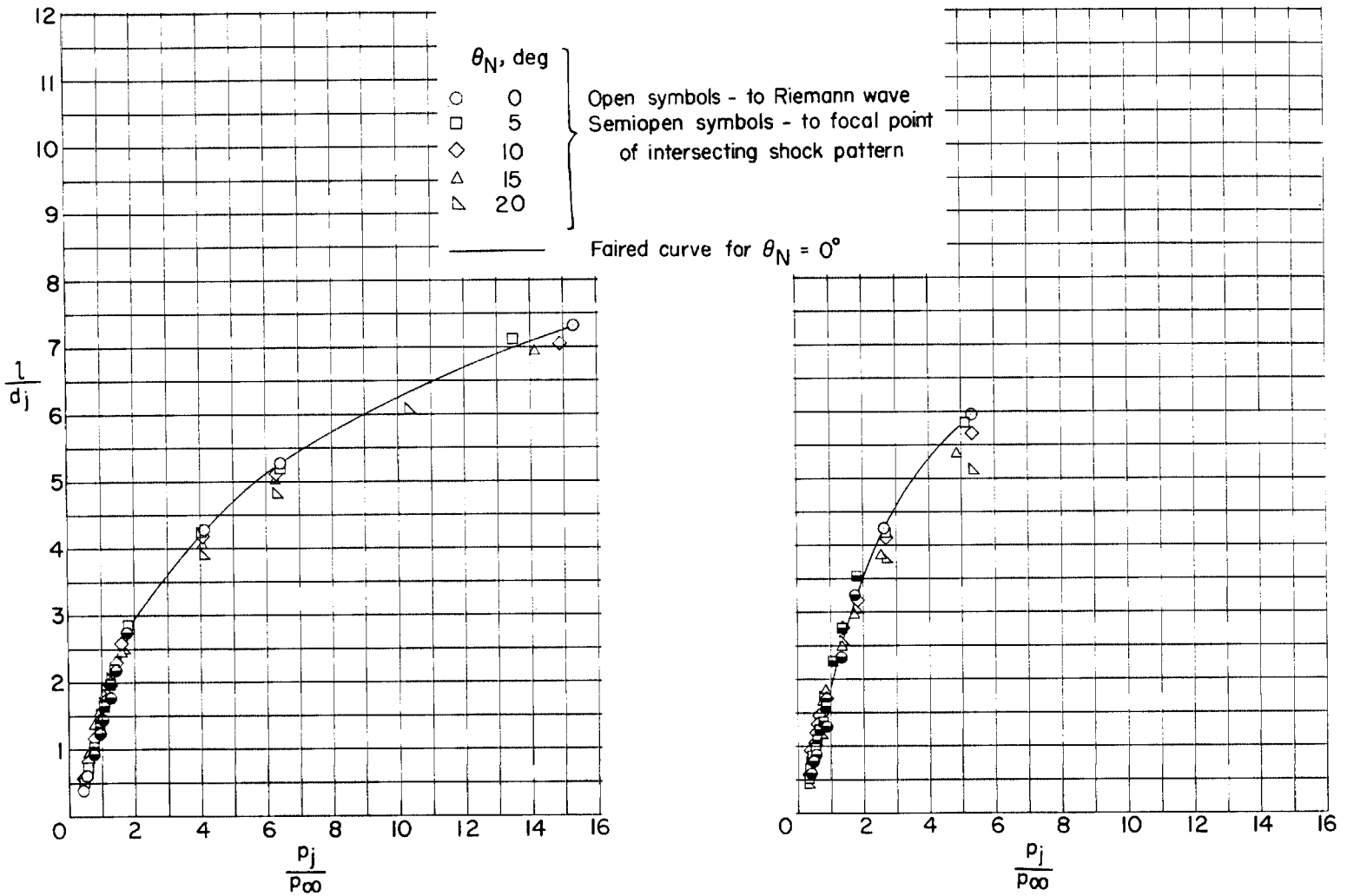

Figure 8.- Concluded.

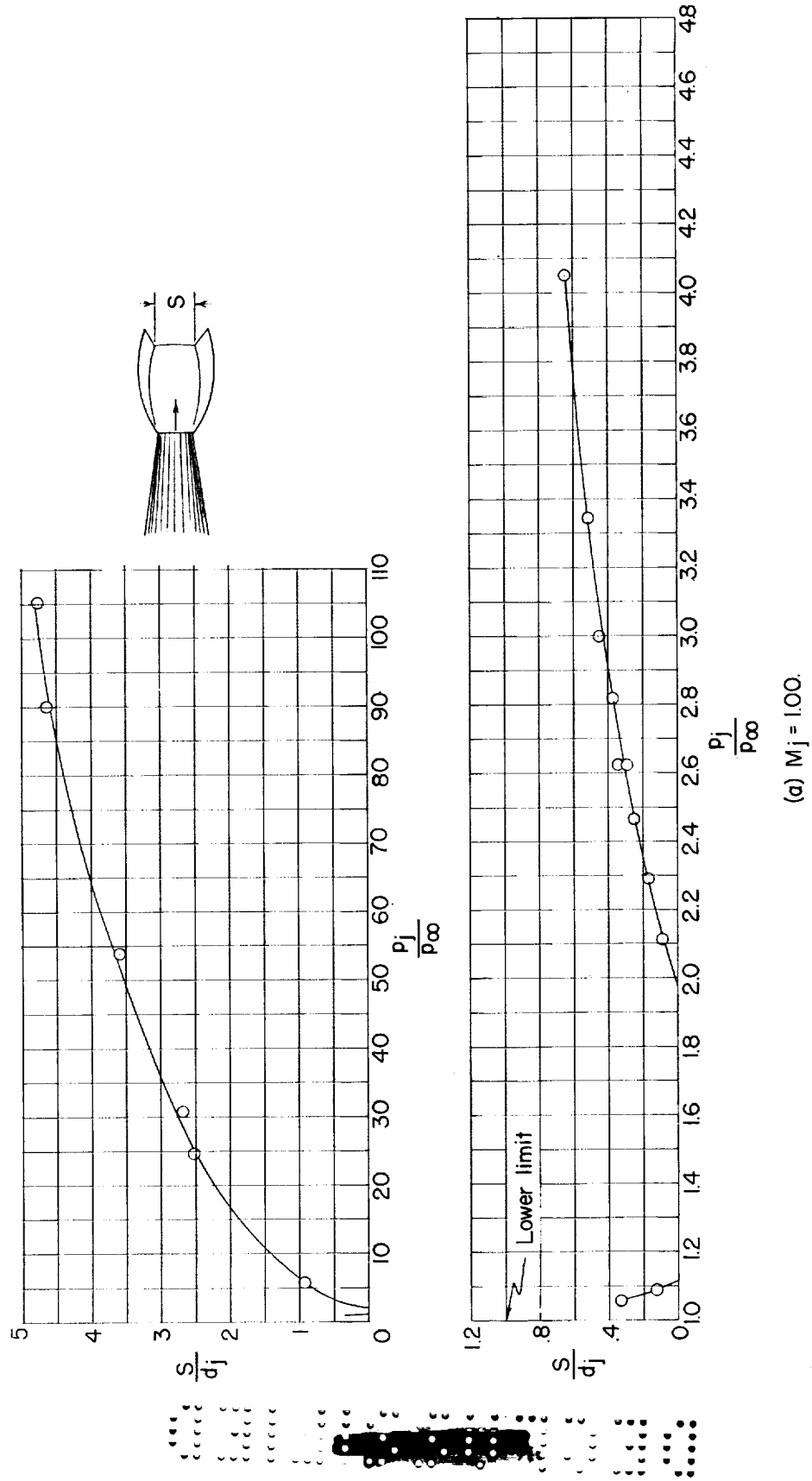

(a) $M_j = 1.00$.

Figure 9.- Effects of jet pressure ratio and nozzle divergence angle upon nondimensional diameter of Riemann wave.

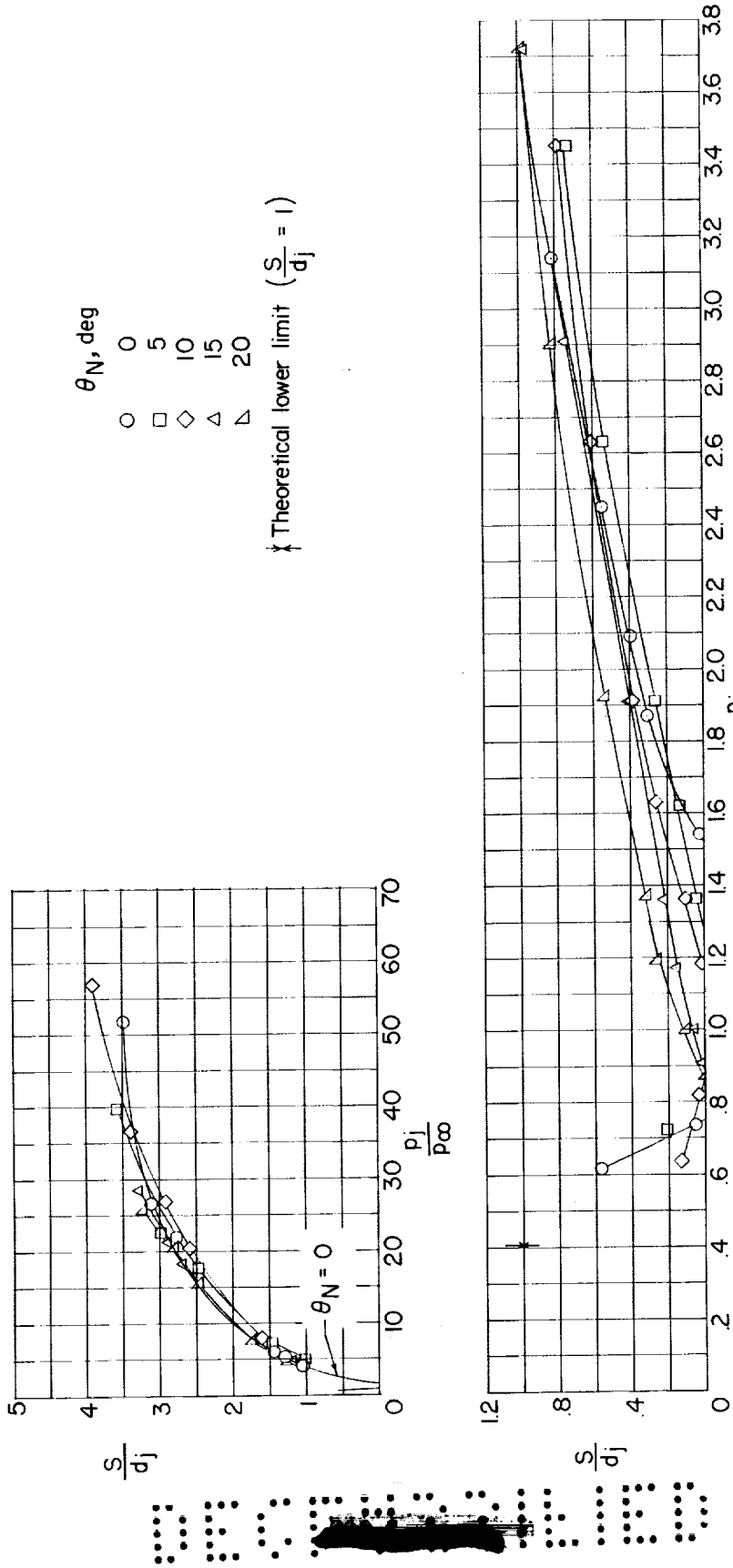

(b) $M_j = 1.50$.

Figure 9.- Continued.

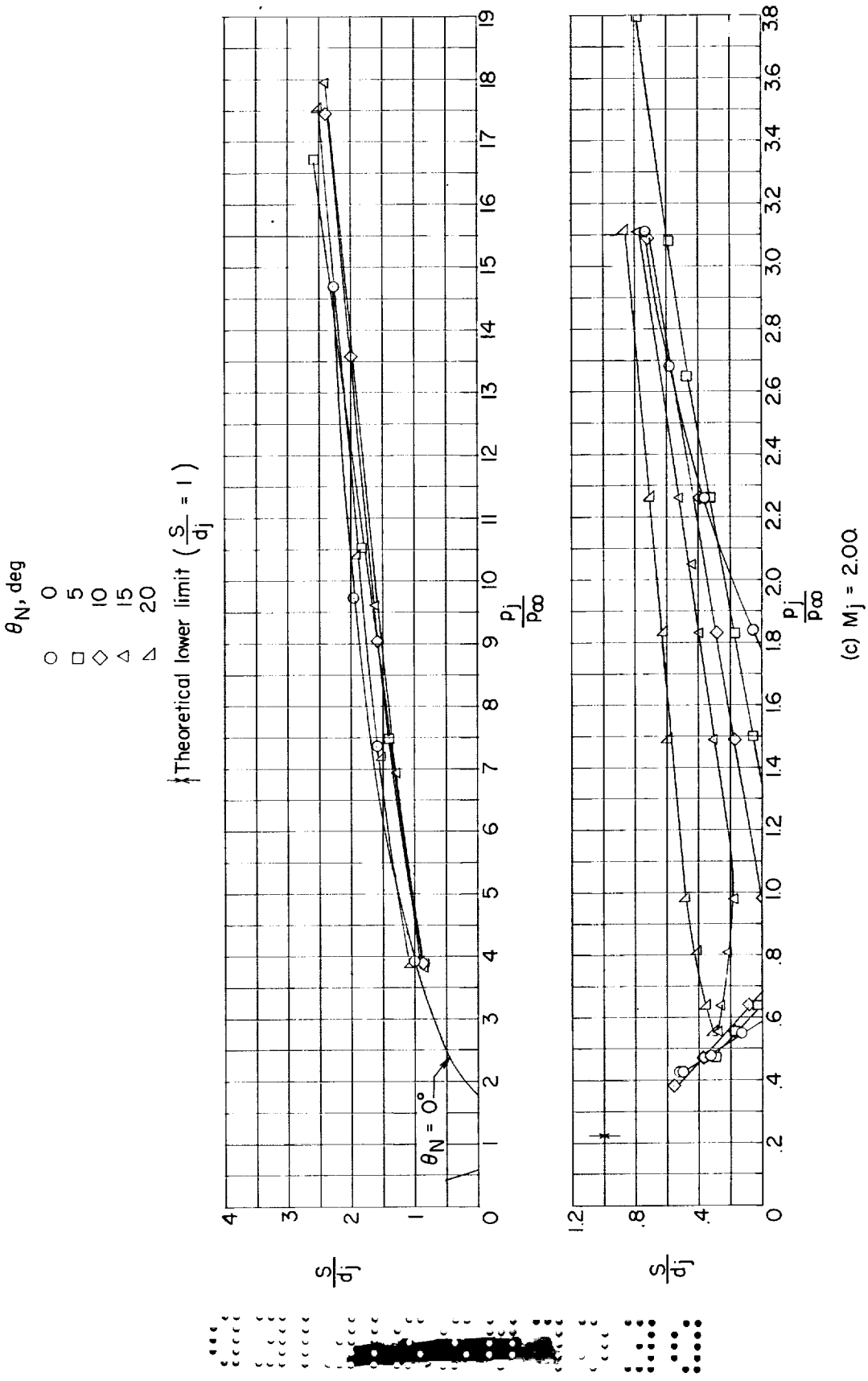

Figure 9.- Continued.

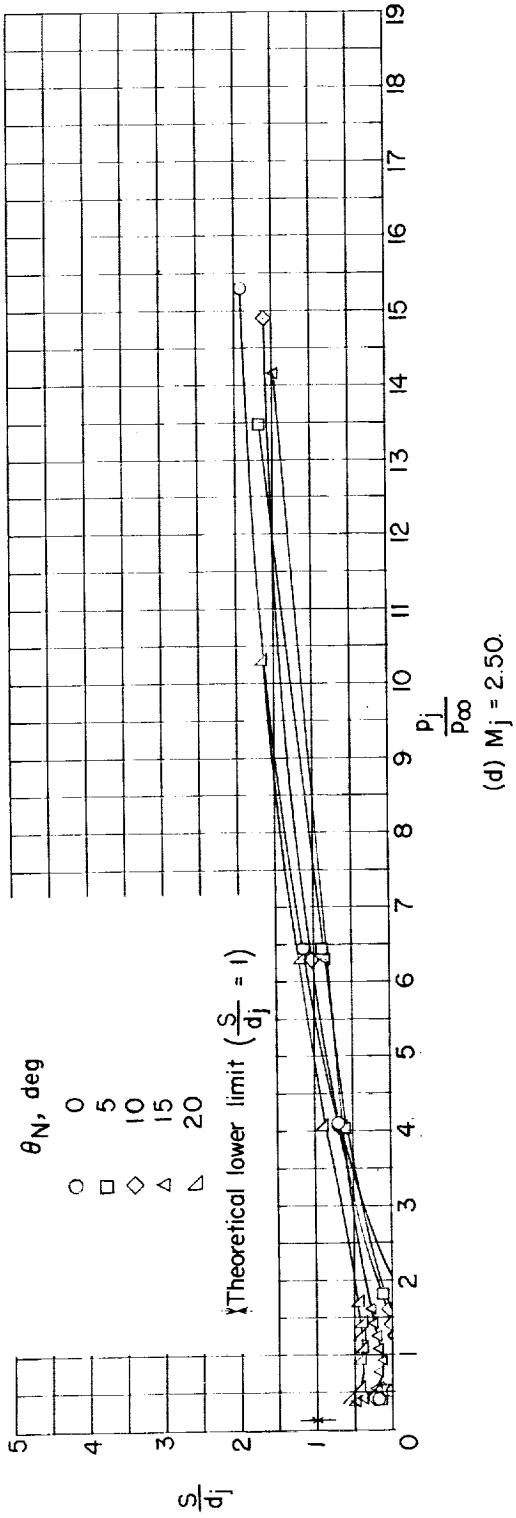

(d) $M_j = 2.50$.

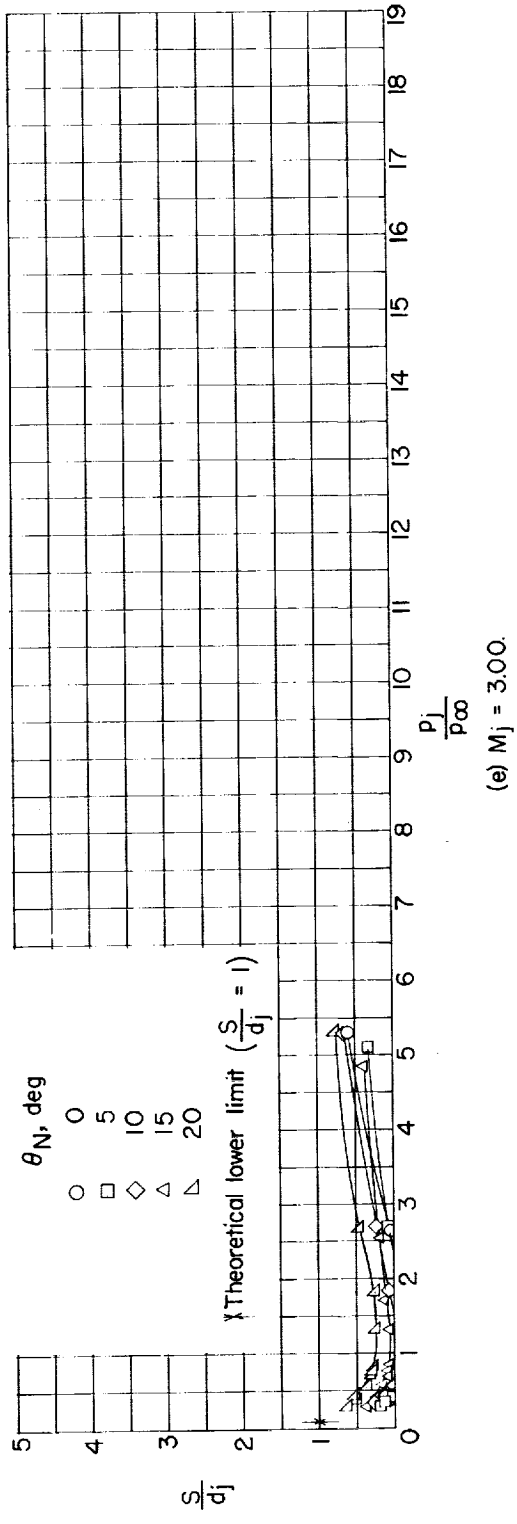

(e) $M_j = 3.00$.

Figure 9.- Concluded.

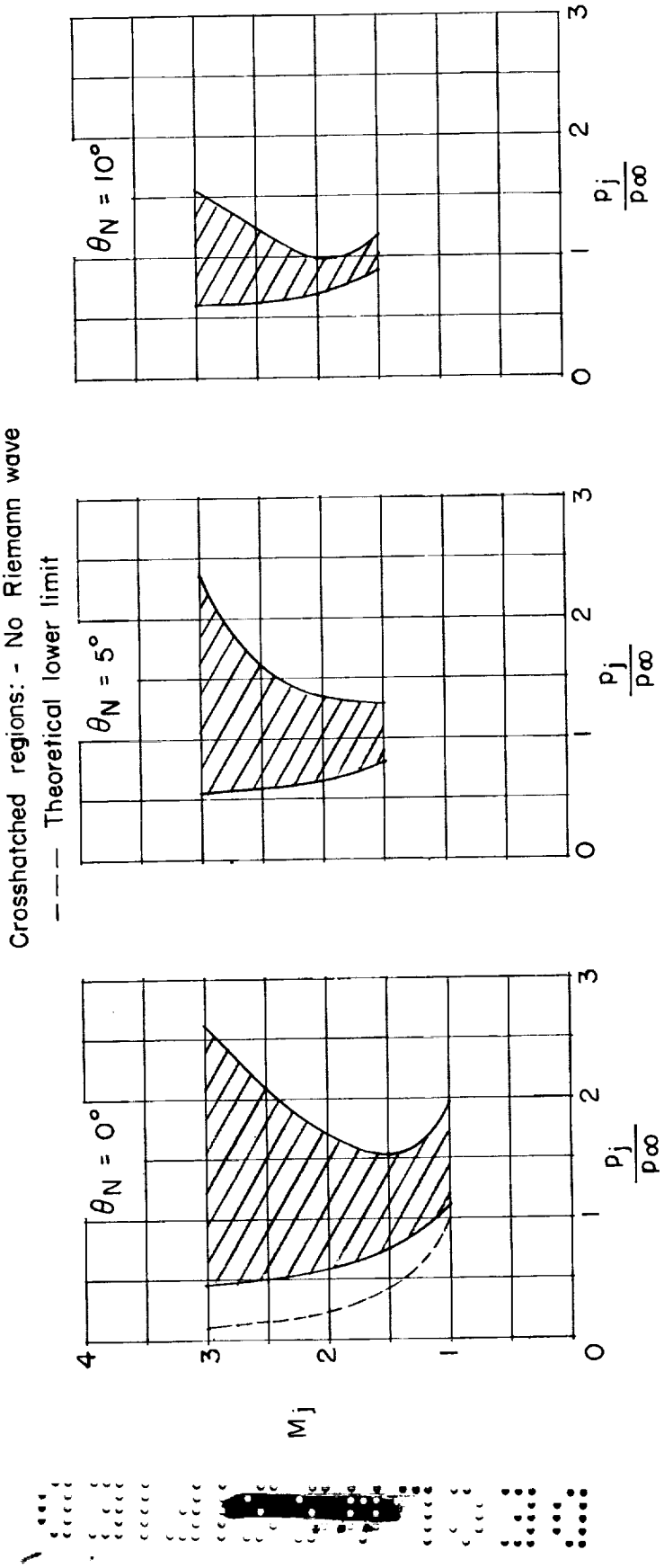

Figure 10.- Range in which no Riemann wave occurs.

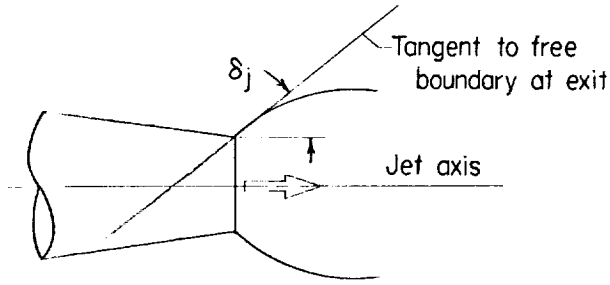

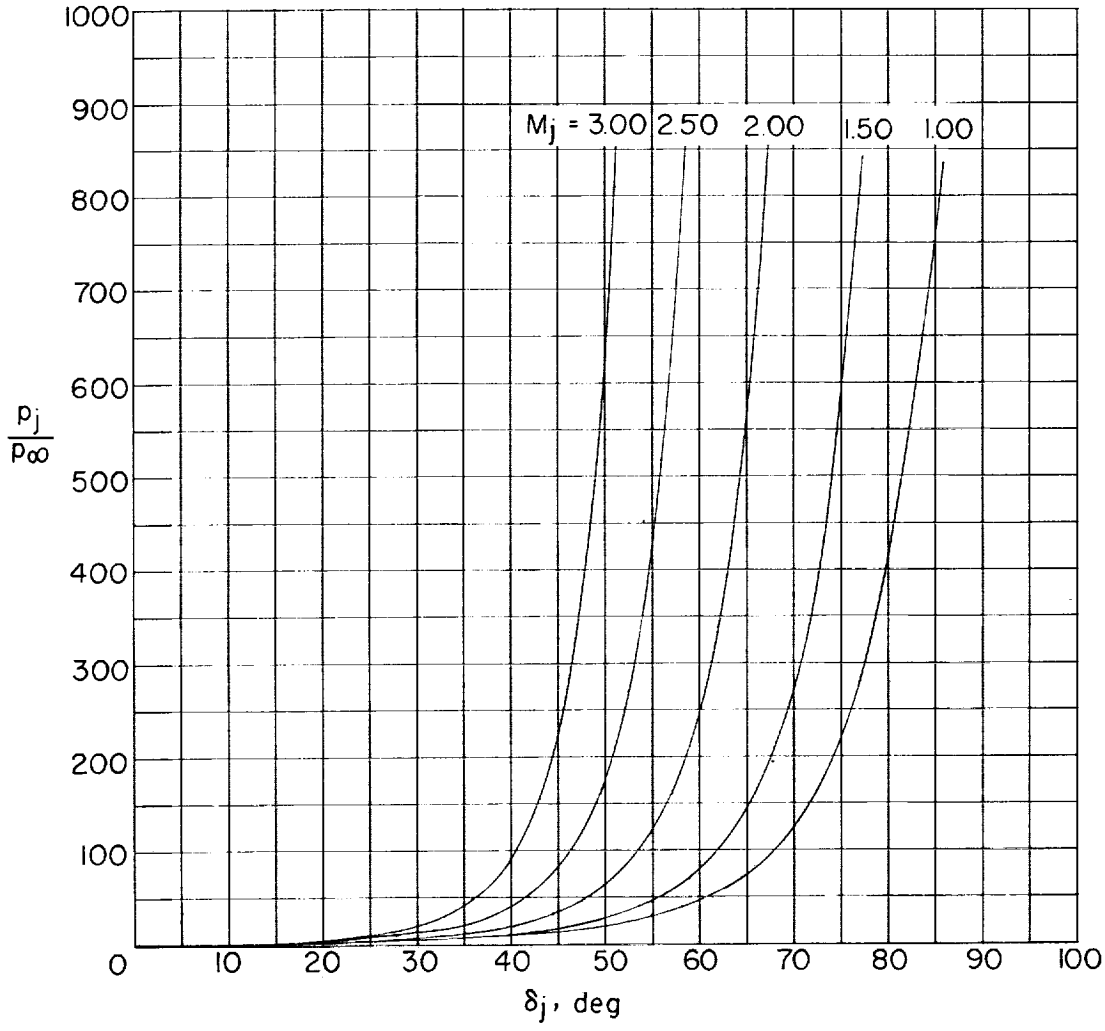

Figure 11.- Theoretical variation in initial inclination of jet boundary with jet pressure ratio and jet Mach number. $\theta_N = 0^\circ$; $\gamma_j = 1.400$.

L-86501

Figure 12.- Example of large initial inclination of jet boundary.

$M_j = 1.00$; $\theta_N = 0°$; $\frac{p_j}{p_\infty} \approx 105$.

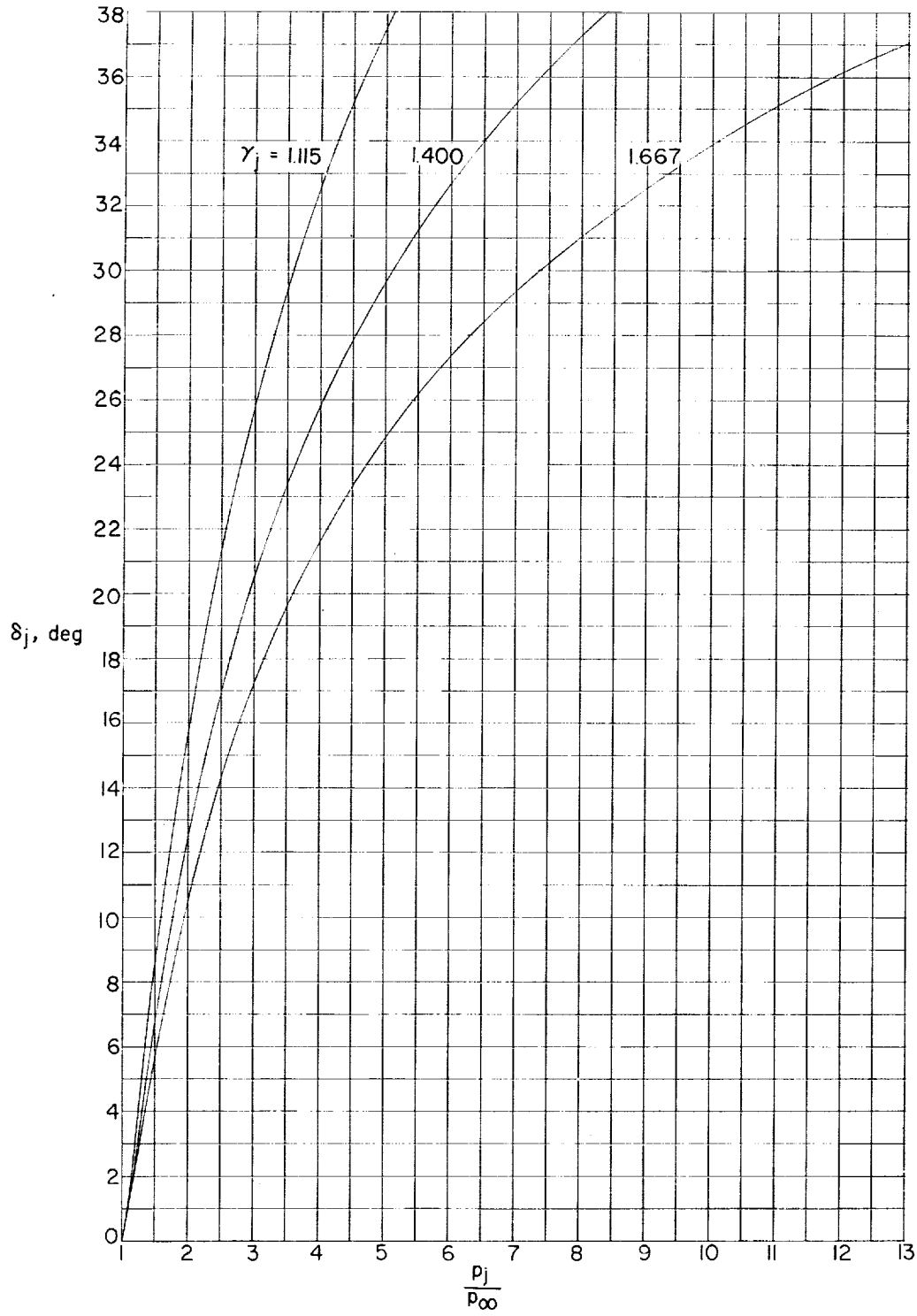

Figure 13.- Effect of the ratio of specific heats of the jet upon the initial inclination of the jet boundary. M_j = 1.00.

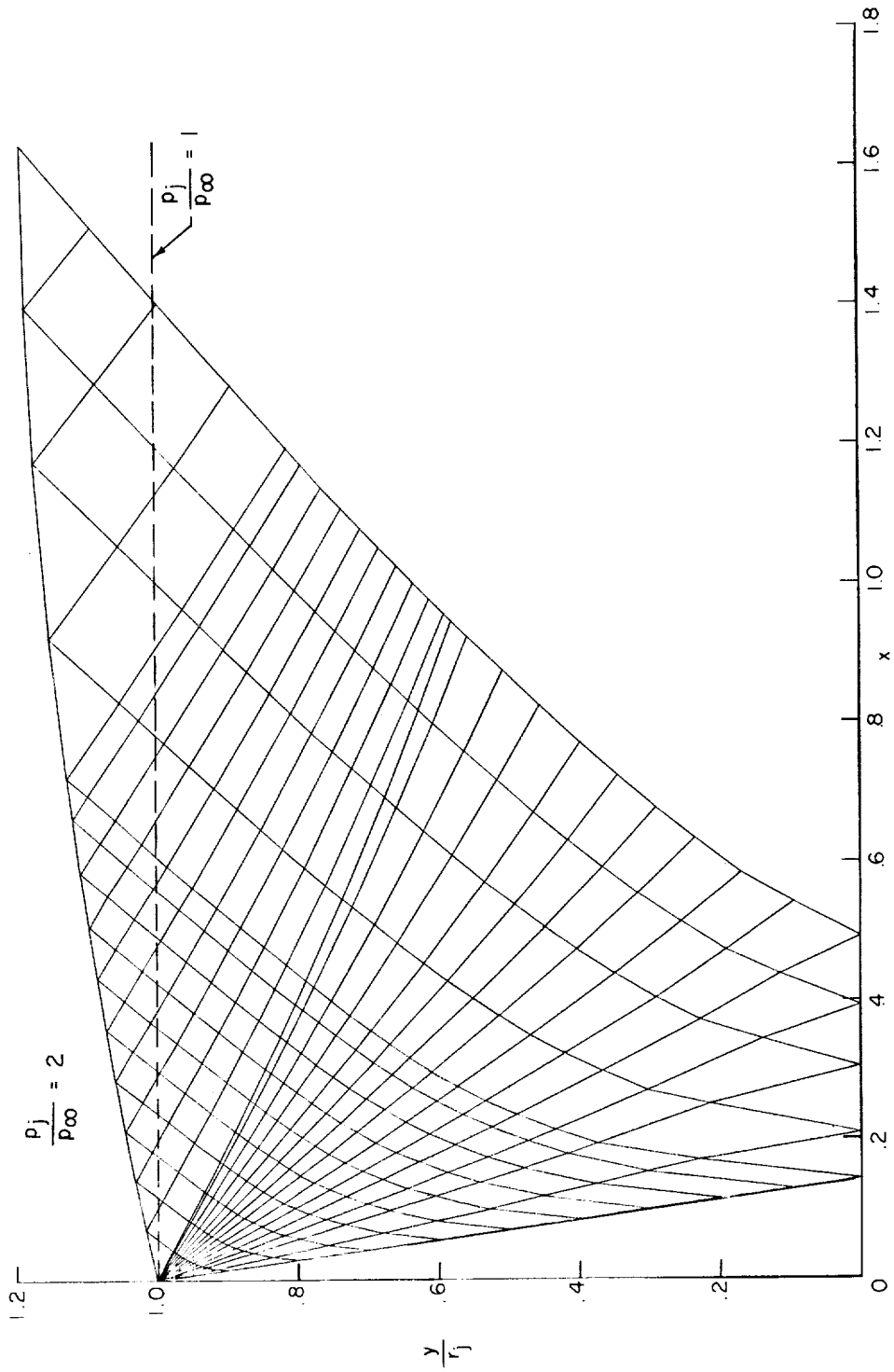

(a) $M_j = 1.01$; $\theta_N = 0°$; $\gamma_j = 1.400$.

Figure 14.- Characteristic nets.

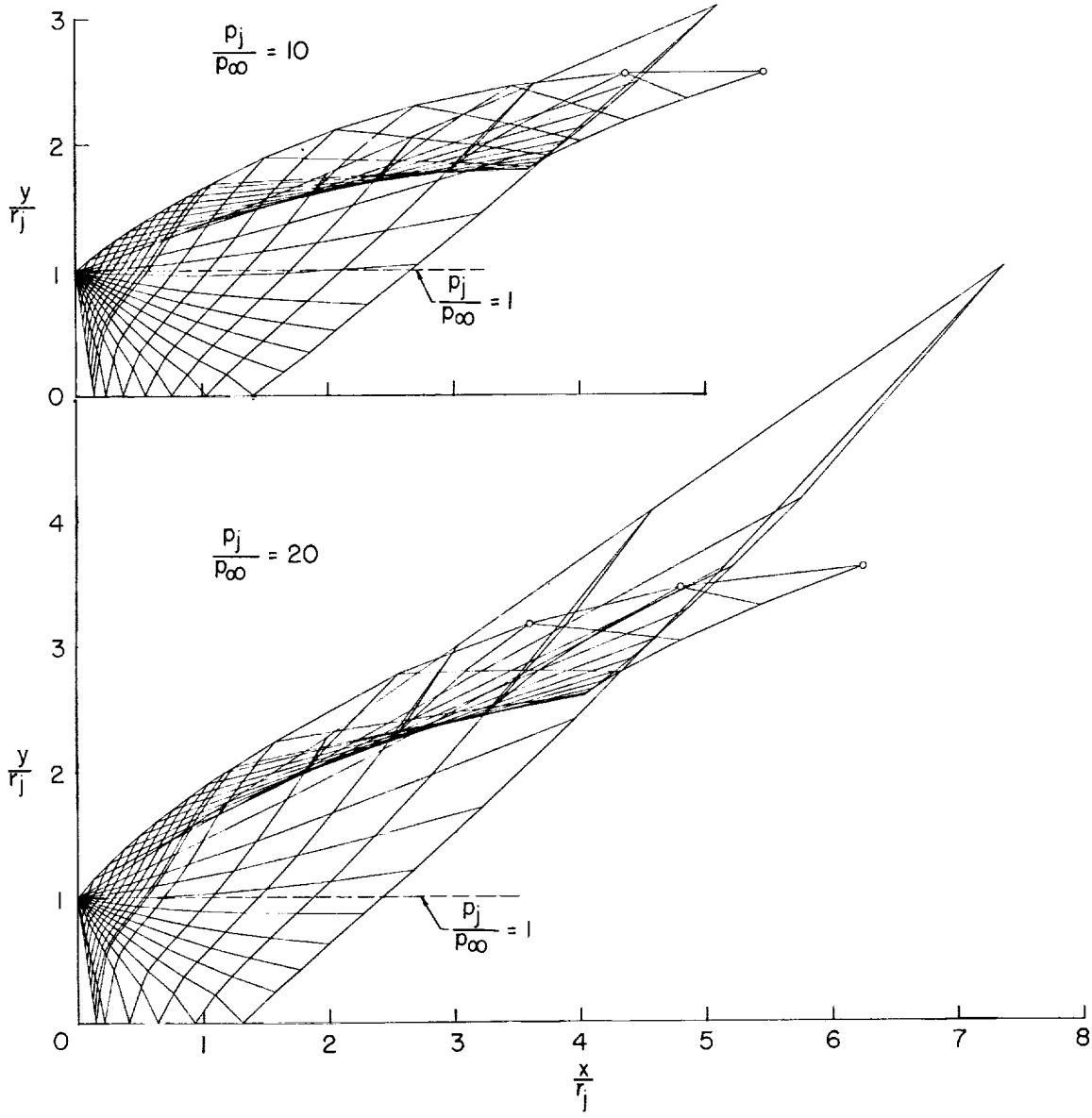

(a) Concluded

Figure 14.- Continued.

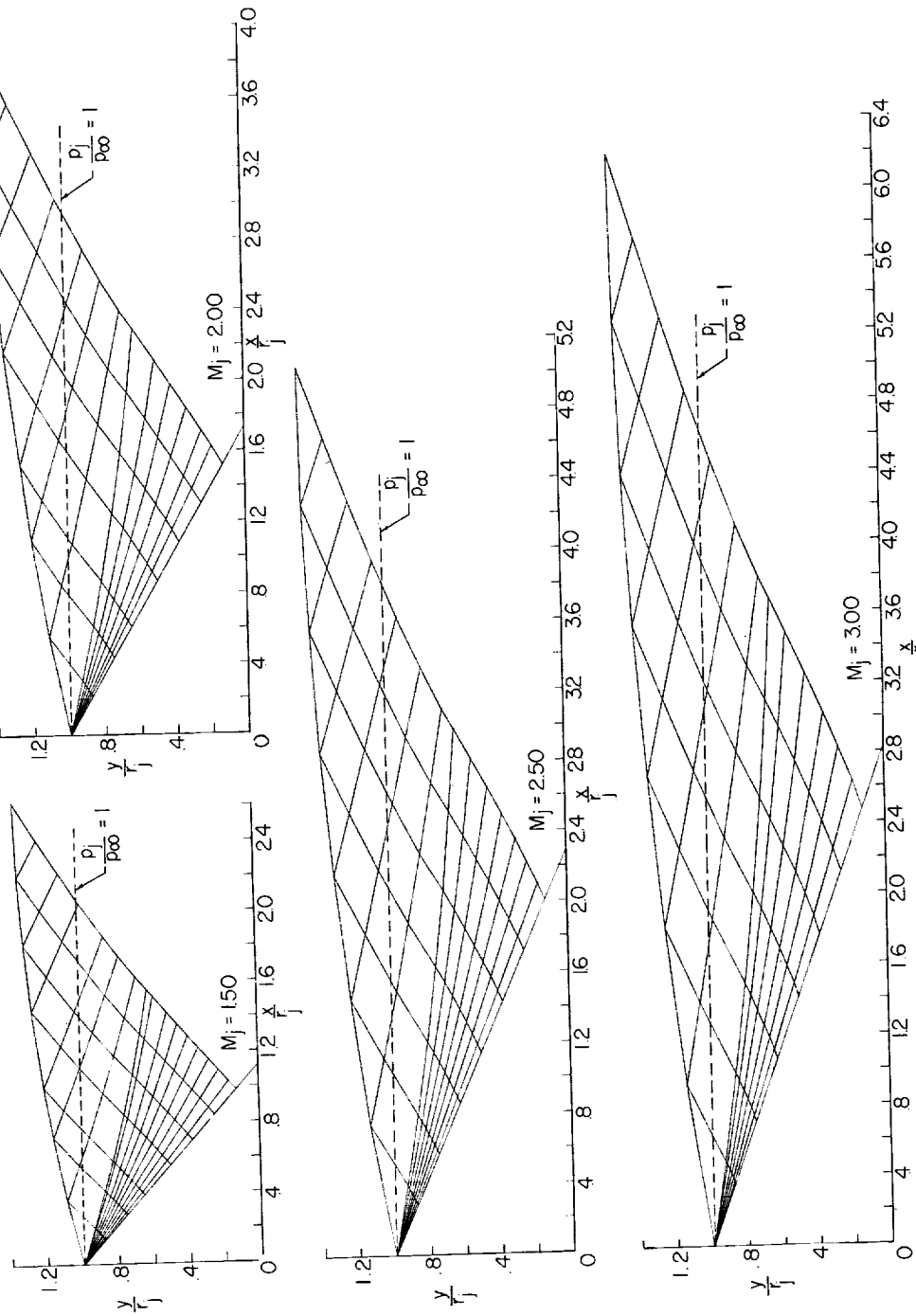

(b) $M_j = 1.50$ to 3.00; $\frac{p_j}{p_\infty} = 2$; $\theta_N = 0°$; $\gamma_j = 1.400$

Figure 14.- Continued.

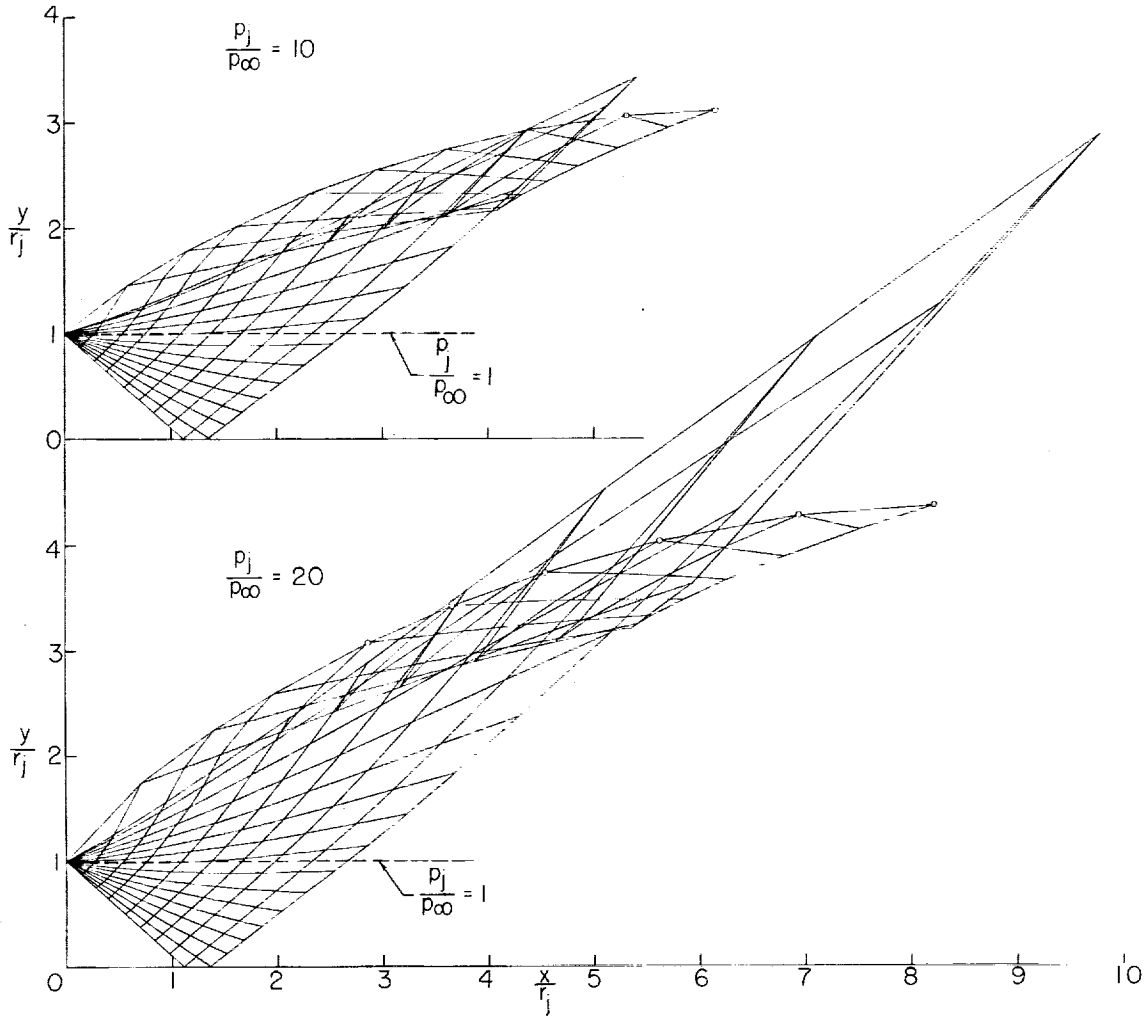

(c) $M_j = 1.50$, $\frac{p_j}{p_\infty} = 10$ and 20; $\theta_N = 0°$; $\gamma_j = 1.400$.

Figure 14.- Continued.

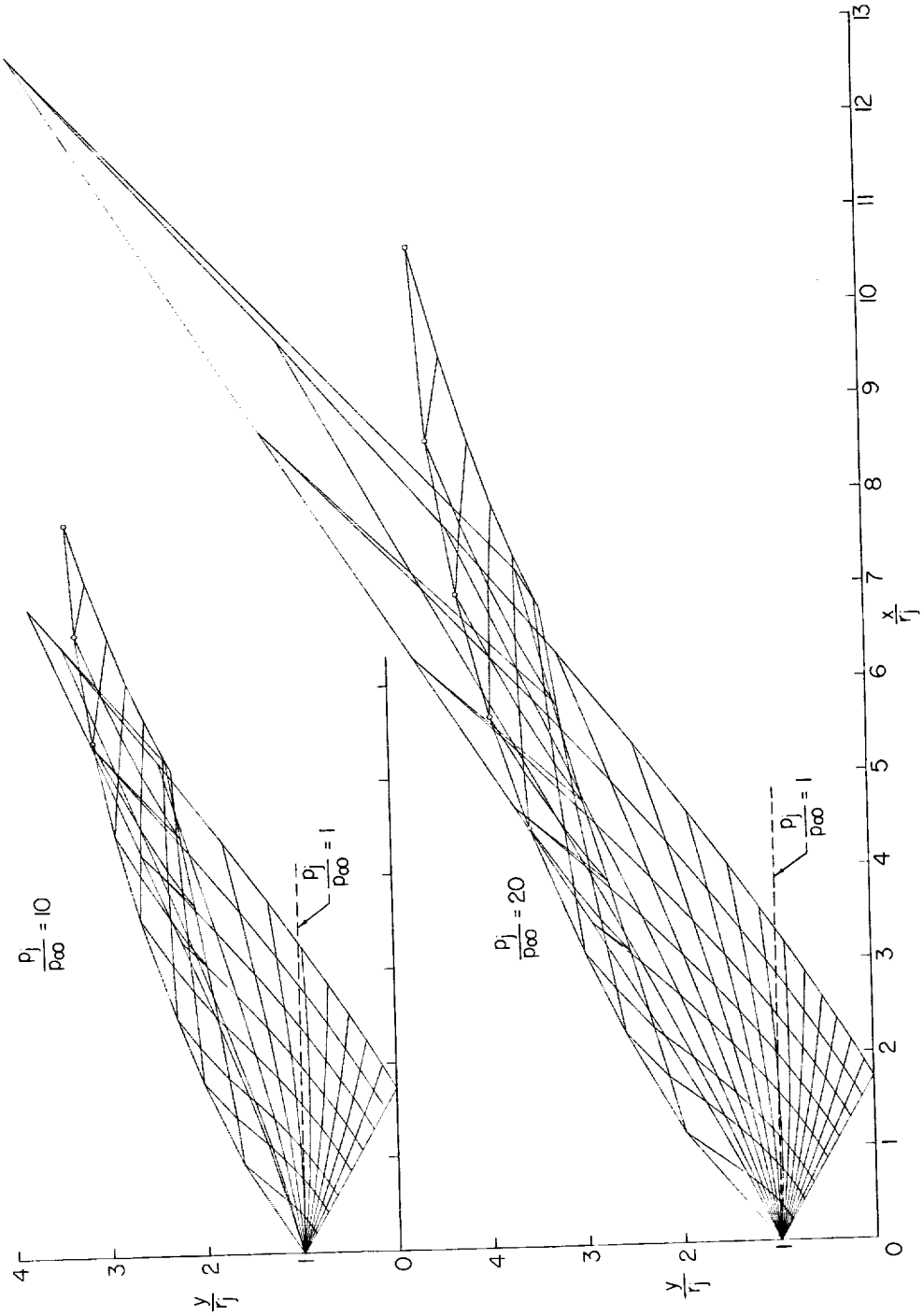

(d) $M_j = 2.00$; $\frac{p_j}{p_\infty} = 10$ and 20, $\theta_N = 0°$; $\gamma_j = 1.400$

Figure 14.- Continued.

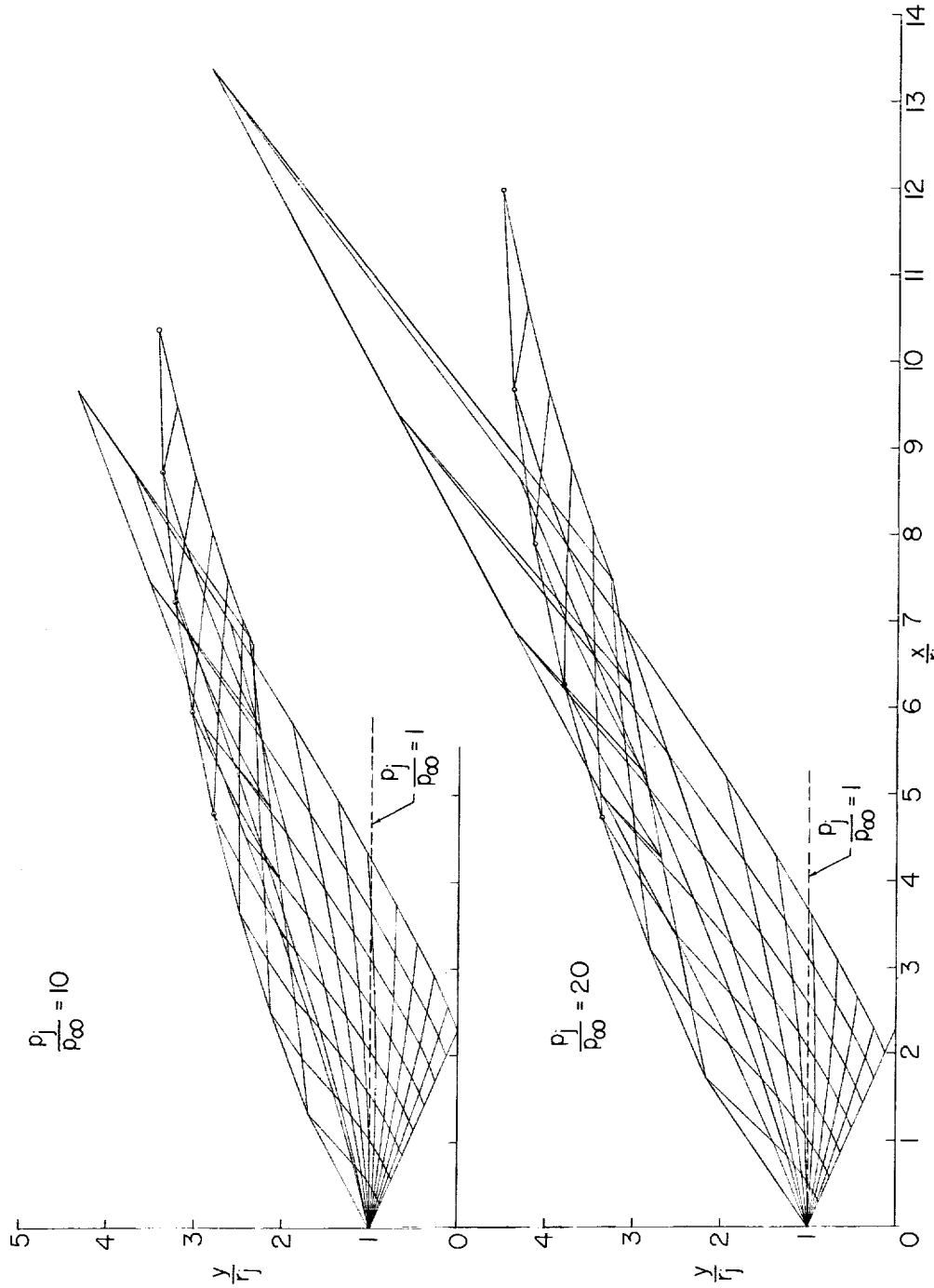

(e) $M_j = 2.50$; $\frac{p_j}{p_\infty} = 10$ and 20; $\theta_N = 0°$; $\gamma_j = 1.400$

Figure 14.- Continued.

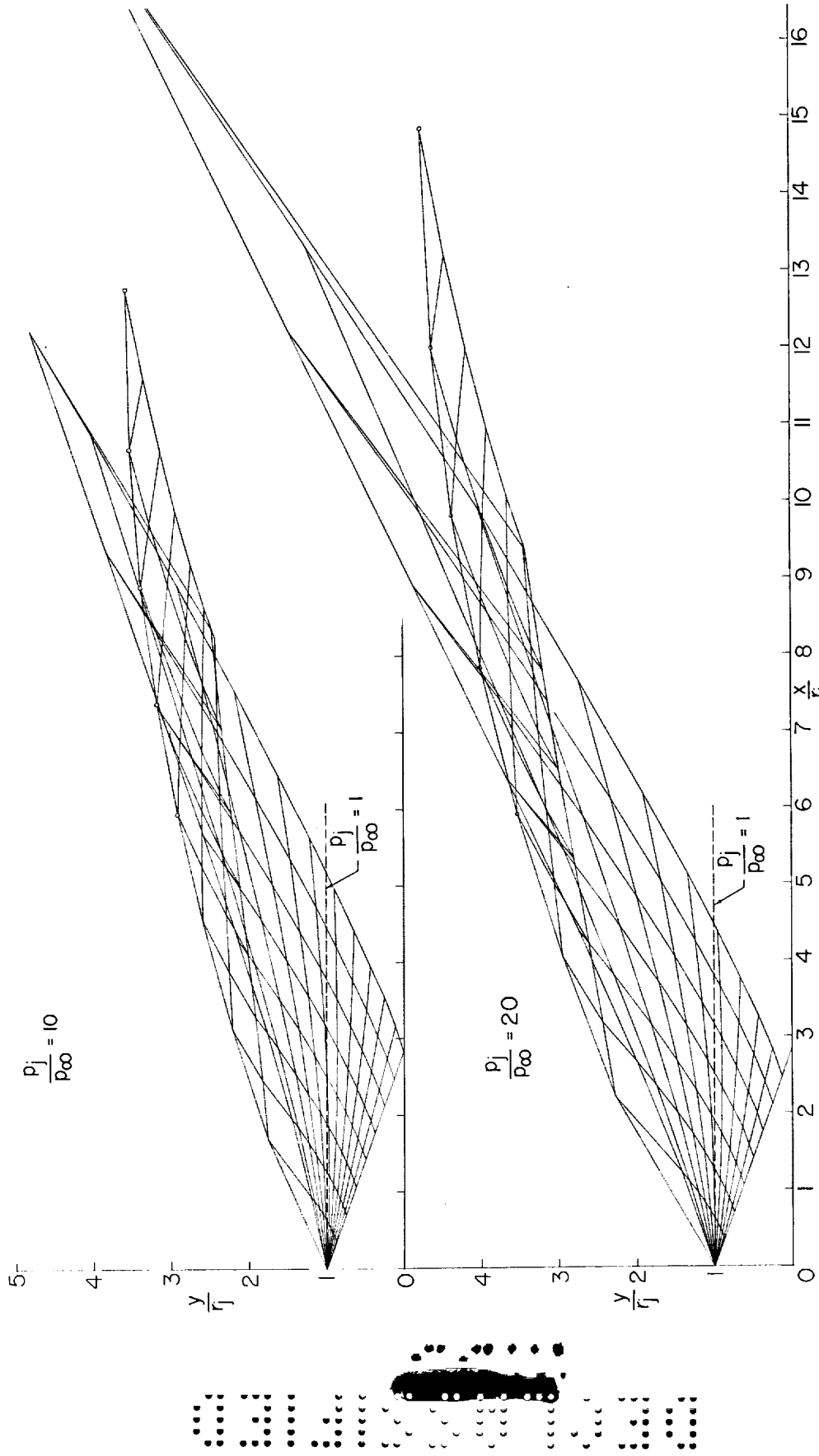

(f) $M_j = 3.00$, $\frac{p_j}{p_\infty} = 10$ and 20, $\theta_N = 0°$; $\gamma_j = 1.400$.

Figure 14.- Continued.

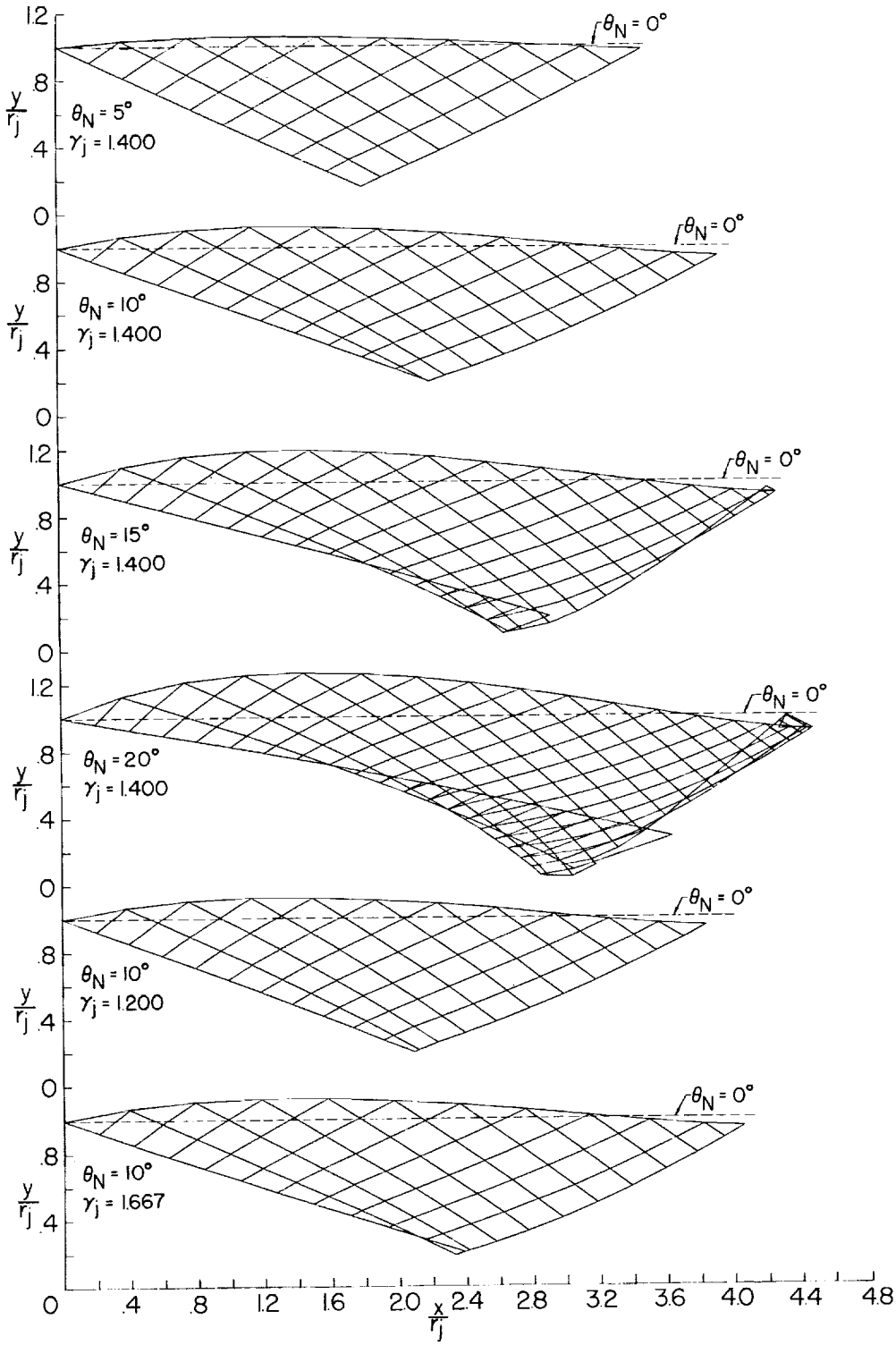

(g) M_j=2.00; $\frac{p_j}{p_\infty}$ = 1; varying θ_N and γ_j.

Figure 14.- Concluded.

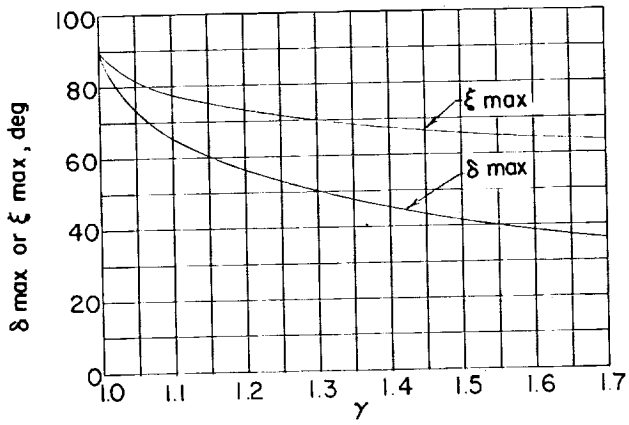

(a) M = ∞.

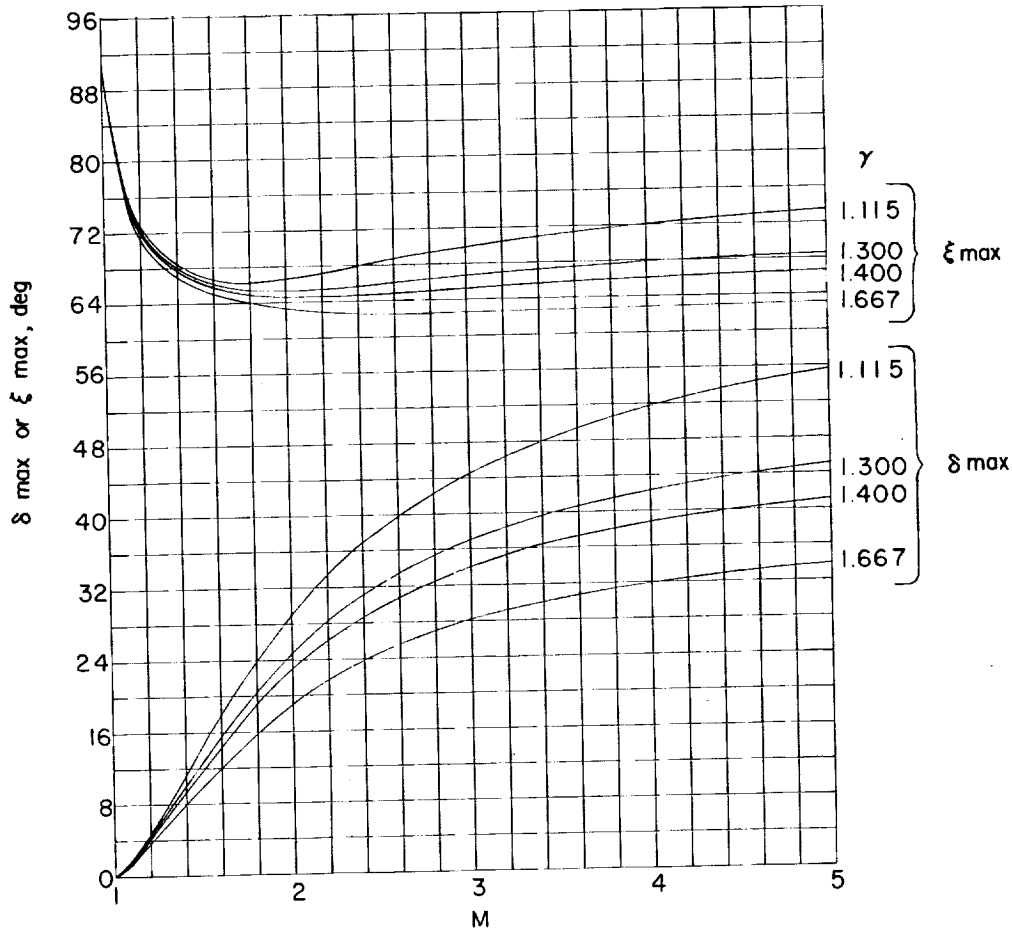

(b) M = 1 to 5.

Figure 15.- Effect of the ratio of specific heats upon the maximum turning of two-dimensional flow through an attached shock and upon the inclination of the shock.

[redacted]

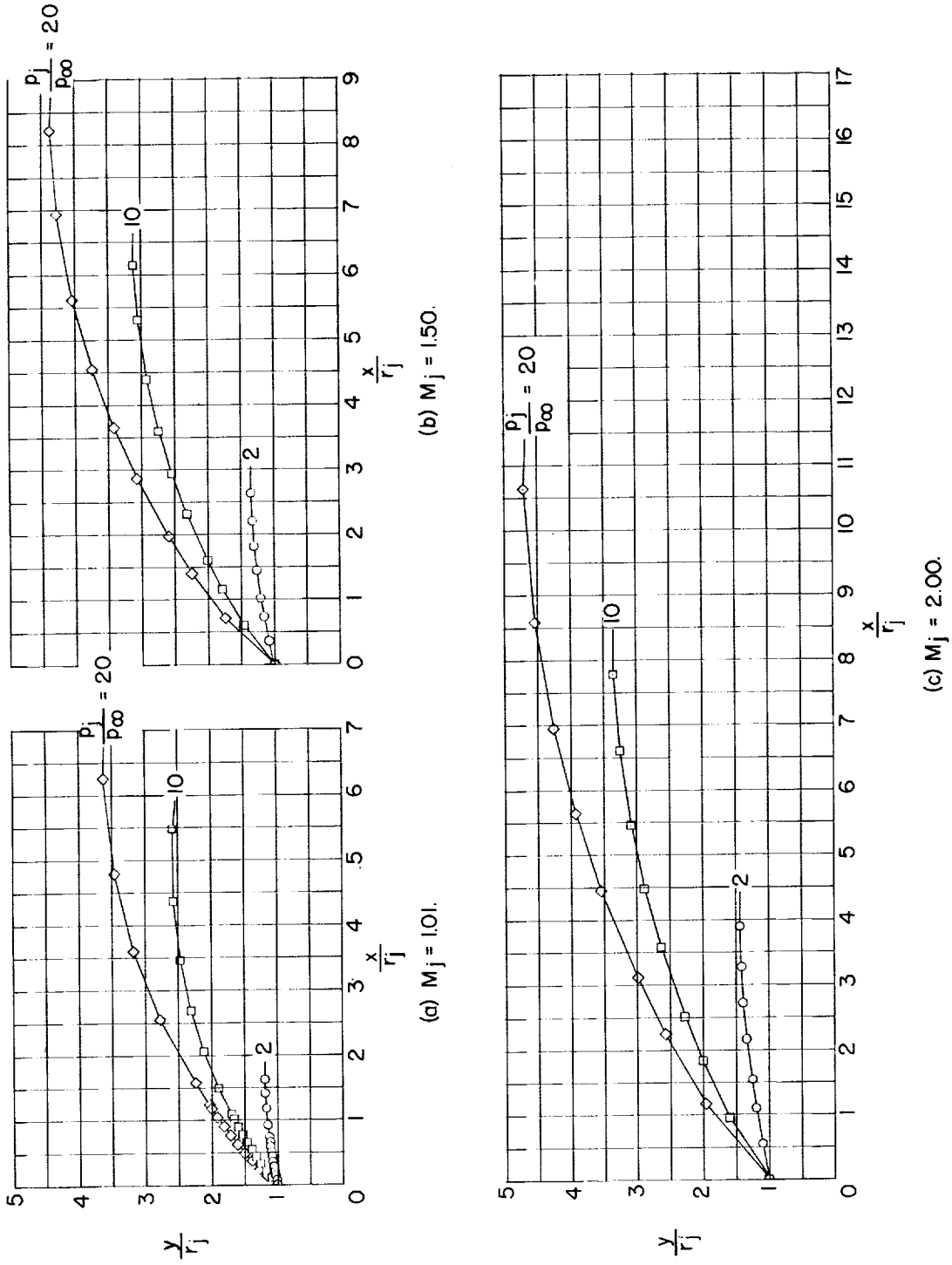

Figure 16.- Theoretical jet boundaries obtained from characteristic calculations. $\theta_N = 0^\circ$; $\gamma_j = 1.400$.

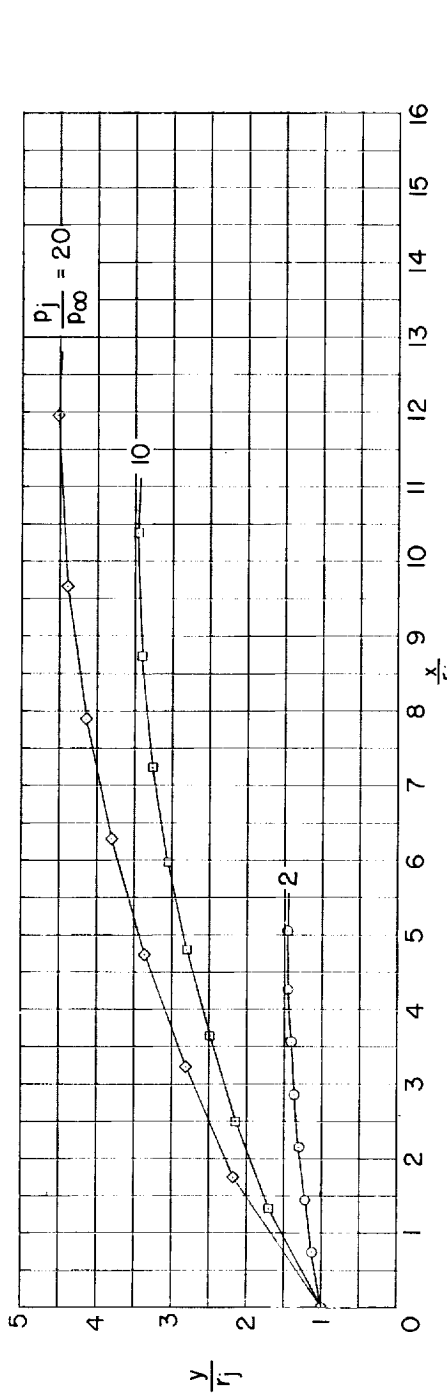

(d) M_j = 2.50.

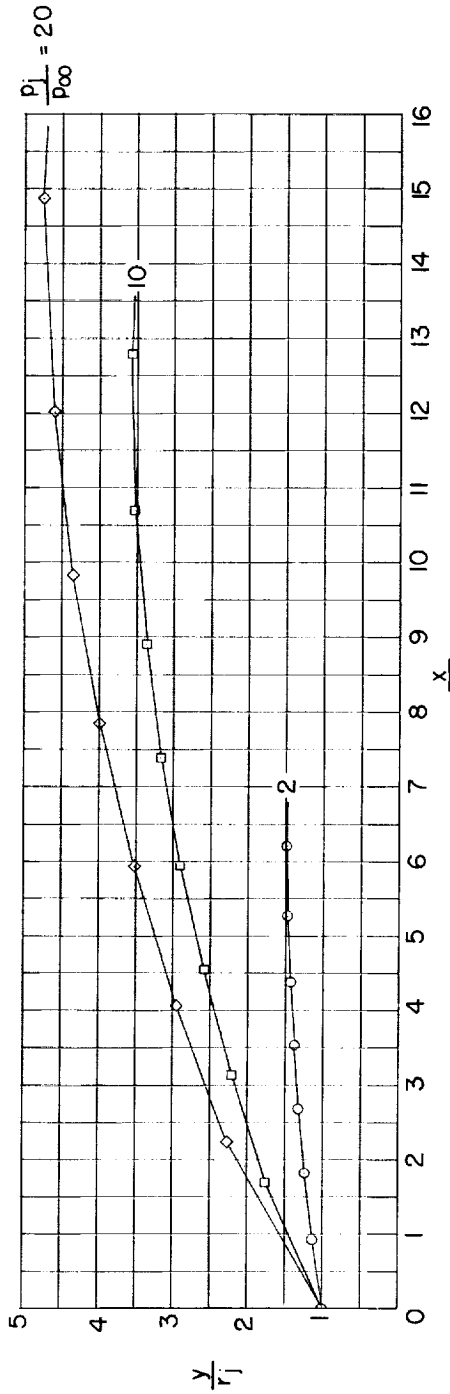

(e) M_j = 3.00.

Figure 16.- Concluded.

[redacted]

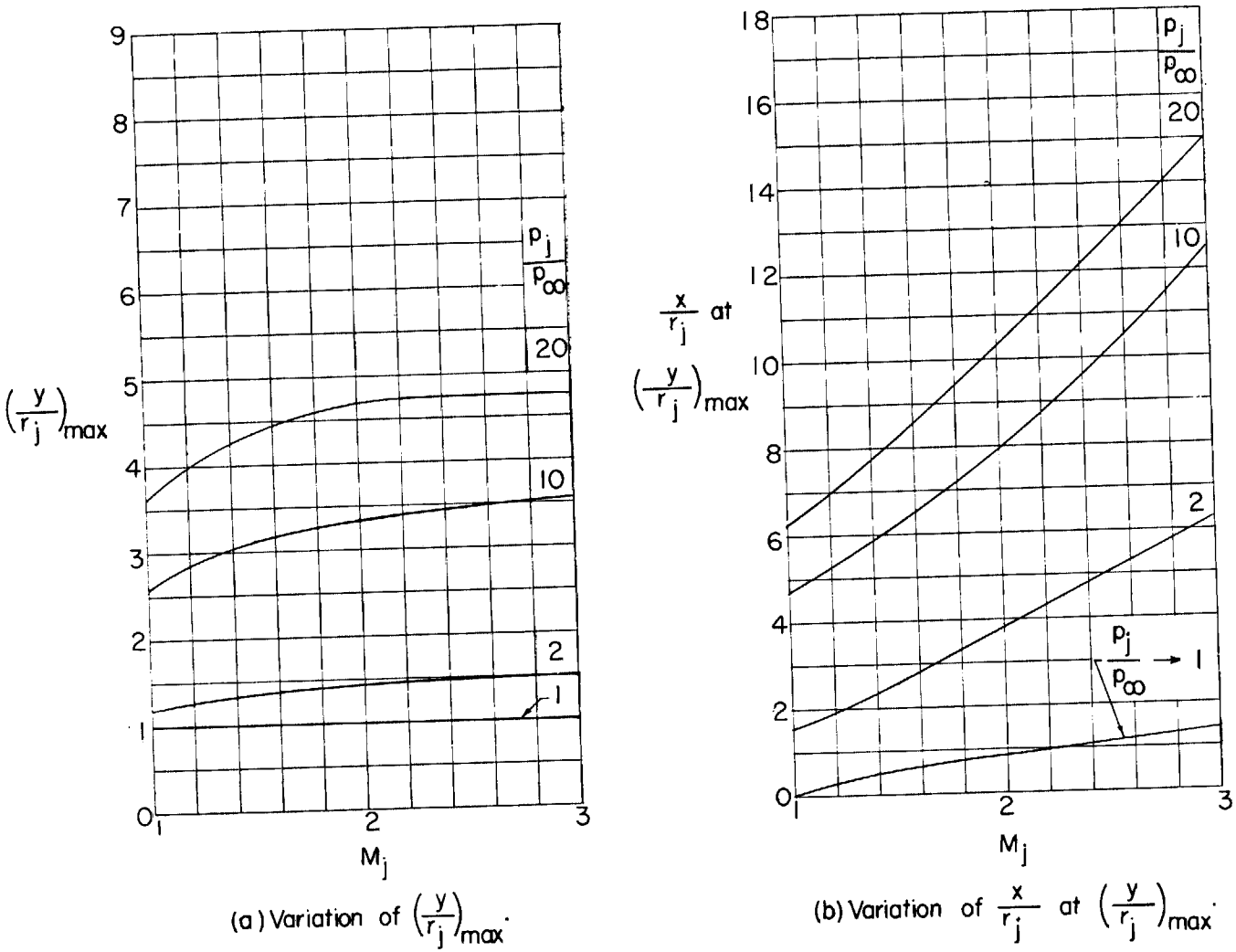

Figure 17.- Maximum height of jet boundary and its location as obtained from characteristic calculations. $\theta_N = 0^\circ$; $\gamma_j = 1.400$.

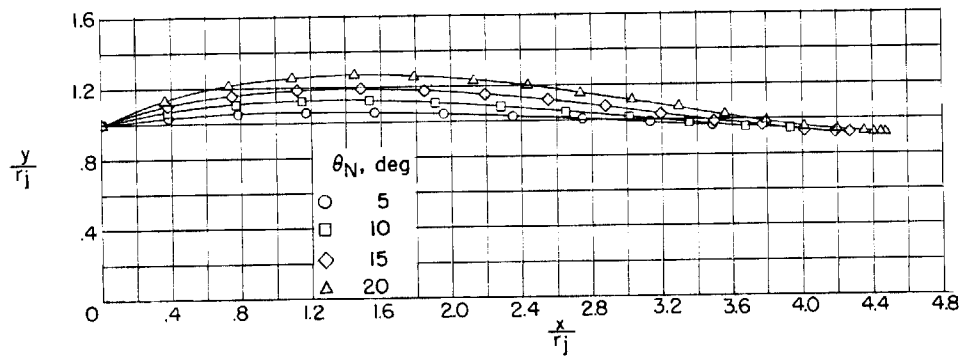

Figure 18.- Effect of nozzle divergence angle upon the shape of the jet boundary as obtained from characteristic calculations. $M_j = 2.00$; $\frac{p_j}{p_\infty} = 1$; $\gamma_j = 1.400$.

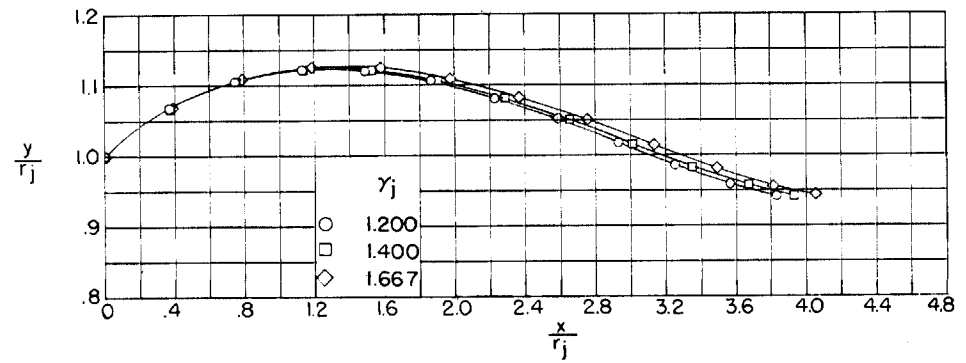

Figure 19.- Effect of ratio of specific heats of the jet upon the shape of the jet boundary as obtained from characteristic calculations. $M_j = 2.00$; $\frac{p_j}{p_\infty} = 1$; $\theta_N = 10^\circ$.

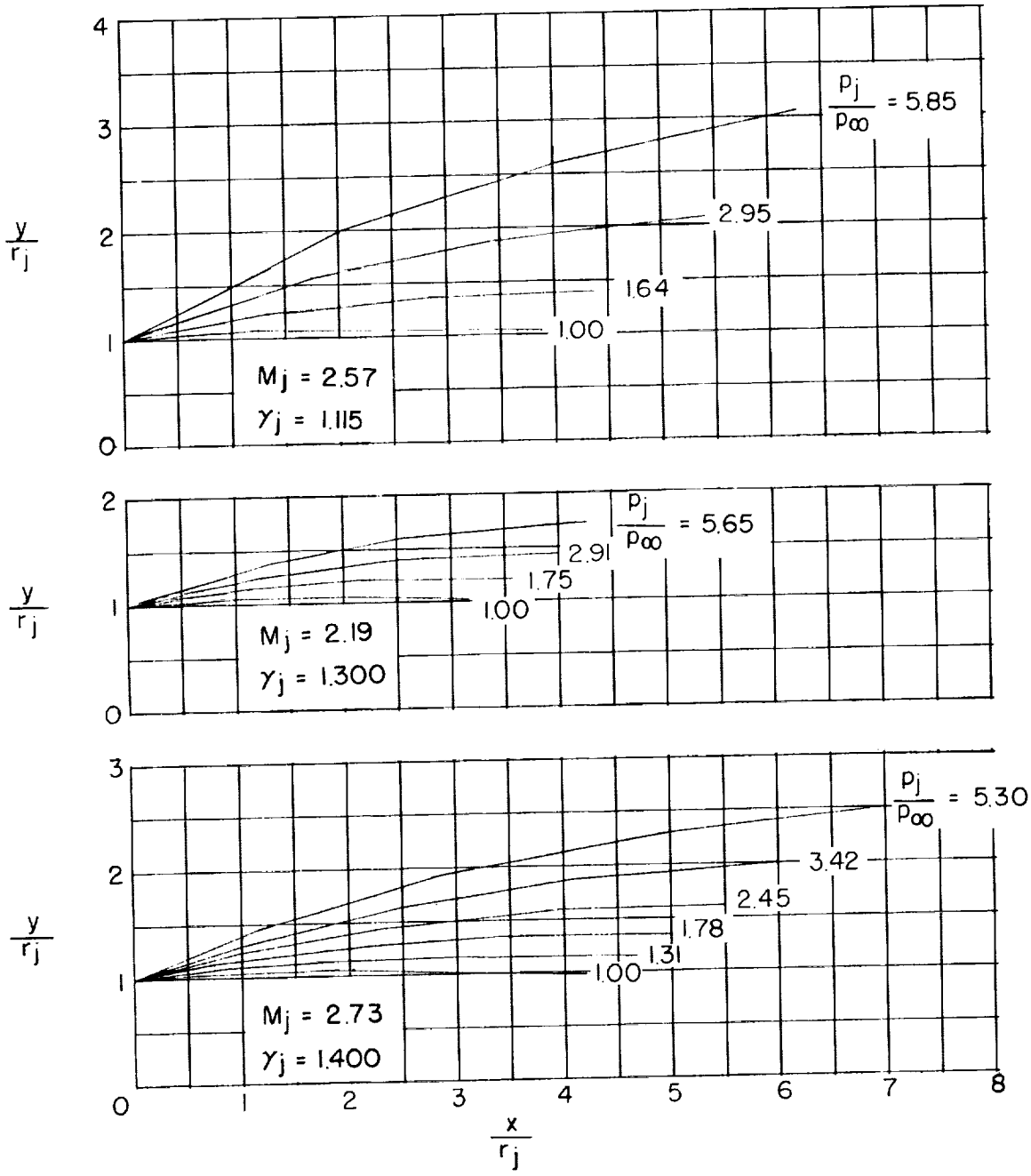

Figure 20.- Calculations of jet boundaries by Johannesen (ref. 5). $\theta_N = 4^\circ$.

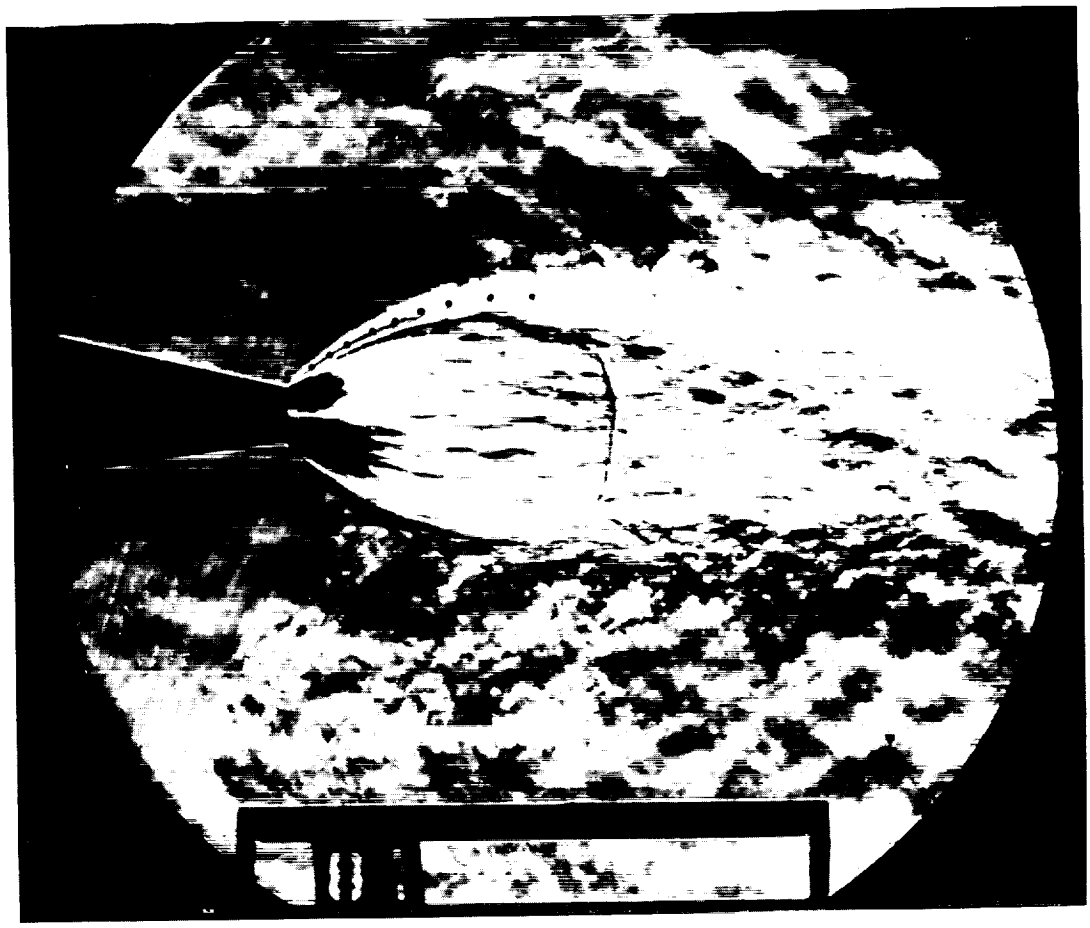

L-86502

Figure 21.- Comparison of theoretical boundary (dots) and shock location (dashes) for $\frac{p_j}{p_\infty} = 20$ with experimental observation for $\frac{p_j}{p_\infty} = 21.9$. $M_j = 1.50$; $\theta_N = 0^\circ$; $\gamma_j = 1.400$.

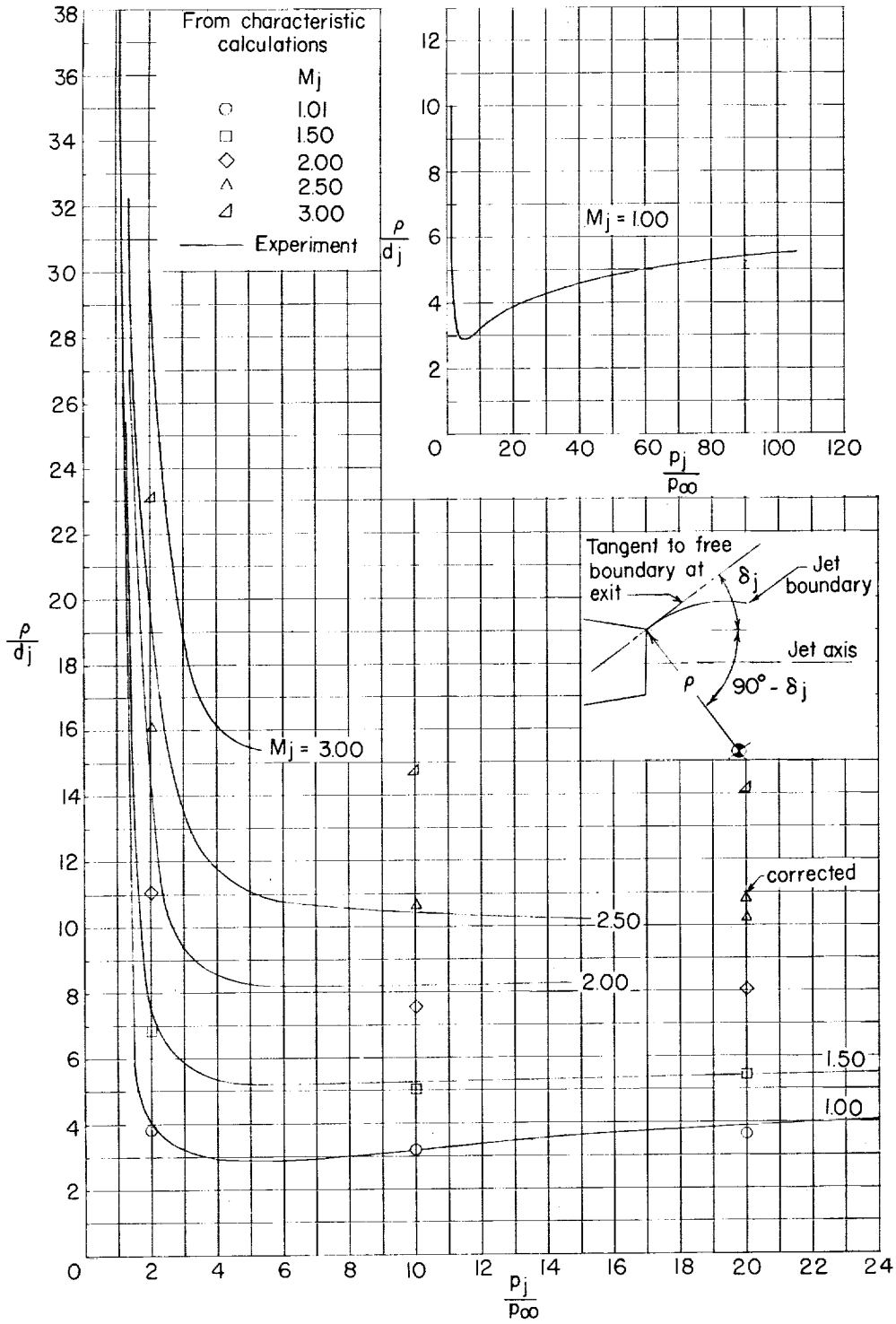

(a) $\theta_N = 0°$.

Figure 22.- Effects of jet pressure ratio and jet Mach number upon the nondimensional average radius of curvature of the jet boundary.

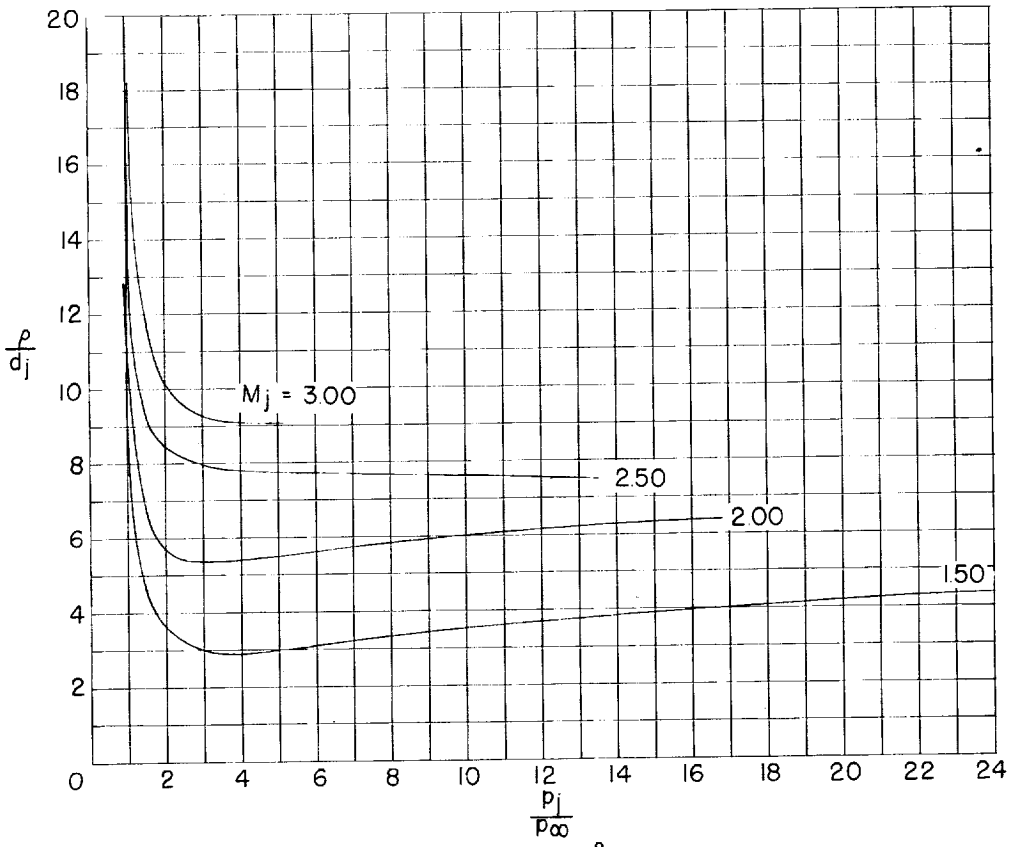

(b) $\theta_N = 5°$.

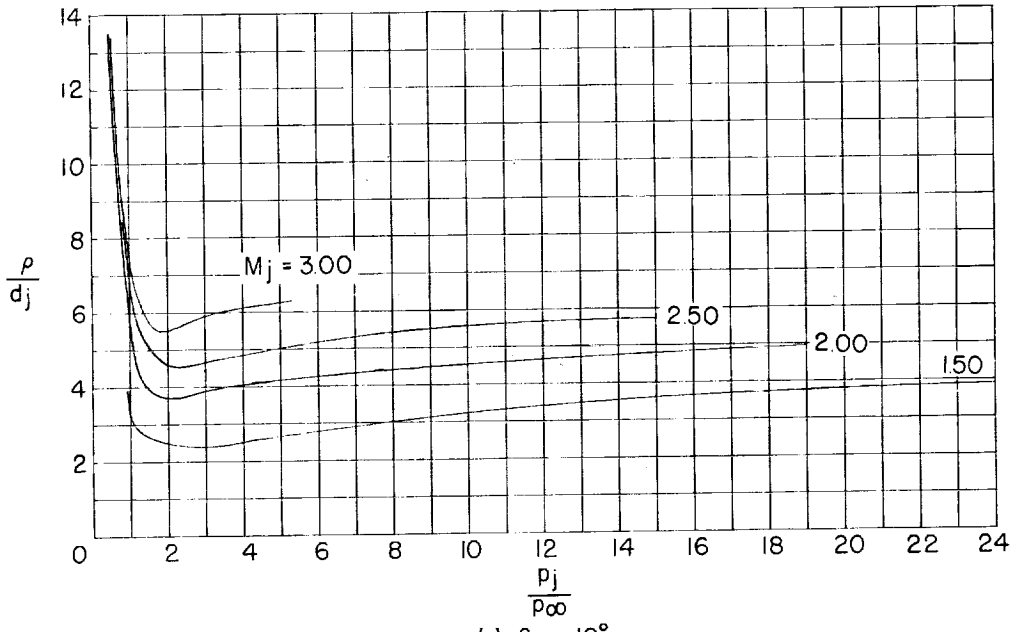

(c) $\theta_N = 10°$.

Figure 22.- Continued.

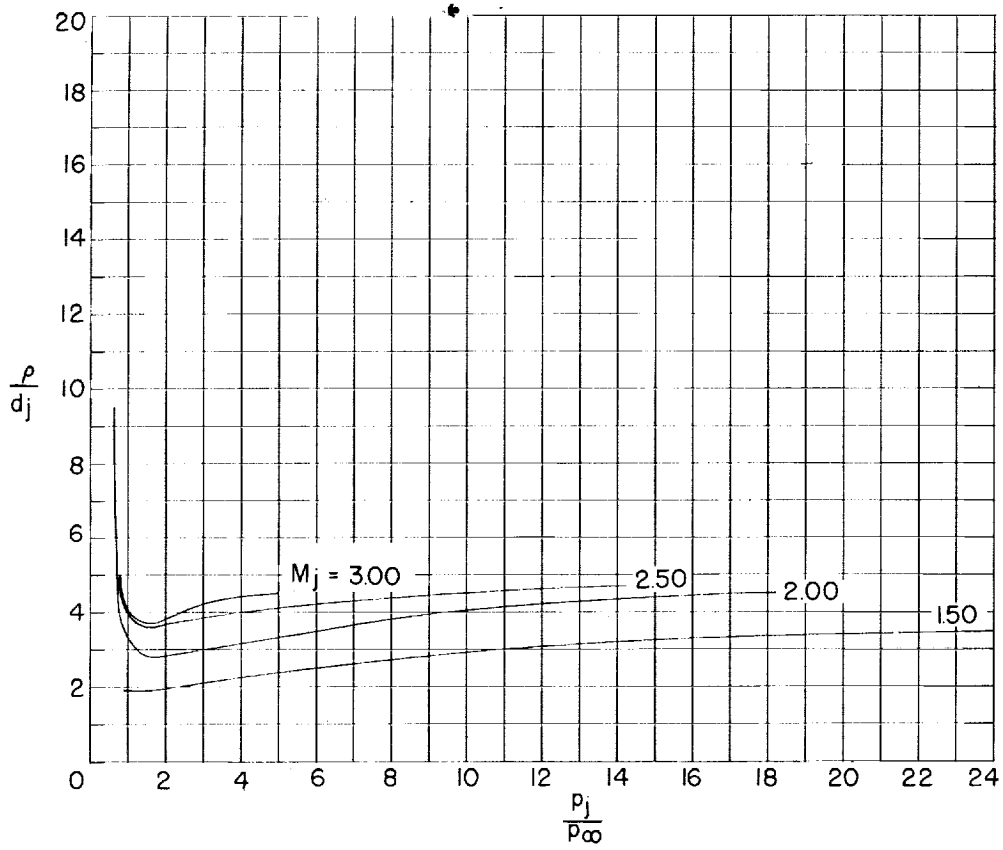

(d) θ_N = 15°.

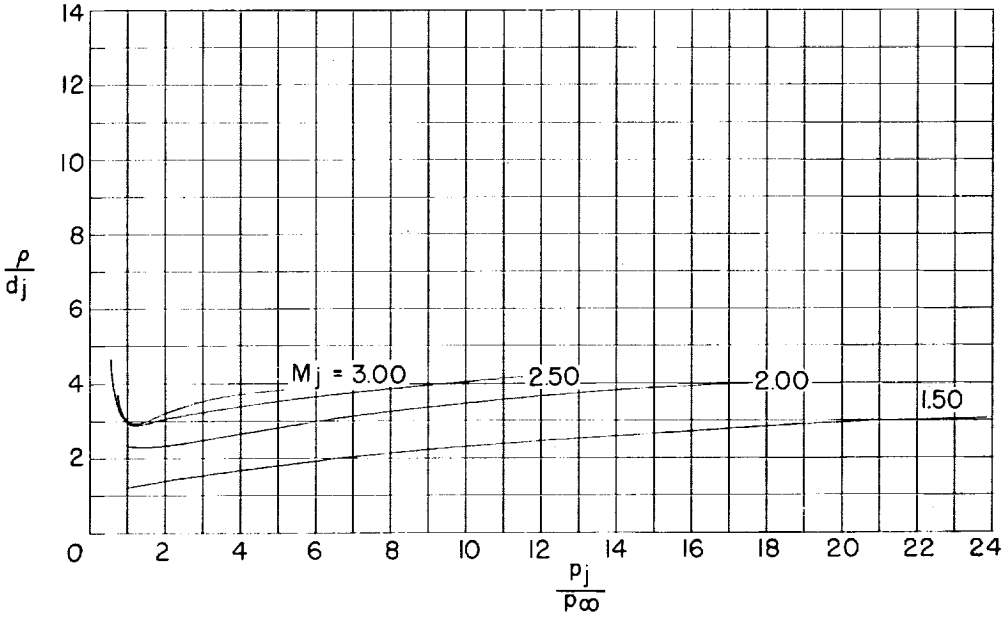

(e) θ_N = 20°

Figure 22.- Concluded.

[redacted]

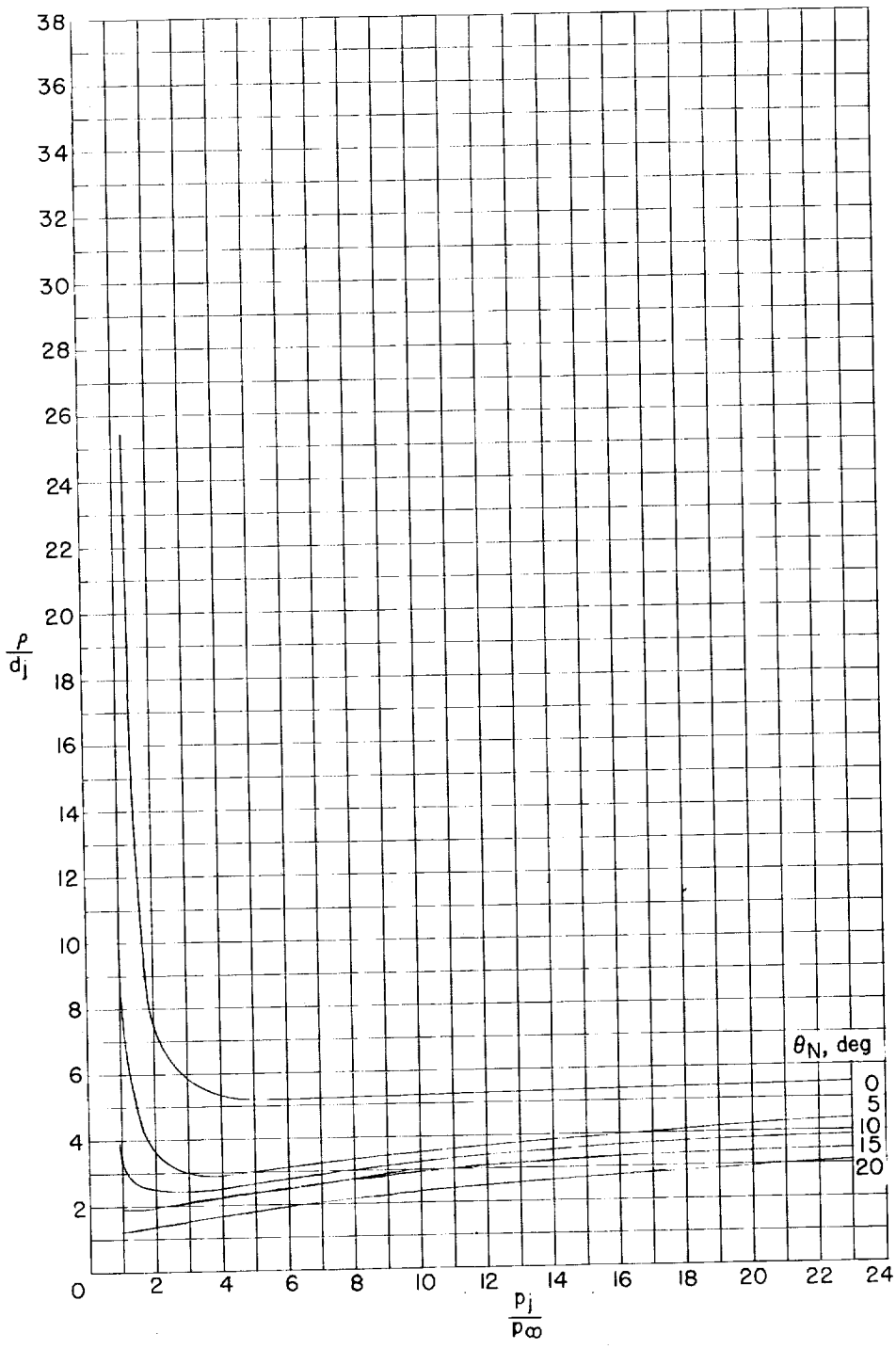

(a) $M_j = 1.50$.

Figure 23.- Effects of jet pressure ratio and nozzle divergence angle upon the nondimensional average radius of curvature of the jet boundary.

[redacted]

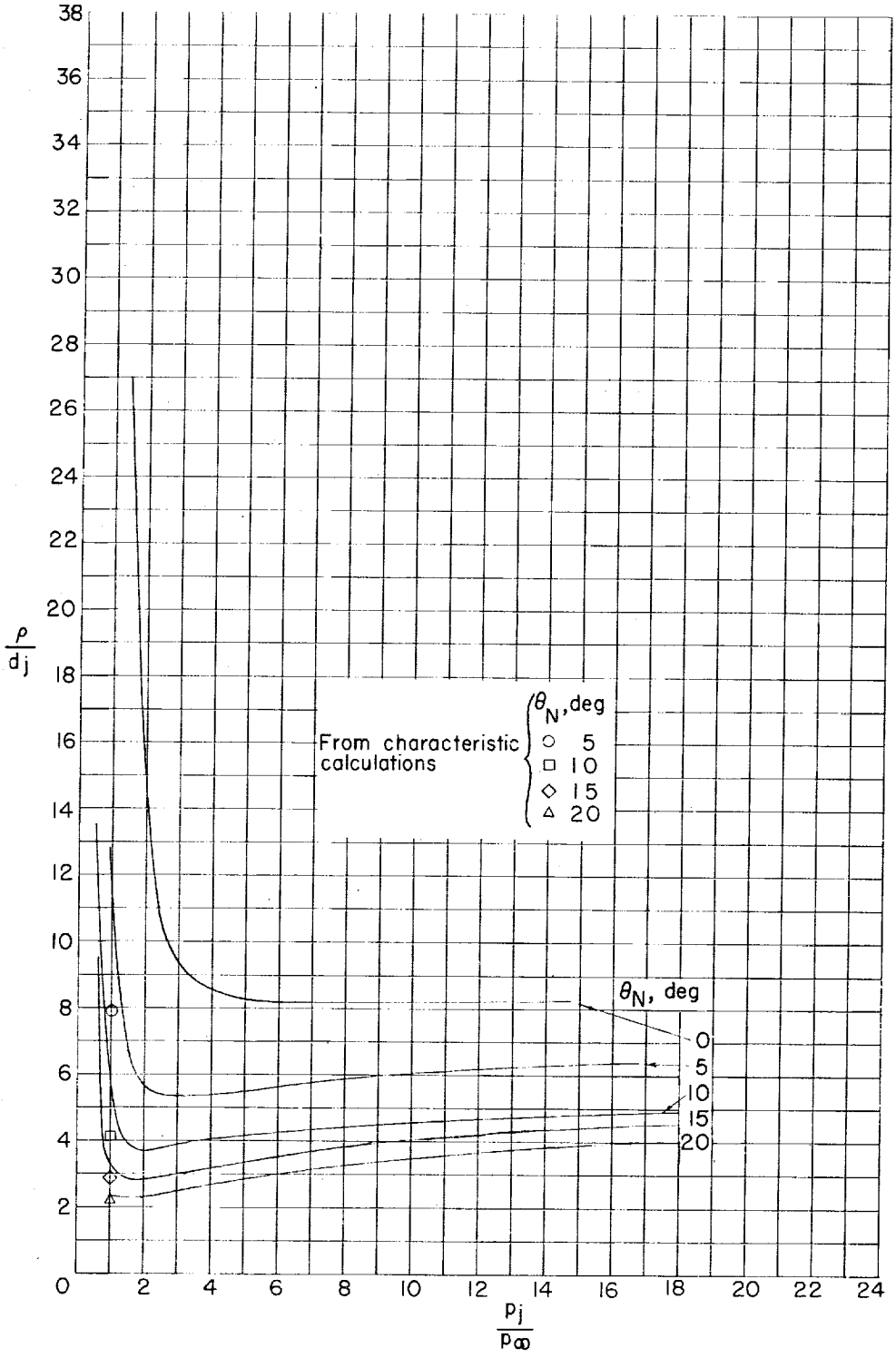

(b) Mj = 2.00.

Figure 23.- Continued.

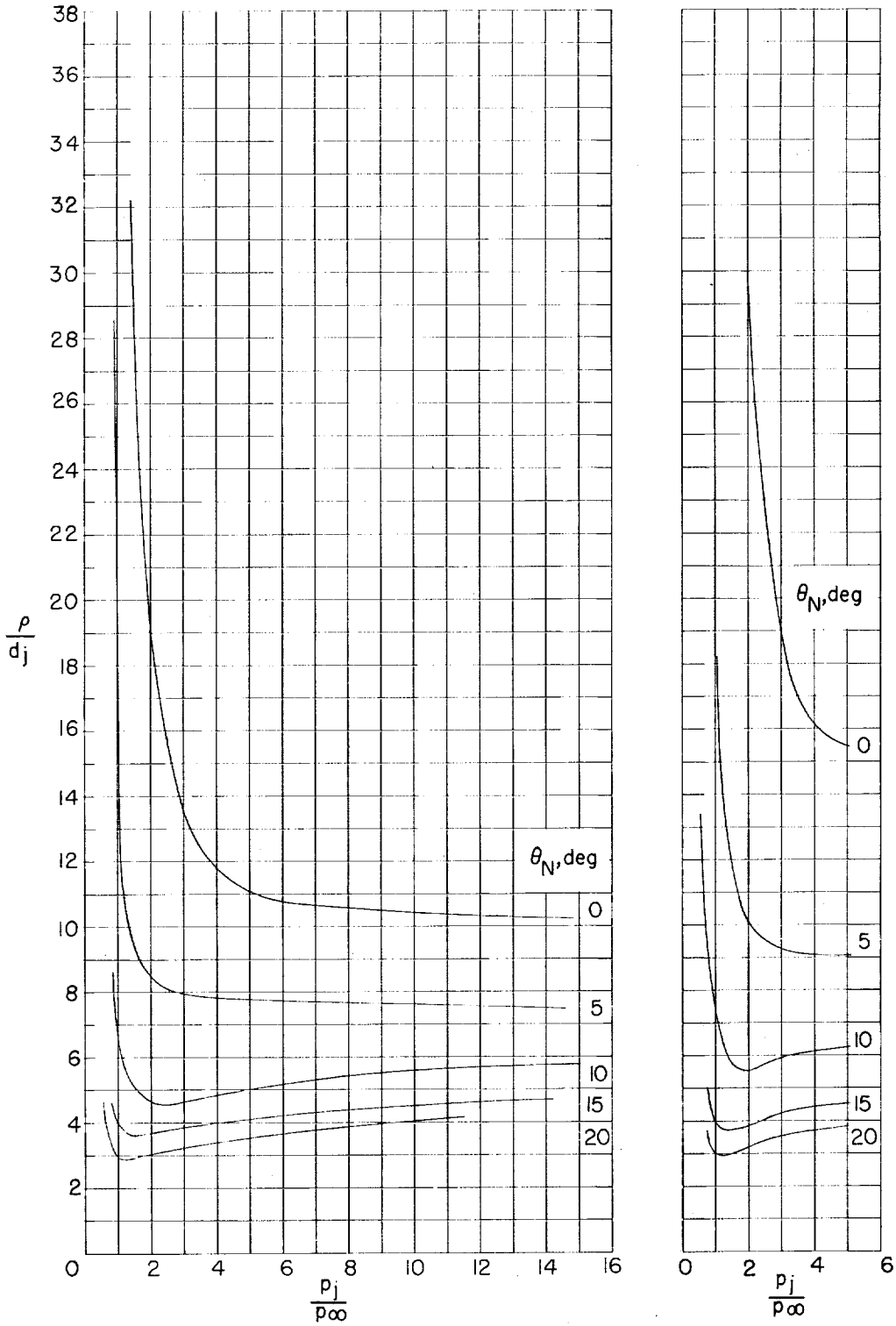

Figure 23.- Concluded.

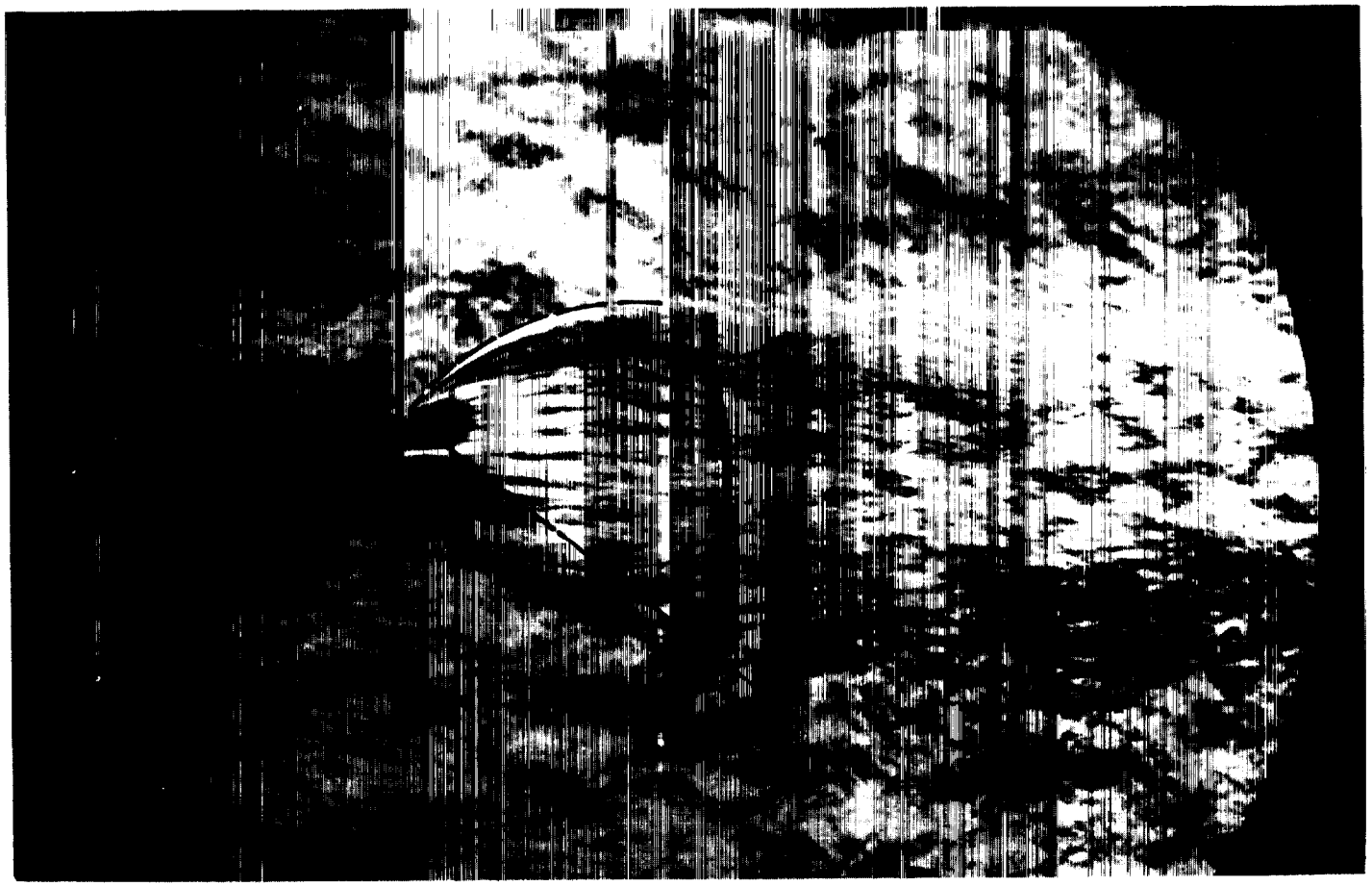

(a) $M_j = 1.0$; $\theta_N = 0^\circ$; $\frac{p_j}{p_\infty} = 24.6$. L-86503

Figure 24.- Examples of circular-arc boundaries given by $\frac{\rho}{d_j}$ superposed on schlieren photographs.

L-86504

(b) $M_j = 2.0$; $\theta_N = 15°$; $\frac{p_j}{p_\infty} = 6.97$.

Figure 24.- Continued.

L-86505

(c) $M_j = 2.5$; $\theta_N = 5°$; $\frac{p_j}{p_\infty} = 6.43$.

Figure 24.- Continued.

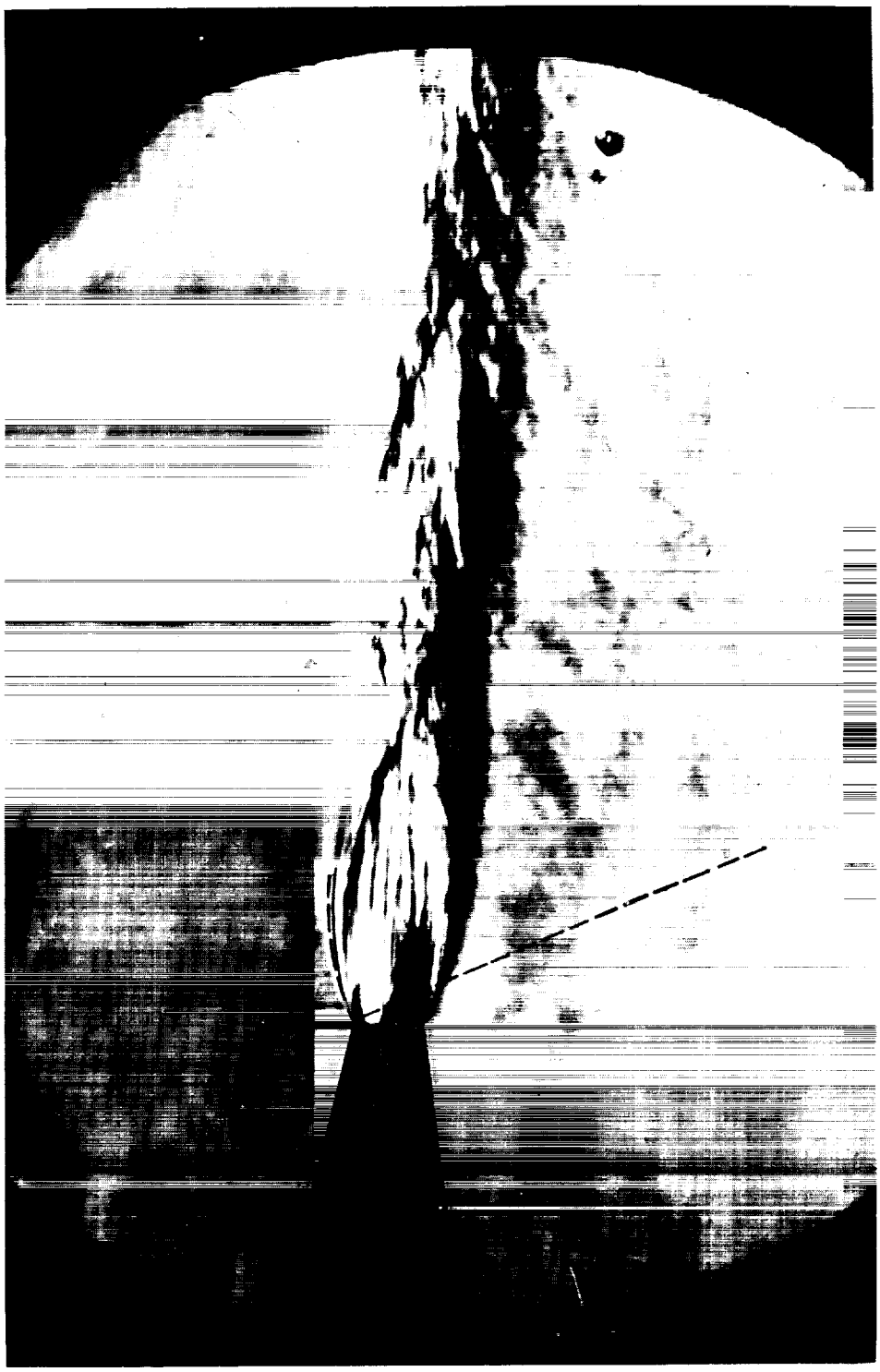

L-86506

(d) $M_j = 3.0$; $\theta_N = 15°$; $\frac{p_j}{p_\infty} = 2.54$.

Figure 24.- Concluded.

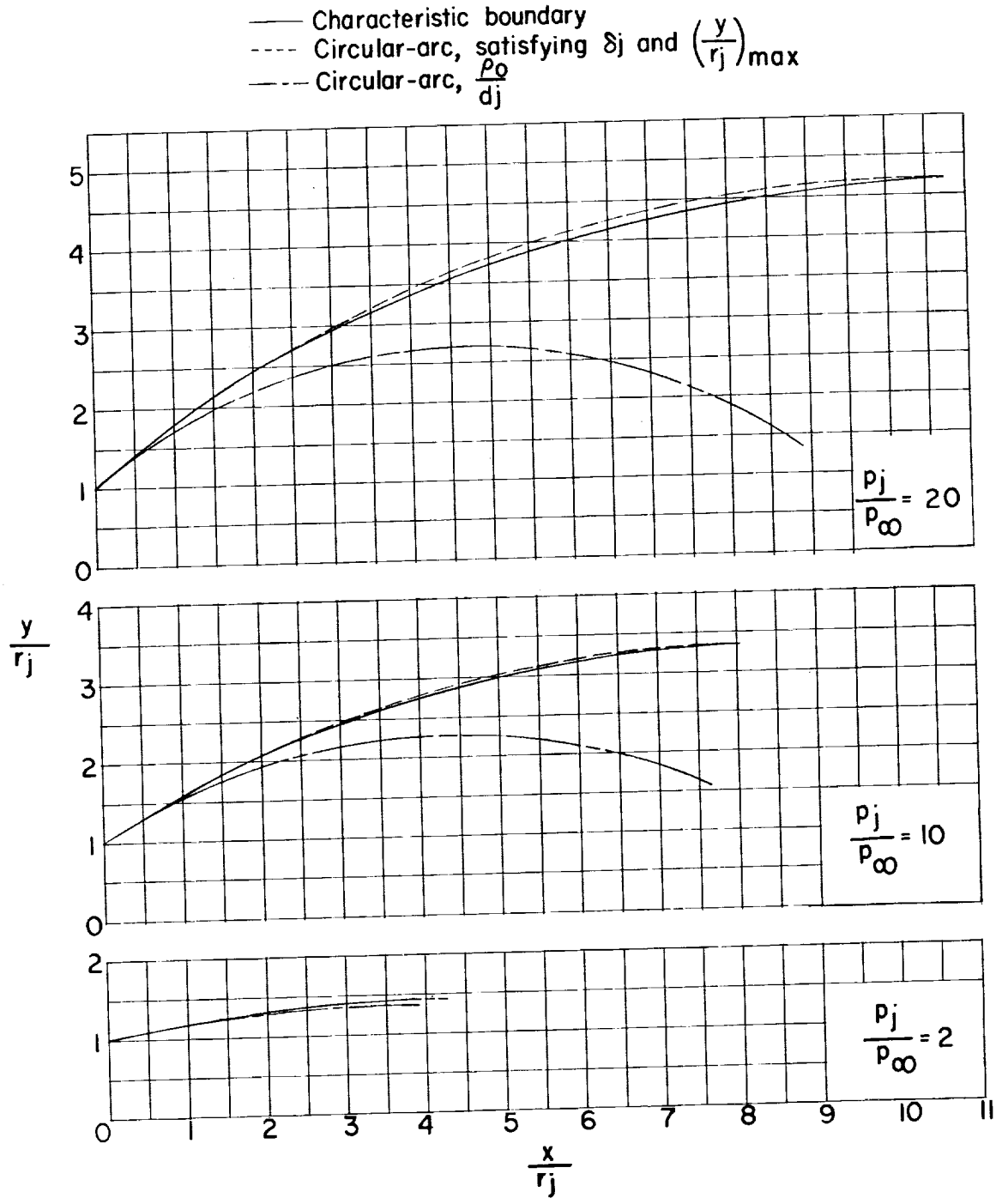

Figure 25.- Comparison of jet boundary given by characteristic calculations, circular-arc boundary passing through $\left(\frac{y}{r_j}\right)_{max}$, and the circular-arc defined by initial radius of curvature. $M_j = 2.00$.

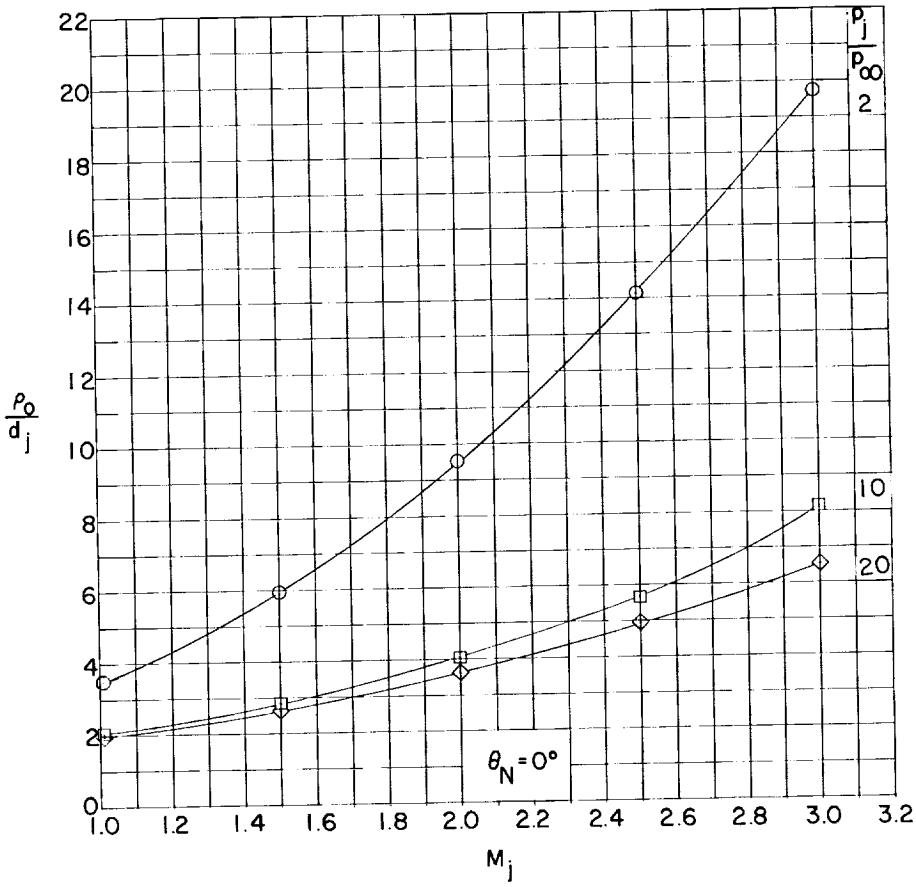

(a) Effects of jet Mach number and jet pressure ratio.

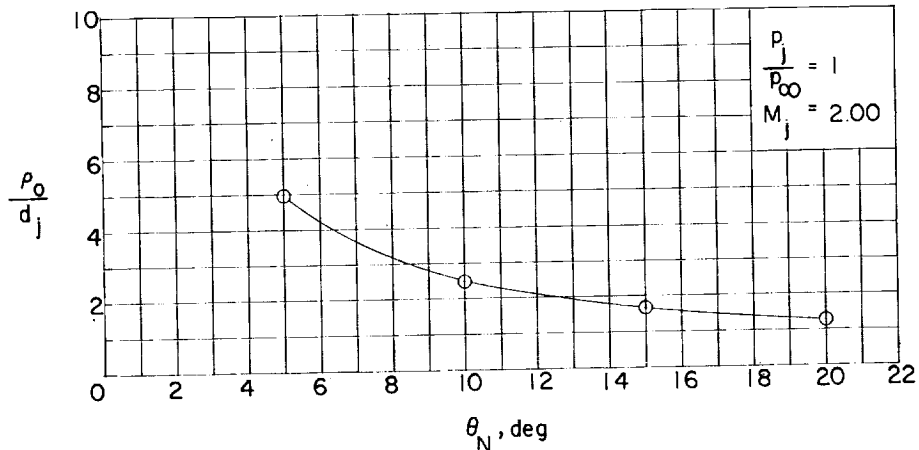

(b) Effects of nozzle divergence angle.

Figure 26.- Theoretical calculations of the nondimensional initial radius of curvature of the jet boundary. $\gamma_j = 1.400$.

[redacted]

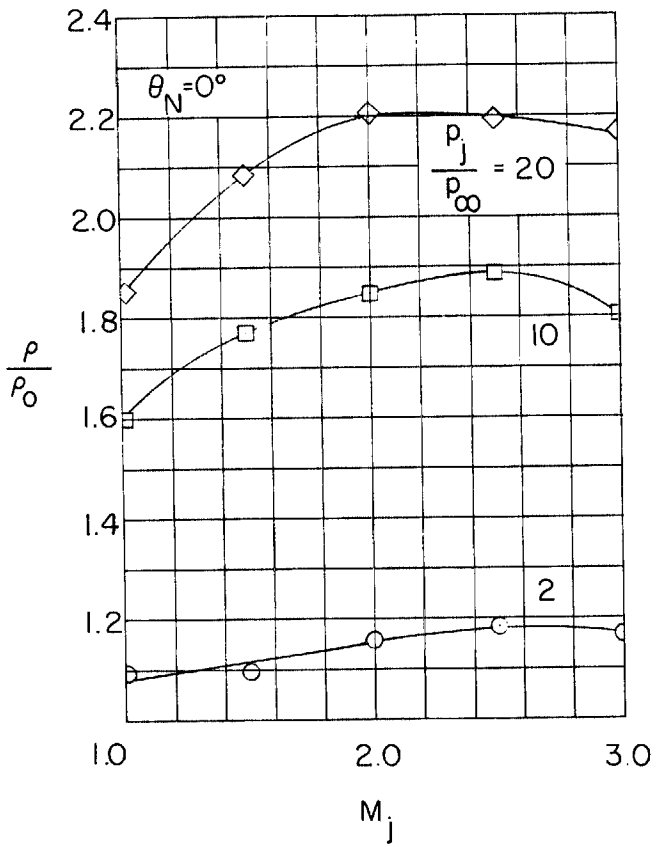

(a) Effects of jet Mach number and jet pressure ratio.

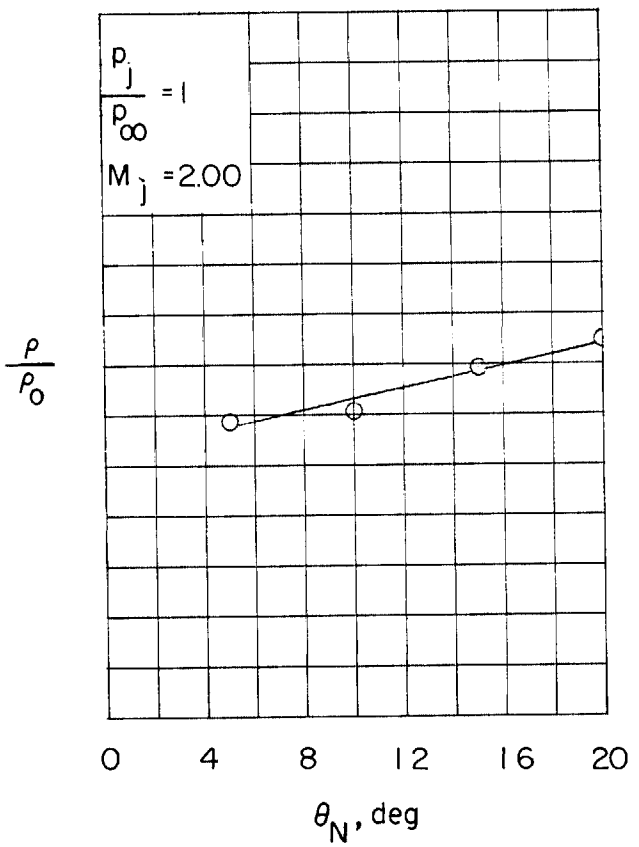

(b) Effects of nozzle divergence angle.

Figure 27.- Ratio of average radius of curvature, as obtained from characteristic solution for $\left(\frac{y}{r_j}\right)_{max}$, to theoretical initial radius of curvature of jet boundary. $\gamma_j = 1.400$.

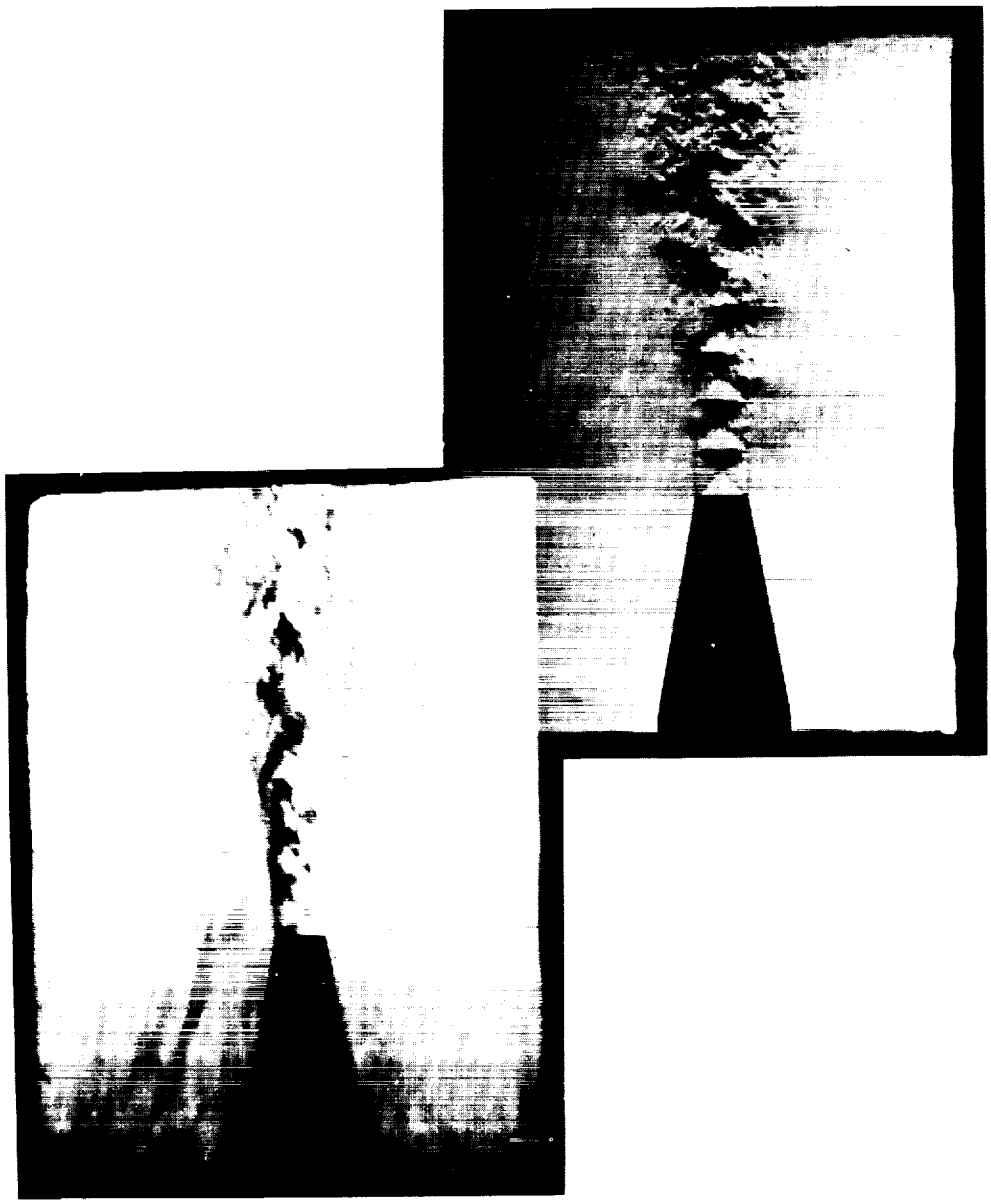

L-86507

(a) $\frac{p_j}{p_\infty} = 1.41$.

Figure 28.- Examples of alternate deflection and degeneration of jet structure. $M_j = 1.00$; $\theta_N = 0^\circ$.

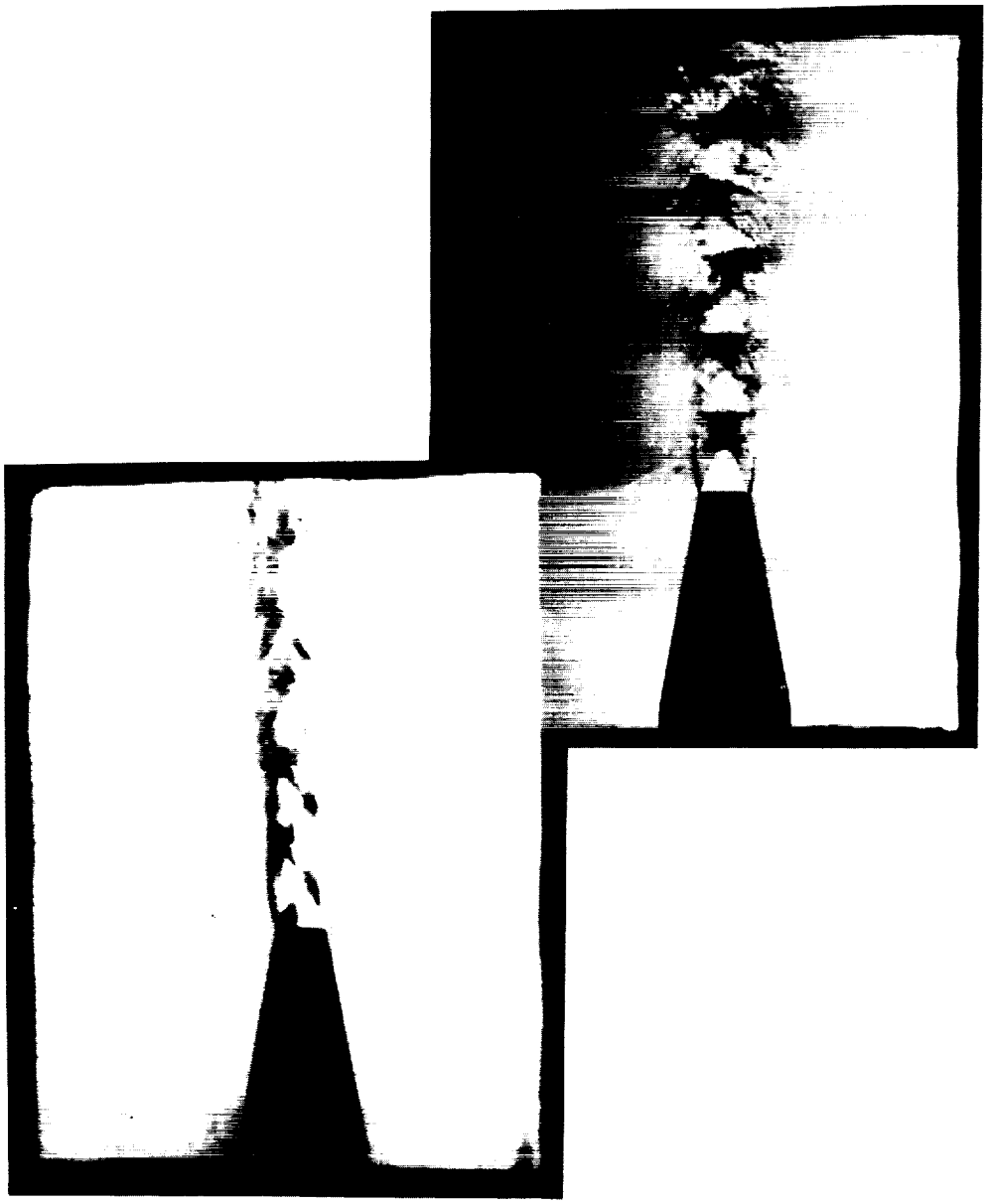

L-86508

(b) $\frac{p_j}{p_\infty} = 2.11$.

Figure 28.- Concluded.

(a) $\frac{p_j}{p_\infty} = 1.76$.

L-86509

Figure 29.- Examples of sound waves associated with the degeneration of jet structure. $M_j = 1.00$; $\theta_N = 0^\circ$.

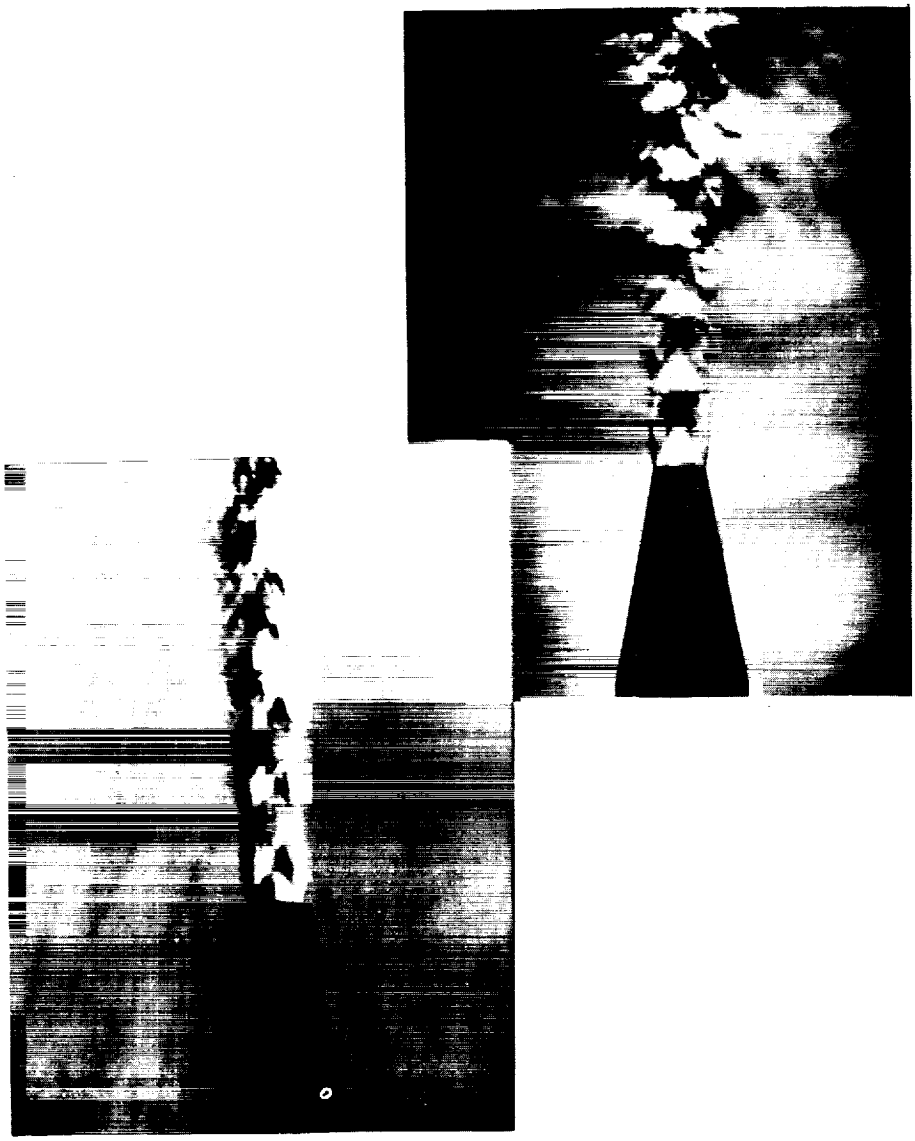

L-86510

(b) $\frac{p_j}{p_\infty} = 1.94$.

Figure 29.- Concluded.

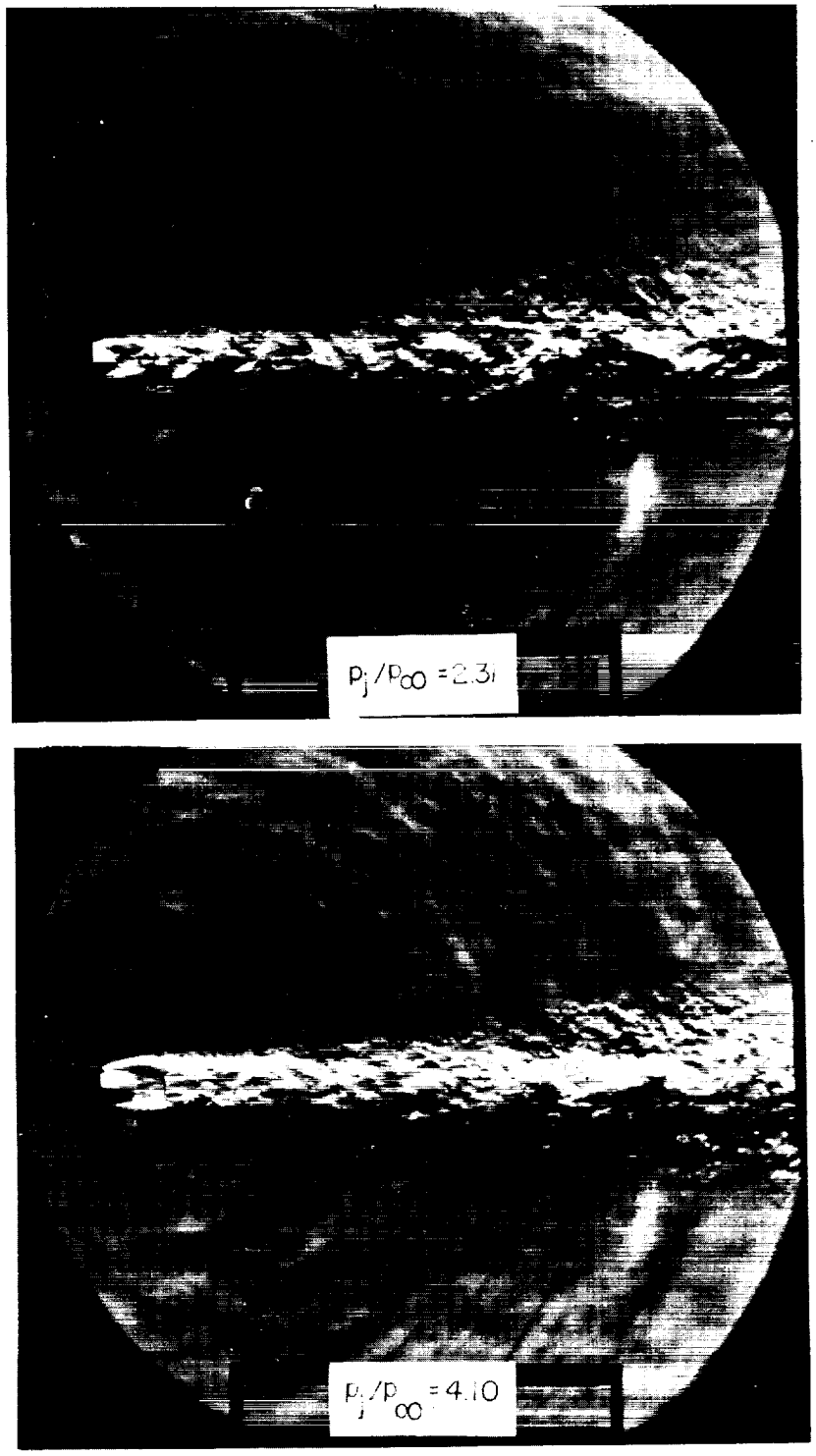

L-86511

Figure 30.- Photographs of sound waves generated by jet beyond jet pressure ratio for reappearance of Riemann wave. $M_j = 1.00$; $\theta_N = 0^\circ$.

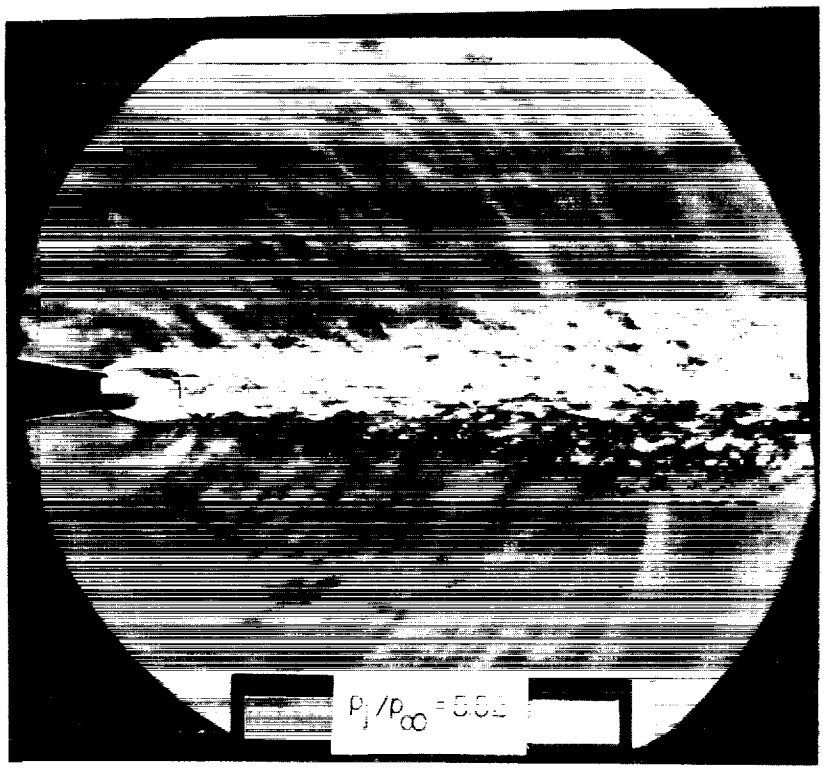

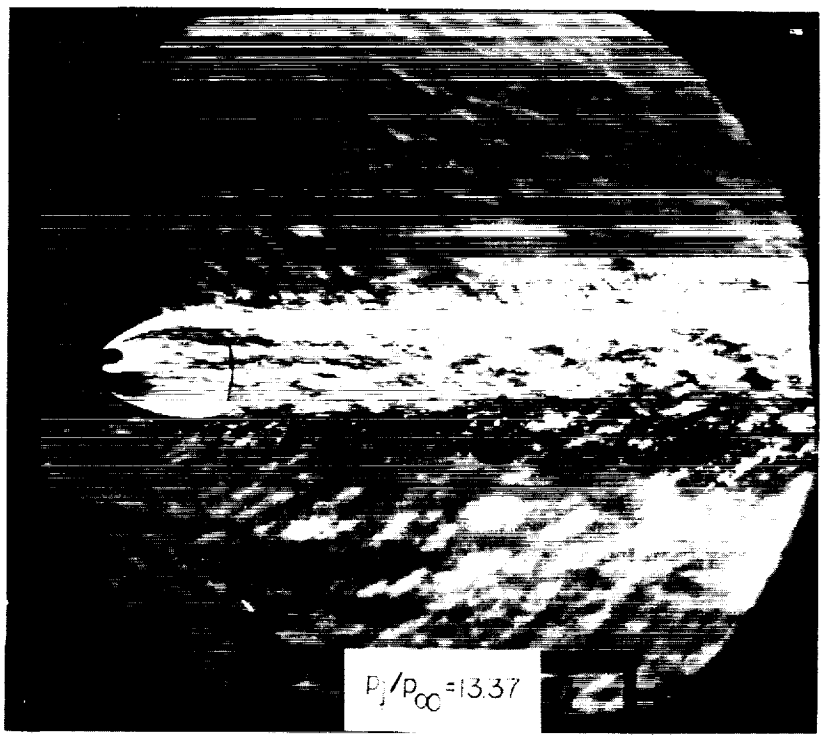

Figure 30.- Concluded. L-86512

L-86513

Figure 31.- Example of oblique compression waves generated in ambient air by supersonic eddy convection velocity. $M_j = 3.00$; $\theta_N = 0$; $\frac{p_j}{p_\infty} = 0.86$.

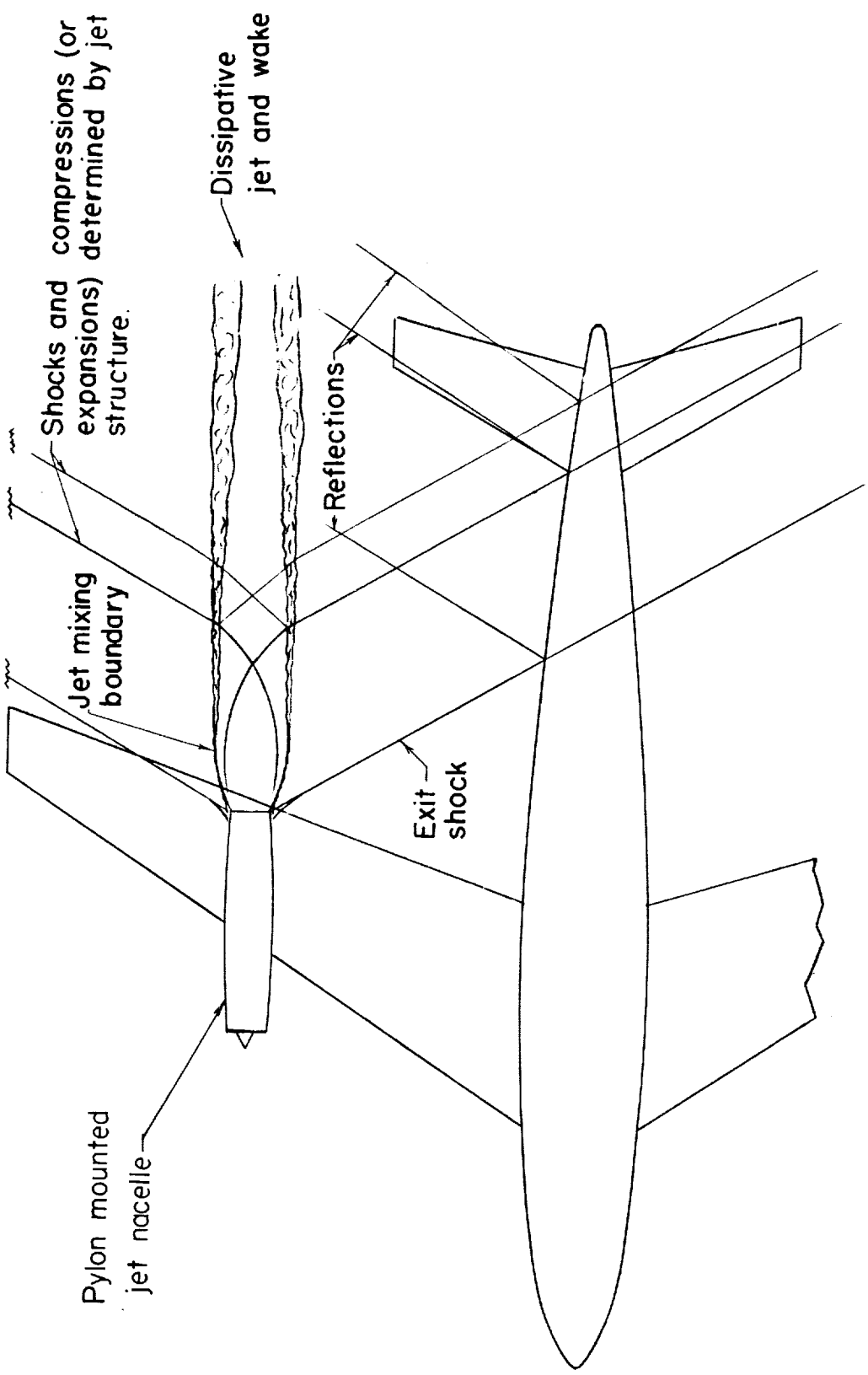

Figure 32.- Illustrative sketch of interference flow field created by jet. Mixing boundary assumed to be supersonic throughout.

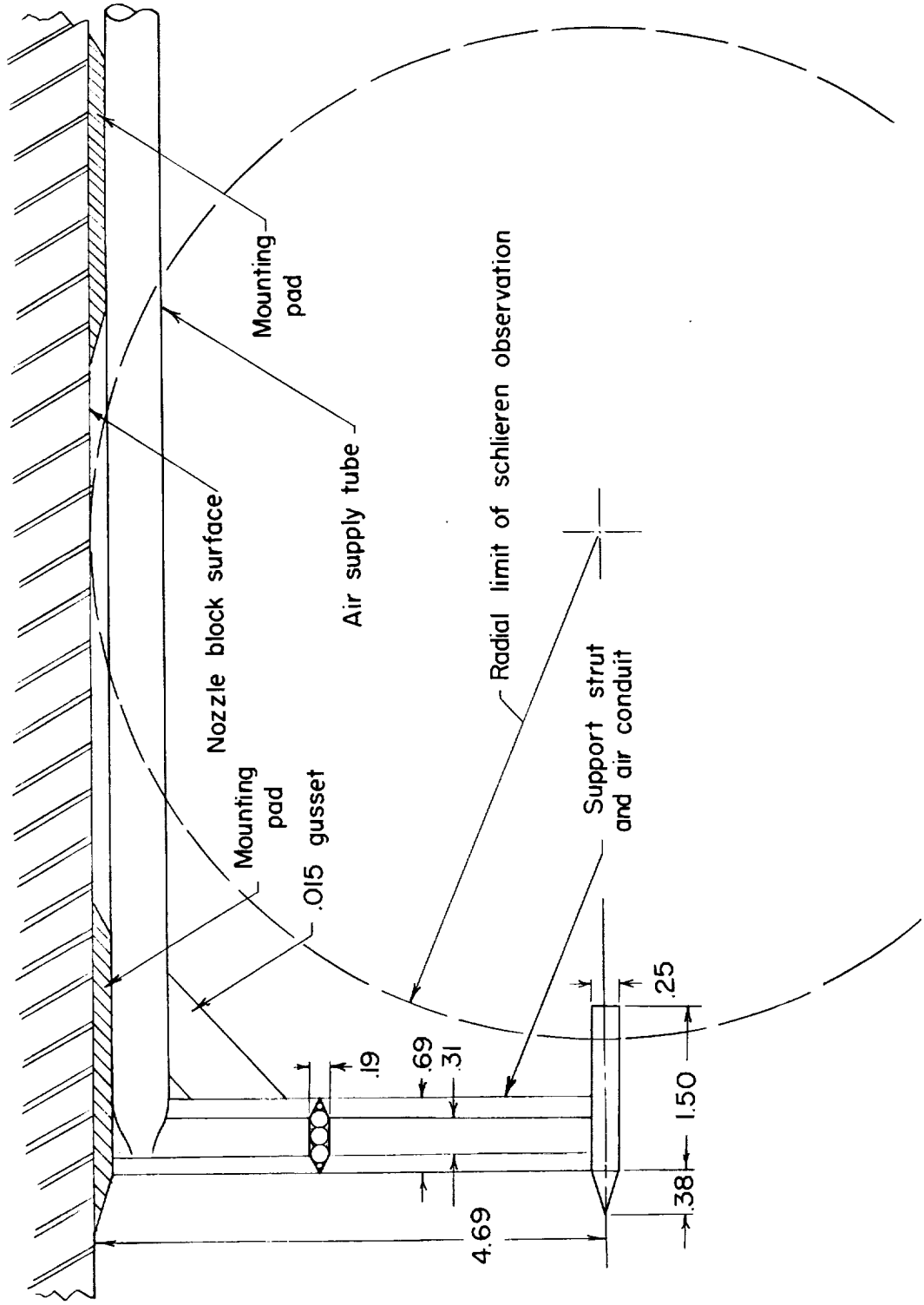

Figure 33.- Sketch of model employed in visual studies of jet exhausting into supersonic stream. All dimensions are in inches.

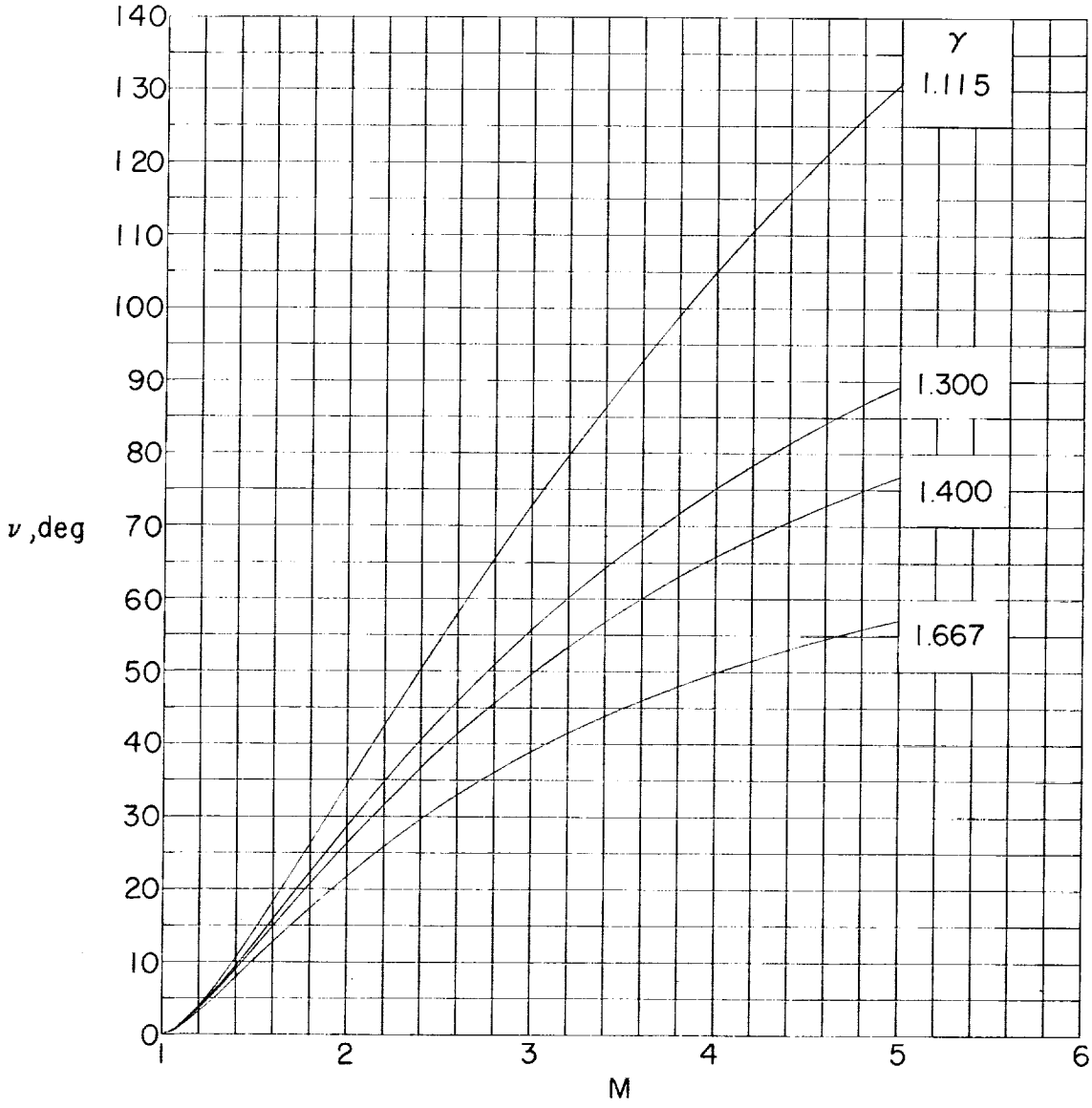

Figure 34.- Effect of the ratio of specific heats upon the variation in Prandtl-Meyer turning angle from sonic velocity with Mach number.

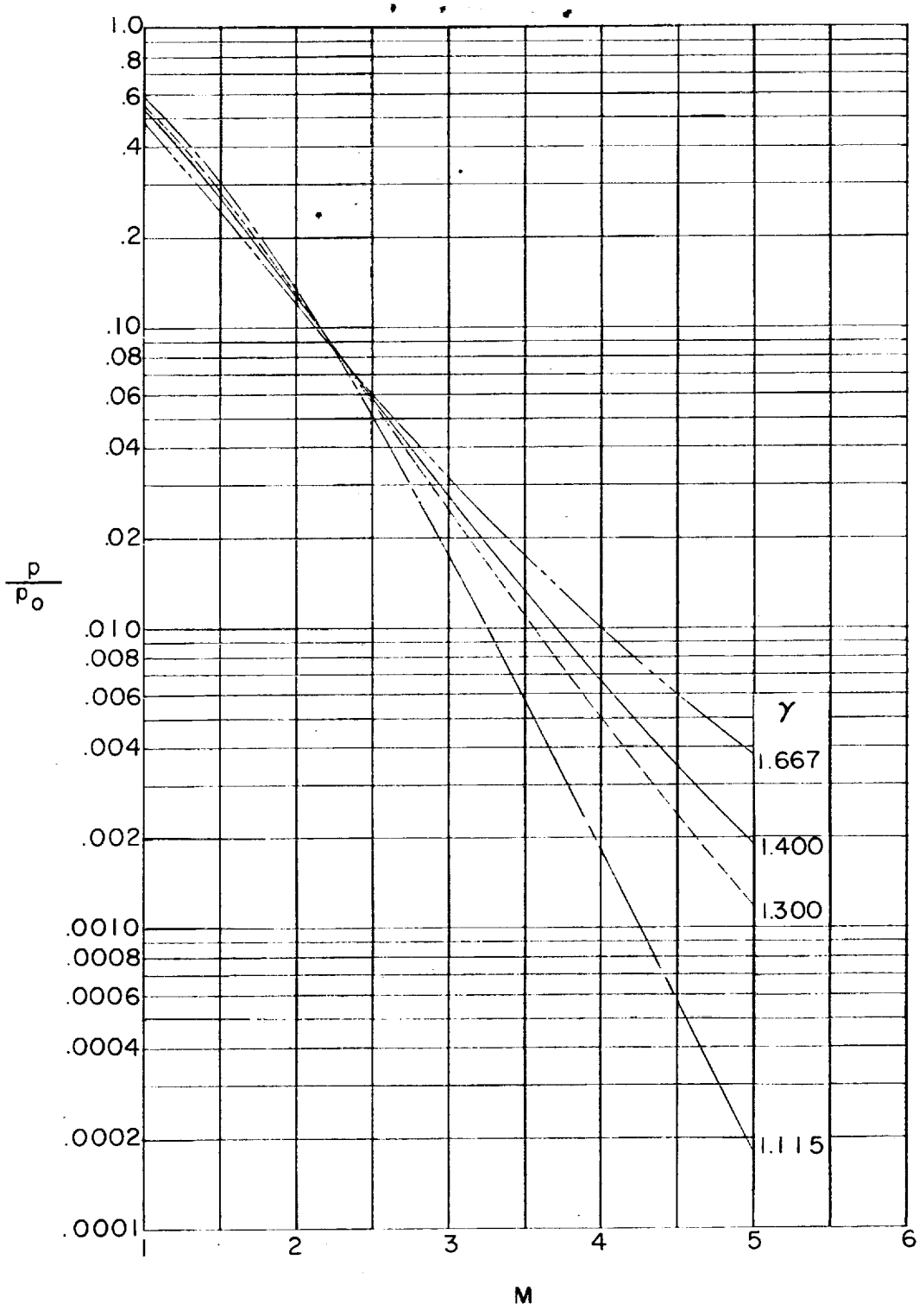

Figure 35.- Effect of the ratio of specific heats upon the variation in the ratio of static to stagnation pressure with Mach number.

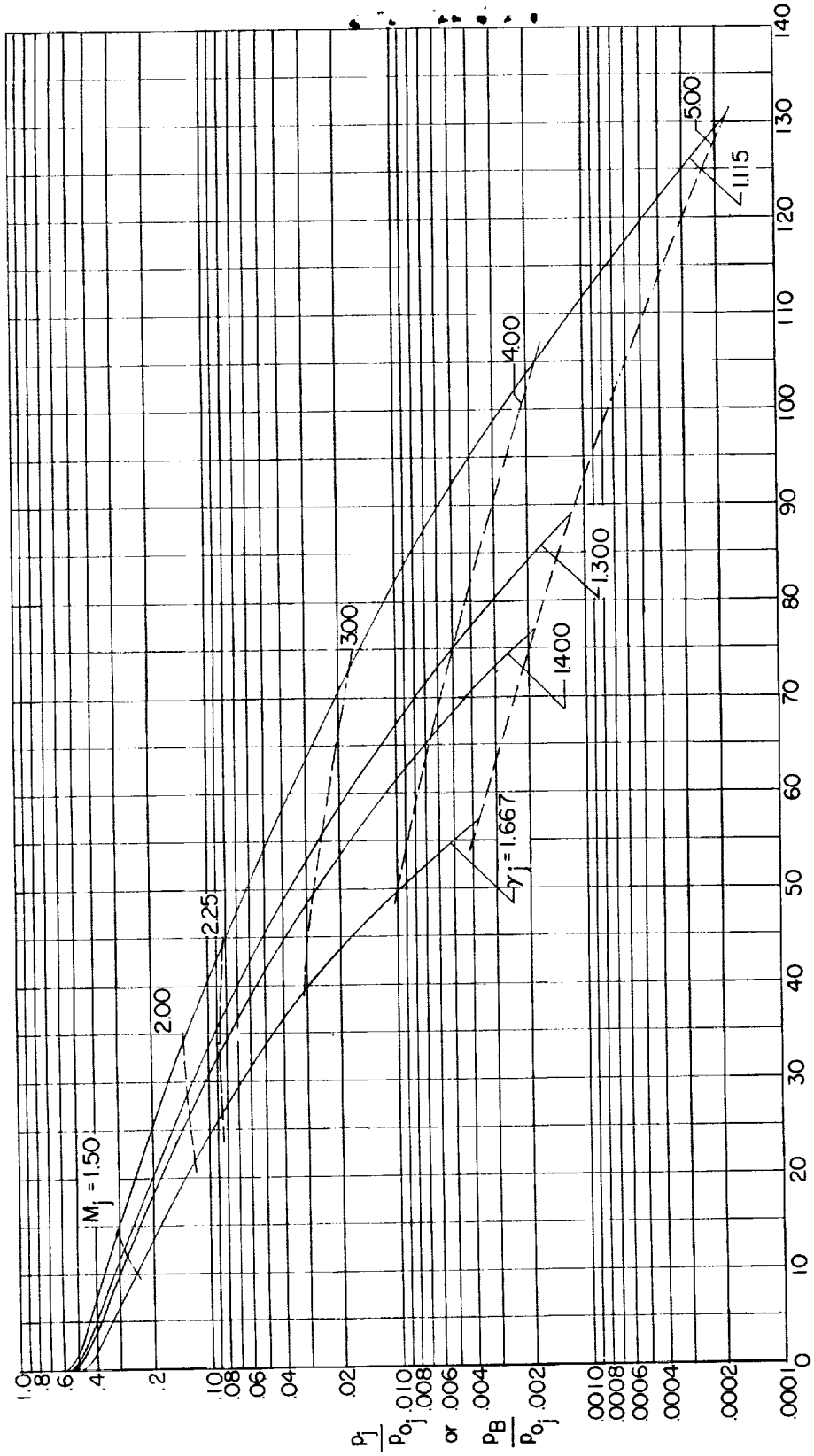

Figure 36.- Curves for correcting base-pressure data for a change in the ratio of specific heats of the jet.

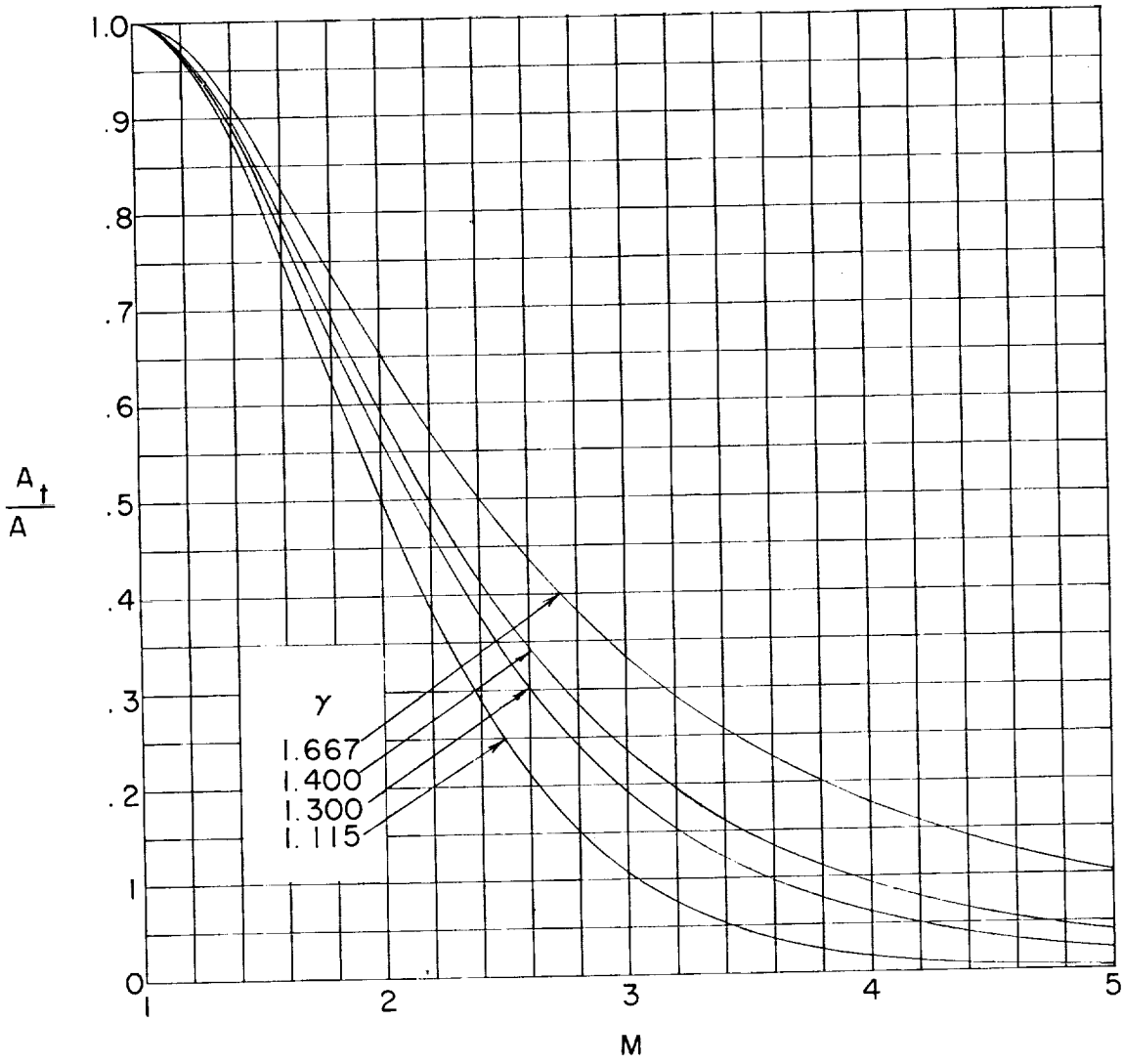

Figure 37.- Effect of the ratio of specific heats upon the variation in nozzle area ratio with Mach number.

[redacted]

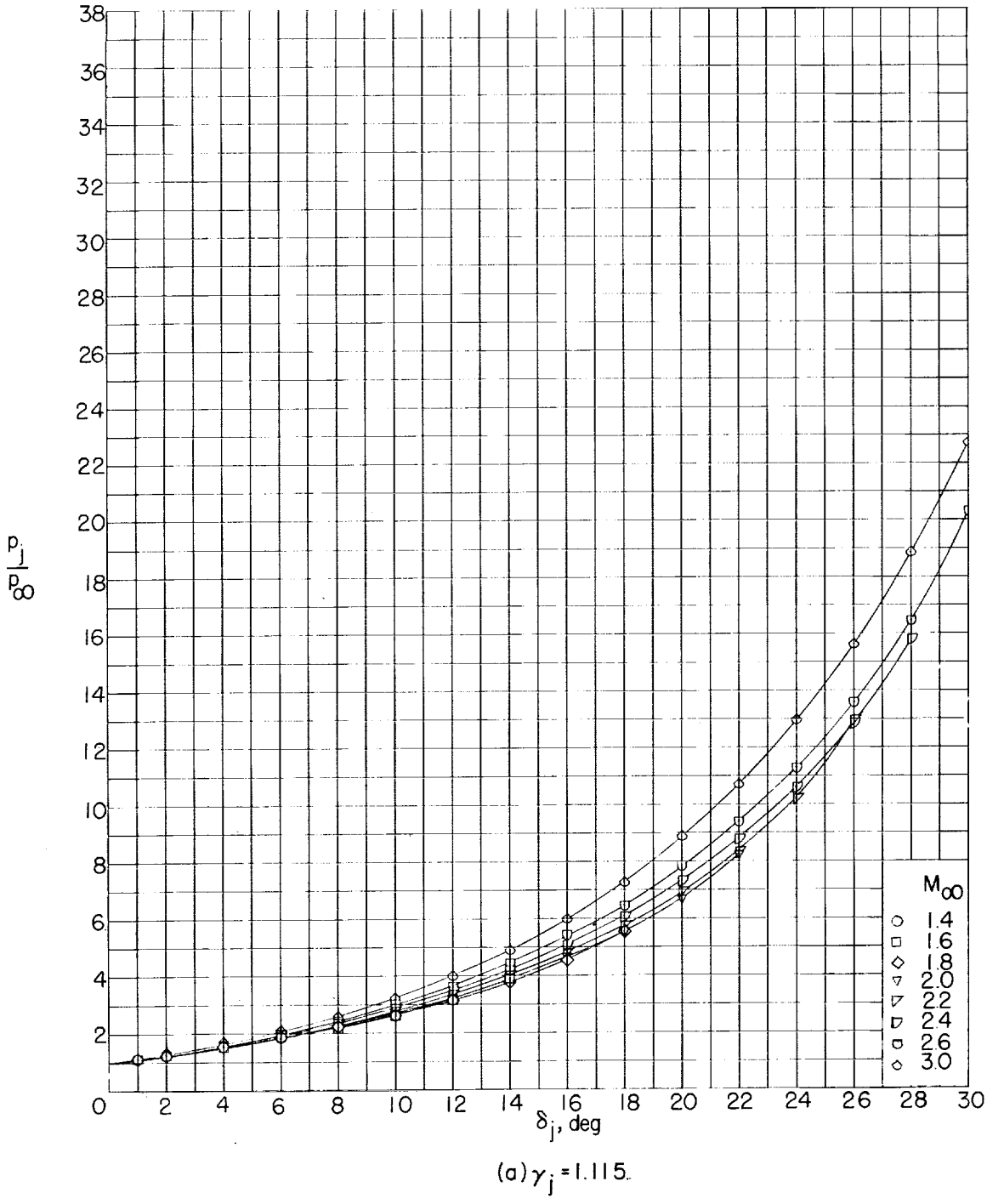

Figure 38.- Variation of initial inclination of jet boundary with jet pressure ratio for several free-stream Mach numbers and ratios of specific heats of the jet. $M_j = 1.00$; $\theta_N = 0^\circ$.

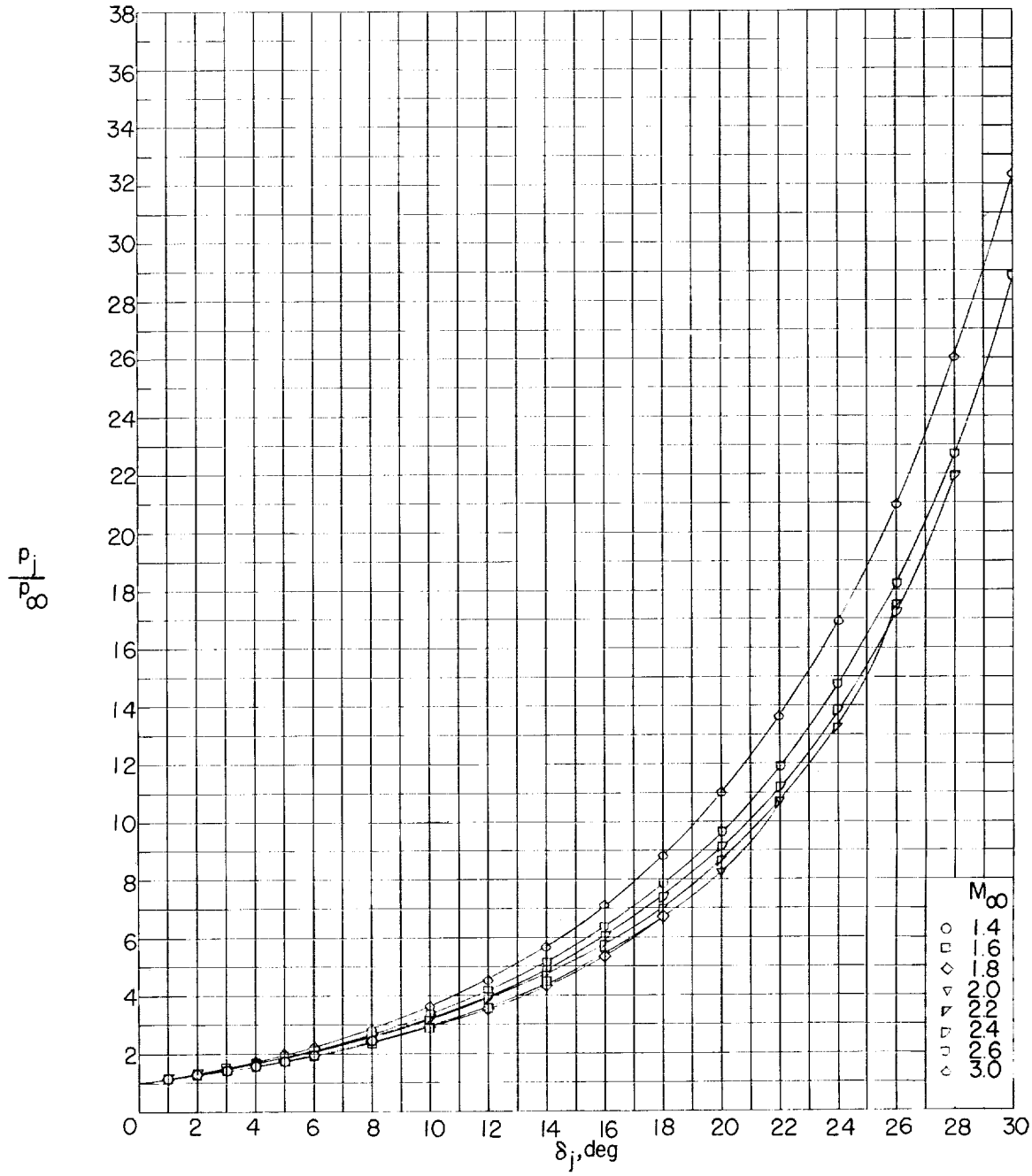

(b) $\gamma_j = 1.400$

Figure 38.- Continued.

[redacted]

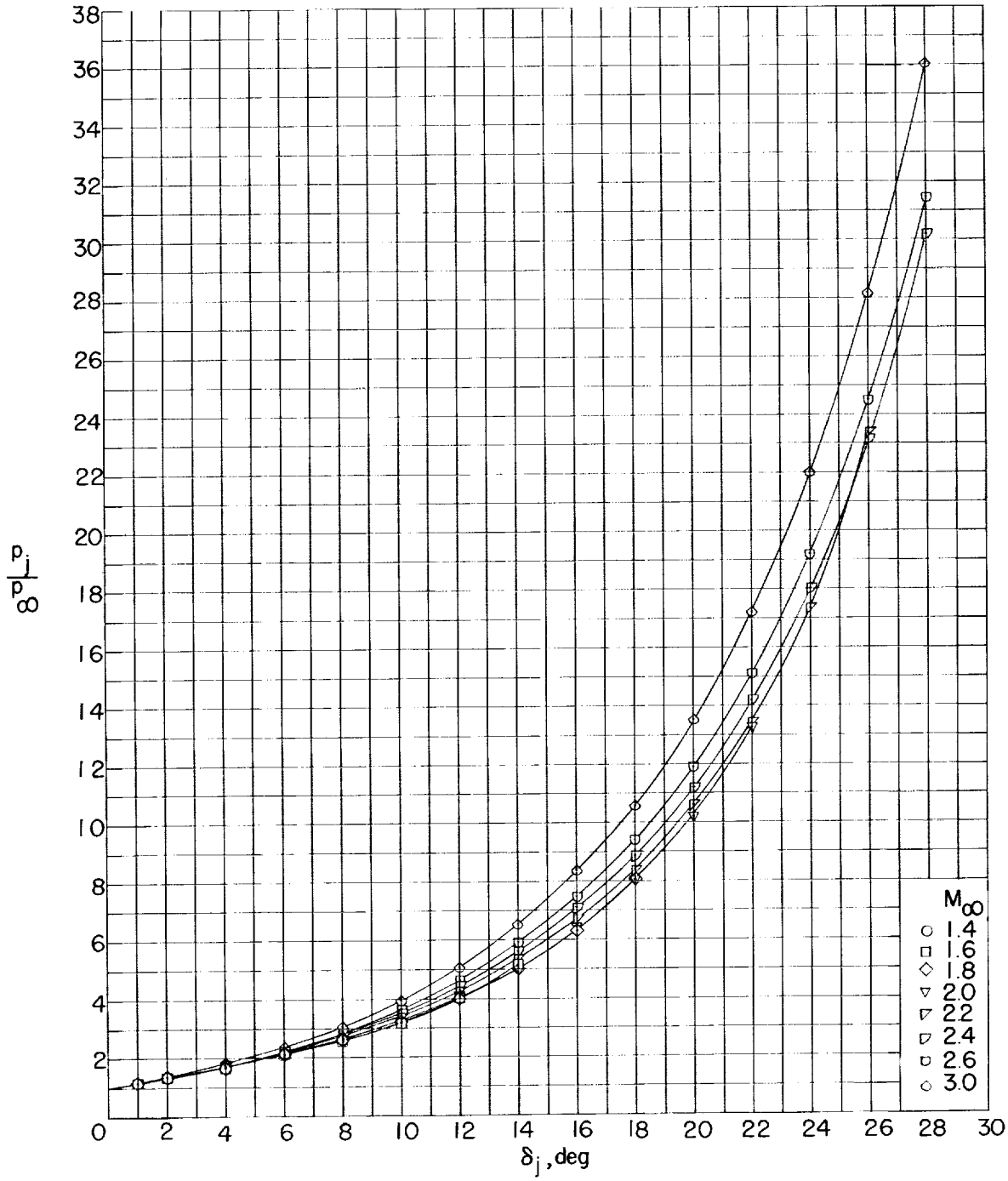

(c) $\gamma_j = 1.667$

Figure 38.- Concluded.

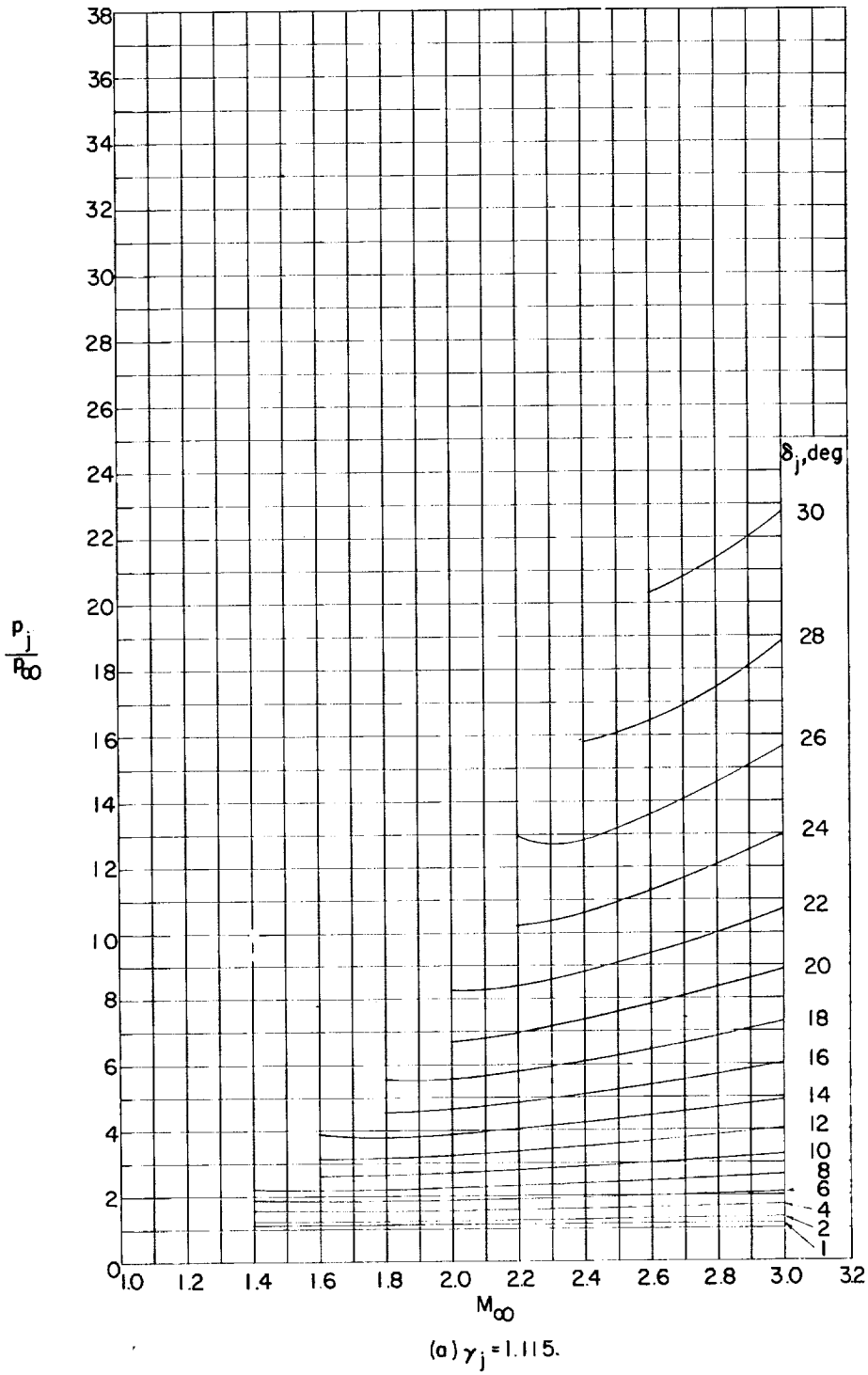

Figure 39.- Variation of jet pressure ratio with free-stream Mach number for several initial inclinations of the jet boundary and ratios of specific heats of the jet. $M_j = 1.00$; $\theta_N = 0^\circ$.

[redacted]

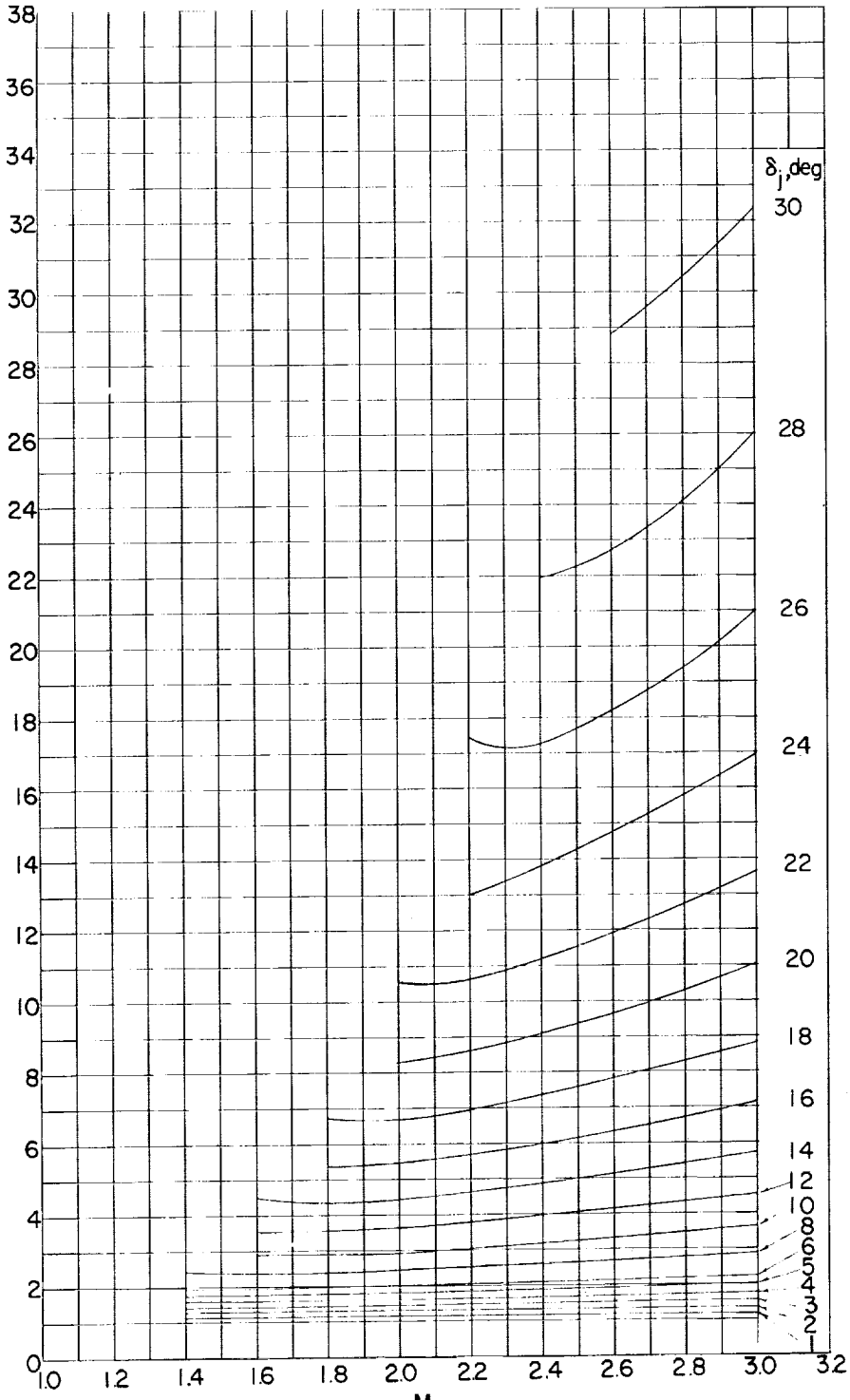

(b) $\gamma_j = 1.400$.

Figure 39.- Continued.

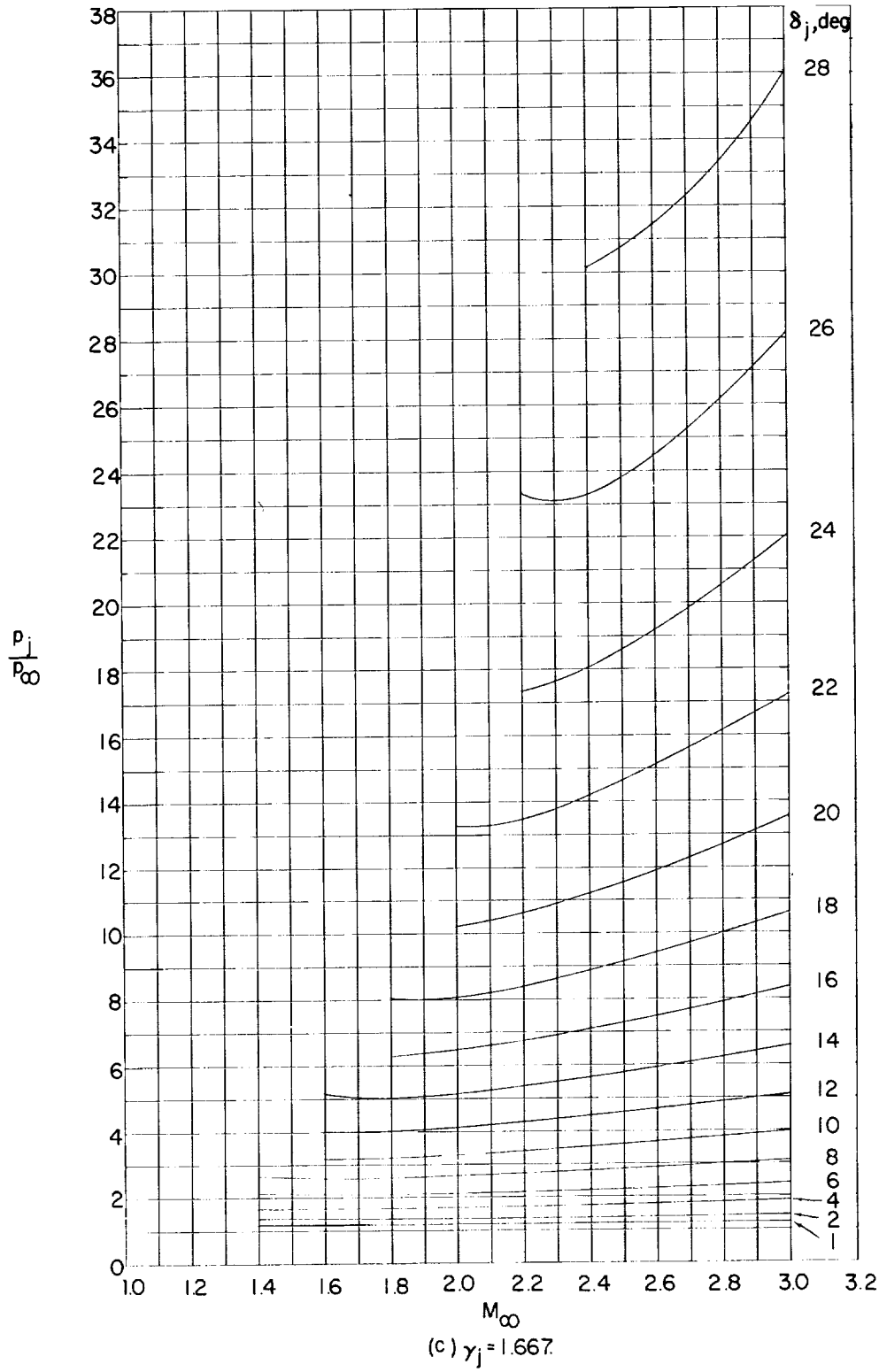

(c) $\gamma_j = 1.667$

Figure 39.- Concluded.

[redacted]

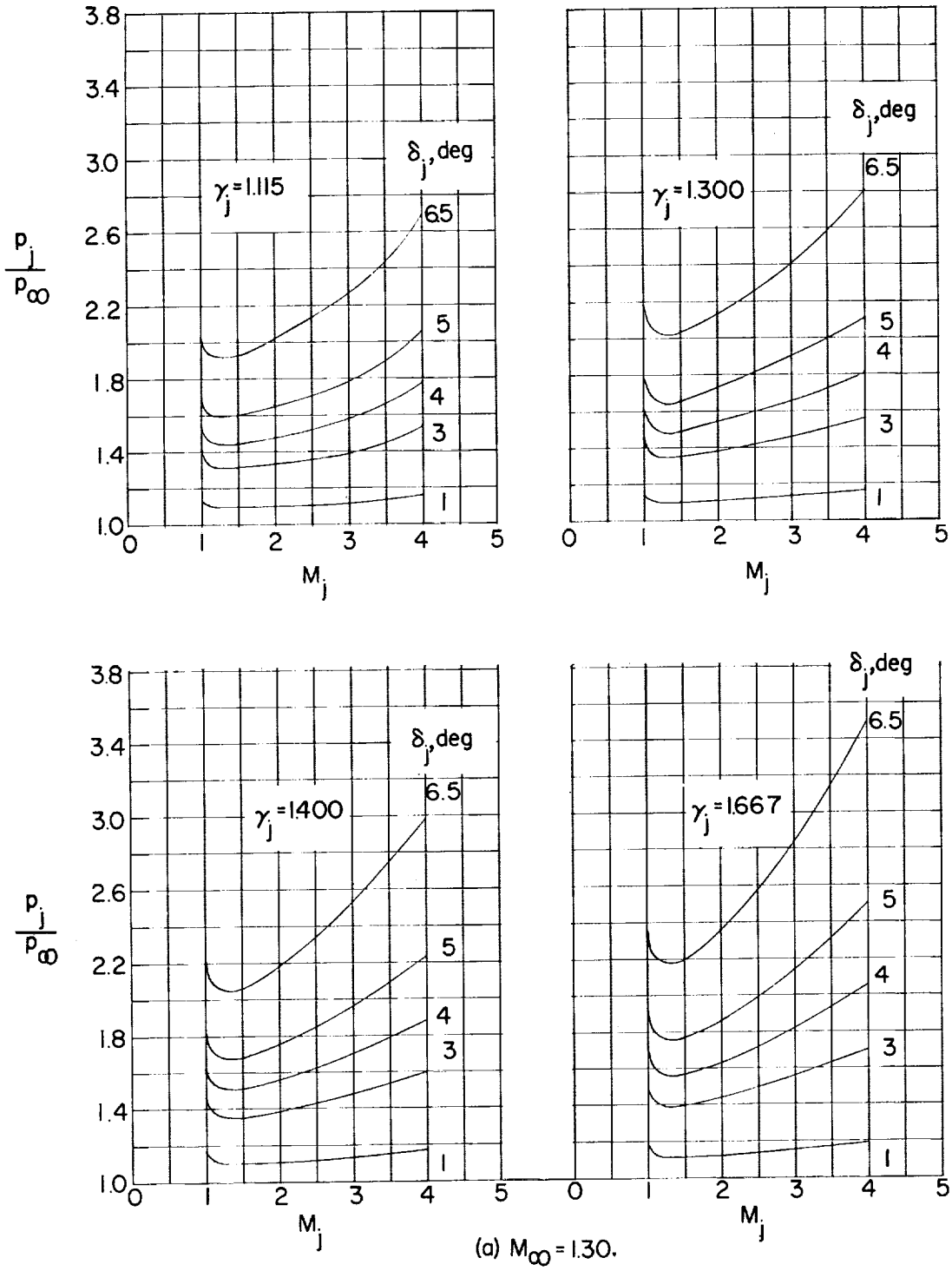

Figure 40.- Variation of jet pressure ratio with jet Mach number for several initial inclinations of the jet boundary and ratios of specific heats of the jet. $\theta_N = 0^\circ$.

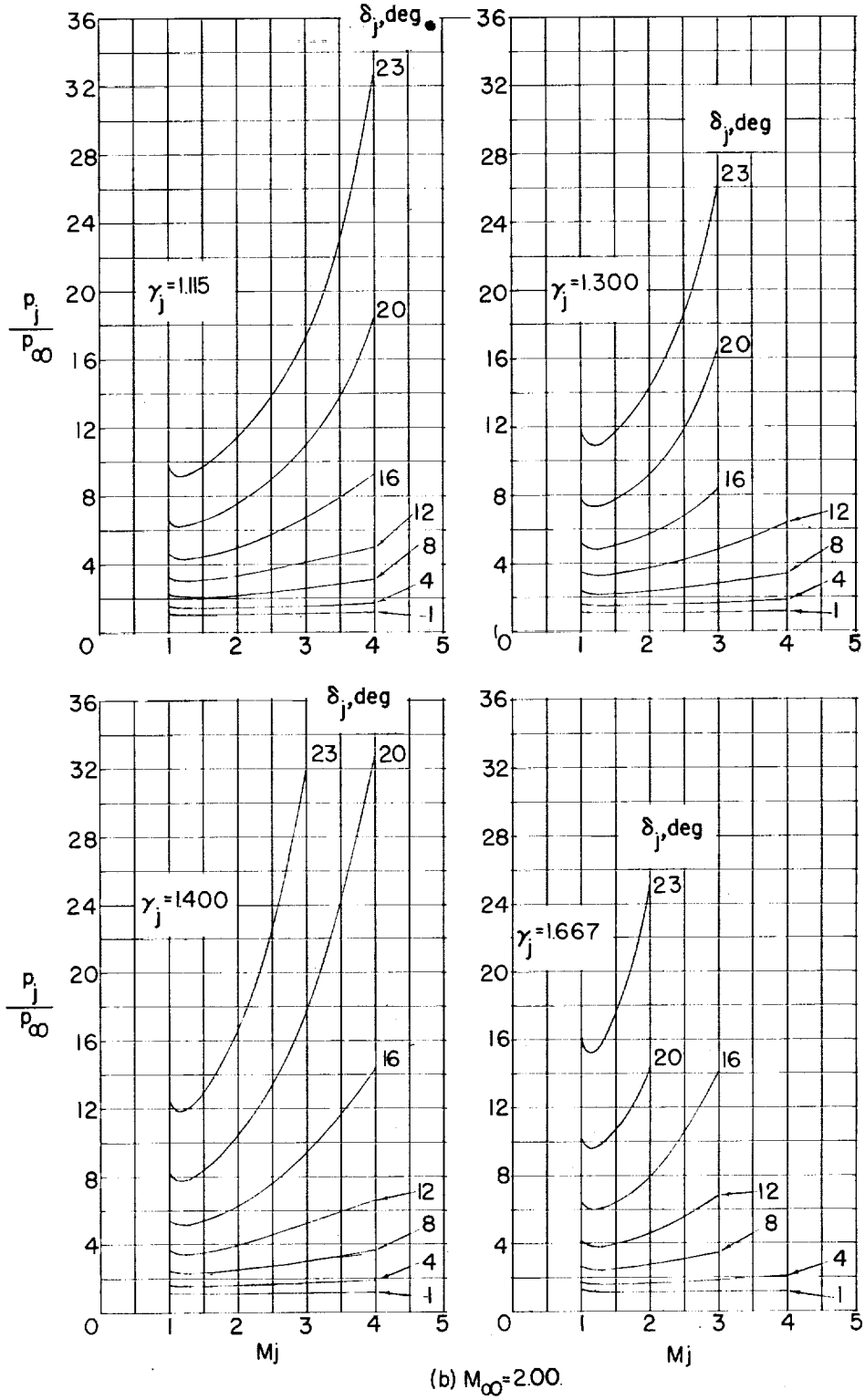

Figure 40.- Concluded.

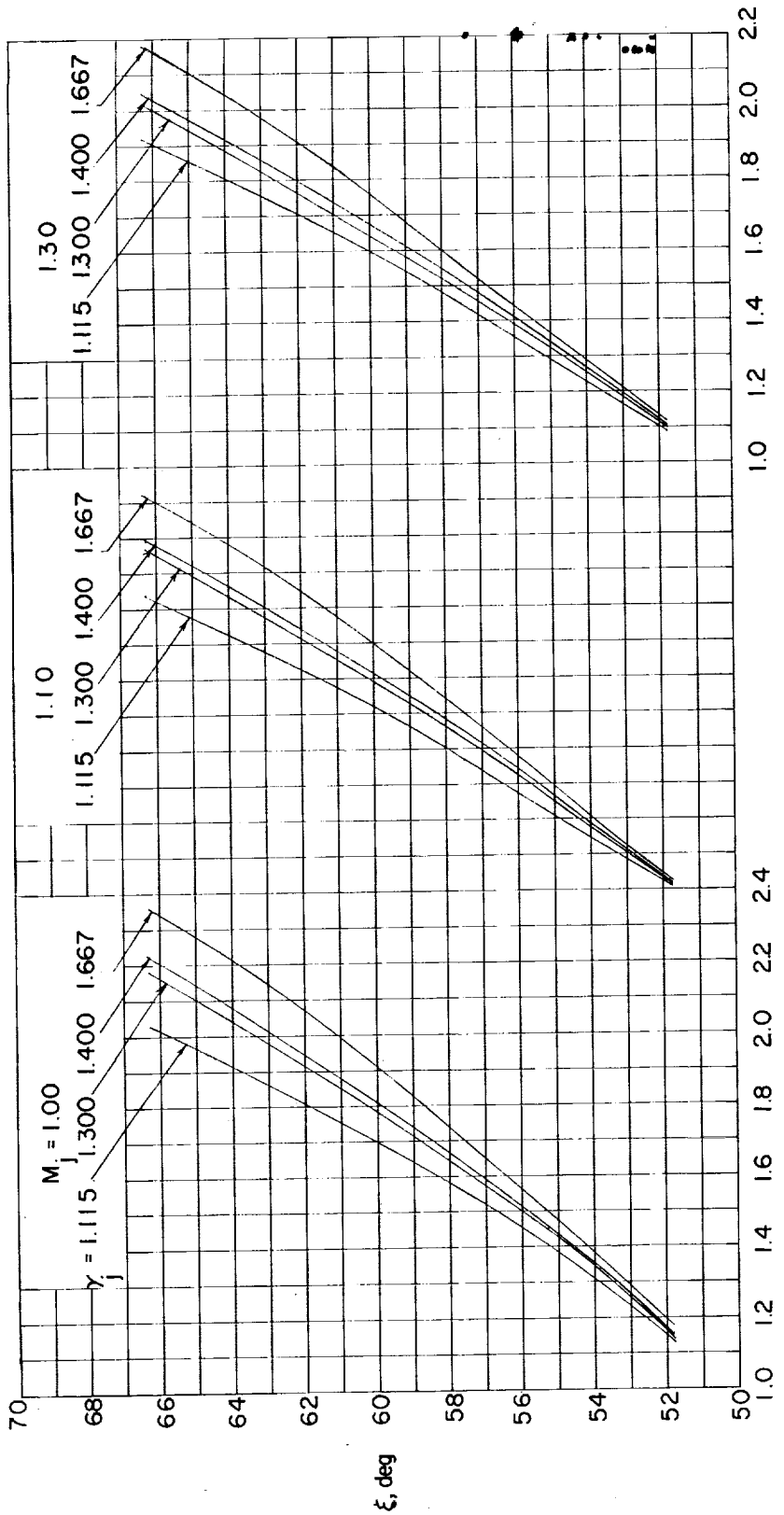

Figure 41.- Variation of inclination of exit shock with jet pressure ratio for several jet Mach numbers and ratios of specific heats of the jet. $\theta_N = 0^\circ$.

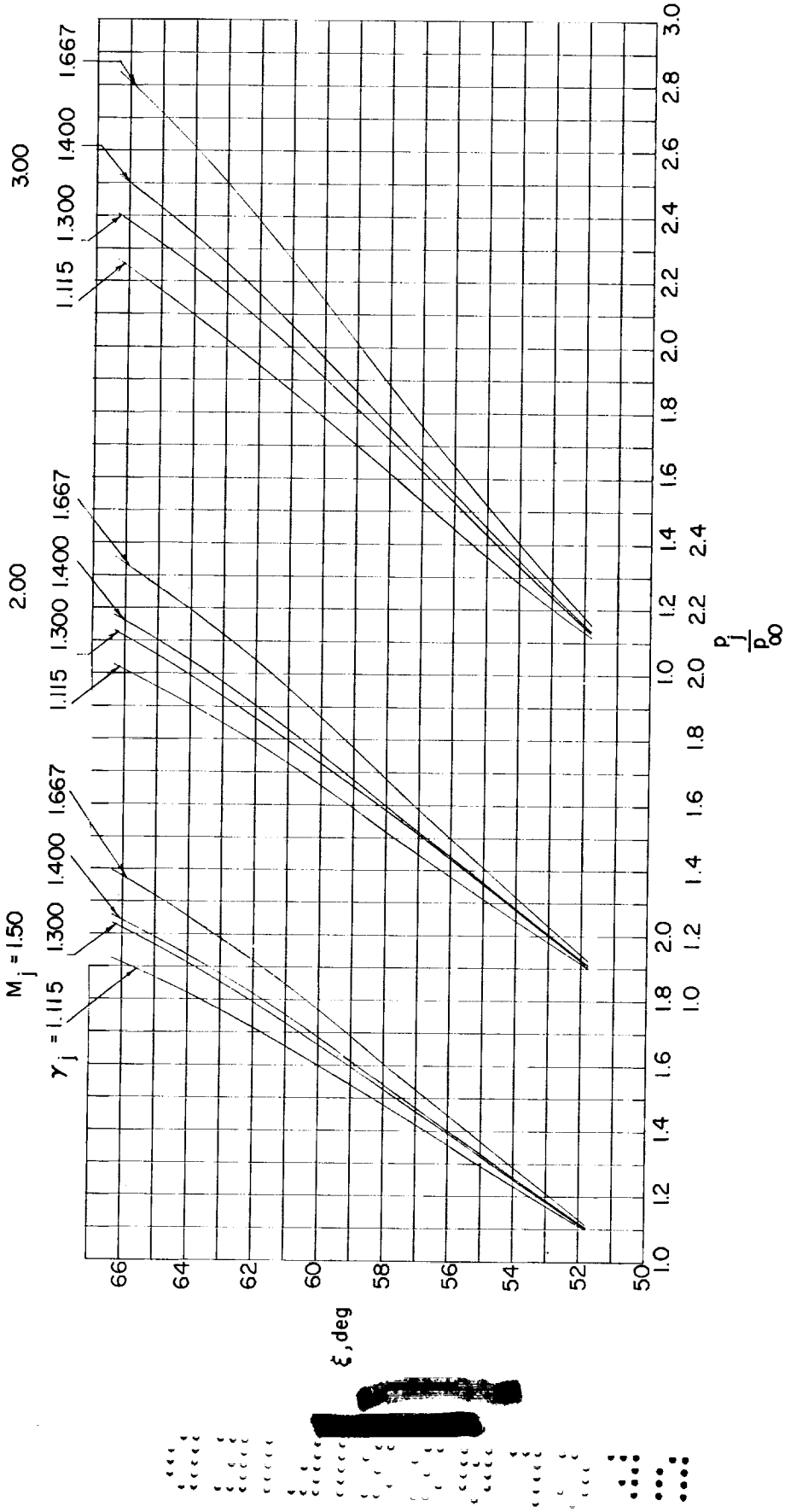

(a) Continued.

Figure 41.- Continued.

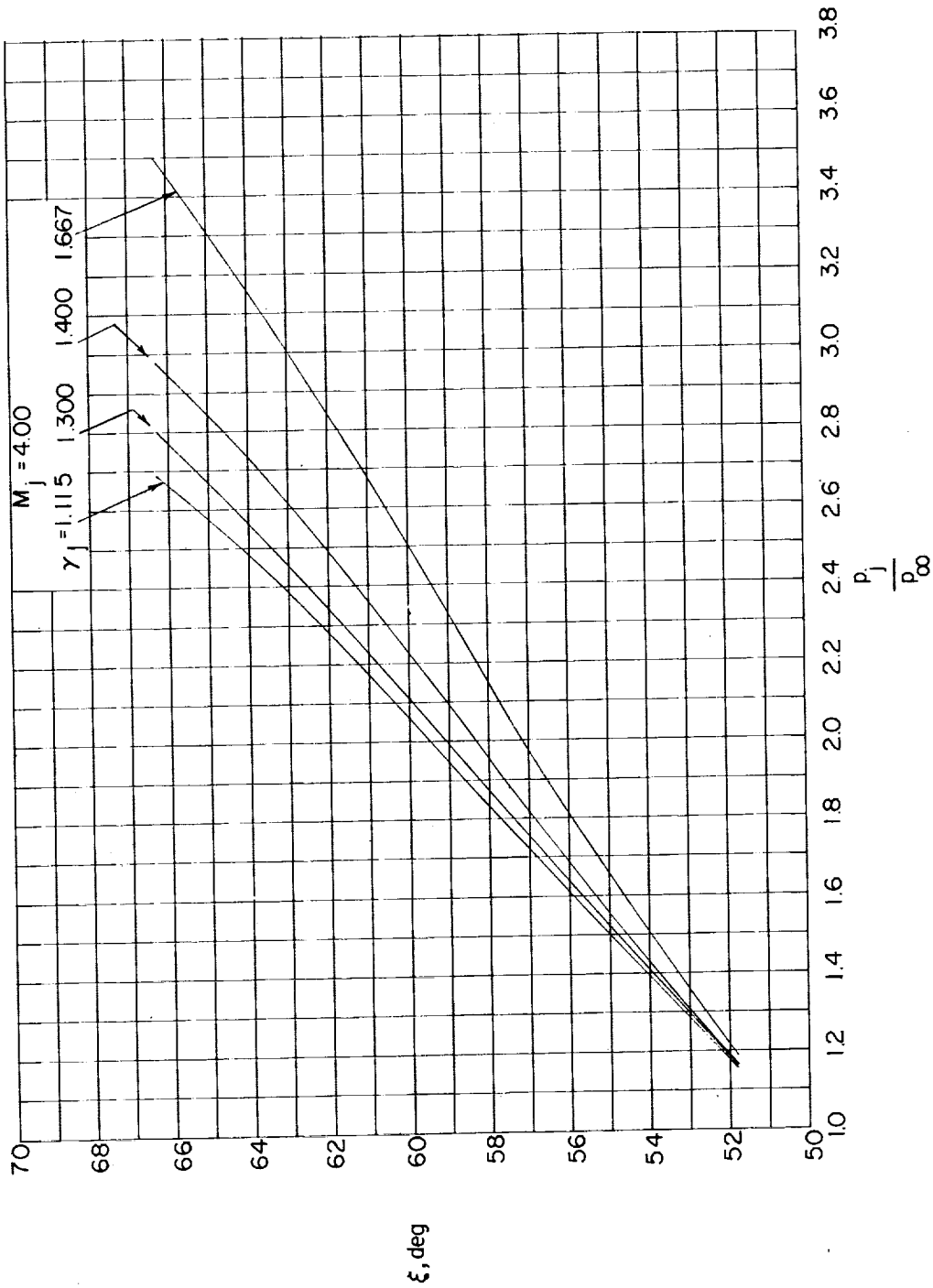

(a) Concluded.

Figure 41.- Continued.

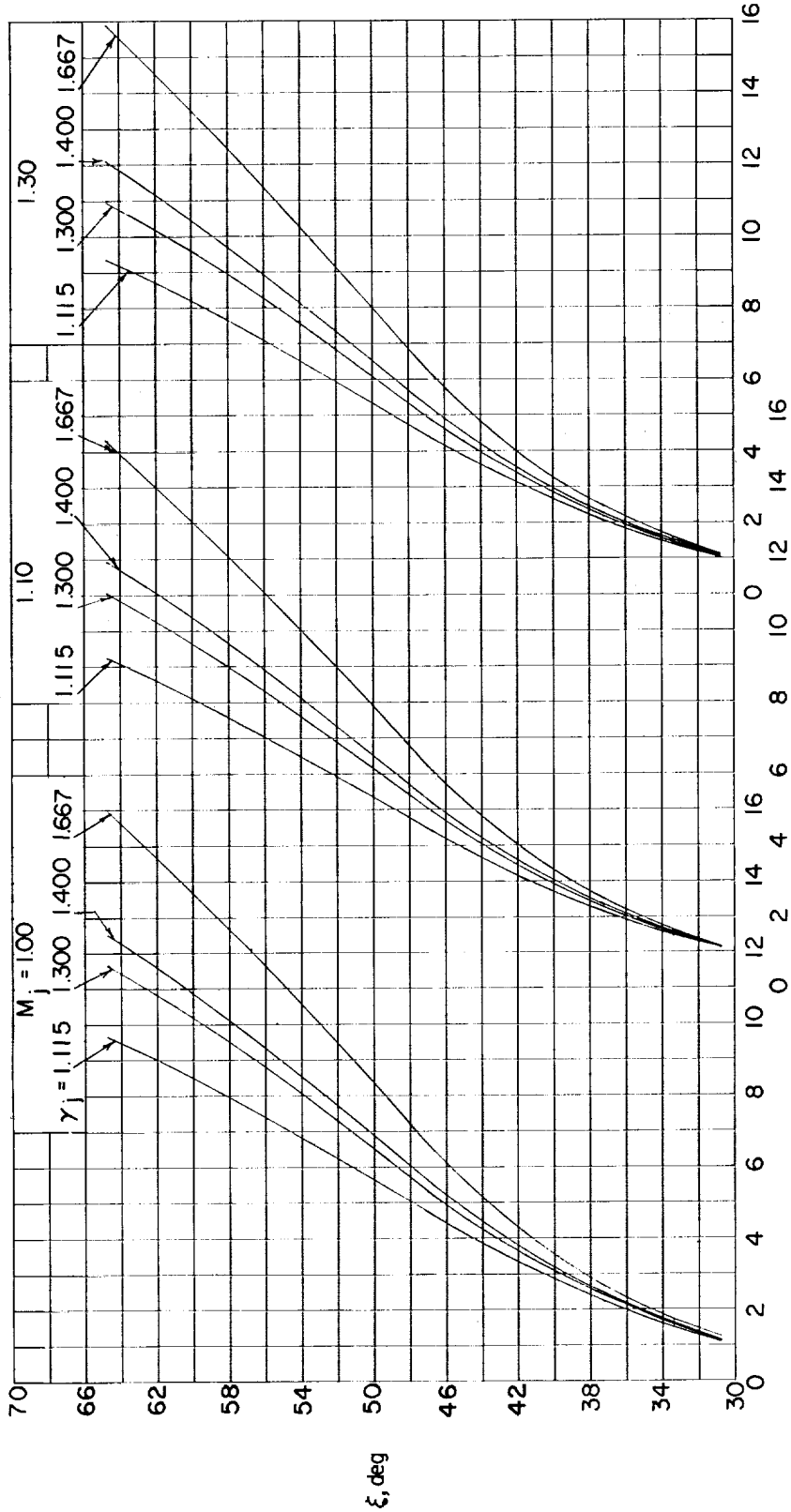

(b) M_∞=2.00.

Figure 41.- Continued.

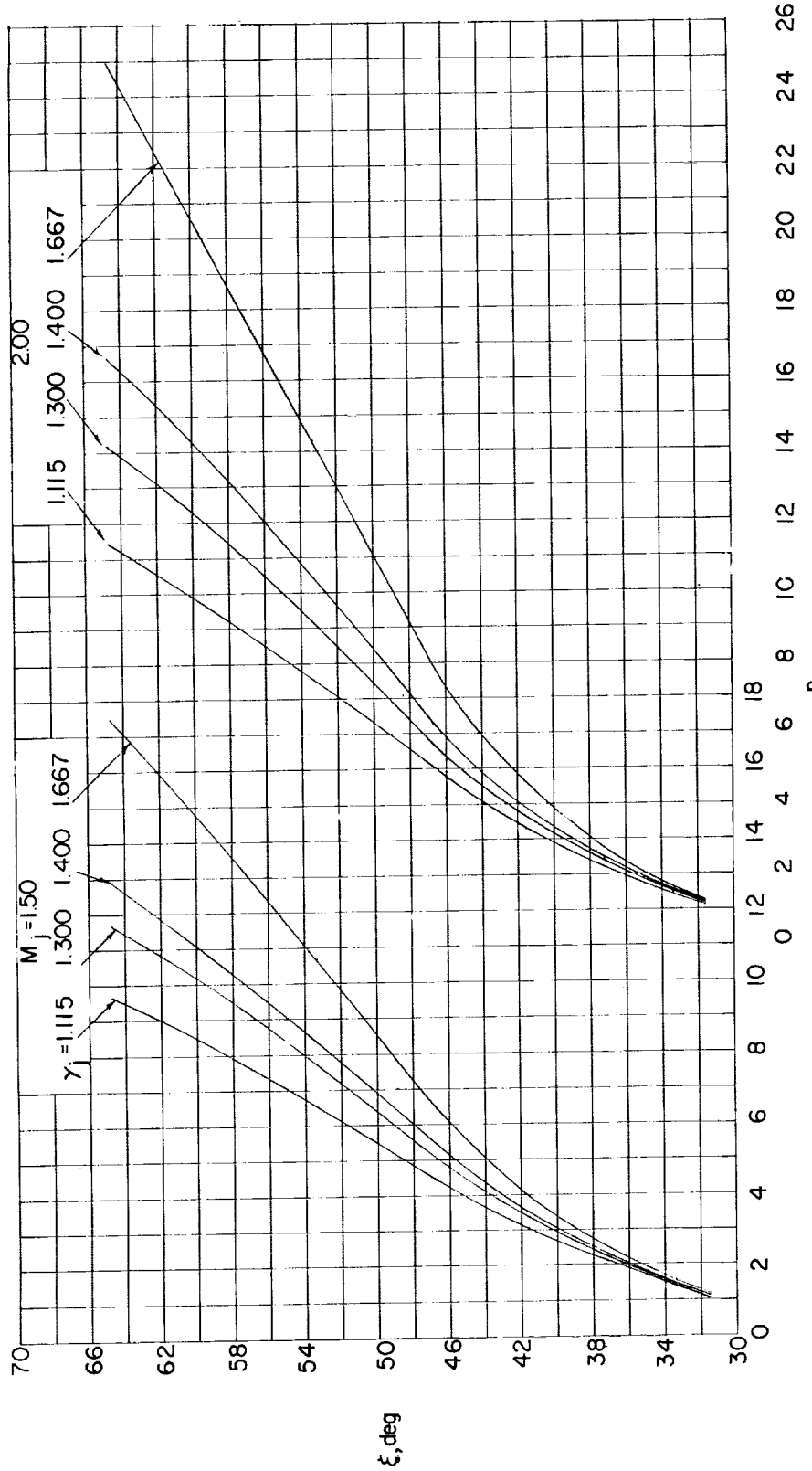

(b) Continued.

Figure 41.- Continued.

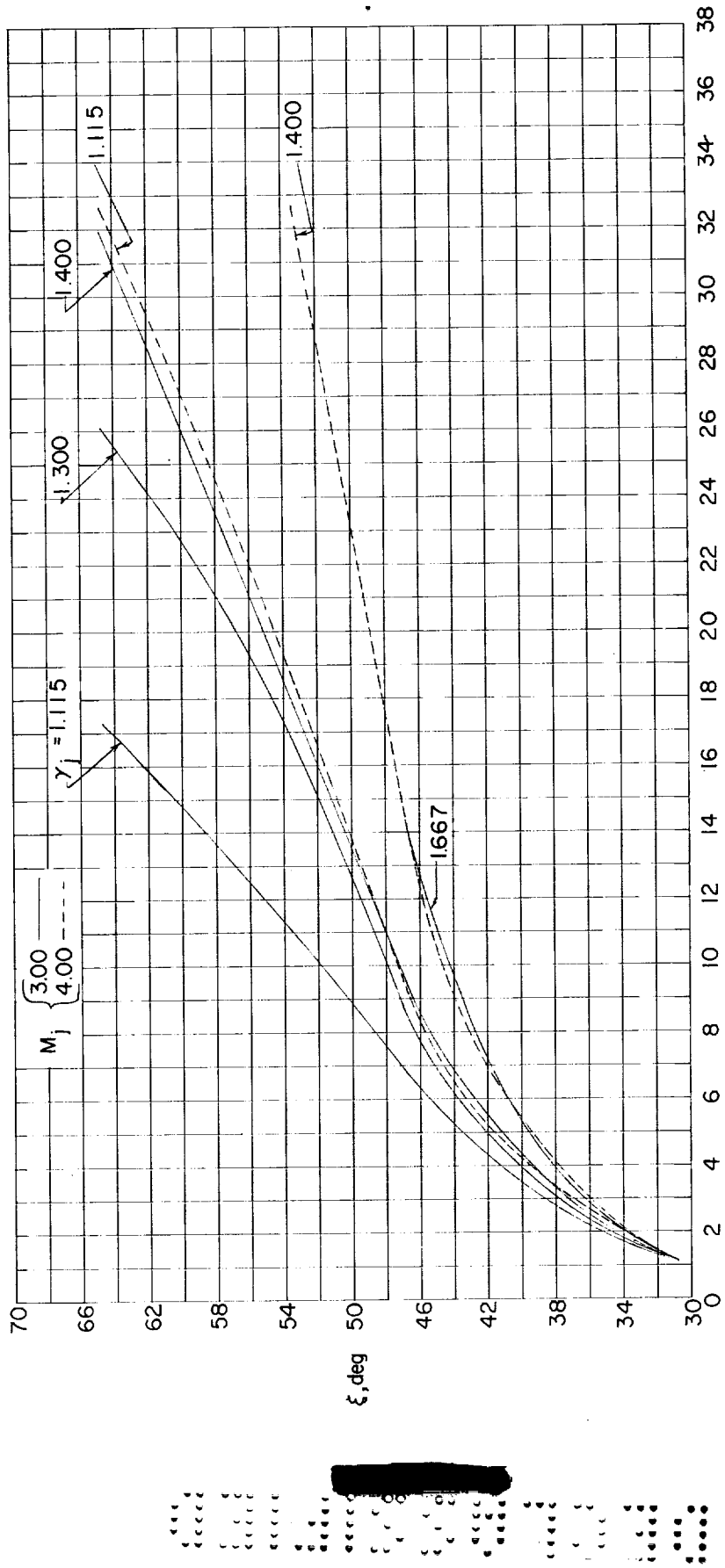

(b) Concluded.

Figure 41.- Concluded.

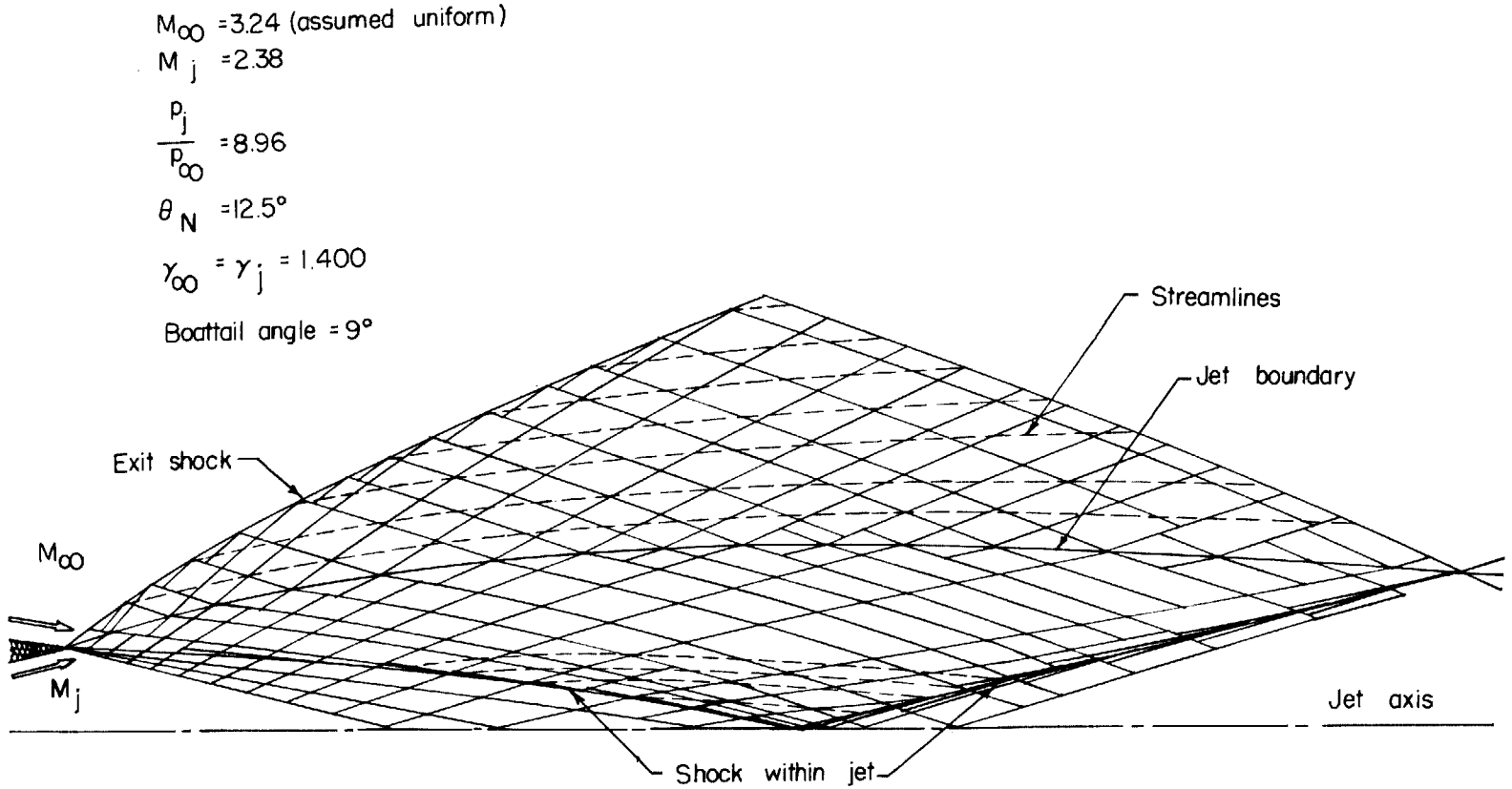

Figure 42.- Characteristic calculation by Schäfer of a supersonic jet exhausting into a supersonic stream.

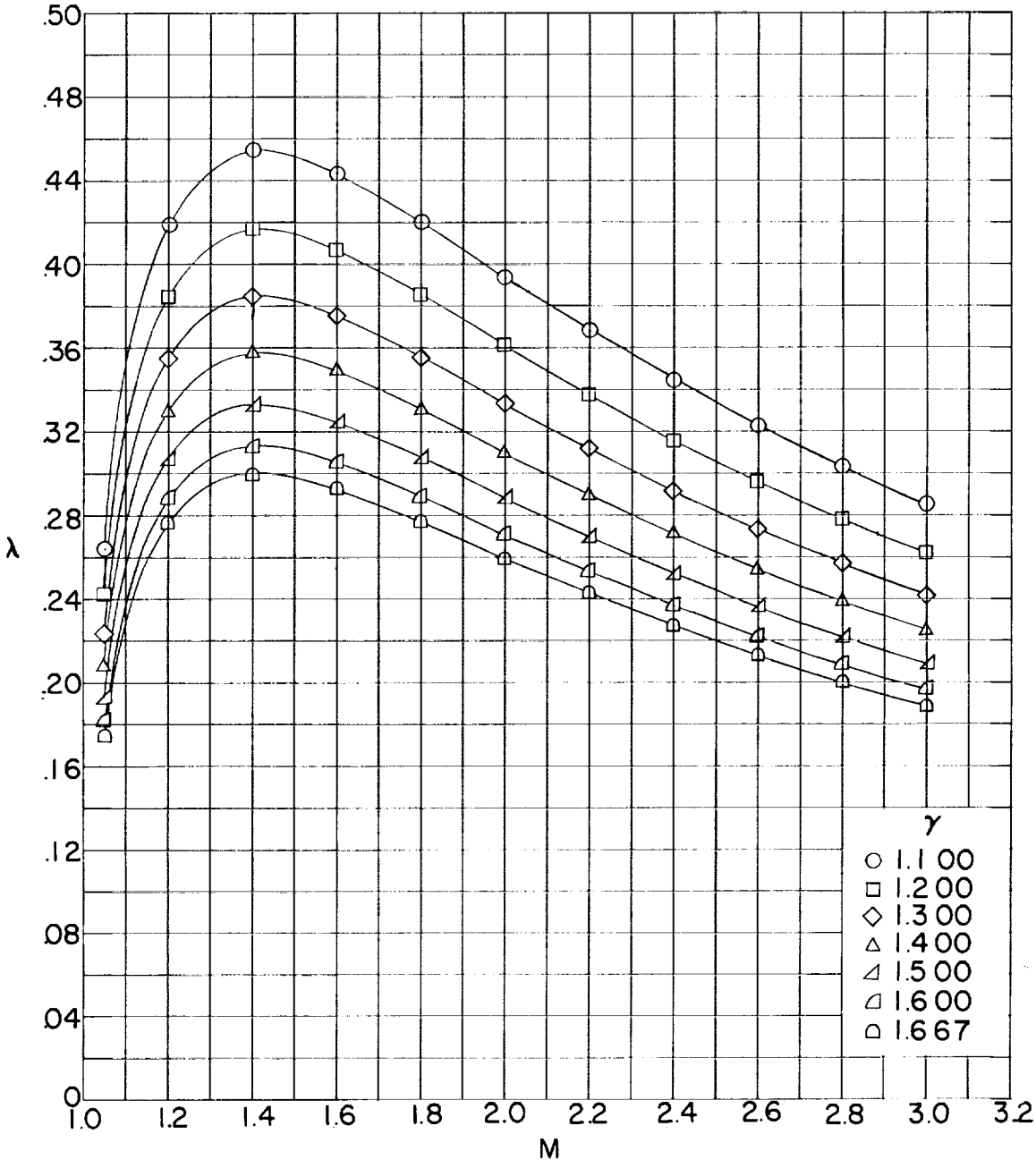

Figure 43.- Variation of basic Kawamura parameter with Mach number for several ratios of specific heats.

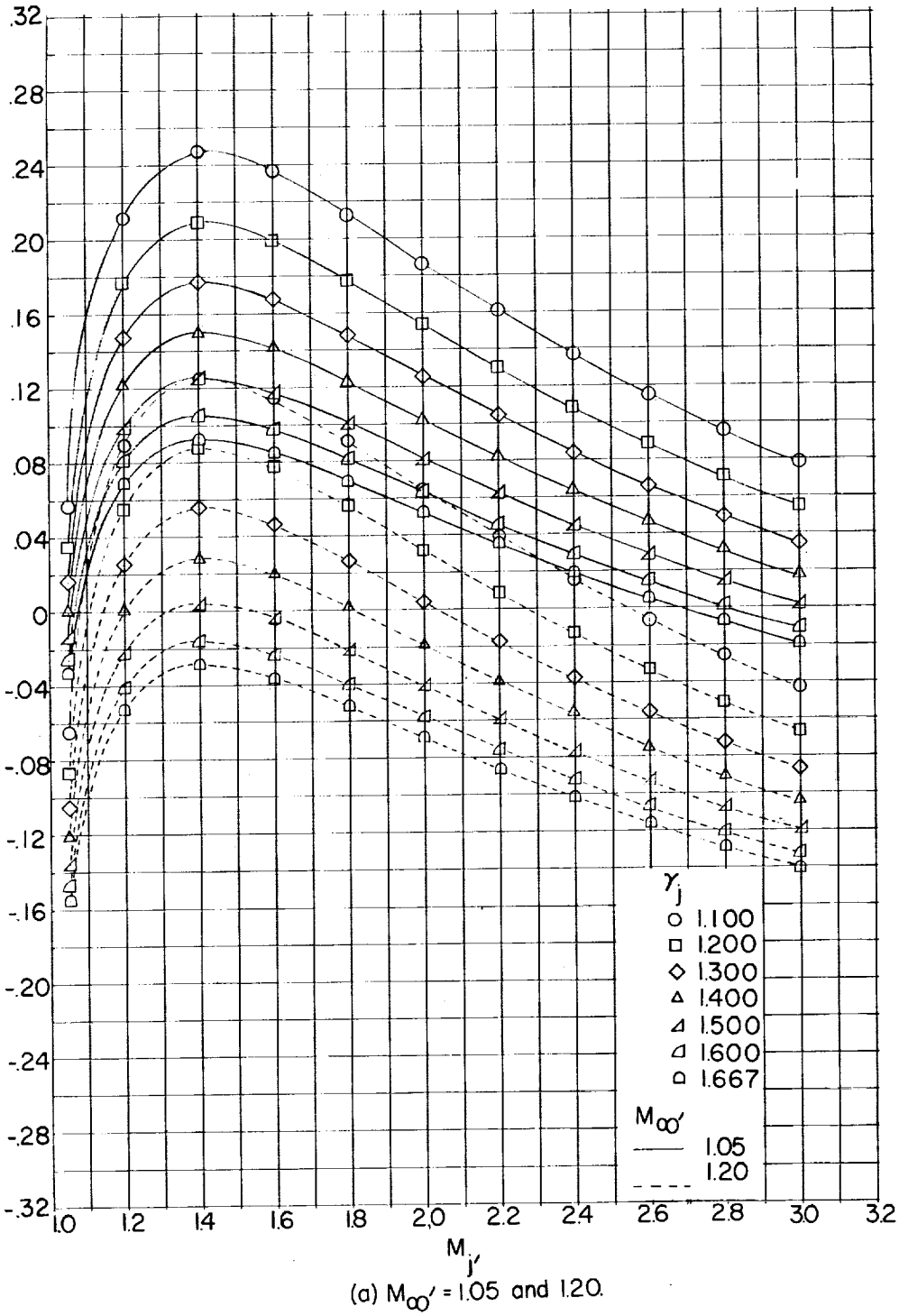

(a) $M_{\infty'} = 1.05$ and 1.20.

Figure 44.- Variation of the Kawamura difference parameter with local Mach number at the boundary in the free jet and in the free stream for several ratios of specific heats of the jet.

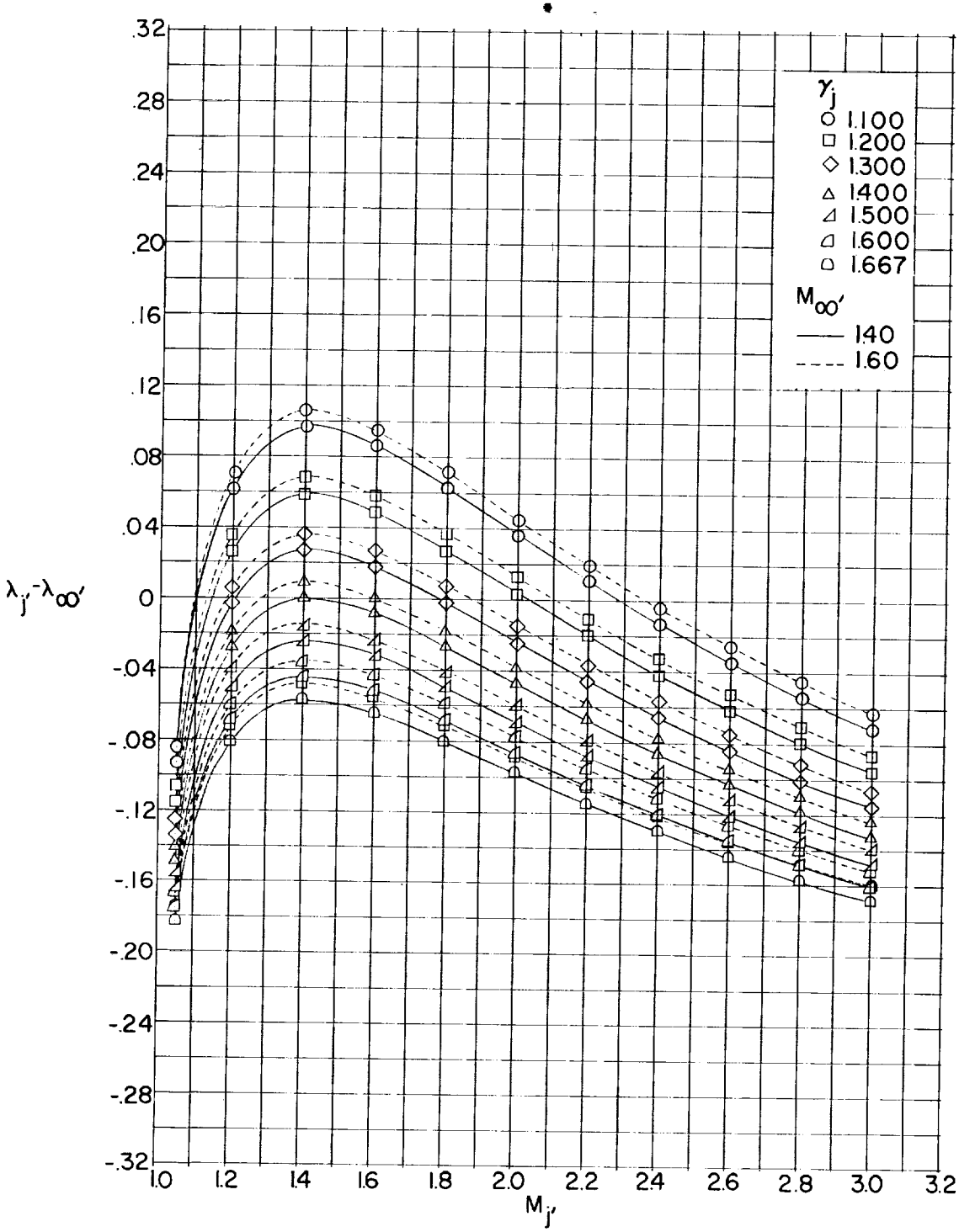

(b) $M_{\infty'}$= 1.40 and 1.60.

Figure 44.- Continued.

[redacted]

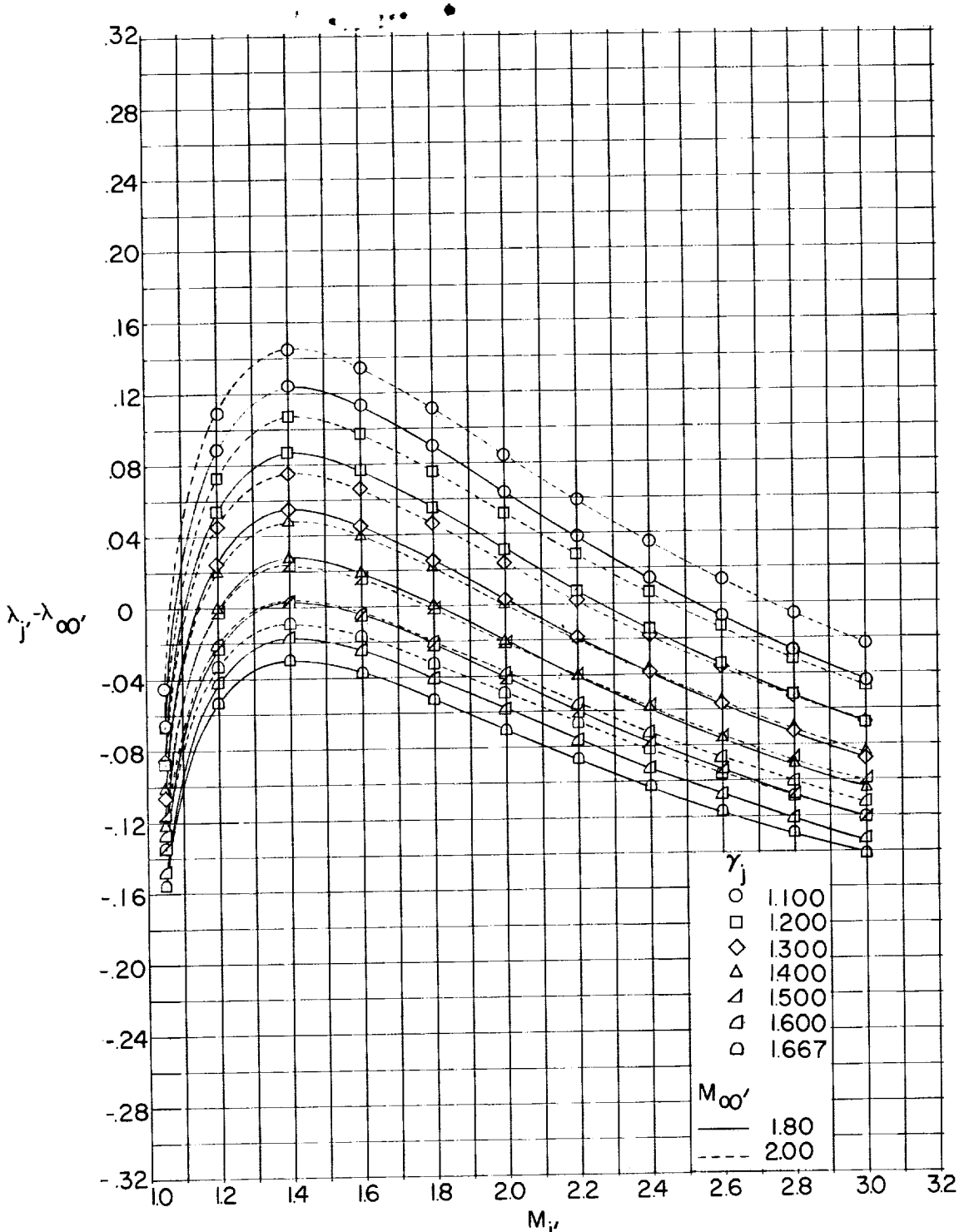

(c) $M_{\infty'}$ = 1.80 and 2.00.

Figure 44.- Continued.

[redacted]

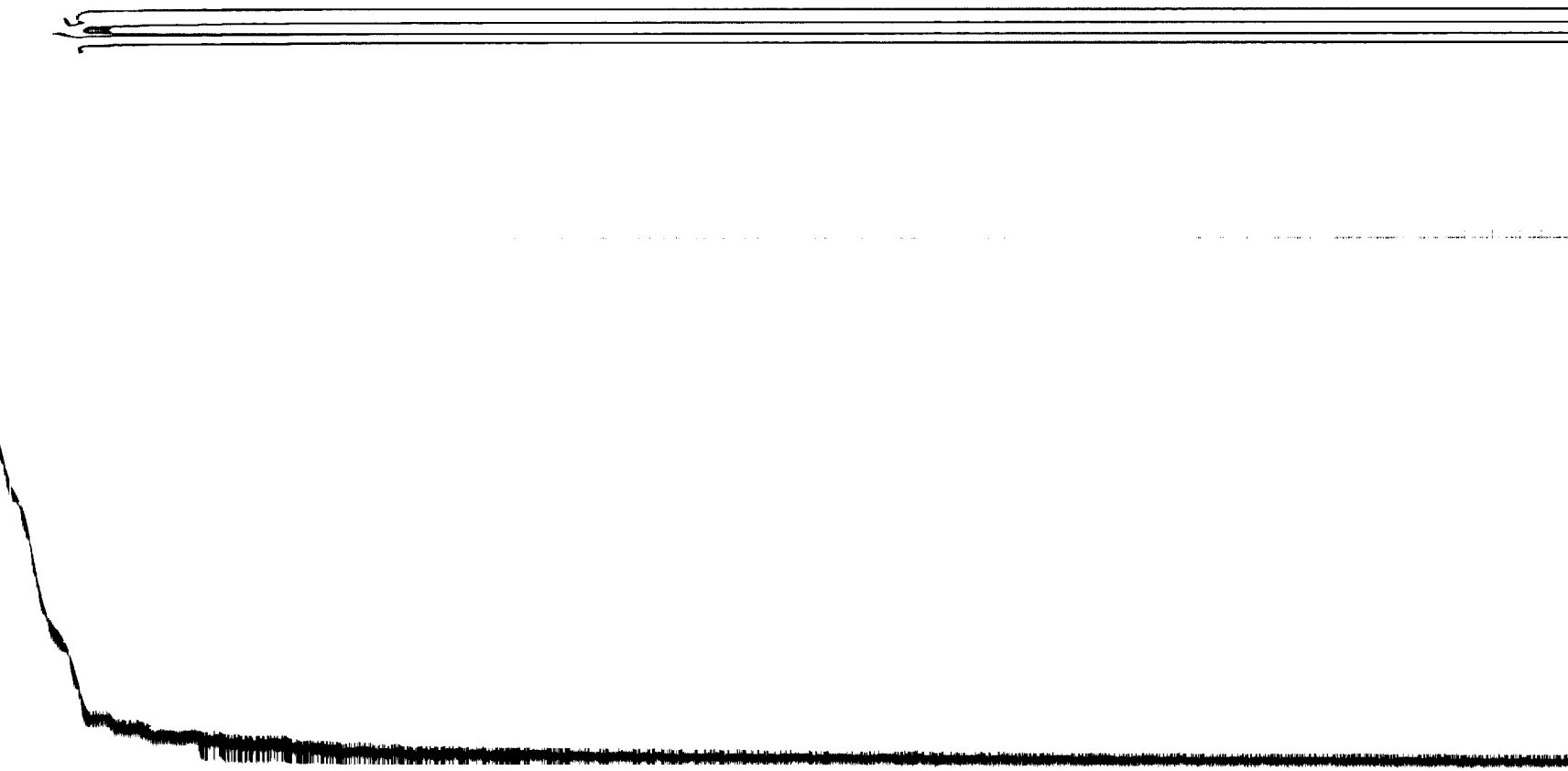

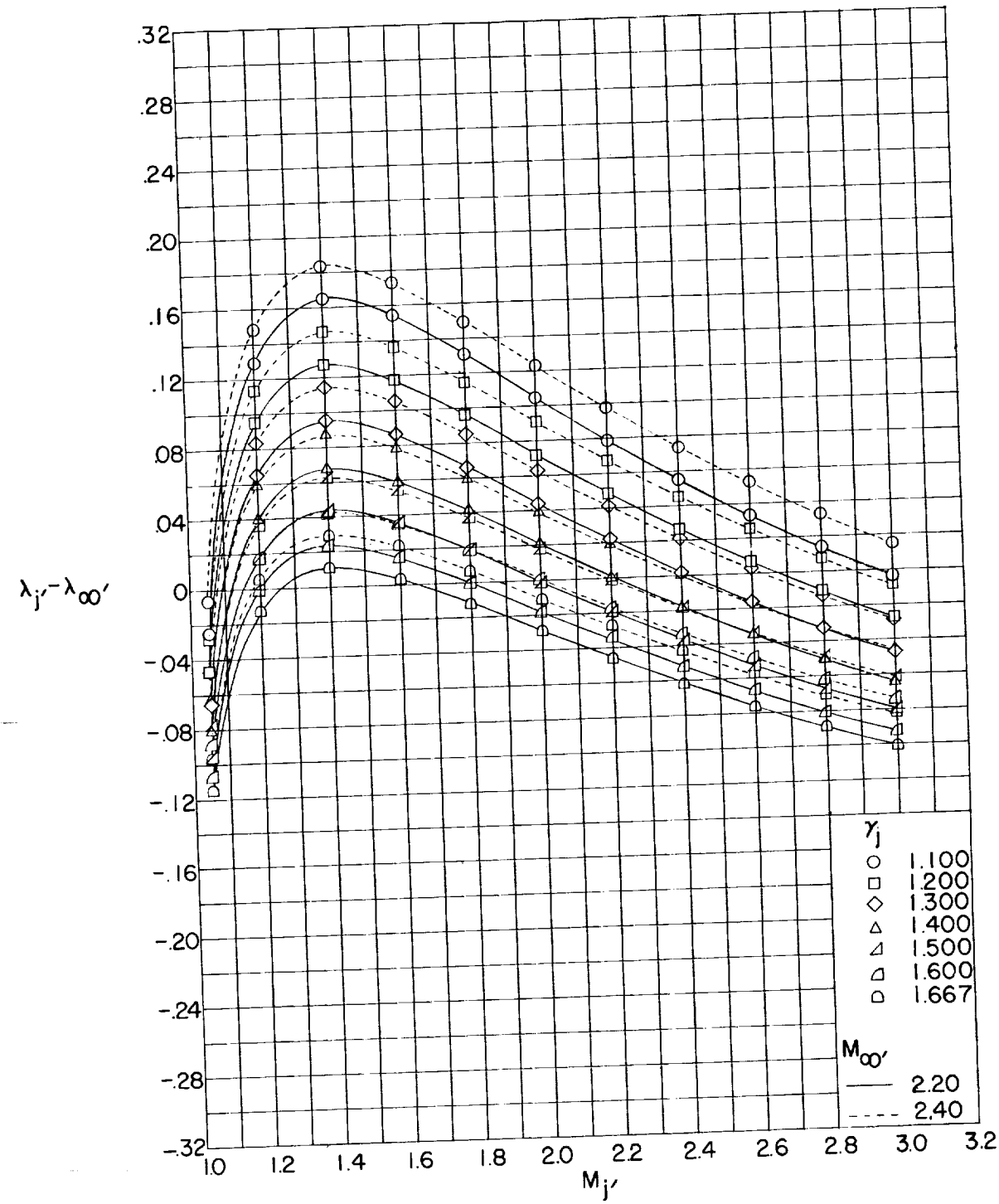

(d) $M_{\infty'}$ = 2.20 and 2.40.

Figure 44.- Continued.

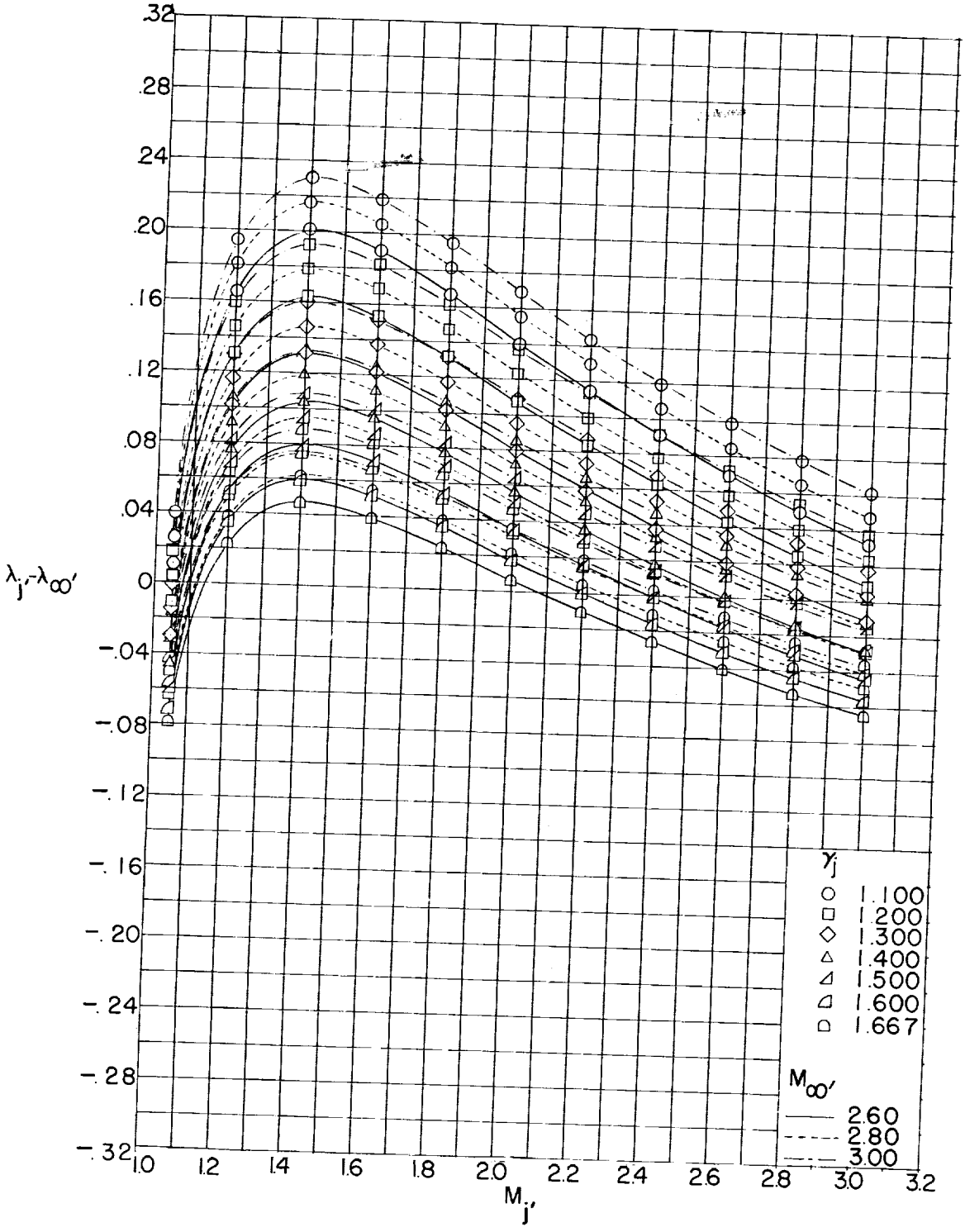

(e) $M_{\infty'}$ = 2.60, 2.80, and 3.00.

Figure 44.- Concluded.

[redacted]

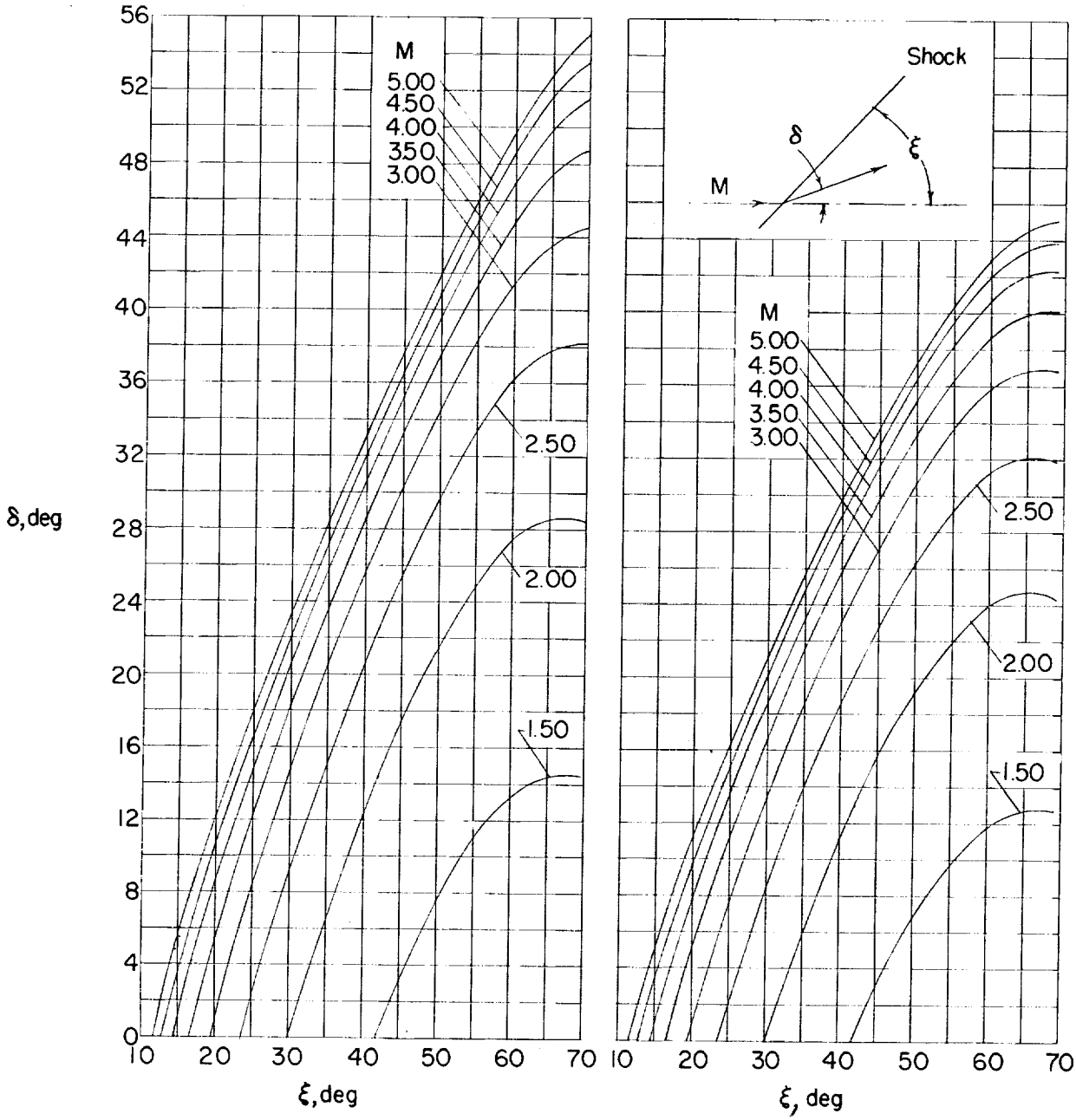

(a) $\gamma = 1.115$.

(b) $\gamma = 1.300$.

Figure 45.- Variation of shock inclination with turning angle for several values of Mach number and ratio of specific heats.

[redacted]

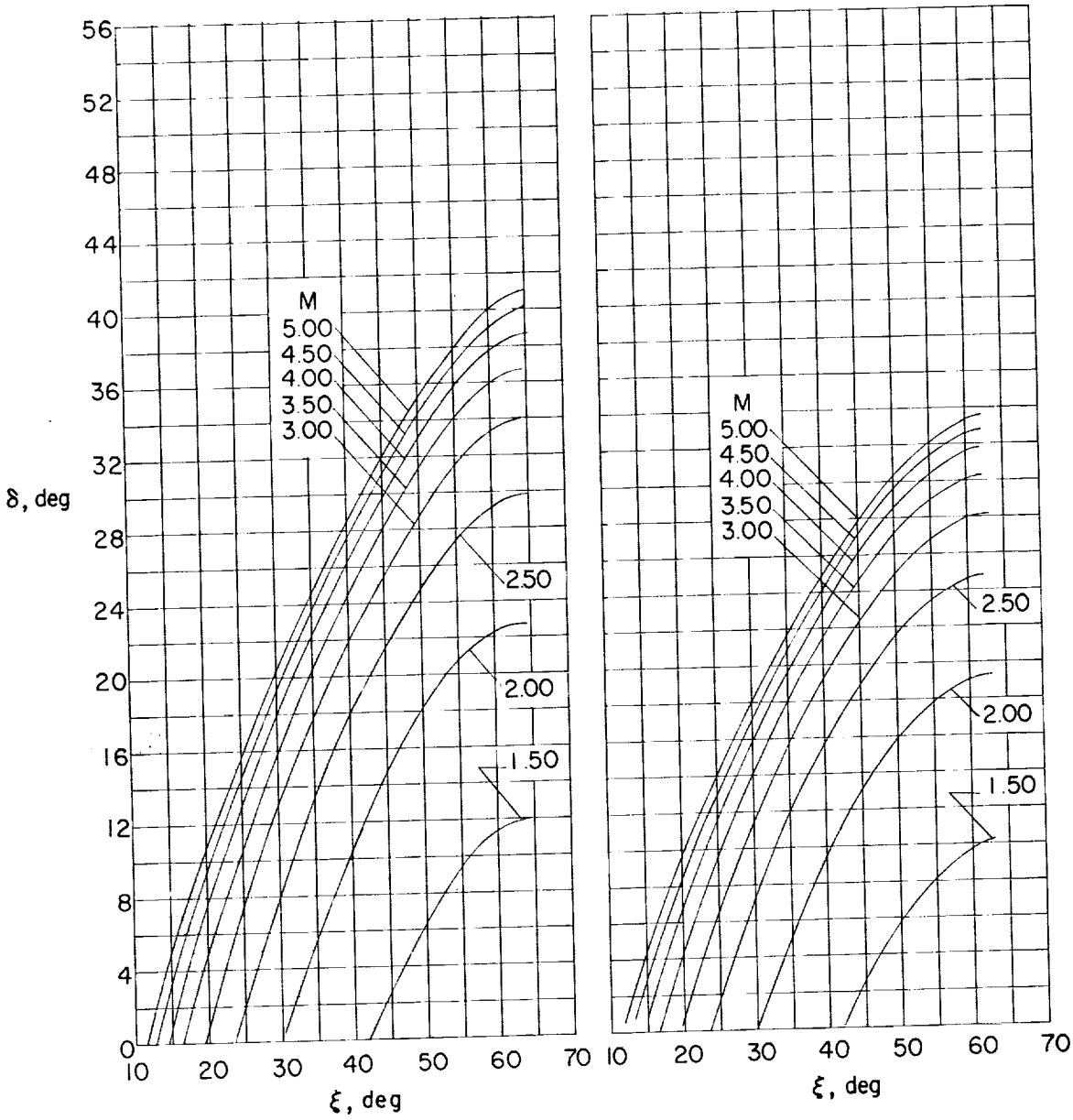

(c) $\gamma = 1.400$.

(d) $\gamma = 1.667$.

Figure 45.- Concluded.

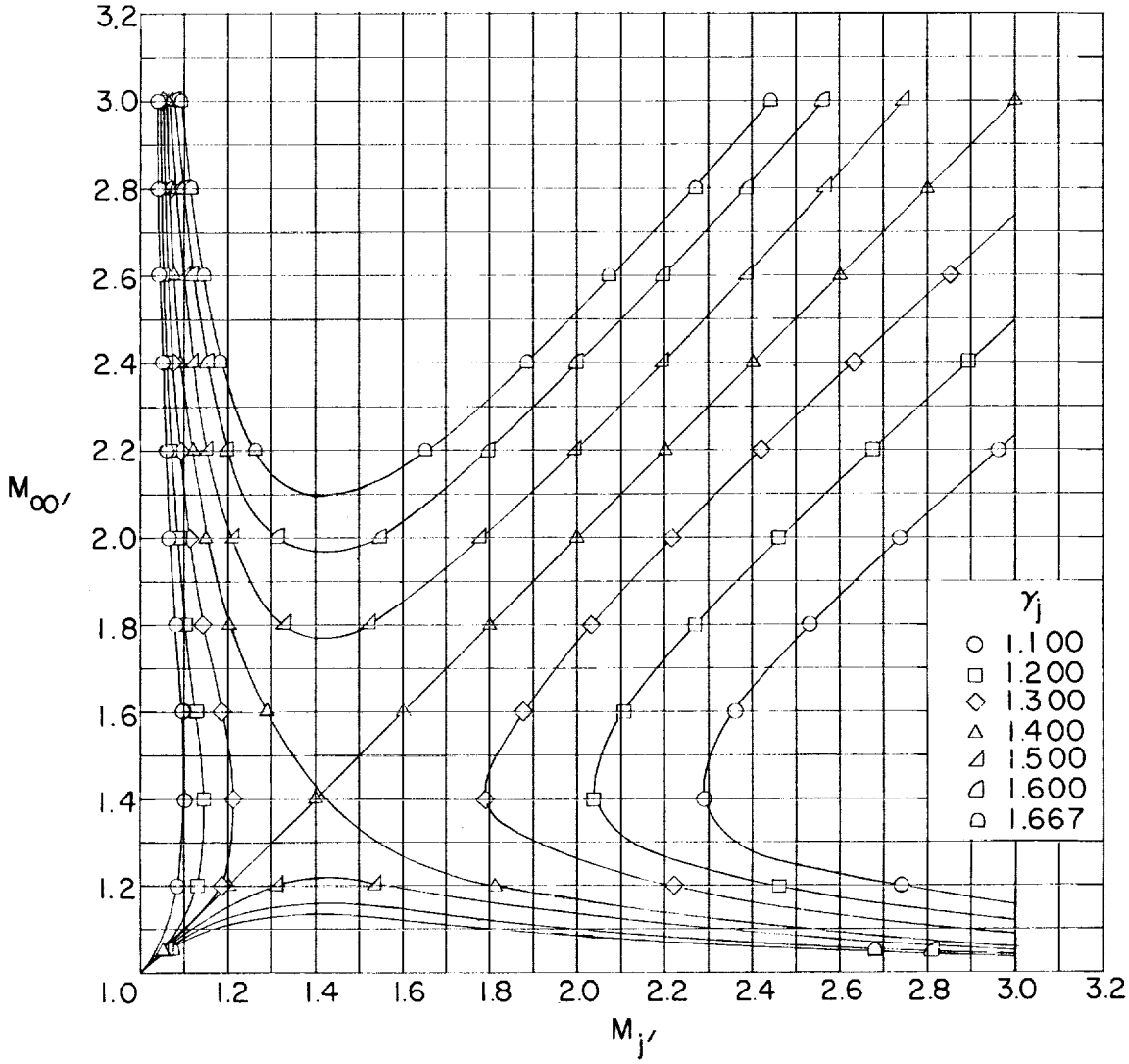

Figure 46.- Relation between the ratio of specific heats of the jet and the local Mach numbers at the boundary in the free jet and in the free stream for no reflection.

[redacted]

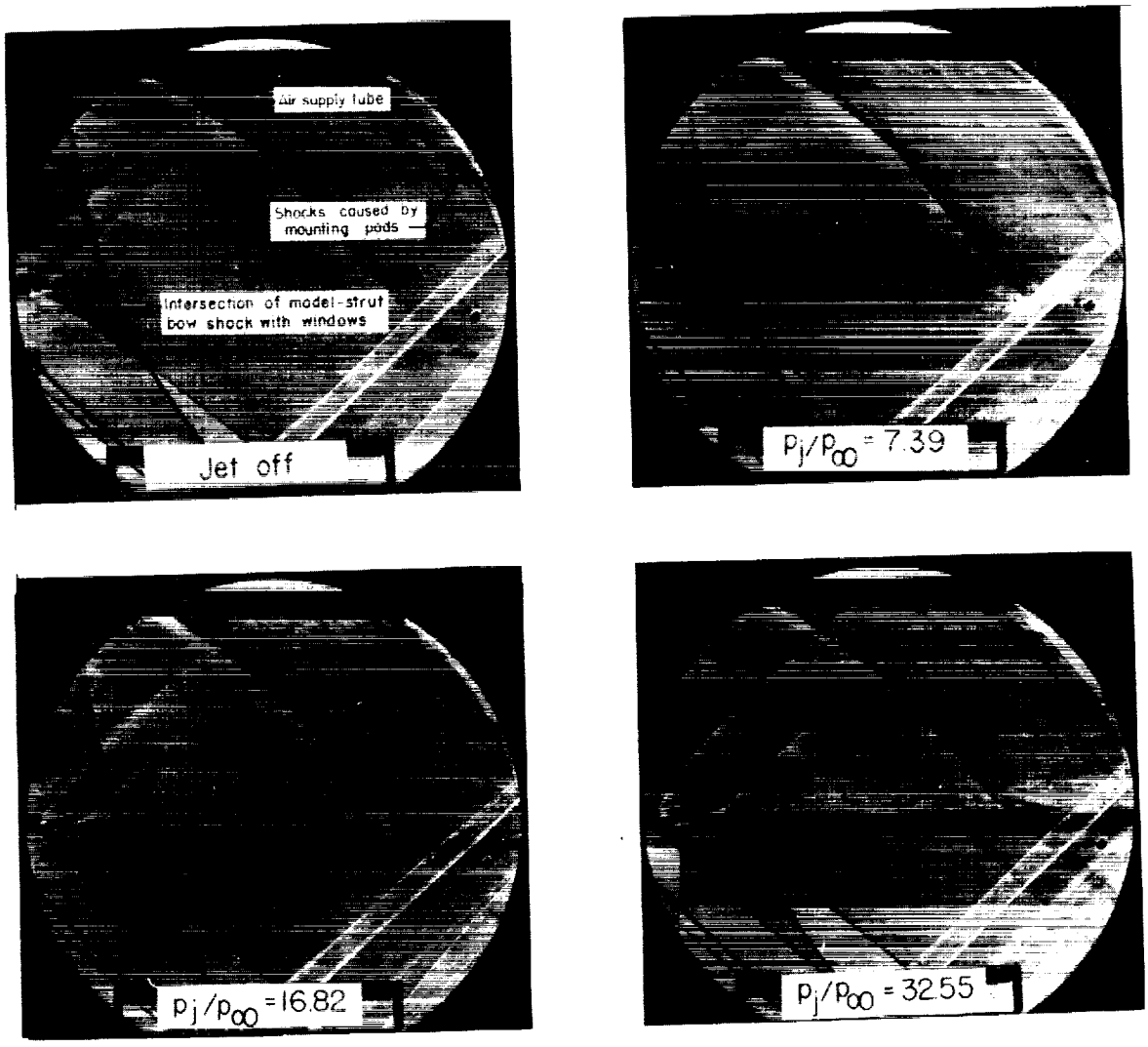

(a) $M_j = 1.00$; $\theta_N = 0°$. L-86514

Figure 47.- Schlieren photographs at a free-stream Mach number of 1.62 of jet exhausting from sonic and supersonic nozzle at varying jet pressure ratio.

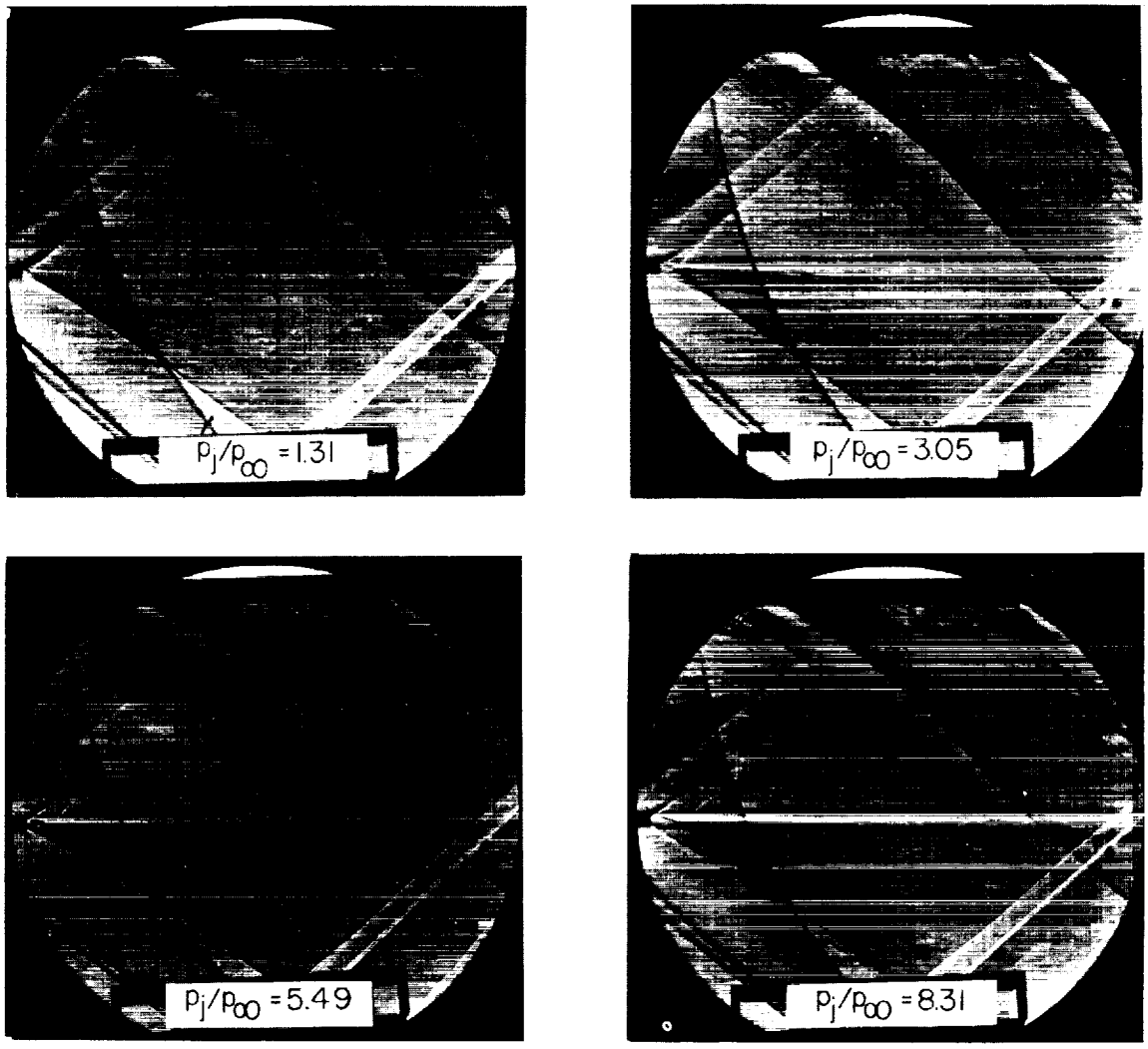

(b) $M_j = 2.50$; $\theta_N = 10^\circ$. L-86515

Figure 47.- Concluded.

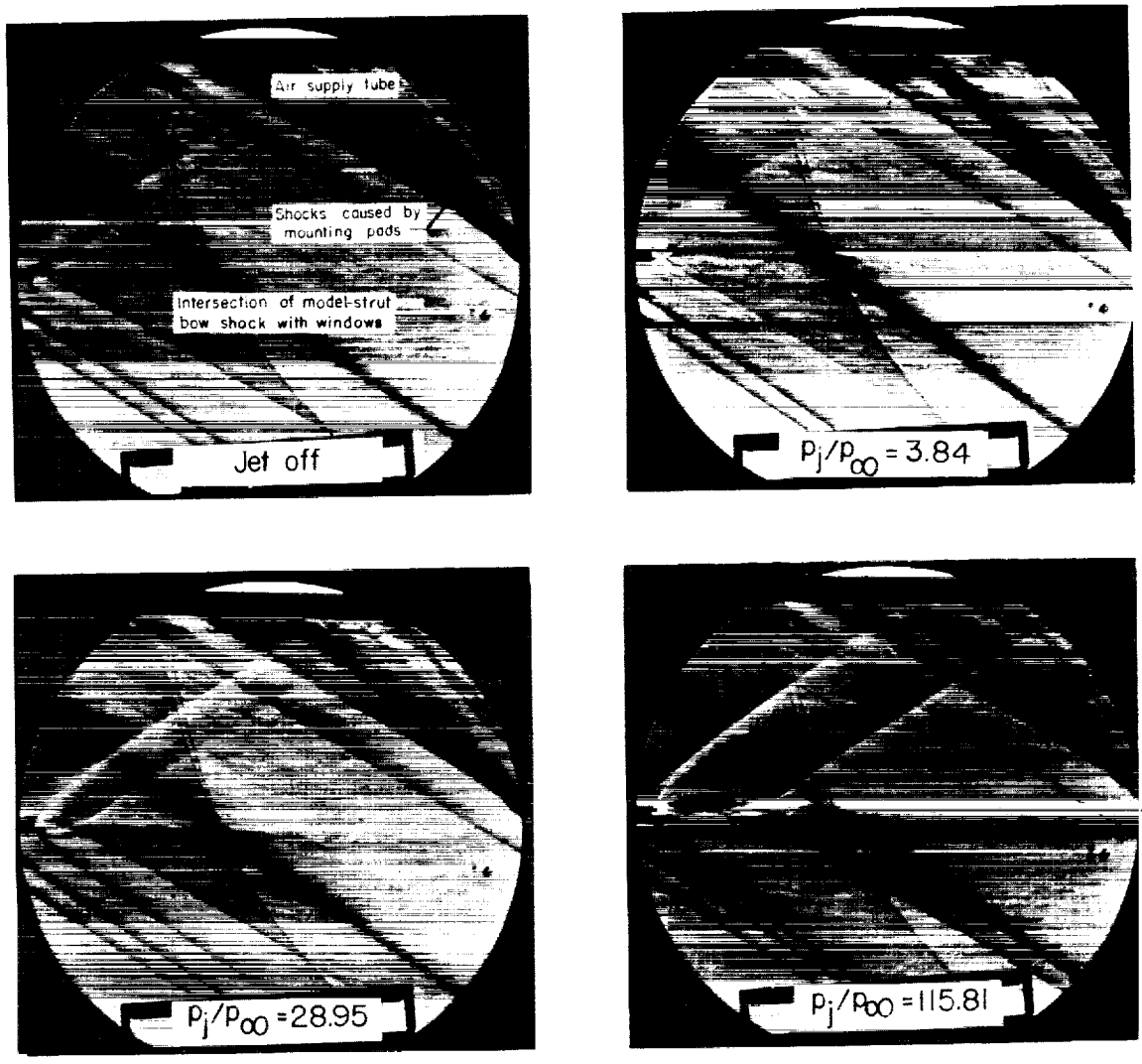

(a) $M_j = 1.00$; $\theta_N = 0^\circ$. L-86516

Figure 48.- Schlieren photographs at a free-stream Mach number of 1.94 of jet exhausting from sonic and supersonic nozzle at varying jet pressure ratio.

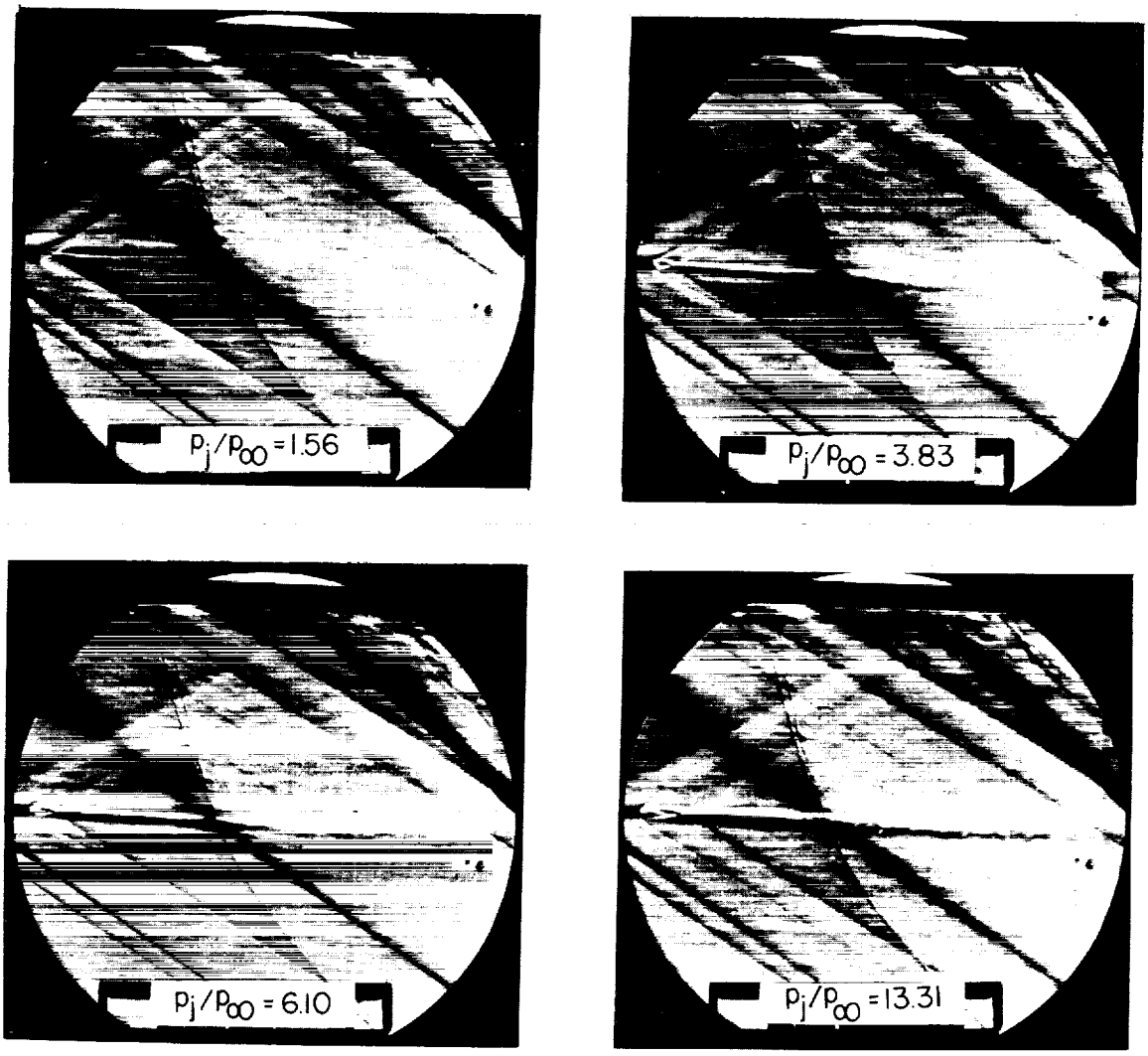

(b) $M_j = 2.50$; $\theta_N = 10^\circ$. L-86517

Figure 48.- Concluded.

[redacted]

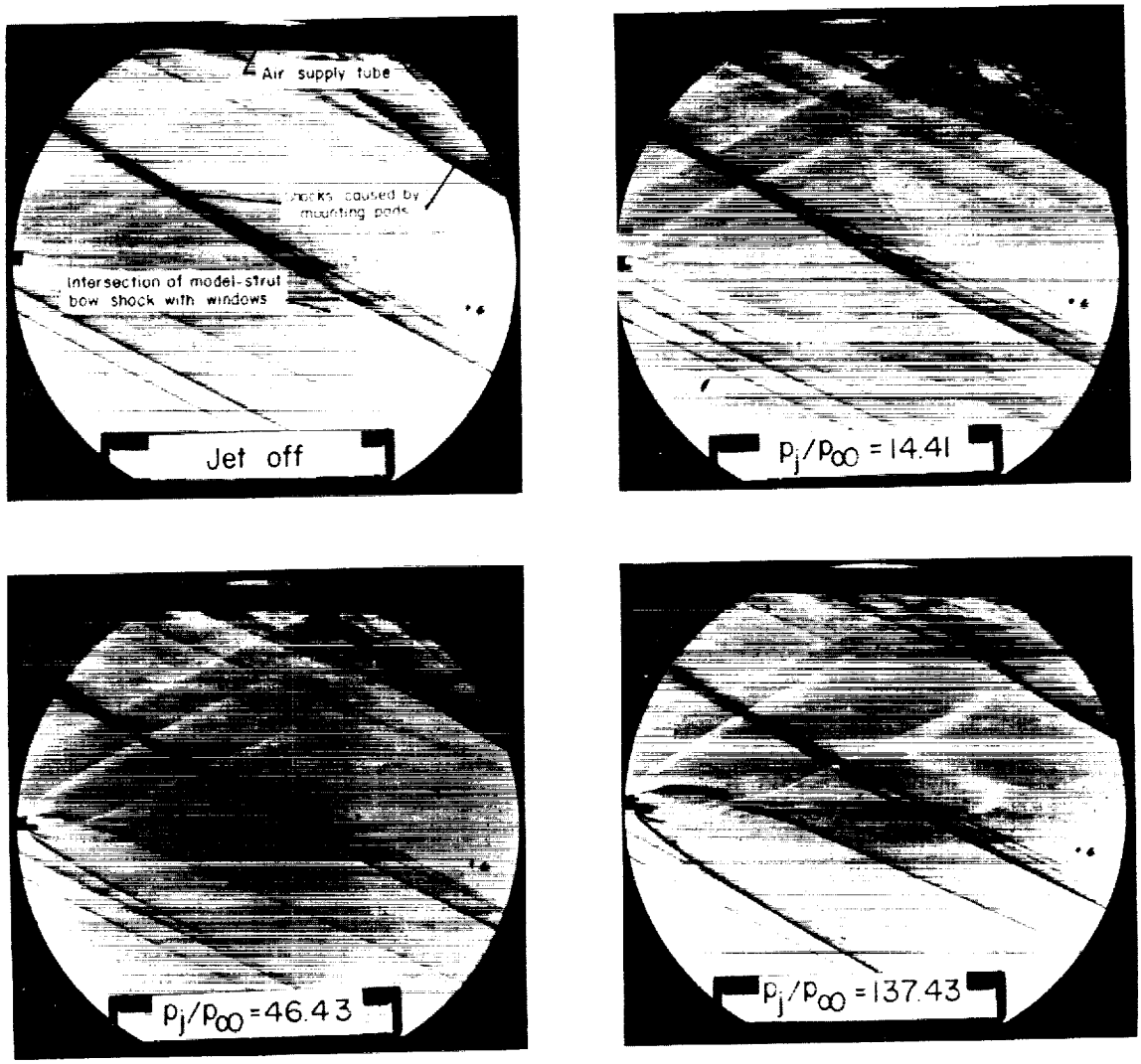

(a) $M_j = 1.00$; $\theta_N = 0^\circ$. L-86518

Figure 49.- Schlieren photographs at a free-stream Mach number of 2.41 of jet exhausting from sonic and supersonic nozzle at varying jet pressure ratio.

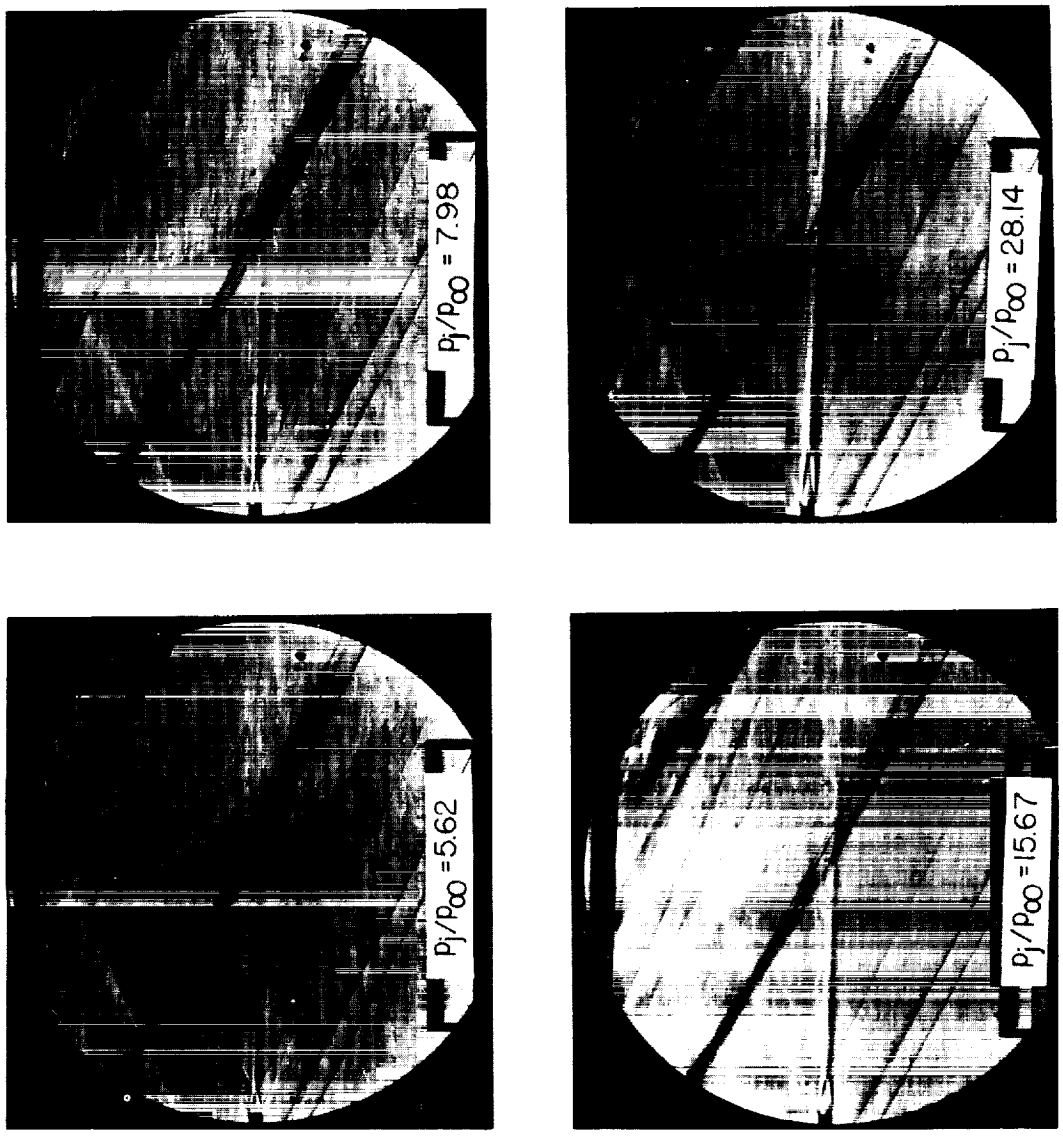

L-86519

(b) $M_j = 2.50$; $\theta_N = 10°$.

Figure 49.- Concluded.

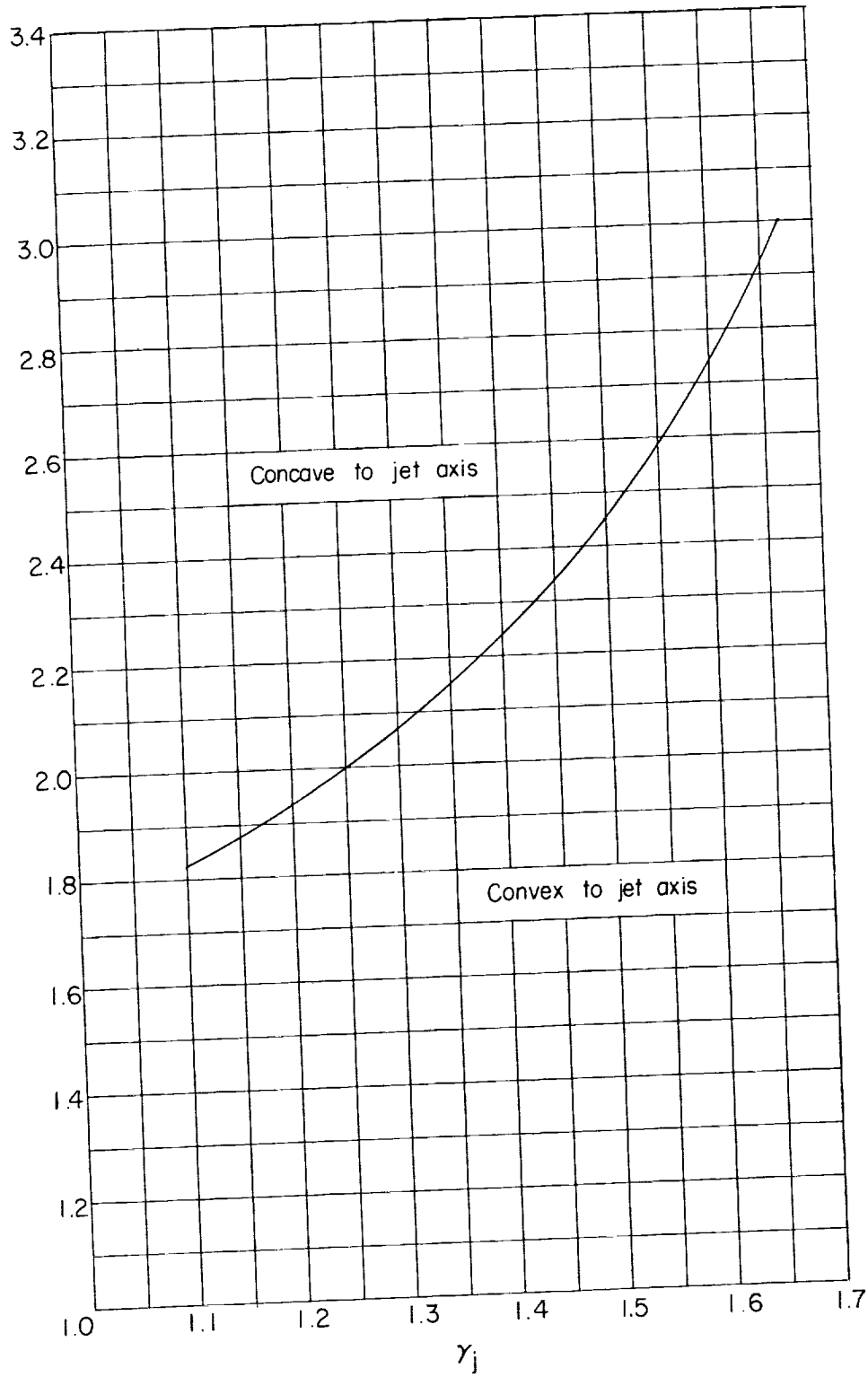

Figure 50.- Curvature of leading characteristic line in expansion of flow from conically divergent nozzles.

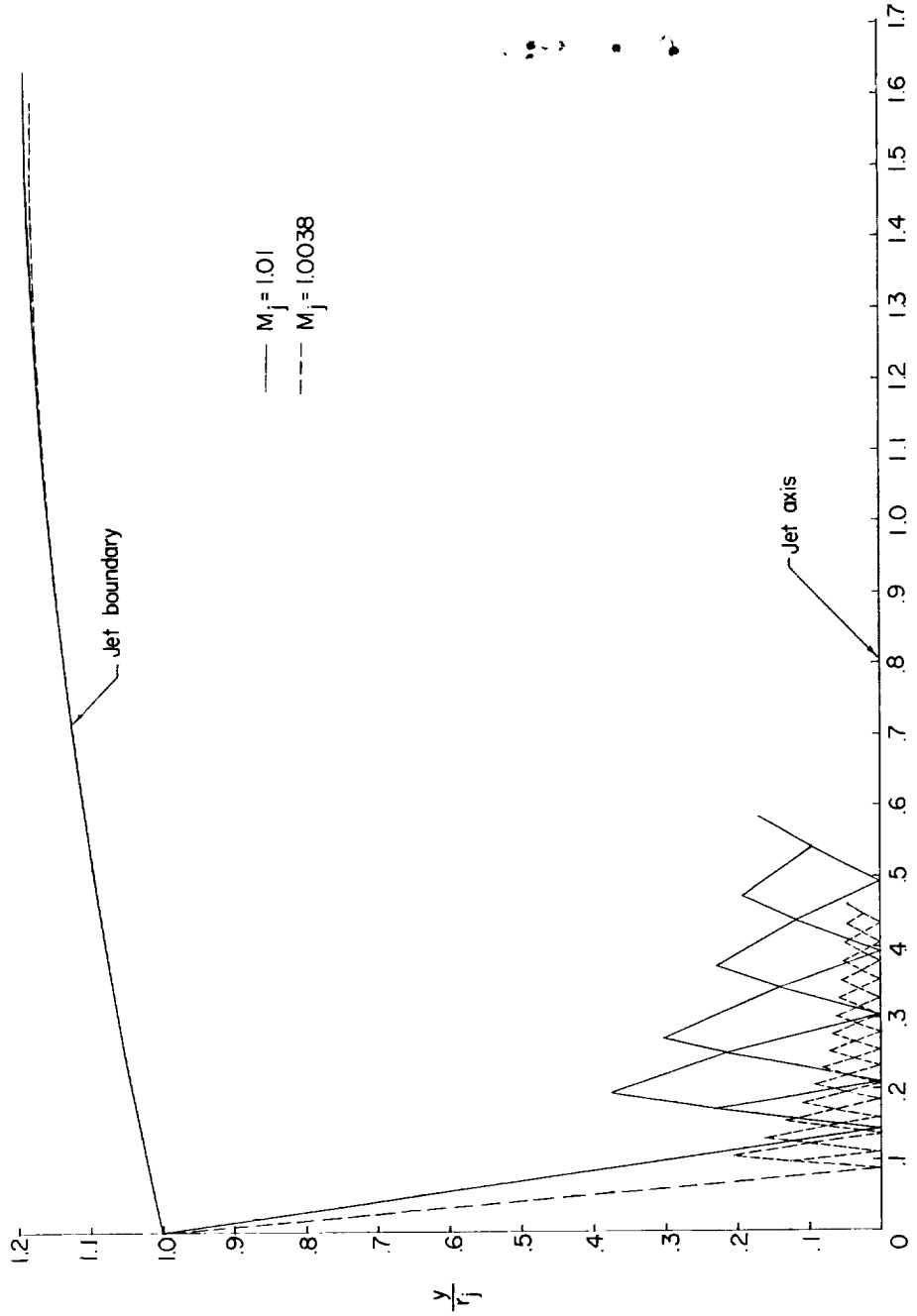

Figure 51.- Comparison of characteristic calculations for near-sonic exit to show effect of errors in flow field near jet axis upon jet boundary.

$\gamma_j = 1.400$; $\frac{p_j}{p_\infty} = 2.$

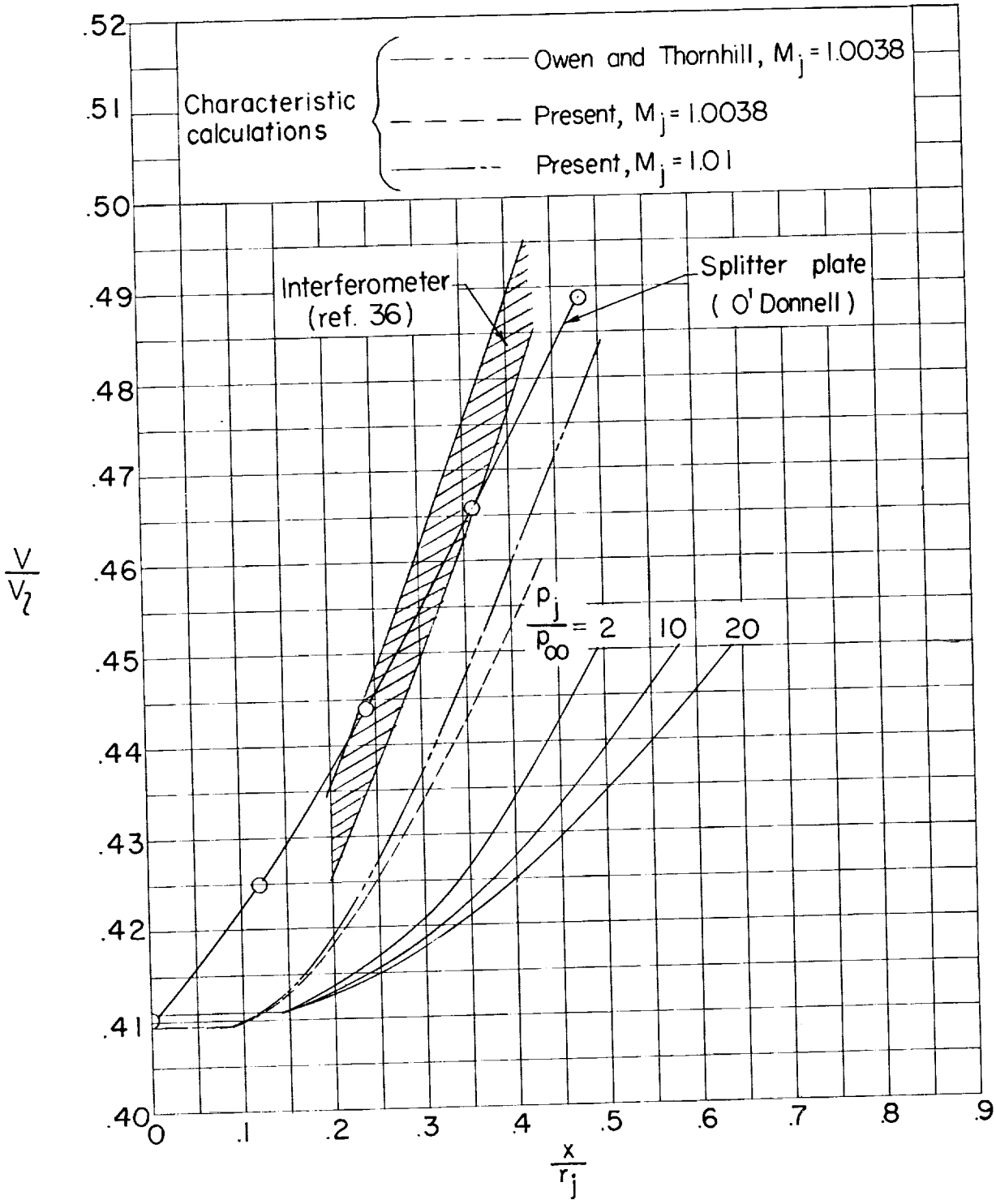

Figure 52.- Comparison of nondimensional velocity distributions along jet axis for sonic or near-sonic exits.